Imperial College London

Department of Chemistry
&
Department of Chemical Engineering

Direct measurement of the interactions between cationic surfactant bilayers

Matthew A Leivers

Submitted in partial fulfilment for the award of the degree of

DOCTOR OF PHILOSOPHY

in Physical Chemistry

September 2019

Declaration of originality

I hereby declare that this thesis and all work contained within is the work of the author and any work of others has been appropriately acknowledged.

Matthew Leivers

Copyright Declaration

The copyright of this work rests with the author and is made available under the Creative Commons Attribution Non-Commercial No Derivatives licence. Researchers are free to copy, distribute or transmit this work on the condition that they appropriately attribute it, they do not use it for commercial purposes and that they do not alter, transform or build upon it. For reuse or redistribution, researchers must make clear to others the licence terms of this work.

Acknowledgements

I would like to acknowledge the contributions of Procter and Gamble who provided the raw materials and funding for this project. The Chemical Biology CDT and the EPSRC for the funding of the project, and Royal Dutch Shell for providing the JPK Nanowizard Atomic Force Microscope. I would also like to personally thank my supervisors, Professors John Seddon and Paul Luckham, for their invaluable help, support, and guidance throughout my PhD.

Abstract

Understanding the interactions between vesicles within a vesicle dispersion is key to understanding the stability of the dispersion. If the interactions between the vesicles are sufficiently repulsive the system will be stable. Whilst this behaviour is relatively easy to predict for simple colloid and vesicle dispersions. In complex systems, containing various additives such as salts, polymers, and polyelectrolytes, the interactions effecting the stability of the dispersion are more complex.

In this study methodologies for directly measuring the interactions between two supported cationic surfactant bilayers using the colloidal probe atomic force microscopy technique were successfully developed.

The surfactant vesicle system of interest in this work was the double tailed, cationic surfactant DIPEDMAMS, often used in commercial fabric softeners. The system was observed to form two co-existing lamellar phases which melt to forma a single fluid lamellar phase at around 40 °C. The addition of different alkyl alcohols was used to modify the transition temperature to create supported bilayers for the colloidal probe technique.

Electrolytes were observed to decrease the repulsive interactions between the bilayers with the identity of the salt determining the strength of the effect. Polyelectrolytes whilst having a similar impact as to the salts the depletion attraction was also observed and shown to be dependent on the molecular weight of the polymer. The interactions with uncharged polymers were complex due to the absorption of the polymer to the bilayers as observed by AFM imaging. The addition of fatty acids to simulate the breakdown of the surfactant molecules within the bilayers exhibited complex behaviour dependent on the nature of the fatty acid in question. All these measurements were supported by AFM imaging and x-ray scattering to decouple changes to the supported bilayers and the interactions between them. Finally, direct force measurements were compared to the behaviour of the bulk vesicle dispersions.

Contents

1 Thesis Overview **1**

2 Theoretical Background **5**

2.1 Amphiphiles: Lipids and Surfactants 5

2.1.1 Structure and Properties 5

2.1.2 Self-Assembly Behaviour 6

2.1.3 The Packing Parameter 8

2.1.4 Liquid Crystalline Phases 9

2.1.5 Lamellar phases 13

2.1.6 Vesicles 15

2.2 Colloids and colloidal stability 17

2.3 Intermolecular Forces 19

2.3.1 Van der Waals Forces 19

2.3.2 Electrical Double Layer Forces 24

2.3.3 DLVO Theory 27

2.3.4 Born Repulsion 29

2.3.5 The Hydrophobic interaction 31

2.3.6 Hydrophilic Interactions 32

2.3.7 Depletion Interaction 33

2.4 Directly Measuring Intermolecular Forces 34

2.4.1 Surface Forces Apparatus 35

2.4.2 Colloidal Probe Atomic Force Microscopy 39

3 Tools and Techniques **47**

3.1 Atomic Force Microscopy 47

3.1.1 Theoretical Principle 47

3.1.2 Experimental protocol 49

3.1.3 Image Processing 50

3.2 Force Spectroscopy and the Colloidal Probe Technique 51

3.2.1 Theoretical Principle 51

3.2.2 Experimental protocol 52

3.2.3 Data processing 53

3.3 Small and Wide Angle X-ray Scattering 54

3.3.1 Theoretical Principle 54

3.3.2 Experimental protocol 57

3.3.3 Data processing 57

3.4 Differential Scanning Calorimetry 58

3.4.1 Theoretical Principle 58

3.4.2 Experimental protocol 59

3.5 Dynamic Light Scattering and Zeta Potential 59

3.5.1 Theoretical Principle 59

3.5.2 Experimental protocol 60

3.6 Sample Preparation 60

3.6.1 Bulk surfactant/water systems 60

3.6.2 Vesicle Dispersions 60

3.6.3 Supported Bilayers 61

4 The Self-Assembly Behaviour of Double Tailed Cationic Surfactants 63

4.1 Introduction 63

4.2 Experimental 65

4.2.1 Preparation of DIPEDMAMS/water systems 65

4.2.2 Small and Wide Angle X-ray Scattering 66

4.2.3 Differential Scanning Calorimetry 66

4.2.4 Atomic Force Microscopy 66

4.3 Results and Discussion 67

4.3.1 SAXS/WAXS Study of the self-assembly behaviour of DIPEDMAMS/water systems . . . 67

4.3.2 The effect of temperature on the self-assembly behaviour of DIPEDMAMS/water systems . . . 77

4.3.3 DSC of the DIPEDMAMS/water system . . . 89

4.3.4 Effect of Temperature on supported bilayers . . . 93

4.4 Conclusions . . . 101

5 Measuring the Interactions between Supported Cationic Surfactant Bilayers 103

5.1 Introduction . . . 103

5.2 Experimental . . . 105

5.2.1 Preparation of Alkyl Alcohol Modified DIPEDMAMS Systems 105

5.2.2 Differential Scanning Calorimetry . . . 105

5.2.3 Small and Wide Angle X-ray Scattering . . . 105

5.2.4 Atomic Force Microscopy . . . 105

5.3 Results and Discussion . . . 107

5.3.1 Issues with formation of bilayers on probe . . . 107

5.3.2 Alkyl Alcohol Modification . . . 110

5.3.3 Alkyl Alcohol Modification: Force Spectroscopy . . . 123

5.3.4 Measurement of Bilayer-Bilayer interactions by Colloidal Probe Atomic Force Spectroscopy . . . 130

5.4 Conclusions 137

6 Impact of Halide Salts on the Structure of, and Interactions between, Supported Cationic Surfactant Bilayers 141

6.1 Introduction 141

6.2 Experimental 144

6.2.1 Preparation of supported lipid bilayers 144

6.2.2 Atomic Force Microscopy 144

6.2.3 Small Angle X-ray Scattering (SAXS) 146

6.2.4 Dynamic Light Scattering and Zeta Potential 146

6.3 Results and Discussion 147

6.3.1 Interaction between supported cationic surfactant bilayers with increasing NaCl concentration 147

6.3.2 Role of Counterion in Bilayer-Bilayer Interactions 153

6.3.3 AFM Imaging 163

6.3.4 Small Angle X-ray Scattering 169

6.3.5 Particle sizing and Zeta Potential of Vesicles 175

6.4 Conclusions 178

7 Impact of Polymers and Polyelectrolytes on Bilayer-Bilayer Interactions 181

7.1 Introduction 181

7.2 Experimental 184

7.2.1 Preparation of supported lipid bilayers 184

7.2.2 Atomic Force Microscopy 185

7.2.3 Dynamic Light Scattering and Zeta Potential 186

7.3 Results and Discussion 186

7.3.1 The impact of polyelectrolytes on the measured interactions between supported cationic bilayers 186

7.3.2 The impact of PEO on the measured interactions between supported cationic bilayers 198

7.3.3 AFM Imaging 208

7.3.4 Particle sizing and Zeta Potential of Surfactant Vesicles 217

7.4 Conclusions 223

8 The Impact of Fatty Acids on Bilayer-Bilayer Interactions to Simulate Surfactant Ageing 227

8.1 Introduction 227

8.2 Experimental 228

8.2.1 Preparation of supported lipid bilayers 229

8.2.2 Atomic Force Microscopy 229

8.2.3 Small Angle X-ray Scattering (SAXS) 230

8.2.4 Dynamic Light Scattering and Zeta Potential 230

8.3 Results and Discussion 231

8.3.1 The impact of bilayer compositions on the interactions measured between supported cationic bilayers 231

8.3.2 AFM Imaging 241

8.3.3 Small and Wide Angle X-ray Scattering 250

8.3.4 Particle sizing and zeta potential of vesicles 256

8.4 Conclusions 260

9 Conclusions and Outlook **263**

References **266**

List of Figures

2.1 Examples of typical ionic, zwitterionic, and non-ionic amphiphiles highlighting the hydrophilic and hydrophobic regions of each molecule. 7

2.2 Surfactant packing parameters for different amphiphile shapes and the structures they typically adopt. 10

2.3 A hypothetical phase diagram showing the impact of increasing surfactant concentration on a binary amphiphile/water system where the transitions are controlled by the solvent content alone. [5] 13

2.4 Diagram showing the typical bilayer structures of the most common lamellar phases. 14

2.5 The main types of surfactant vesicles. 16

2.6 Diagram showing the three main components of the van der Waals forces: permanent dipole - dipole interactions; permanent dipole - induced dipole interactions; and the instantaneous dipole - induced dipole forces. Orientation dependant variables are illustrated for each interaction. 20

2.7 Diagram describing the three main components of the van der Waals forces: the Keesom interaction, the Debye Force, and the London dispersion force. 22

2.8 Diagram showing the different double layer models with sketches of how the potential changes with distance from the surface. 26

2.9 The theoretical DLVO interactions showing the impact of deceasing surface potential on the model interactions. 28

2.10 Diagrammatic representation of the depletion attraction. 33

2.11 Simplified schematic of the surface forces apparatus. 36

2.12 Simplified schematic of the colloidal probe atomic force microscopy technique. 41

3.1 Simplified schematic of an atomic force microscope. 48

3.2 Diagram showing the three main AFM imaging modes: contact mode, non-contact mode, and quantitative imaging mode. 49

3.3 Impact of the line fitting algorithm on AFM images showing the raw data and the final processed image. 50

3.4 The operation of the colloidal probe force spectroscopy technique with theoretical force curves showing the types of interactions measured at different points in the force ramp. 52

3.5 Preprocesses used in the data processing of force curves. Showing the impact of each process on the raw data. 54

3.6 Simplified schematic of a combined SAXS/WAXS system similar to I22. 55

3.7 Diagrammatic representation of Bragg diffraction. Showing the elastic scattering of two incident beams by two different atoms within the sample. 56

4.1 Structure of the DIPEDMAMS surfactant, were R is a fatty alkyl chain originating from a fatty acid mixture of C16, C18 and C18:1. . 64

4.2 Full detector image of the SAXS pattern for a 20 wt% DIPEDMAMS/water system at 25 °C. 68

4.3 Linear intensity plot for the SAXS pattern of a 20 wt% DIPEDMAMS/water system produced by the radial integration of the raw SAXS image. 69

4.4 Cropped SAXS images of DIPEDMAMS/water systems at 25 °C at surfactant concentration a) 1 wt%, b) 5 wt% c) 10 wt%, d) 20 wt%, e) 30 wt%, f) 50 wt%. 70

4.5 Linear intensity plots of the SAXS patterns of DIPEDMAMS/water systems, at 25 °C, and surfactant concentrations 1 - 50 wt%. The insert shows an enlarged section of the linear intensity plots focusing on the 1 - 10 wt% range. 71

4.6 Plots of d-spacing as a function of a) DIPEDMAMS concentration and b) water to surfactant ratio including extrapolation to zero water content for a calculation of the intrinsic surfactant bilayer thickness. . 72

4.7 WAXS images of DIPEDMAMS/water systems at 25 °C at surfactant concentration a) 1 wt%, b) 5 wt% c) 10 wt%, d) 20 wt%, e) 30 wt%, f) 50 wt%. 75

4.8 Linear intensity plots of the WAXS patterns of DIPEDMAMS/water systems, at 25 °C, and surfactant concentrations 1 - 50 wt%. 76

4.9 Cropped SAXS images of 20 wt% DIPEDMAMS/water systems at a) 15 °C, b) 25 °C, c) 35 °C, d) 45 °C, e) 55 °C. 78

4.10 Linear intensity plots of the SAXS patterns of DIPEDMAMS/water systems with increasing temperature at surfactant concentrations a) 1 wt%, b) 5 wt% c) 10 wt%, d) 20 wt%, e) 30 wt%, f) 50 wt%. 79

4.11 WAXS images of 20 wt% DIPEDMAMS/water systems at a) 15 °C, b) 25 °C, c) 35 °C, d) 45 °C, e) 55 °C. 82

4.12 Linear intensity plots of the WAXS patterns of DIPEDMAMS/water systems with increasing temperature at surfactant concentrations a) 1 wt%, b) 5 wt% c) 10 wt%, d) 20 wt%, e) 30 wt%, f) 50 wt%. For clarity the y-axis has been offset by the temperature of the sample. . 84

4.13 Structure of the DIPEDMAMS surfactant, where R is a fatty alkyl chain originating from a fatty acid mixture of C16, C18 and C18:1. . 86

4.14 SAXS linear intensity plots of a) 30 wt% and b) 50 wt% DIPEDMAMS water systems with i) increasing and ii) decreasing temperature. Temperature range of 20 - 60 °C. 87

4.15 Proposed phase diagram for the DIPEDMAMS/water system as a function of surfactant concentration and temperature. 88

4.16 DSC curves for the DIPEDMAMS surfactant system at surfactant concentrations a) 1 wt%, b) 5 wt% c) 10 wt%, d) 20 wt%, e) 30 wt%, f) 50 wt%. Scan conducted at 5 °C min^{-1} between 15 and 55 °C. Scans shown are the second cycle. 90

4.17 Typical QI AFM topographical images, with associated typical maps of surface adhesion and measured slope, for DIPEDMAMS bilayers on mica with increasing temperature from 25 - 65 °C. 94

4.18 Typical QI AFM topographical images, with associated typical maps of surface adhesion and measured slope, for DIPEDMAMS bilayers on mica with decreasing temperature from 65 - 25 °C. 95

4.19 Typical 5 x 5 µm QI AFM topographical images, with associated cross-sections, for DIPEDMAMS bilayers on mica with increasing temperature from 25 - 55 °C. 97

4.20 Typical 5 x 5 µm QI AFM topographical images, with associated cross-sections, for DIPEDMAMS bilayers on mica with decreasing temperature from 25 - 55 °C. 98

5.1 DIPEDMAMS bilayer formed at room temperature on freshly cleaved mica. Imaging was done in QI mode and the topographical, adhesion and measured slope maps are shown. A crossection of the topographical image is included as well as an example of the QI force curves for upper (left) and lower (right) regions. 108

5.2 Approach force distance plots of the interaction measure between a glass colloidal probe and mica both before and after incubation with a DIPEDMAMS vesicle dispersion at room temperature. 109

5.3 Structure of perillyl alcohol. 110

5.4 Second heating cycle of normalised DSC curves for DIPEDMAMS/water systems containing 10 mol% alkyl alcohol. 113

5.5 Linear intensity plots of the SAXS patterns of DIPEDMAMS/water systems, at 25 °C, containing 10 mol% alkyl alcohols. 115

5.6 Linear intensity plots of the WAXS patterns of DIPEDMAMS/water systems, at 25 °C, containing 10 mol% alkyl alcohols. 116

5.7 Typical QI AFM topographical images, with associated typical maps of surface adhesion and measured slope, for DIPEDMAMS bilayers on mica containing 10 mol% alkyl alcohol. All bilayers formed and imaged at room temperature. 118

5.8 Typical QI AFM topographical images, with associated typical maps of surface adhesion and measured slope, for DIPEDMAMS bilayers on mica. Top row show images of bilayers containing only DIPEDMAMS formed at room temperature, the middle row show pure DIPEMAMS bilayers formed at 60 °C and the bottom row shows bilayers contain 10 mol% perillyl alcohol formed at room temperature. 121

5.9 Approach force distance curves measured between a sharp AFM probe and DIPEDMAMS bilayers containing 10 mol% alkyl alcohol. The top plot shows forces measured against the higher areas and the bottom figure those measured against the lower areas. 124

5.10 Approach force distance curves measured between a sharp AFM probe and DIPEDMAMS bilayers. The top and bottom plots show the forces measured against the higher areas and lower areas of the bilayers respectively. 127

5.11 Colloidal probe AFM force distance curves measured on approach between a glass colloidal probe and a mica surface. Each plot shows the measured force both before and after bilayer formation. 131

5.12 Colloidal probe AFM force distance curves measured on approach between a glass colloidal probe and a glass surface. Each plot shows the measured force both before and after bilayer formation. 136

6.1 Schematic of the colloidal probe experimental set up used for the direct measurement of interactions between two cationic surfactant bilayers. 145

6.2 Forces measured between DIPEDMAMS on approach in solutions of increasing NaCl concentration. 148

6.3 Forces measured between DIPEDMAMS on approach in solutions of increasing NaCl concentration, on a semi-log scale. Solid red lines show the theoretical DLVO fitting for each electrolyte environment and the solid black lines show the theoretical EDL forces. See table 6.1 for fitting parameters. 151

6.4 Forces measured between DIPEDMAMS bilayers on approach in electrolyte solutions with increasing concentration.. Halide concentrations and salt identity are shown in the figure. 154

6.5 Forces measured between DIPEDMAMS bilayers on approach in electrolyte solutions with increasing concentration. Halide concentrations and salt identity are shown in the figure. 155

6.6 Forces measured between DIPEDMAMS bilayers on approach in electrolyte solutions with increasing concentration, on a semi-log scale. Solid black lines show the theoretical model EDL interactions interactions for each environment. Halide concentrations and salt identity are shown in the figure. See table 6.2 for fitting parameters. 157

6.7 Forces measured between DIPEDMAMS bilayers on approach in electrolyte solutions with increasing concentration, on a semi-log scale. Solid black lines show the theoretical model EDL interactions interactions for each environment. Halide concentrations and salt identity are shown in the figure. See table 6.2 for fitting parameters. 158

6.8 Schematic showing a) a classic EDL with stern layer and diffuse layer b) ionic pair model for a surfactant bilayer. 162

6.9 AFM images, 5 x 5 μm and associated cross-sections for a)i0.01 mM NaCl a)ii 100 mM NaCl b)i 0.01 mM NaBr b)ii 100 mM NaBr. 164

6.10 AFM images, 5 x 5 μm and associated cross-sections for a)i0.01 mM NaI a)ii 100 mM NaI b)i 0.005 mM $CaCl_2$ b)ii 50 mM $CaCl_2$. 165

6.11 Typical QI AFM topographical images, with associated typical maps of surface adhesion and measured slope, for supported DIPEDMAMS bilayers imaged in increasing concentrations of NaBr. Concentrations shown in figure. 168

6.12 Linear intensity plots of the SAXS patterns of DIPEDMAMS/water systems with varying electrolyte concentrations. Electrolyte concentrations and identity are shown in the figure. 170

6.13 Plot of the d-spacing of DIPEDMAMS lamellar phases as a function of halide concentration for all electrolytes investigated. 172

6.14 Plots of the mean particle diameter and zeta potential of a DIPEDMAMS vesicle dispersion as a function of increasing electrolyte concentration. 176

7.1 Forces measured between DIPEDMAMS bilayers on approach in increasing concentrations of high molecular weight poly-DADMAC. Polyelectrolyte concentrations are shown in figure. Insert shows the forces from 5×10^{-3} to 0.05 wt% poly-DADMAC on a smaller scale. 187

7.2 Forces measured between DIPEDMAMS bilayers on approach in increasing concentrations of medium molecular weight poly-DADMAC. Polyelectrolyte concentrations are shown in figure. Insert shows the forces from 5×10^{-3} to 0.05 wt% poly-DADMAC on a smaller scale. . 188

7.3 Forces measured between DIPEDMAMS bilayers on approach in increasing concentrations of low molecular weight poly-DADMAC. Polyelectrolyte concentrations are shown in figure. Insert shows the forces from 5×10^{-3} to 0.05 wt% poly-DADMAC on a smaller scale. 189

7.4 Forces measured between DIPEDMAMS bilayers on approach in increasing concentrations of different molecular weights of poly-DADMAC, on a semi-log scale. Solid black lines show the theoretical model EDL interactions interactions for each environment. Polyelectrolyte concentrations and molecular weights shown in figure. 191

7.5 Forces measured between DIPEDMAMS bilayers on approach in increasing concentrations of different molecular weights of poly-DADMAC, on a semi-log scale. Solid black lines show the theoretical model EDL interactions interactions for each environment. Polyelectrolyte concentrations and molecular weights shown in figure. 192

7.6 Forces measured between DIPEDMAMS bilayers on approach in 0.05 wt% poly-DADMAC at different molecular weights. Molecular weights shown in figure. 196

7.7 Forces measured between DIPEDMAMS bilayers on approach in increasing concentrations of different molecular weights of PEO. Polymer concentrations and molecular weights shown in figure. Inserts show the forces from 5×10^{-3} to 0.05 wt% PEO on a smaller scale. . 199

7.8 Forces measured between DIPEDMAMS bilayers on approach in increasing concentrations of different molecular weights of PEO. Polymer concentrations and molecular weights shown in figure. Insert shows the forces from 5×10^{-3} to 0.05 wt% PEO on a smaller scale. . 200

7.9 Forces measured between DIPEDMAMS bilayers on approach in increasing concentrations of different molecular weights of PEO, on a semi-log scale. Solid black lines show the theoretical model EDL interactions interactions for each environment. Polymer concentrations and molecular weights shown in figure. 202

7.10 Forces measured between DIPEDMAMS bilayers on approach in increasing concentrations of different molecular weights of PEO, on a semi-log scale. Solid black lines show the theoretical model EDL interactions interactions for each environment. Polymer concentrations and molecular weights shown in figure. 203

7.11 Typical QI AFM topographical images, with associated typical maps of surface adhesion and measured slope, for supported DIPEDMAMS bilayers imaged in increasing concentrations of 400,000 Mw PEO. Concentrations shown in figure. 209

7.12 AFM images, 5 x 5 μm and associated cross-sections in PEO solutions a)i 5×10^{-5} wt% high molecular weight a)ii 0.5 wt% high molecular weight. 211

7.13 AFM images, 5 x 5 μm and associated cross-sections in PEO solutions b)i 5×10^{-5} wt% medium molecular weight b)ii 0.5 wt% medium molecular weight. 212

7.14 AFM images, 5 x 5 μm and associated cross-sections in PEO solutions a)i 5×10^{-5} wt% low molecular weight a)ii 0.5 wt% low molecular weight. 213

7.15 Typical QI AFM topographical images, with associated typical maps of surface adhesion and measured slope, for supported DIPEDMAMS bilayers imaged in increasing concentrations of medium poly-DADMAC. Concentrations shown in figure. 214

7.16 AFM images, 5 x 5 μm and associated cross-sections in poly-DADMAC solutions a)i 5×10^{-5} wt% high Mw a)ii 0.5 wt% high Mw b)i 5×10^{-5} wt% low Mw b)ii 0.5 wt% low Mw. 216

7.17 Plots of the mean particle diameter and zeta potential of a DIPEDMAMS vesicle dispersion as a function of increasing poly-DADMAC concentration and molecular weights. 218

7.18 Plots of the mean particle diameter and zeta potential of a DIPEDMAMS vesicle dispersion as a function of increasing PEO concentration and molecular weights. 220

8.1 Forces measured on approach between DIPEDMAMS bilayers containing increasing concentrations of stearic acid and palmitic acid. Fatty acid concentrations and identity are shown in the figure. 233

8.2 Forces measured on approach between DIPEDMAMS bilayers containing increasing concentrations of oleic acid and tallow mixture. Fatty acid concentrations and identity are shown in the figure. 234

8.3 Forces measured on approach between DIPEDMAMS bilayers containing increasing concentrations of stearic acid and palmitic acid on a semi-log scale. Solid black lines show the theoretical model EDL interactions interactions for each composition. Fatty acid concentrations and identity are shown in the figure. 236

8.4 Forces measured on approach between DIPEDMAMS bilayers containing increasing concentrations of oleic acid and the tallow mixture on a semi-log scale. Solid black lines show the theoretical model EDL interactions interactions for each composition. Fatty acid concentrations and identity are shown in the figure. 237

8.5 Typical QI AFM topographical images, with associated typical maps of surface adhesion and measured slope, for supported DIPEDMAMS bilayers containing increasing concentrations of stearic acid. Concentrations shown in figure. 242

8.6 AFM images, 5 x 5 μm and associated cross-sections of DIPEDMAMS bilayers containing a)i 1 mol% stearic acid a)ii 20 mol% stearic acid b)i 1 mol% palmitic acid b)ii 20 mol% palmitic acid. 244

8.7 Typical QI AFM topographical images, with associated typical maps of surface adhesion and measured slope, for supported DIPEDMAMS bilayers containing increasing concentrations of oleic acid. Concentrations shown in figure. 245

8.8 Typical QI AFM topographical images, with associated typical maps of surface adhesion and measured slope, for supported DIPEDMAMS bilayers containing increasing concentrations of the tallow fatty acid mixture. Concentrations shown in figure. 247

8.9 AFM images, 5 x 5 μm and associated cross-sections of DIPEDMAMS bilayers containing a)i 1 mol% oleic acid a)ii 20 mol% oleic acid b)i 1 mol% tallow b)ii 20 mol% tallow. 249

8.10 Linear intensity plots of the SAXS patterns of DIPEDMAMS/water systems with varying fatty acid content. Fatty acid concentrations and identity are shown in the figure. 251

8.11 Plot of the d-spacing of DIPEDMAMS lamellar phases as a function of increasing fatty acid content. 253

8.12 Linear intensity plots of the WAXS patterns of DIPEDMAMS/water systems with varying fatty acid content. Fatty acid concentrations and identity are shown in the figure. 254

8.13 Plots of the mean particle diameter and zeta potential of a DIPEDMAMS vesicle dispersion as a function of increasing fatty acid content. 258

List of Tables

2.1 Types of colloidal dispersions 18

6.1 Fitting parameters used in DLVO and EDL fits to the CP-AFM data in figure 6.3 152

6.2 Fitting parameters used in DLVO and EDL fits to the CP-AFM data in figure 6.6 and 6.7 159

7.1 Fitting parameters used in DLVO and EDL fits to the CP-AFM data in figure 7.4 and 7.5 193

7.2 Fitting parameters used in DLVO and EDL fits to the CP-AFM data in figure 7.9 and 7.10 205

8.1 Fitting parameters used in DLVO and EDL fits to the CP-AFM data in figure 7.9 and 7.10 239

Chapter 1

Thesis Overview

Liquid fabric enhancers are complex multi-component colloidal dispersions. These systems are based around an aqueous surfactant vesicle dispersion containing polymers, fragrances, and salts. Cationic surfactants are the active compound in liquid fabric enhancers as they are used to modify the fabric's surface properties. Fabrics, such as cotton, become negatively charged over their lifetime, caused by the deprotonation of hydroxyl groups on the cellulose fibres during repeated washing and drying cycles. When added towards the end of a wash cycle, cationic surfactant molecules adhere electrostatically to the surface of the fabric exposing a lipophilic functional group to the air resulting in reduced friction between the fibres. this gives the fabric a fabric a "softer" feel to the touch which is an effect desired by consumers. This lipophilic layer also helps to prevent staining as water based solutions are somewhat repelled, as well as reducing hydrogen bonding between strands which reduces wrinkling. The other components in a fabric conditioner are present to adjust the rheological properties, improve coating, or to enhance the customer experience. These additives add additional variables and interactions which are not present in a simple colloidal dispersion. This makes predicting and understanding the long term stability of these products difficult.

The surfactant of interest in this work is di(alkyliso-propyl ester) dimethyl ammonium methylsulfate (DIPEDMAMS), a cationic, double tailed surfactant, with a

quaternary ammonium head group and ester linkages to the aliphatic tails. It is a key component of some fabric conditioning systems. The aim of this work is to understand the behaviour and stability of aqueous DIPEDMAMS vesicle dispersions by investigating the interactions between the surfactant vesicles. This will be achieved by the direct measurement of the interactions between supported DIPEDMAMS bilayers.

Chapter 2 describes the theoretical background of the behaviour of surfactants and other amphiphiles in aqueous dispersions, the stability of colloidal and vesicle dispersions, and intermolecular interactions. The chapter then goes onto look at the previous work done on the direct interactions between surfaces and bilayers by SFA and the colloidal probe technique. Chapter 3 describes the techniques used in this study.

Chapter 4 focuses on understanding the aqueous self-assembly phase behaviour of the DIPEDMAMS/water system and the effect of temperature on the bulk structure. This is then compared with the structure of supported DIPEDMAMS bilayers on mica as studied by temperature controlled quantitative imaging atomic force microscopy (AFM). Chapter 5 moves onto the development of colloidal probe force techniques for the direct measurement of bilayer - bilayer interactions. It was necessary to reduce the gel to fluid transition temperature of the DIPEDMAMS/water system in order to fabricate complete surfactant bilayers at room temperature. The effect of several alkyl alcohols on the bulk structure, transition temperature, topography and nanomechanics of the supported bilayers was investigated. This lead to the formation of complete surfactant bilayers at room temperature which were suitable for colloidal probe force microscopy.

Chapter 6 investigates the impact of different electrolytes on the directly measured interactions between the supported DIPEDMAMS bilayers. This was supported by investigating the impact of the electrolyte on the structure and properties of the supported bilayers and the impact on the bulk lamellar structure. Finally the behaviour of the DIPEDMAMS vesicle dispersions with the addition of the different electrolytes was investigated to directly compare the measured interactions and the stability of the vesicle dispersions.

Chapter 7 looks at the impact of polymer and polyelectrolytes on the directly measured interactions between supported DIPEDMAMS bilayers. Investigating the impact of charged and uncharged polymers and the role of the molecular weight of the polymers. The interaction between these polymers and the supported bilayers is investigated to understand how the polymers and polyelectrolytes impact on the bilayers themselves as opposed to just mediating the interactions between them. The impact of these polymers and the impact of their molecular weight on DIPEDMAMS vesicle dispersion was investigated to directly compare the measured interactions and the stability of the vesicle dispersions.

Chapter 8 looks at the modification of the composition of the DIPEDMAMS bilayers themselves and its impact on the measured forces and the behaviour of the bulk vesicle dispersions. This is to explore the impact of the breakdown of the surfactant molecules into their constituent fatty acids. The impact on the interactions between the bilayers, the structure of the supported bilayer, and the bulk DIPEDMAMS/water with different fatty acids and increasing fatty acid content was investigated. Finally the behaviour of the bulk vesicles dispersions was compared with the directly measured bilayer-bilayer interactions.

Chapter 2

Theoretical Background

2.1 Amphiphiles: Lipids and Surfactants

2.1.1 Structure and Properties

An understanding of the amphiphilic nature of surfactants and the consequences of this is key to understanding the complex surfactant systems such as fabric enhancers. Amphiphiles are compounds which contain both a hydrophilic and a lipophilic moiety. [1] These include many classes of compounds including lipids, surfactants, proteins, and block co-polymers. They can be found as both natural products and as synthetic compounds. [2]

The lipophilic, literally meaning fat loving, moiety can also be also described as hydrophobic or non-polar. [1, 3] However the terms are not synonymous as some functional groups can be considered hydrophobic but not lipophilic, such as fluoroalkanes and siloxanes. [4] For most amphiphiles the lipophilic moiety is typically a long hydrocarbon chain. These chains are generally linear, but some branched chained amphiphiles do exist, the chains can be saturated or unsaturated, and typically have a chain length greater than four. [5]

The hydrophilic, or polar, functional groups generally fall into one of two categories. [6] Ionic groups, which can then be further subdivided into anionic and cationic, and uncharged or non-ionic groups. Anionic groups commonly found in amphiphiles include sulfates, carboxylates, and phosphates. [2] Phosphates being an important group and well studied area as they are the charged moiety found in the biologically important phospholipids. [7–10] Cationic systems are typically derived from ammonium ions and are particularly relevant in surfactant detergent systems, and zwitterionic systems where the hydrophilic group contains both a cationic and anionic functional group. Finally the uncharged category is primarily dominated by alcohols such as diglycerides and sugars found in biology and polyethylene glycols which typically are synthetic. [11] Examples of some of the types of amphiphiles discussed so far are shown in figure 2.1 with the hydrophilic and hydrophobic region highlighted.

2.1.2 Self-Assembly Behaviour

The contrasting natures of the hydrophilic and hydrophobic moieties lead to very different interactions between the two groups. In an aqueous environment these differing interactions between the solvent and the hydrophilic and hydrophobic moieties leads to the self-assembly of the amphiphiles into various structures. [12] This is driven by the tendency of the hydrophobic regions to avoid contact with water and prefer interacting with each other and for the tendency of the hydrophilic regions to remain in contact with the water. At sufficiently high amphiphile concentrations this leads to the formation of micelles, usually spherical structures with the hydrophobic tails pointing towards the centre with the hydrophilic groups facing outwards shielding the hydrophobic regions from the aqueous environment. [13] This minimises the interactions between the hydrophobic regions and the solvent and maximises the interactions between the hydrophilic regions and the water. At higher concentrations, amphiphiles can self-assemble into more complex lyotropic liquid crystalline phases. [14] These can range from simple phases such the micellar cubic formed by the close packing of micelles to complex bicontinuous cubic phases of interwoven bilayer channels. Self-assembly behaviour of amphiphiles also occurs

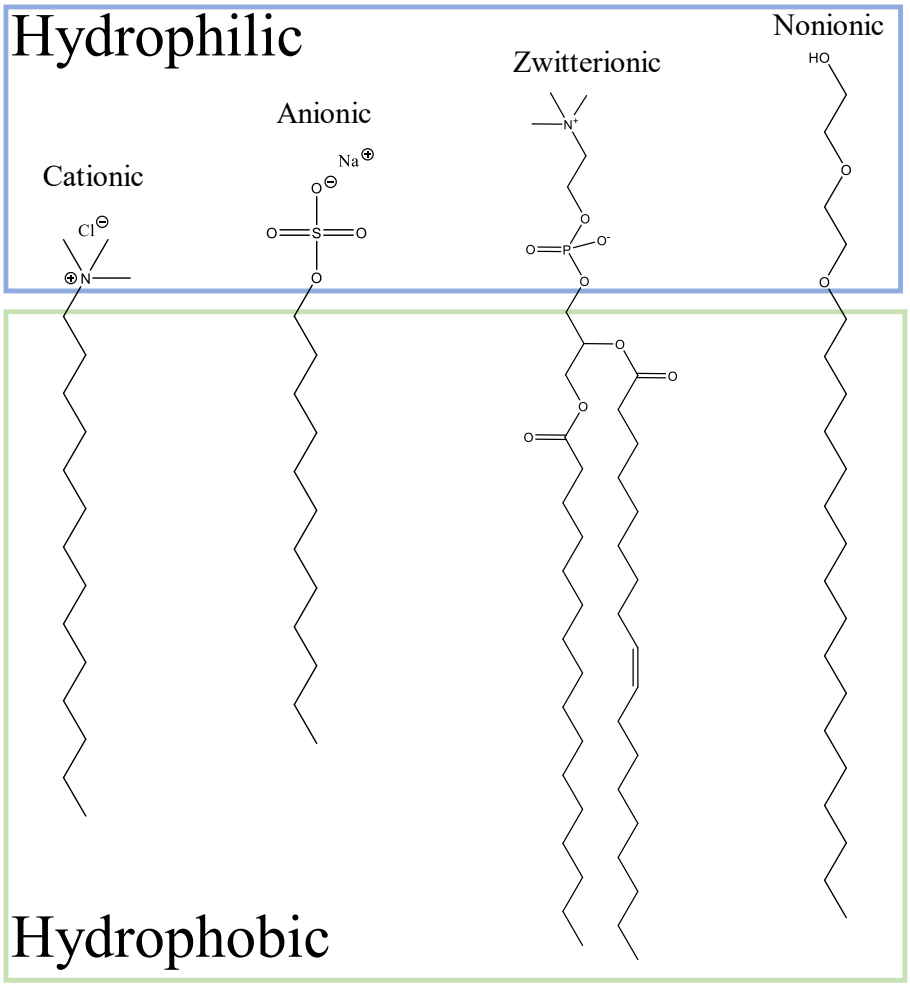


Figure 2.1: Examples of typical ionic, zwitterionic, and non-ionic amphiphiles highlighting the hydrophilic and hydrophobic regions of each molecule.

in other polar and non-polar solvents but will not be considered here as the systems of interest here are in aqueous environments. [15]

The main driver of this self-assembly behaviour is the tendency for the hydrophobic regions to avoid contact with water due to the hydrophobic effect. [16] The driving force behind the this interaction is mainly entropic in nature. Due to hydrogen bonding water forms a loose tetrahedral network. Hydrocarbon chains are not capable of hydrogen bonding, since they break up the bonding between water molecules. This results in the reoriented of the hydrogen bonds tangentially to the surface resulting in a more ordered structure resulting in a loss of entropy. This effect is minimised when the hydrocarbon chains aggregate together. In contrast to this attractive force between the hydrocarbon chains and their unfavourable interactions

with water the polar head groups prefer to remain in contact with the water and experience ionic or steric repulsions between each other. These contrasting forces between the hydrophilic and hydrophobic regions result in the formation of micelles or other more complex structures. [17]

At very low concentrations amphiphiles will sit at the air/water interface. Heads in the water, tails out, as this reduces the interactions between the hydrophobic parts and the water. [2, 5] As the concentration increases, the formation of micelles becomes energetically favourable. The CMC is then the concentration of the surfactant in the bulk at which micelles begin to form. [1] Further increasing the surfactant concentration increases the number of micelles present. Various variables are known to have an impact on the CMC. [18] The CMC of most ionic surfactants are practically independent of temperature but non-ioinc surfactants with ethylene glycol hydrophilic groups become less hydrophilic with increasing temperature resulting in a decrease in the CMC. [19, 20] This is caused by the oxyethylene groups becoming increasingly insoluble with increasing temperature. Increasing temperature in general does cause a small increase in the CMC of ionic surfactants due to increased thermal motion. Non-ioinc surfactants generally have a lower CMC than ionic surfactants as there are no electrostatic repulsion between the head groups of non-ionic surfactants compared with ionic. [21] The larger the head group charge on the ionic surfactants also results in a higher CMC due to increased electrostatic repulsion. An increase in the chain length of the hydrophobic chains results in a decreased CMC as micellisation is favoured. [22] However increasing the chain length above 16 carbon atoms does not yield significant further decreases to the CMC, most probably due to the coiling of the long hydrocarbon chains. [23] The addition of electrolytes can be used to lower the CMC for ionic surfactants but non-ionic surfactants are generally independent of salt concentration. [24]

2.1.3 The Packing Parameter

The packing properties of amphiphilic molecules depend on three parameters. The effective area of the head group a, the volume of the hydrocarbon chain or chains v, and the maximum effective length of the hydrocarbon chains l_c. This is known as

the critical chain length and represents the limit over which the hydrocarbon chains can not be stretched and remain fluid. This is of a similar order to, but less than, the fully extended chain length l_{max}. The following relationships can be used to define the length and volume of a linear hydrocarbon chain made up of n_C carbon atoms. [13]

$$l_c/\text{nm} = 0.154 + 0.127 n_C \tag{2.1}$$

$$V/\text{nm}^3 = (27.4 + 26.9 n_C) \text{ x } 10^{-3} \tag{2.2}$$

From the effective head group area, the critical chain length and the volume of the hydrocarbon chains the surfactant packing parameter or critical packing parameter N_s can be defined. [13]

$$N_s = \frac{V}{a l_c} \tag{2.3}$$

Figure 2.2 shows how the different interactions for the headgroup and hydrocarbon chains influence the critical packing parameter. [25] It suggests that different aggregates can be considered to be the result of the packing of cones, truncated cones, and cylinders. It is important to note that this is a limiting factor and that amphiphiles can assemble into structures that are more cylindrical than suggested, the head group area and the volume, a and v, remain constant but the chain length extension can be less than l_c. However they can not adopt more conical structures as the chain length can not be extended beyond l_c. [2]

2.1.4 Liquid Crystalline Phases

At high concentrations amphiphiles tend to self-assemble into more ordered liquid crystalline phases. Unlike thermotropic liquid crystals, pure materials which display

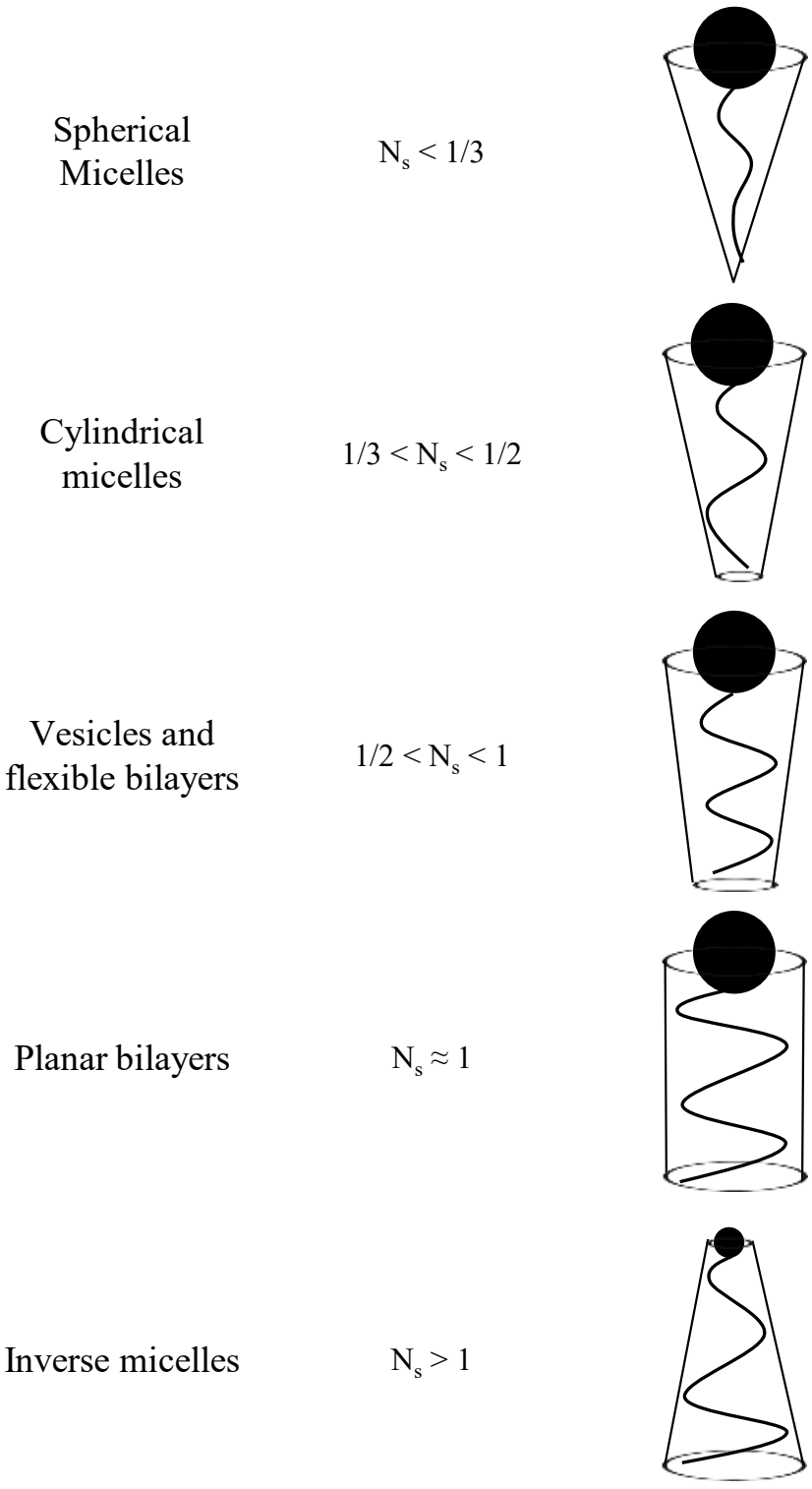


Figure 2.2: Surfactant packing parameters for different amphiphile shapes and the structures they typically adopt.

liquid crystalline properties within a well defined temperature range. [26] Lyotropic liquid crystals are formed by dissolving an amphiphilic compound in a suitable solvent, those formed in water are most widely studied and important. The liquid crystalline phase is dependent on the amphiphile concentration, and the system temperature and pressure. [27]

The liquid crystalline phase formed is dependent on the shape of the individual amphiphile molecules, as described above by the critical packing parameter model. Phases formed where the effective head group size, a, is larger than the lengths and volume of the hydrocarbon tails, v and l_c, are considered "normal" structures. When the effective head group size is much larger than the tails spherical micelles are formed. As the difference is reduced worm like or cylindrical micelles become energetically favourable. As the effective size of the two regions approach parity planer structures such as vesicles and bilayers are preferred. For some asymmetrical amphiphiles complex saddle splayed structures such as the bicontinuous cubic phase are observed. [28, 29] These normal structures are in contrast to inverse structures formed when the tails are larger than the head group and tend to be present in apolar media or at very high amphiphile concentrations. [30]

For a given amphiphile, variation in the amphiphile concentration induces changes in the curvature of the liquid crystal phase. [13] This is described in the critical packing model for a given amphiphile, by changes in the effective area of the head group a with increasing concentration. The effective head group area is governed by the hydrophobic forces which reduce the effective size and the tendency for the head groups to want to maximise their interaction with water increasing which increases the effective area. [17] It is the balance of these two forces which gives the optimal head group area a. In concentrated systems the interactions between the amphiphile aggregates also have an impact. The short range repulsive interactions between the aggregates as the concentration increases results in a decrease of the optimal head group area. [14]

As previously discussed, above the CMC micelles begin to form. This micellar dispersion is often denoted by the short hand L_1. As the concentration is increased the number of micelles increases. At higher concentration the micelles begin to fill

the space given resulting in the close cubic packing, mostly face centred, of the micelles. This is the micellar cubic phase and is often labelled I_1. [31,32] However it is more common for the shape of the micelles to change from spherical to cylindrical with increasing surfactant concentration due to changes in the amphiphile's packing parameter as the effective head group size, a, is decreased by the increasing concentration. [33] The cylindrical micelles, as the concentration increases, pack into a hexagonal structure usually denoted as H_1. [34] At even higher lamellar phases are formed L_α.

Figure 2.3 shows a theoretical phase diagram for an idealised amphiphile system with increasing concentration. In this ideal system the phase changes are driven only by changes in the inter-facial curvature of the amphiphile molecules brought about by the increasing concentration. The digram show the progression from L_1 to H_1 then to L_α, as previously discussed, as the concentration is increased. Intermediate phases are often observed between the L_1 to H_1 phases, region a in the diagram, and between H_1 then to L_α, region b in the diagram. The cubic packed micellar phase is often the intermediate phase observed in region a, between the micellar dispersion and the hexagonal phase. Region b often contains more complex structures such as the bicontinuous cubic phase, between the hexagonal and lamellar phases. The shaded areas in the diagram are biphasic regions where more than one liquid crystal phases are co-existent. [2,5,35]

At sufficiently high amphiphile concentrations, where the amphiphile is the major phase, inverse structures can be formed. Increasing the concentration from the lamellar phase, the most widely observed inverse phase observed is the inverse hexagonal phase, H_{II}. [36, 37] Composed of cylindrical water channels within an amphiphile matrix. Further increases in the concentration may result in the inverse micellar phase, L_2. [38,39] Between the inverse phases, as with the normal phases, intermediate phases are observed. Mirroring those at lower concentrations these are commonly inverse bicontinuous phases and inverse micellar cubic phases.

This theoretical phase diagram, for an idealised amphiphile, is hardly ever observed in its entirely as shown here. [5] Inverse phases may not be formed for all systems, intermediate phases are not always observed, and temperature has not

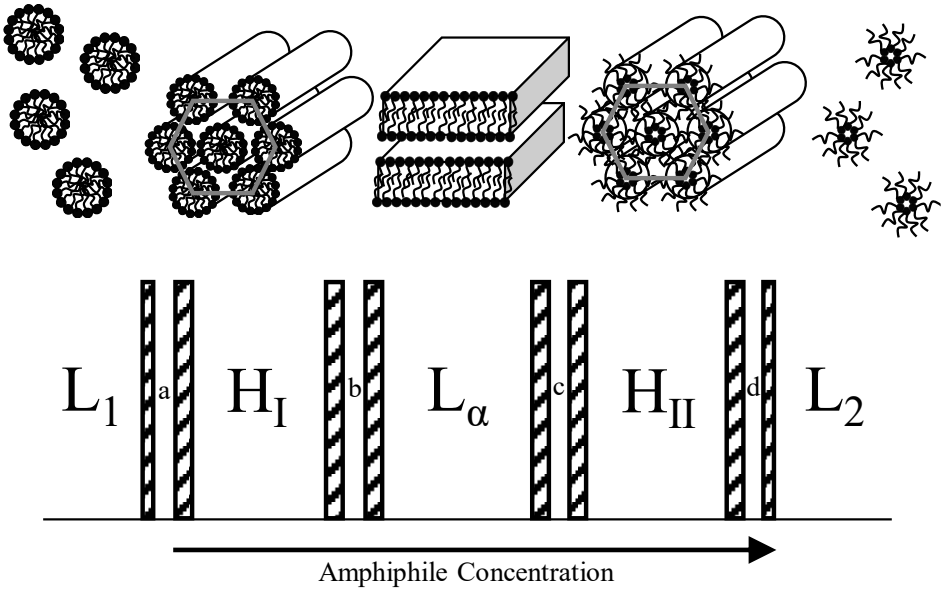


Figure 2.3: A hypothetical phase diagram showing the impact of increasing surfactant concentration on a binary amphiphile/water system where the transitions are controlled by the solvent content alone. [5]

been considered. It is however useful for understanding the dependence of the phase structure on concentration and how different structures are stable at different concentrations. The generalised sequence discussed here is a good approximation to the phase behaviour of many ionic surfactants. Non-ionic surfactants display more complex phase behaviour due the polyethyleneoxide hydrophilic groups being more effected by temperature and concentration than their ionic counterparts.

2.1.5 Lamellar phases

The lamellar phases are some of the most important types of aggregates formed by amphiphiles. The lamellar phases consist of amphiphile bilayers separated by a layer of the solvent, water being the most widely studied. The amphiphiles are oriented so that the hydrophilic head groups are on the outside of the bilayers to maximise their interactions with the water and the hydrophilic tails are sequestered inside the bilayers to minimise hydrophobic interactions. These phases have a low interfacial curvature, as such they are typically formed from amphiphiles where the crossectional area of the head group and the hydrocarbon tails are similar. Double

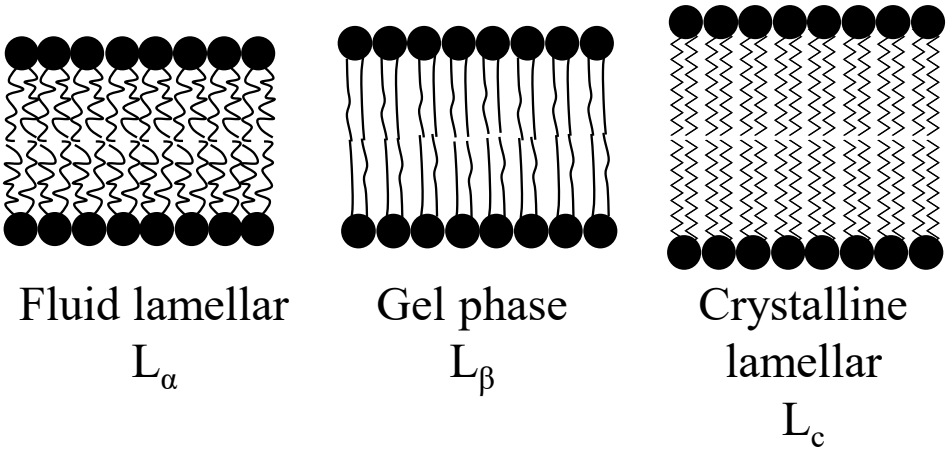


Figure 2.4: Diagram showing the typical bilayer structures of the most common lamellar phases.

chained surfactants and lipids are most likely to form lamellar phases. Many double chained lipids and surfactants tend to form lamellar phases directly from increasing the concentration above the CMC. Lamellar phases can be formed by single chained surfactants and lipids but generally at much higher concentrations and tend to form cylindrical micelles and hexagonal phases first.

Lamellar phases can exist in a crystalline, gel, or fluid phase depending on the temperature and composition of the system, a diagram of these different phases is shown in figure 2.4. [40] At low temperatures lamellar systems adopt a crystalline phase L_c where the amphiphile molecules have no rotational nor positional freedom. As the temperature is increased the molecules first gain rotational freedom, the lamellar gel phase L_β. On further increase the bilayers become completely fluidised and the amphiphiles have both rational and translational freedom as they are able to diffuse within the plane of the bilayer. [41] The temperature at which the bilayers transition to the fluid state is typically known as the transition temperature or the chain melting temperature and is denoted by T_c.

The lamellar phase behaviour is primarily governed by the strength of the van der Waals interactions between the aliphatic tails and the extent to which the amphiphiles are packed together in the bilayers. [42] Longer hydrocarbon chains have a greater area over which to interact with one another which increases the strength of the van der Waals interactions between the tails increasing the packing of the

bilayer. This leads to an increase in the transition temperature. [43] Conversely shorter tailed systems will lead to a decrease in the transition temperature. Unsaturation within the hydrophobic tails can also reduce the transition temperature. [44] The double bond results in a kink in the hydrocarbon chain which causes a disruption in the packing of the amphiphiles within the bilayer due to steric effects. [45] Branched hydrocarbon chains can have a similar impact on the transition temperature to alkenes as they cause disruption of the packing due to steric interactions. The impact of unsaturation and branching on the bilayer fluidity is also dependent on the position of the group in the hydrocarbon chain. Those near the middle of the chain have a greater impact than those located near the ends of the alkane. [46]

The bilayer structures, like those found in the lamellar phases, have been widely studied due to their biological relevance. [47, 48] The cell membrane is a lamellar bilayer formed of various phospholipids and other biological amphiphiles such as cholesterol. [49–51] Numerous studies have been conducting investigating the impact of different lipid composition on the properties of these lipid bilayers. [52] In these complex lipid systems, were at a given temperature one component is predicted to be in the gel phase and another would be in the fluid phase, the two can separate. This leads to the two phases coexisting in spatially separated regions. [53–56] Other systems however show a homogenous bilayer with the transition temperature of the system being impacted by all components. [57–59]

2.1.6 Vesicles

Vesicles are hollow amphiphile aggregates formed from one or more bilayers that have been curved round on themselves to form a sphere, as opposed to the infinite planar bilayers of the true lamellar phase, encapsulating part of the aqueous phase. [60] Vesicles are generally categorised either by their size or structure. Vesicles can vary in size from tens of nanometres, termed nano-vesicles, to giant vesicles which can be tens of micrometers in diameter. [59] There are three main structures of vesicles. Uni-lamellar vesicles, which are formed from a single amphiphile bilayer. Multi-lamellar, or onion, vesicles where the wall of the vesicle is formed of several bilayers, a lamellar phase formed into a sphere. [61] The third type are multi-vesicle vesicles

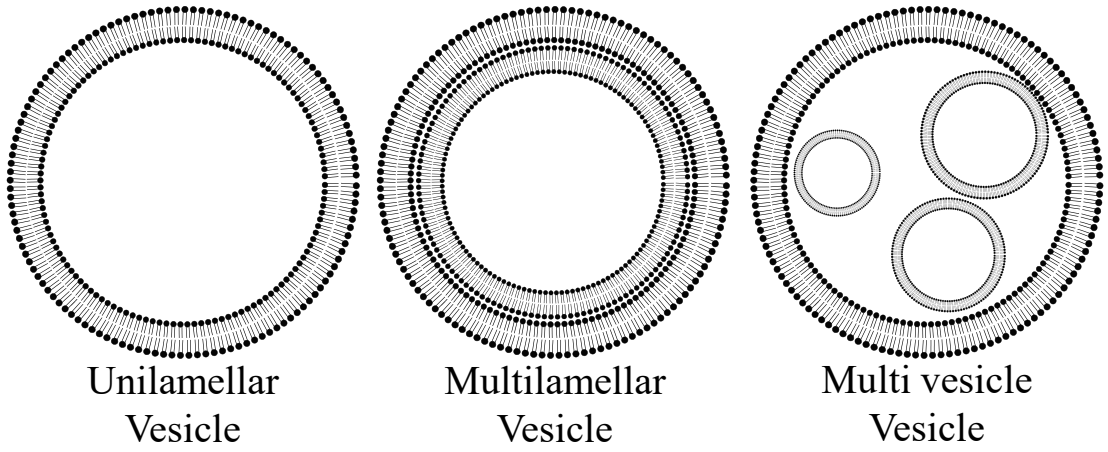


Figure 2.5: The main types of surfactant vesicles.

which contain several smaller vesicles within a larger vesicle. [62] These different structures are shown in figure 2.5.

Vesicles are not usually formed spontaneously like other self-assembled amphiphile structures already discussed without some form of shearing or agitation of the system, although there are some system where this has been observed. [63–65] Vesicles are usually formed from lamellar dispersions. The most common method is by sonication of dilute lamellar phases, where the ultrasound waves break up the lamellar sheets causing them to reform as vesicles. [66] This method generally forms small vesicles with a fairly broad size distribution. Other methods include droplet formation for large unilamellar vesicles, electroformation, and extrusion. These methods are more commonly used to form more monodispersion vesicles for the study of biological systems. [63] In the homecare industry vesicles are generally formed by applying a steady shear to a lamellar phase. [67] This method generally forms multilamellar vesicles with a narrow size distribution. The vesicle size can be controlled by varying the shear rate.

Vesicles have been widely studied due to their use in cosmetic and homecare products and are of particular interest in the biological communities. Vesicles formed of lipids are often referred to a liposomes. The formation, transport, and fusion of vesicles are believed to play a vital role in biological and physiological processes such as mitosis, cell fusion, transport, and cell signalling. [68] Liposomes are often used as simple cell models and bottom up biochemistry as they mimic the cell membrane

but without the added functionality of membrane proteins and polysaccharides. Liposomes are of interest as a technology for drug delivery. [69,70] They are capable of encapsulating a potential drug candidate and carrying the pharmaceutically active compound to the target organ or area whilst minimising release in untargeted areas. Another area where liposomes or vesicles are of interest are in liquid fabric enhancers and detergents as the surfactants in these products exist as vesicles.

Vesicle systems, similar to micellar solutions, have no long range order. The vesicles are considered to be suspended in the aqueous phase and are described as vesicle dispersions as opposed to solutions. If the vesicles, or liposomes, within a dispersion begin to aggregate, or break down, this could have a significant impact on the physical properties of the system, reduce the efficacy of a drug delivery system, or make a commercial product undesirable to consumers. It could even lead to phase separation of the vesicle dispersion.

Surfactant vesicle dispersions, such as those used in liquid fabric enhancers, can be viewed in the same manner as colloidal dispersions. Therefore understanding the properties of colloids, their stability, and the factors that effect their properties and stabilities are important in understanding vesicle dispersions.

2.2 Colloids and colloidal stability

A colloid is a microscopically heterogeneous system where one component has dimensions on the order of nanometres to micrometres and is dispersed within another phase. [71] In contrast to a solution, where the solute and solvent are considered to be one phase, a colloidal system consists of a dispersed phase suspended within a continuous phase, or dispersion medium. The terminology for colloidal systems can sometimes be ambiguous with the term colloid being used to refer to both the dispersed phase or to the entire system. [72] To avoid confusion the entire system will be referred to as a colloidal dispersion or system whilst the dispersed phase will be referred to as colloidal particles.

There are many different types of colloidal systems but they are most usefully defined by the state of mater of the dispersed phase and the dispersion medium, see table 2.2.

Table 2.1: Types of colloidal dispersions

Medium/phase		**Dispersed Phase**		
		Solid	**Liquid**	**Gas**
Dispersion medium	**Solid**	Solid suspension	Gel	Solid Foam
	Liquid	Colloidal dispersion	Emulsion	Foam
	Gas	Solid aerosol	Liquid aerosol	N/A

The main focus here will be on solid-liquid and liquid-liquid colloidal systems. These system can generally be viewed as small particles or colloidal spheres suspended within the liquid phase. Micellar solutions, vesicle and liposome dispersion fall into this category.

The particles in a colloidal dispersion under go Brownian motion, the colloidal particles are under random motion due to collisions with fast moving molecules with in the fluid. [73] When two colloidal particles encounter one another it is the balance of the repulsive and attractive forces between them that dictate their behaviour and hence the behaviour of the entire dispersion. If the repulsive interactions are sufficiently strong to balance any attractive interactions then the two particles will experience an over all repulsive interaction and they will move apart. The dispersion would be considered stable. [74] However, if the attractive interactions are comparably strong enough to overcome any repulsive interactions then the two particles will attract one another. This would lead to the aggregation of the particles and the colloidal dispersion would be considered unstable. [75]

If the aggregation process is reversible the process of aggregation is generally termed flocculation. [6] Loose associations of colloidal particles are formed, called flocs, which stay suspended with in the dispersion media. [76] An equilibrium is generally formed between the flocs and the free colloidal particles. [77] If the aggregation process is irreversible the aggregation process is generally referred to as coagulation. Unlike flocs coagulated aggregates separate out from the dispersion media. If the aggregates are denser than the dispersion media they separate by sedimentation, and if the aggregates are less dense than the dispersion media they

separate via creaming.

The stability of a colloidal dispersion is determined by the interactions between the colloidal particles. Due to the small size of colloidal particles, the surface to volume ratio of colloids is very large. Therefore in order to begin to understand the stability of colloidal dispersions, such as surfactant vesicle dispersions, one needs to explore and understand the intermolecular forces, surface forces, and surface chemistry between the colloidal particles.

2.3 Intermolecular Forces

2.3.1 Van der Waals Forces

The van der Waals forces are attractive interactions between uncharged atoms or molecules. [35, 78] They arise primarily from the interactions between dipoles. A dipole moment arises when two opposite charges of magnitude q are separated by a distance of r. The magnitude of the dipole moment μ can be expressed as follows: [79]

$$\mu = qr \tag{2.4}$$

Some molecules contain permanent dipoles which arise when two adjacent atoms have significantly different electronegativities. [80] This is a measure of the tendency of an atom to attract electrons, or electron density, towards itself, conversely electropositivity is a measure of an atom's ability to donate electrons. [81, 82] When two adjacent atoms have significantly different electronegativities the electron density will be concentrated towards the more electronegative species, resulting in it becoming more negatively charged whilst the less electronegative species becomes more positivity charged. This creates a permanent dipole moment. A good example of a molecule that contains a permanent dipole is water, where the electronegativity of the oxygen atom results in it becoming more negatively charged than the

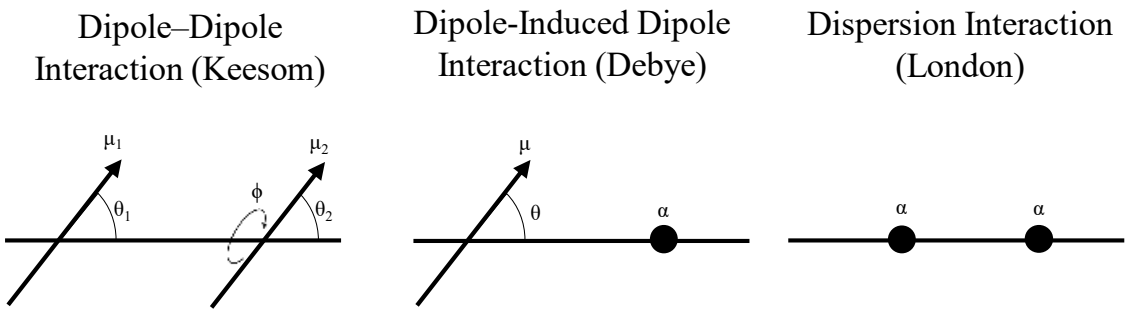


Figure 2.6: Diagram showing the three main components of the van der Waals forces: permanent dipole - dipole interactions; permanent dipole - induced dipole interactions; and the instantaneous dipole - induced dipole forces. Orientation dependant variables are illustrated for each interaction.

hydrogen atoms. [83]

The van der Waals forces can be divided into three different interactions: permanent - permanent dipole interactions, permanent - induced dipole interactions, and instantaneous dipole - induced dipole interactions. [84]

The first to be considered are the attractive interactions between two permanent dipoles. For two permanent dipoles with dipole moments of μ_1 and μ_2 separated by distance r the interaction energy V can be given by equation 2.5. Where ε_0 is the permittivity of free space ε_r is the dielectric constant of the surrounding media and θ_1 θ_2 and ϕ describe the orientation of the two dipoles, as shown in figure 2.6. [85]

$$V = -\frac{\mu_1\mu_2}{4\pi\varepsilon_0\varepsilon_r r^3}[2\cos\theta_1\cos\theta_2 - \sin\theta_1\sin\theta_2\cos\phi] \tag{2.5}$$

From equation 2.5 it is noted that the interactions between two permanent dipoles is dependent on their orientation. The largest attraction occurs when the the two dipole are in line with each other whilst the minimum interaction occurs when the two dipoles are oriented parallel to each other. This equation is only valid where $r > 3l$, where l is the length of the dipole. Below this separation it would be necessary to view the interactions as interactions between individual charges.

Averaging the interactions over all angles and orientations leads to equation 2.6 for the interactions between two freely rotating permanent dipoles, where k_B is

the Boltzman constant and T is the temperature in kelvin. [35, 86] The rotation averaged interactions between two permanent dipoles is often referred to as the Keesom interaction. [87]

$$V = -\frac{\mu_1^2 \mu_2^2}{3(4\pi\varepsilon_0\varepsilon_r)^2 k_B T r^6} \tag{2.6}$$

Note that with freely rotating dipoles the interactions are inversely dependent on the temperature of the system this is due to the dipoles rotating less freely at lower temperatures. The interaction energy for freely rotating permanent dipoles is dependent on the inverse sixth power of the separation between the dipoles, compared with the inverse third power dependency for two fixed dipoles. This suggests that the permanent - permanent dipole interactions are very short range.

The second of the van der Waals interactions to be considered is the attractive interaction due to the interactions between a permanent dipole and non-polar molecules. [84] This involves the induction of a dipole moment in a non-polar molecule by an external electric field, in this case a field emanating from a near by permanent dipole. The polarisability α of a molecule is a measure of the strength of an induced dipole moment μ_{ind} the molecule can develop in the presence of an electric field E. [88, 89] All molecules are polarisable to some degree.

$$\mu_{ind} = \alpha E \tag{2.7}$$

The induced dipoles arise from the displacement of the non-polar molecule's electron cloud relative to the nucleus. Different functional groups have different polarisabilities with those with more delocalised electrons generally being more polarisable. [88] The overall polarisability of a molecule can be estimated by the summation of the polarisabilities of its different functional groups. [90]

At a fixed angle the interaction energies between a permanent dipole and a polar molecule with an induced dipole is given by equation 2.8, where μ is the permanent dipole moment and α is the polarisability of the non-polar molecule. [91]

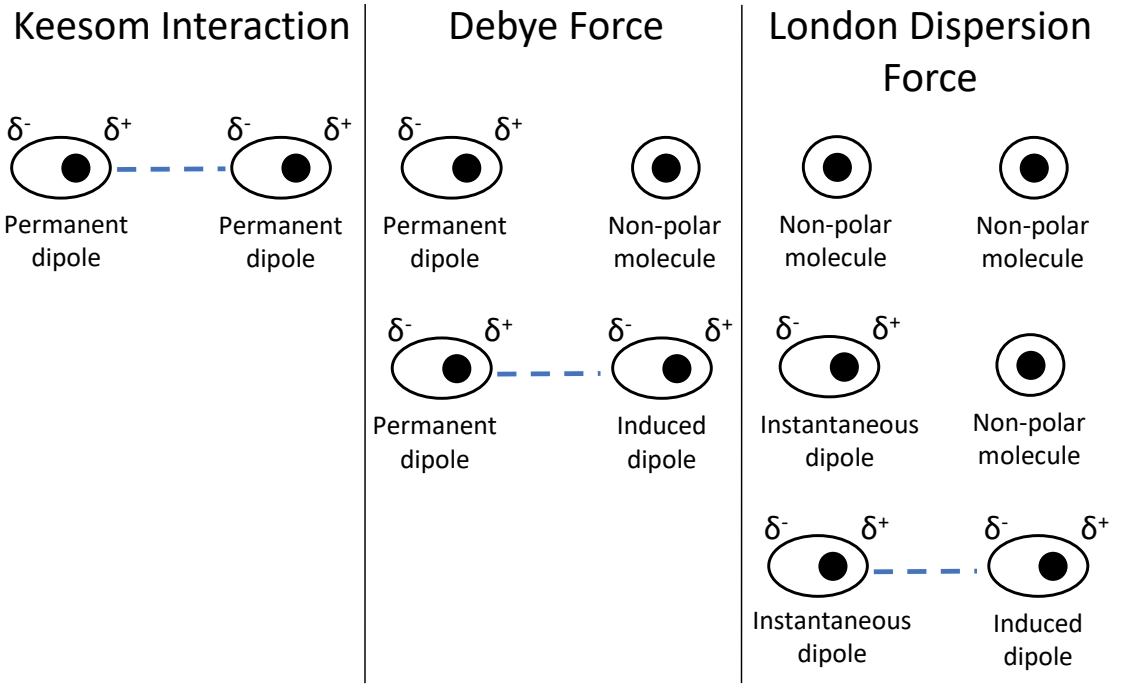


Figure 2.7: Diagram describing the three main components of the van der Waals forces: the Keesom interaction, the Debye Force, and the London dispersion force.

$$V = -\frac{\mu^2\alpha(1+3\cos^2\theta)}{2(4\pi\varepsilon_0\varepsilon_r)^2 r^6} \tag{2.8}$$

The strength of this interaction is not usually sufficient to cause the permanent orientation of the dipole and the induced dipole. Therefore the angle averaged interaction between a free spinning permanent dipole and a non-polar molecule is given by equation 2.9. [35]

$$V = -\frac{\mu^2\alpha}{(4\pi\varepsilon_0\varepsilon_r)^2 r^6} \tag{2.9}$$

This is often known as the Debye interaction, or induction interaction. Again the interaction energy is dependent on the inverse sixth power of the separation between the molecules as with the two freely rotating permanent dipoles. The induction interactions are considerably weaker than the permanent - permanent dipole interactions.

The final and most significant component of the van der Waals forces are the instantaneous dipole - induced dipole interactions. These are also known as the London or dispersion forces. [92, 93] The are quantum mechanical in nature and are the result of random fluctuation in the electron cloud of any given molecule. For a non-polar molecule the time averaged dipole moment is zero, however at any given instant in time due to the random fluctuation with its electron cloud a dipole moment can exist due to the position of the electrons and the nucleus. This instantaneous dipole produces an electric field, as any other dipole, which in turn induces a dipole moment in a nearby non-polar molecule. The resultant interaction between the two dipoles results in an attractive force, as discussed above. The London dispersion forces are typically larger for atoms with larger electron clouds and molecules that have a higher polarisability. [94, 95] The significance of the London dispersion forces is that as all molecules and atoms are to some extent polarisable, these interaction are found between all atoms and molecules. In contrast to the Keesom or Debye interactions which require a permanent dipole and explains why noble gases liquefy at low temperature.

The dispersion interaction between two identical atoms or molecules is shown in equation 2.10, where E_i is the first ionisation potential.

$$V = -\frac{C_{disp}}{r^6} = -\frac{3}{4}\frac{\alpha^2 E_i}{(4\pi\varepsilon_0\varepsilon_r)^2 r^6} \tag{2.10}$$

It is noted from equation 2.10 that the interaction energy is dependent on the inverse sixth power of the separation between the molecules. This is the same distance dependency as seen for the other two dipole interaction, the Keesom and Debye forces. Whilst the London forces are the weakest of the three interactions that constitute the van der Waals forces they are considered to be the most significant as they are present between all materials. [96]

The van der Waals interactions between macroscopic bodies, e.g. colloids, vesicles, bilayers, is often understood in terms of Hamaker's work. [97] This involves the integration of the van der Waals interactions between all the atoms of the system.

$$V_{VdW} = -\frac{AR_1R_2}{6(R_1 + R_2)r} \tag{2.11}$$

The model for two spherical particles is shown in equation 2.11, where R_1 and R_2 are the radii of the two spheres and A is the Hamaker constant as defined in equation 2.12, where ρ_1 and ρ_2 are the number densities of the two particles and C is the coefficient of particle–particle pair interaction. [35, 98]

$$A = \pi^2 C \rho_1 \rho_2 \tag{2.12}$$

Note from equation 2.11 that the interactions are now much longer range than between two atoms. They are dependent on the inverse of the separation between the particles as opposed to the inverse sixth power as observed between individual molecules. Whilst the Hamaker approach is generally good for describing the van der Waals interactions between individual particles, it assumes pairwise additivity with multi-molecule particles. It assumes that each pair of molecules interact independently of their environment. [99, 100] The Lifshitz theory was developed to describe the Van der Waal's interactions between macromolecules taking into account the dielectric properties of this intervening medium and the influence of neighbouring molecules on the interactions between each pair of particles in the two particles. [101, 102]

2.3.2 Electrical Double Layer Forces

Electric double layer forces arise from the interactions between charged objects, such as cationic surfactant bilayers, in a liquid environment, most commonly water or an electrolyte solution. It is the result of the interactions between two electrical double layers. [35]

Electrical double layers are structures that form at the surface of a charged object immersed in a liquid environment. The surface charge can arise from the

dissociation of surface groups, e.g. -OH to -O^- + H^+, the adsorption or binding of ions from the liquid phase, or inherently ionic surface groups. [103] The double layer refers to the ordering of ions attracted to the charged surface by Coulombic interactions. These ordered layers screen the surface charge. Several models of the electrical double layer have been proposed and built upon over time.

One of the first models of the double layer was proposed by Helmholtz who studied electrodes, charged surfaces, in electrolyte solutions. [104] He suggested that the charged electrode immersed in an electrolyte solution repels like charged ions whilst attracting counterions towards the charged surface. The interactions at he electrode are considered to be purely electrostatic in nature and no electron transfer interaction occur. This leads to a tightly bound layer of counterions, the Helmholtz layer, the drop in charge and a potential is confined to this region.

Whilst the Helmoholtz model provided a basis for the understanding of the behaviour of ions in this region it does not account for many factors, such as diffusion within the liquid phase. The Gouy-Chapman model, also looked at electrodes, observed that the capacitance was dependent on the applied potential and the electrolyte concentration, which could not be understood by the previous model. [105] The Gouy-Chapman model describes the double layer as a charged surface surrounded by a diffuse layer of mobile ions. The concentration of counterions is enriched in the diffuse layer and decreases with increasing distance from the charged surface until the concentration is identical to the bulk electrolyte concentration. This leads to the electrical charge and potential to decrease exponential from the charged surface. [106]

The Stern model combines both the Gouy-Chapman and the Helmholtz models. It allows some ions to adhere to the charged surface, similar to that suggested by Helmholtz, now called the Stern layer, followed by a diffuse layer as suggested by the Gouy-Chapman model. This leads to an initial fall in the surface charge or potential across the Stern layer followed by an exponential decrease across the diffuse layer. [107] An illustration of the double layer structure for all three models discussed is shown in figure 2.8.

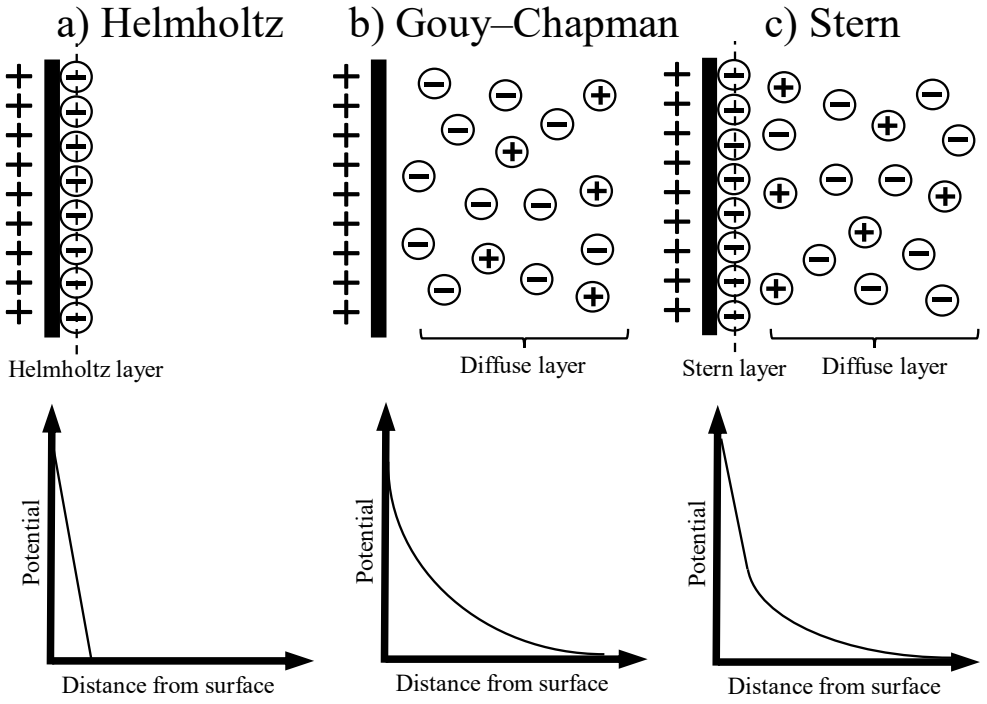


Figure 2.8: Diagram showing the different double layer models with sketches of how the potential changes with distance from the surface.

The thickness of the diffuse layer is known as the Debye length, κ^{-1}. The Debye length is typically tens of nanometers in length and decreases with increasing electrolyte concentration. [108] Equation 2.13, where k_B is the Boltzman constant, N_A is Avogadro's number, and I is the electrolyte concentration in $mole/m^3$, can be used to calculate the Debye length. [109]

$$\kappa = \sqrt{\frac{2e^2 N_A I}{\epsilon_0 \epsilon_r k_B T}} \tag{2.13}$$

When two like charged surfaces approach one another in a liquid environment a repulsive force is exerted between the two surfaces. [110] However the origin of this interaction is not Coulombic nor electrostatic in nature. The origin of the repulsive interaction between two charged surfaces in an electrolyte solution is entropic, also termed osmotic, in nature. [111] On bringing the two surfaces together the diffuse layers overlap. This creates a localised increase in ion concentration resulting in an osmotic repulsion. [112]

The EDL interactions between two charged planar surfaces in an electrolyte solution can be described by equation 2.14, where n is the bulk electrolyte concentration in $mol.m^{-3}$, k_B is the Boltzmann constant, γ is the reduced surface potential given by $\gamma = \tanh(ze\psi_0/4k_BT)$. Where e is the elementary charge, z is the valence, and ψ_0 is the surface potential. [35]

$$V_{edl} = \frac{64nk_BT\gamma^2}{\kappa} \exp^{-\kappa r} \tag{2.14}$$

Note that the interaction energy is dependent on the negative exponential of the separation between the molecules. This means that the interactions between the charged plates decreases exponentially with increasing separation.

2.3.3 DLVO Theory

The Derjaguin–Landau–Verwey–Overbeek (DLVO) theory is often used to explain the interactions between particles in an aqueous dispersion. It generally describes the total interactions between two charged surfaces in an electrolyte solution. It was developed independently by Derjaguin and Landau in 1941, and Verwey and Overbeek in 1948. [113, 114] The theory was developed to describe the stability or instability of colloidal dispersions and combines the effect of the attractive van der Waals forces and the repulsive electric double layer interactions.

The DLVO interactions between two particles, or two surfaces, can be expressed by equation 2.15.

$$W_{DLVO} = W_{vdw} + W_{edl} \tag{2.15}$$

The van der Waals forces for the interaction between two given particles or surfaces can generally be considered fixed, they are not significantly impacted by changes in the electrolyte concentration or pH. [115] At short distances the van der

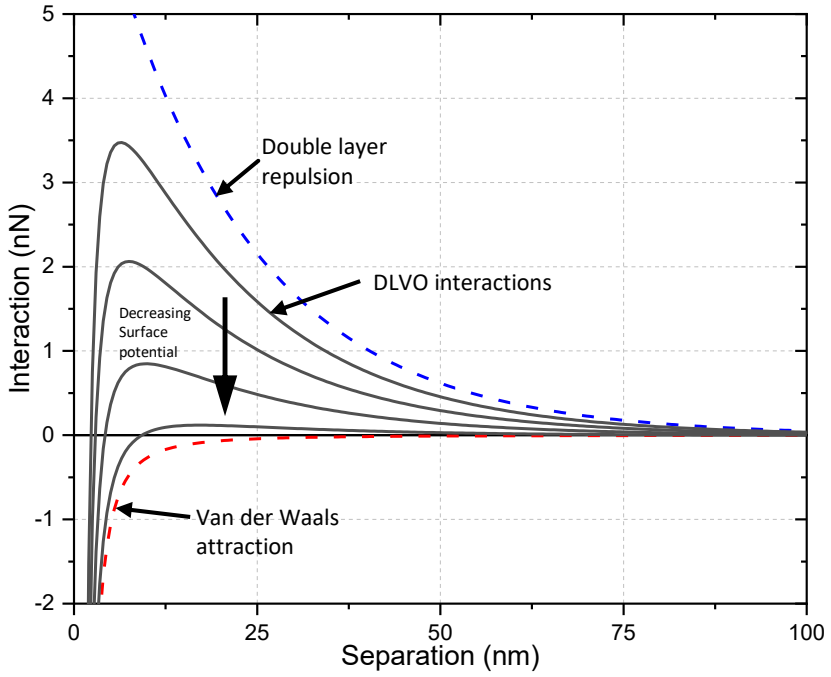


Figure 2.9: The theoretical DLVO interactions showing the impact of deceasing surface potential on the model interactions.

Waals interactions will dominate the repulsive double layer interactions due to the the difference in dependencies of the two interactions on the separation. From the relationships $W_{WdV} \propto -1/r$ and $W_{EDL} \propto e^{-r}$ it can be seen that the double layer interactions rise more slowly as $r \to 0$ compared with corresponding decrease in the van der Waals interactions.

Figure 2.9 show a schematic of how the double layer and van der Waals interactions between two similarly charged particles in a monovalent electrolyte solution combine to give the DLVO interactions. The figure shows the interactions for particles or surfaces with different surface charges. For highly charged particle or surfaces in low electrolyte concentrations the DLVO theory predicts a strong long range repulsion with a clear peak at short separation after which a strong attractive force is observed. In terms of dispersion stability, this peak can be seen as an energy barrier that needs to be overcome to bring the surfaces or particles into contact, often called the primary minimum. [35] If the particles in the dispersion do not have enough energy to overcome the repulsive peak they will be repelled from each other and the dispersion is considered to be stable. [116]

For systems with a smaller surface charge, or in more concentrated electrolyte solutions the van der Waals interactions are relativity constant but the range of the double layer forces is decreased. This can result in a secondary minimum before the repulsive peak. This could result in the particle in a dispersion sitting in the secondary minimum. For particles with a low surface charge or in high electrolyte solutions the van der Waals forces will be more dominant and the repulsive peak much lower potentially allowing the particles to overcome it and come into contact. This would result in the aggregation and flocculation of the dispersion. As the surface charge approaches zero, or in very high electrolyte concentrations, the double layer forces are negligible and the interaction become purely van der Waals resulting in an attraction between the particles at all separations.

DLVO theory is good for predicting the stability of simple charged and neutral colloids suspended in a simple solvent or electrolyte. It is able to predict the effect of ionic concentration on the stability of systems, increased ionic concentration decreases Debye length which decreases the electrostatic interactions which means that the attractive van der Waals' forces dominate the equation leading to the destabilisation of the colloidal system. The theory can also explain and predict the effect of the surface charge on the colloid particles, which increases the electrostatic repulsion and the effect of the size of the colloids. However, the theory begins to break down at short distances as it does not take into account short range interactions such as hydration forces, which add a short ranged repulsion between the colloids due the adsorption of water molecules, or the deformability of colloids such as vesicles, where the flattening of vesicles at contact can increase the van der Waals interactions adding an extra destabilising factor to the system. [117, 118] Additives to the liquid phase, such as polymers, add additional forces which cannot be predicted by DLVO theory these include steric interactions and depletion forces.

2.3.4 Born Repulsion

At very small separations a strong repulsive interaction is observed for all atoms, molecules and particles. [119] This repulsion is due to the overlap of the atom's electron clouds and ultimately determines how close two atoms or molecules can

approach one another. This is often called steric repulsion or Born repulsion. [5] These interactions are very short range and the repulsion increases extremely rapidly as the separation between the two molecules or atoms is decreased. [120]

The steric interaction is quantum mechanical in nature and there are no general equations for understanding the distance dependence of the interaction. However there are some equations used to try to describe the interactions. The most common is the hard sphere potential which considers atoms to be hard, incompressible, impenetrable spheres, where the radius of the spheres is set at the atomic radii of the atom or molecule of interest. [121]

The hard sphere potential is often described by equation 2.16, where σ is the hard sphere diameter.

$$V = +(\sigma/r)^n \quad \text{where } n \to \infty \tag{2.16}$$

This expression describes the hard sphere model well. Where $r > \sigma$ the interaction is zero and where $r < \sigma$ the interaction becomes infinite.

Another model often used to describe the relationship between steric interactions and separation is the exponential potential. This is described by equation 2.17, where c is an adjustable constant.

$$V = +ce^{-r/\sigma} \tag{2.17}$$

This expression is potentially a more realistic description of the steric interactions as it allows for the finite compression of atoms or molecules. However, whilst there is some theoretical justification, these expression are used more for their convenience in describing the forces rather than being based on empirical observations. [5]

The steric interaction is combined with the van der Waals to give the Lennard-Jones potential. This is a simple mathematical model which is often used to describe

the interactions between a pair of uncharged atoms or molecules, in this case $n = 12$.

2.3.5 The Hydrophobic interaction

The hydrophobic interaction describes the strong attractive interaction between hydrophobic molecules and surfaces in water which are stronger than their interactions in air or vacuum. The interactions between hydrophobic, non-polar, molecules are expected to be dominated by the van der Waals interactions, however these interaction are expected to be reduced in water not enhanced, as discussed in section 2.3.1. The hydrophobic interaction is considered to arises from the implication of the hydrophobic effect. [118, 122]

The hydrophobic effect describes the interaction between water and non-polar molecules such as alkanes. Water molecules have a strong desire to form hydrogen bonds between each other forming a loose tetrahedral structure. Hydrophobic molecules however are not capable of forming hydrogen bonds, so when water comes into contact with such a molecule therefore in order to disrupt the fewest hydrogen bonds the water molecules must reorient around the non-polar solute. If the hydrophobic molecule is not too large it is possible for the water molecules to pack around it in a manner that does not give up any of the hydrogen bonds. However for larger molecules this may necessitate the bending of the hydrogen bonds away from their normal configuration.

Whilst the interaction between water molecules and hydrophobic molecules in itself are not unfavourable. The interactions are generally attractive due to Debye interactions between polar and non-polar molecules and the ubiquitous London dispersion interactions. The rearrangement of the water molecules around them, to maximise hydrogen bonding, creates a more ordered structure compared with the bulk water phase. This is entropically unfavourable and is what lies behind the observation that non-polar molecules are only sparingly soluble in water.

Considering two hydrophobic molecules approaching one another in water it can be understood from the hydrophobic effect why their aggregation would be entrop-

ically favourable. Combining the two molecules would reduce the overall area that is in contact with water therefore reducing the number of water molecules needed to form more ordered structures around the molecules. However this combining of polar molecules may lead to the formation of larger aggregates and to more structured systems, such as the various ordered and liquid crystalline surfactant phases discussed in section 2.1. The formation of an ordered structure is also entropically unfavourable, however the energy cost in forming these ordered structures is less than that required to "solvate" each hydrophobic molecule.

Whilst some attempts have been made to measure and propose equations to describe the hydrophobic interactions, with some suggesting the range of this interaction to be up to seven times greater than that of the van der Waals interactions alone. The exact mechanism for this attractive interaction is still not well understood. [123, 124]

2.3.6 Hydrophilic Interactions

In comparison with the hydrophobic interactions are the interactions between hydrophilic molecules in water, their impact on the water structure and how that relates to the observed interactions. Whilst there are no hydrophobic interactions per se, it is important to understand why some molecules, hydrophilic, are water soluble and appear to strongly repel each other in water whilst others, hydrophobic, are practically insoluble and show a strong attraction in water. [5, 125]

As mentioned earlier water molecules like to form hydrogen bonds between each other and that this is disrupted by a hydrophobic molecule. In contrast to this hydrophilic molecules are capable of forming hydrogen bonds with water. This leads to the strong and directional binding of water to the hydrophilic molecule or surface. This creates an additional steric barrier around the hydrophilic molecule increasing its effective size and therefore the range of the interaction.

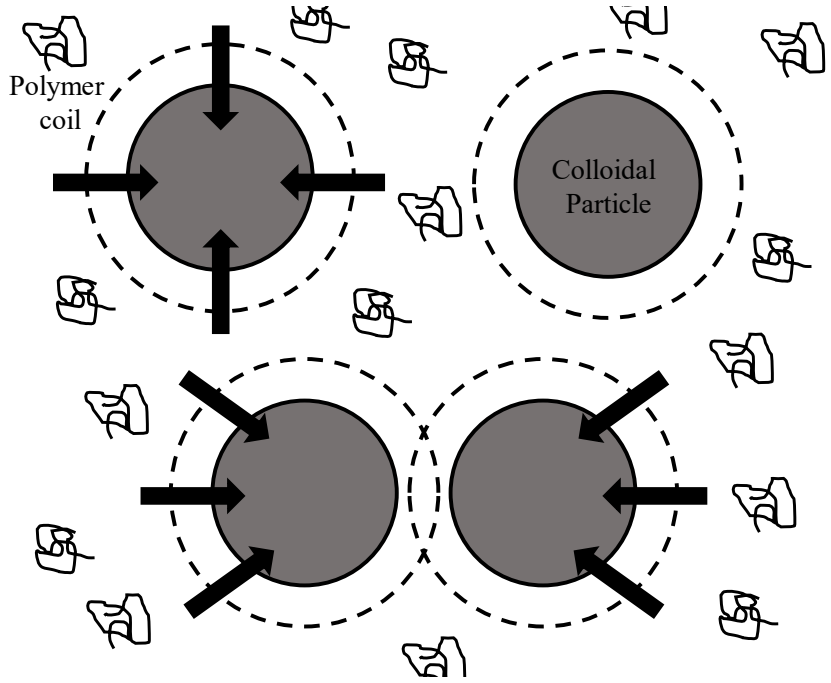


Figure 2.10: Diagrammatic representation of the depletion attraction.

2.3.7 Depletion Interaction

The depletion force is the attractive force observed between two colloids in a solution containing non-adsorbing polymers. This attractive force between colloids is osmotic in nature. [126] We can understand the nature of this force if we consider the concentration distribution of polymer within the solution. In the bulk solution we can consider the polymer concentration to be the maximum but at the surface of the colloids it can be considered zero. This means that there is a concentration gradient from the colloid surface to the bulk solution if we simplify this we can imagine a region around each colloid which has a polymer concentration of zero, a depletion layer. This results in an osmotic pressure gradient, which for an isolated colloid is equal in all directions so there is no overall net force. However, as two colloids approach their depletion regions overlap. This creates a region between the colloids that is devoid of polymer. This leads to an overall osmotic vector which drives the two colloids together. This osmotic vector is the depletion force. If the depletion force is large enough the colloids will aggregate, which may induce phase separation leading to a polymer enriched phase and a colloid enriched phase.

Depletion interactions were first measured by Asakura and Oosawa in 1954 who showed that two parallel plates submerged in a solution of non-adsorbing polymers were attracted to one another. [127] They developed an equation to calculate the osmotic pressure inside and outside of the region between the plates. This allowed the calculation of the osmotic pressure difference as a function of the distance between the plates. The integration of this equation gives the interaction potential between the plates as a function of D/R_g where D is the distance between the plates and R_g is the radius of gyration of the polymer in solution. Expanding on this work Asakura and Oosawa described the interaction between two spheres in a non-adsorbing polymer solution. [128] In this model the polymers are simplified as penetrable hard spheres. Penetrable hard spheres can freely permeate another penetrable hard sphere but are considered hard spheres when they interact with the colloids. This gives the following equation for the interaction potential between two spheres:

$$V = -\frac{1}{2}\pi(R/R_g)n_p kt(1 - D/R_g)^2 \tag{2.18}$$

Where D is the separation between spheres, n_p is the bulk polymer concentration. Later Lekkerkerker et al developed an osmotic equilibrium model for colloids and penetrable hard spheres, which took into account the partitioning between the two phases. [129] Using this model it was possible to calculate phase boundaries which were compared favourably to the experimental phase diagram. Experimentally these models were very accurate below a/R 0.5 but deviation appeared above this ratio.

2.4 Directly Measuring Intermolecular Forces

As previously stated the main aim of this work is to directly measure the interactions between two cationic surfactant bilayers using the colloidal probe AFM technique and then to study the impact of additives on the measured interactions in an attempt to predict or at least further understand the stability of this system.

Some of the first reported measurements of intermolecular forces were those measured between glass and quartz plates in vacuum by Overbeek in 1952. [130] A long range attractive force was measured between the plates but the measurements were difficult due to dust particles and surface roughness. A similar experiment was carried out by Derjaguin in 1956 between a convex glass lens and a flat glass surface in both vacuum and in air. [131] Attractive interactions were also measured with difficulties due to surface roughness.

There are two key techniques for the direct measurement of intermolecular interactions. The surface forces apparatus (SFA) and colloidal probe atomic force microscopy (CP-AFM). SFA is the older of the two techniques and has been used to measured and refine our understanding of some of the fundamental intermolecular forces discussed in section 2.3. The colloidal probe technique is a more recent development but is considered to be experimentally more versatile and a potential successor technique.

2.4.1 Surface Forces Apparatus

The surface forces apparatus measures the interactions between two surfaces as they are brought together then retracted from each other. The surfaces are generally two curved pieces of mica in a crossed cylinder geometry. [35,132] Mica is the most commonly used surface as is atomically smooth and relatively easy to prepare, but other surfaces have been used. [133–136] The separation of the two surfaces is controlled by a series of mechanisms but the most important and the one used during force measurements is a piezoelectric crystal which controls the fine < 0.1 nm movement. [137] The surface not controlled by the piezoelectric crystal is held by a cantilever spring, the deflection of which can be used to calculate the force between the two surfaces. Multiple beam interferometry is used to measure the absolute surface separation, the contact area, and any surface deformation. [138–141] A simplified diagram of a typical SFA is shown in figure 2.11

The first description of an SFA was published by Tabor and Winterton in 1969. [142] The instrument measured the interactions between two crossed mica cylinders

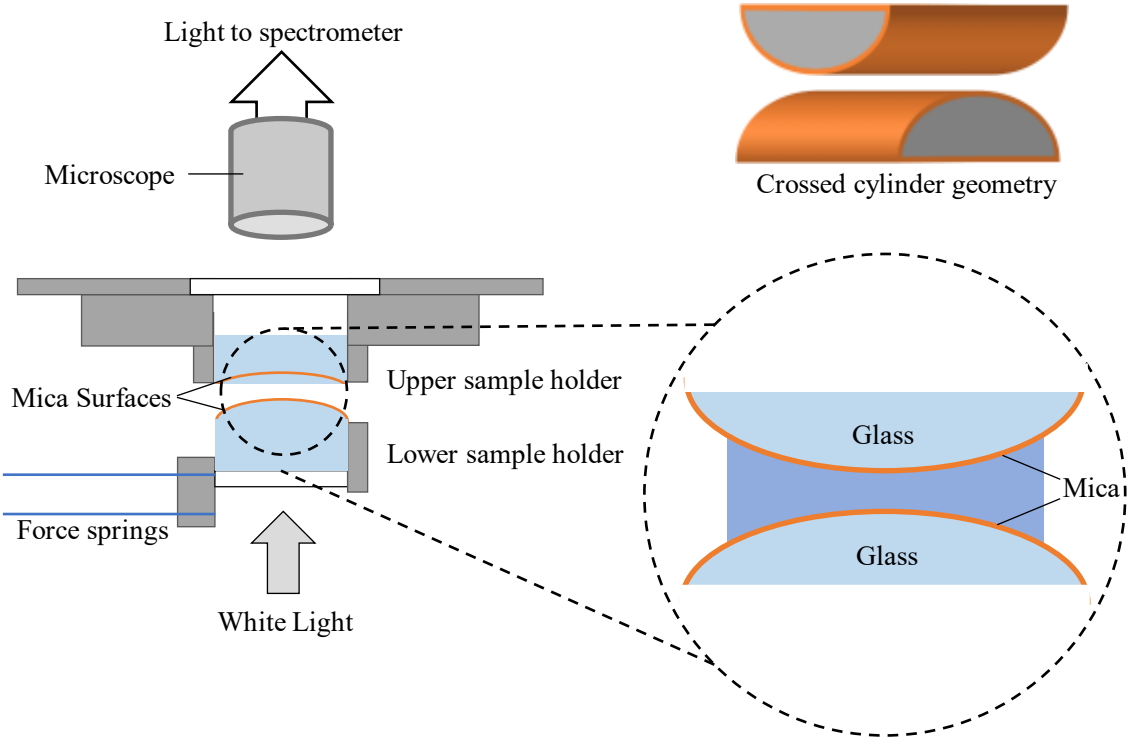


Figure 2.11: Simplified schematic of the surface forces apparatus.

measured for separations as low as 5 – 30 nm One of the cylinders was held by a spring the other controlled by a piezoelectric transducer. The distance was measured by multiple beam interferometry. Improvements were made by Israelachvili and Tabor in 1972 which allowed forces to be measured at smaller separation down to 1.5 nm. [143] They were able to measure the normal and retarded van der Waals interactions between the two mica surfaces which compared well with the previously discussed theory of the van der Waals forces. At this time they also showed the usefulness of the method for measuring forces in air between monolayers deposited on mica surfaces.

Further developments by Israelachvili and Adams in 1976 enabled the measurement of forces between surfaces immersed in liquids. [144] This iteration used a piezoelectric crystal to drive the mica surfaces enabling measurements at separations down to the Angstrom level and enabled one of the first direct measurements of the repulsive double layer forces. Further developments and refinements were made over the years increasing the range of forces that can be measured as well as making the instrument easier to clean, assemble, and operate. [145–147]

As mentioned the first SFA to be able to function in an aqueous environment was developed by Israelachvili and Adams in 1976. [144] This allowed for the direct measurement of the DLVO interactions between two surfaces. In their first full publication using this method they investigated the impact of electrolyte solutions on the interactions. [148] The results showed a long range repulsive interaction giving way to an attractive interaction at ≈ 5 nm separation. The attractive interaction was suggested to be the van der Waals interactions whilst the repulsive was attributed to the double layer repulsion. The range of the repulsive force decreased with increasing electrolyte concentration but the surface potential remained constant. Whilst the van der Waals attractions were largely independent of electrolyte concentration. Overall the paper showed the interactions to be compatible with the DLVO theory. The effect of other electrolytes on the forces have also been studied with other monovalent, bivalent and multivalent electrolytes. [149–151] The interactions measured in these studies mostly followed the DLVO theory as the electrolyte concentration was varied. However at higher electrolyte concentration an additional short range repulsive forces were observed, these were ascribed to hydration effects, and were studied further elsewhere. [152–154]

The interactions between mica plates in non-polar solvents has also been investigated. [155–157] These works mostly focus on the measurement of structural forces caused by the compression and displacement of the ordering within the non-polar solvents.

Due to the role of polymers in the stability of colloidal systems there has been several investigations into the impact of aqueous polymer dispersions on the interactions measured between the two mica plates of the SFA. [158] The majority of this work shows the adsorption of the polymer coils onto the mica surfaces. As such they generally focus then on the interactions between the polymer coated surfaces as opposed the interactions between the surfaces modified by the polymer solution. [159–163] The interactions between the surfaces with neutral polymers were generally repulsive but were attractive with low surface coverage. Others investigated the effect of polyelectrolytes. [164–166] Cationic polymers were shown to absorb to the mica surface, similar to the uncharged polymers, but show double layer like repulsion between the two surfaces. Anionic polyelectrolytes in compari-

son did not show adoption to the mica surfaces but did have a strong impact on the interactions between the sheets.

The initial work investigating the surface forces involved with lipids and surfactants focused on formation of surfactant monolayers and the forces between them.The hydrophobic interactions between surfactant monolayers have been investigated using single tailed and double tailed surfactants by Israelachvili and Pashley. [167–169] These studies showed a much stronger and longer range attractive interaction between the hydrophobic surfaces than would be expected from the van der Waals interaction. The strength of this attractive interaction depended strongly on the hydrophobicity of the surface and was thought to be due to the impact of the surface on the water structure surrounding it, although it is now believed that this very long ranged interaction is in fact due to nano-bubbles on the surface of the hydrophobic surface. [170, 171]

The interactions measured between non-ionic and zwitterionic lipid bilayers in water and air were dominated by the van der Waals interactions and compared well with theoretical models. [172–174] In electrolyte solutions the interactions between uncharged bilayers did not change significantly however repulsive double layer forces were measured between zwitterionic bilayers. [172,175] This was suggested to be due to the binding of ions creating a surface charge. Temperature dependence of non-ionic has also been investigated. [176]

The interactions measured between bilayers of ionic surfactants, both single and double chained, exhibited both double layer repulsion and short range attractive van der Waals interactions. Increases in the electrolyte concentration decreased the range of the double layer interactions but didn't appear to impact on the attractive interactions significantly. All in keeping with the DLVO theory. Some papers observed an additional short range repulsive interaction, 1 - 10 Å, which appeared with increasing electrolyte concentration. This was proposed to be the result of steric effects caused by counterion binding. [172, 175, 177, 178] Others however did not observe the short range van der Waals attraction at small separations but just observed an additional strongly repulsive short range interaction. [179] This was proposed to be due to stearic and hydration interactions due to the size of the sur-

factant head groups. The SFA has also been used to study the fusion of lipid or surfactant bilayers by using the apparatus to apply forces between two bilayers in contact with each other. [180]

More recently there have been some investigations looking at the interactions between cationic surfactant bilayers in aqueous polymer and polyelectrolyte solutions. In the presence of oppositely charged polyelectrolytes the supported surfactant bilayers were shown to be disrupted and break apart. [181] Anderson et al. reported to have measured the depletion interaction between the supported bilayers in the presence of uncharged and oppositely charged polymers. [182] However this is observed as a small additional adhesive interaction on retraction and not by an additional attractive interaction on approach. It may not be possible to measure the depletion attraction with SFA due the size and curvature of the crossed mica cylinders, making it hard for the depletion region to form on approach of the surfaces.

2.4.2 Colloidal Probe Atomic Force Microscopy

Atomic force microscopy (AFM) is a type of scanning probe microscopy developed from the scanning tunnelling microscopy invented in the 1980s. [183] The STM enabled the imaging of atoms for the first time but was limited to conducting or semiconducting samples. [184–186] The AFM, first reported by Binnig et al., was able to image the topography of conducting and insulating surfaces. [187] The resolution was generally not as good as the STM but atomic resolution has been possible in some cases.

The atomic force microscope measures the interactions between a sharp tip mounted on the end of a cantilever and the surface of interest. As the tip is scanned across the surface the interactions between the surface and the tip are measured by monitoring the deflection of the cantilever. A topographical image of the surface is obtained by keeping a constant force or deflection between he sample and tip and then plotting the height of the sample stage against the probe position. The height of the sample is controlled by a feed back loop which attempts to maintain a constant force between the sample and the tip. The interaction between the tip and

sample used for imaging is generally the short range repulsion due to the overlap of electron orbitals.

The sample position is controlled using a piezoelectric crystal which controls both the lateral position, for scanning, and the height of the sample relative to the probe. Depending on the instrument design the piezo can either be used to control the position of the sample, with he probe being in a fixed position, or to control the position of the probe with the sample being stationary. The deflection of the cantilever is most commonly measured using the optical lever technique. [188, 189] This involves focusing a laser beam on the back of the cantilever and monitoring the position of the reflected beam using a split photodiode. Deflection of the cantilever can then be converted into the force applied via Hooke's law. Whilst the instrument was originally developed for topographical imaging, due to the imaging principal it can also be used to measure forces between the tip and surface as a function of distance. By moving the probe towards the sample in the vertical axis and recording the cantilever deflection force distance curves can be plotted, of referred to as force curves.

The invention of the AFM allowed molecular and surface forces to be measured on a near molecular scale for the first time on any surface. Forces have been measured in air [190–192] and in water, [193–197] and the frictional forces on the tip have also been investigated. [198] In these studies, the force was measured between a sharp tip and a flat surface. Unfortunately, because the geometry of the tip was not simple, or more usually, was not even known, comparison with theory proved difficult.

The main problem with this as a direct force measuring technique is the geometry of the tip. Therefore in 1991 Ducker attached a small sphere to the tip creating the first colloidal probe AFM technique. [199] A diagram of the colloidal probe technique is shown in figure 2.12.

Ducker's first measurements were between a silica sphere and a silica surface. [200] The interactions showed a long range repulsion which fitted well with the DLVO theory above 3 nm separation. A van der Waals minimum was not observed due to additional repulsive interactions at small separations. The force distance

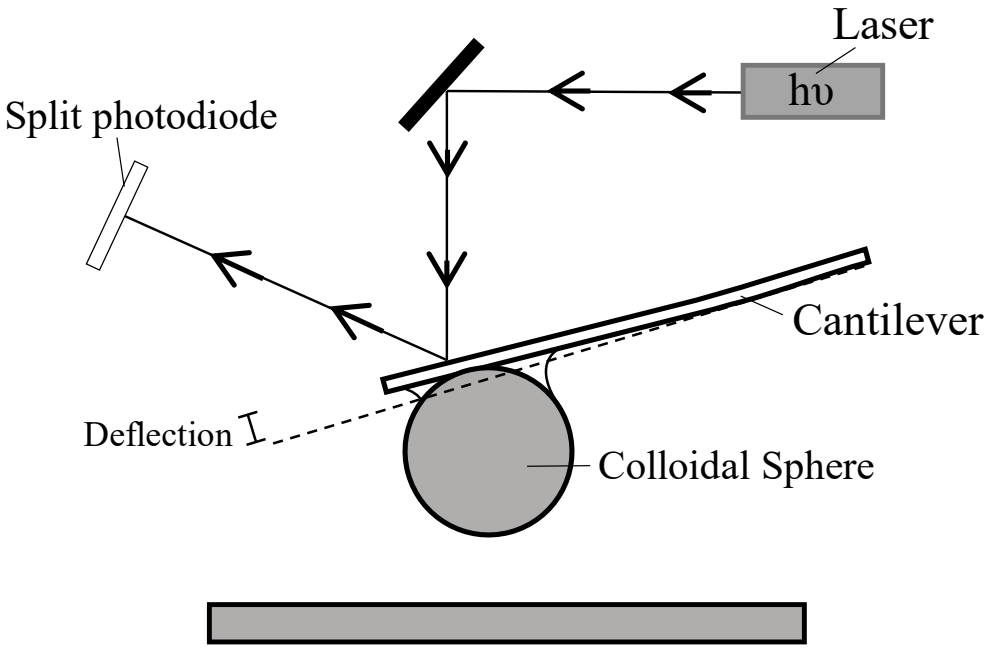


Figure 2.12: Simplified schematic of the colloidal probe atomic force microscopy technique.

curves collected were compared with those measured between two silica surfaces using SFA and were found to be in good agreement. [135, 201] They also showed how changing the pH of the system impacted on the measured interactions due to the changing surface charge of the silica. At a similar time Meagher used the the colloidal probe technique to also measure the interactions between a silica sphere and and plate. They were able to observe the attraction due to van der Waals forces at high $CaCl_2$ concentrations and at high pH. [202]

Moving on from these initial experiments the interactions between other materials have been investigated. [203] Li et al. looked at polystyrene, showing long range repulsion and short range attraction. Repulsion decreased with increasing electrolyte but adhesion remained unaffected. [204] Various other surfaces have been investigated including silicon, silicon-nitride, silicon oxide, borosilicate glass, latex, and ZnS. [203, 205–210] People have also investigated asymmetrical systems such as a silica sphere and a mica surface. [211] The interactions measured using this technique between a colloidal sphere and a flat substrate generally exhibit DLVO interactions with the exception for some samples where an additional short range repulsion was observed. The repulsive interaction due to the double layer interaction

decreased with increasing electrolyte concentration whilst the short range attraction due to van der Waals forces we not significantly effected.

More recent work has looked at the role of monovalent and multivalent salts on the interactions between colloidal particles using the colloidal probe technique. [212] These have been studied as both co-ions and counter ions to the colloidal surface. The forces between a colloidal probe and a flat surface in the presence of multivalent co-ions, has been studied by Ruiz-Cabello et al. [213] They observed that the repulsive interactions had a longer range in multivalent co ion salts compared with monovalent salts. Co-ions are not expected to adsorb onto the surfaces and are therefore not expected to affect the surface charge. However they are suggested to strongly modify the structure of the electric double layer. Multivalent counterions have been studied in several papers. [214–216] Multivalent counter ions are shown to decrease the range of the double layer interactions in agreement with the DLVO theory. However additional non-DLVO forces have been observed. These include an additional repulsive interaction at short range which has also been observed for multivalent ions with SFA believed to be due to hydration and steric effects caused by the counterions adsorbing to the surfaces. [149–151] Some have shown short range attraction with the addition of multivalent counter ions with increasing concentration with a repulsive interaction re-emerging as the concentration is increased further. [212, 214]

Another non-DLVO interaction of particular importance to the stability of colloid dispersion is the depletion attraction. Attempts have been made to directly measure this interaction using the SFA. [182] However these only measured an increased adhesion rather than a short range attraction on approach. One of the earliest direct measurements of the depletion attraction caused by an aqueous polymer solution was performed by Milling. [217] Where the interactions between silica spheres and a flat silica surface were measured in aqueous solutions of sodium poly(styrenesulfonate). They observed a long range repulsive interaction due to the double layer interactions between the surfaces, as observed in electrolyte solutions, but also minimum which was though to be due to the depletion of the polymer. Oscillatory forces due to structuring of the polymer coils were also reported in some instances. These depletion and structuring interactions were also observed in a later

paper with uncharged polymers. [218] Further work looking at structuring behaviour was conducted later. [219]

The effect of the molecular weight of the polymer on the measured depletion interactions was investigated by Biggs et al. [220] They observed that the depth and range of the depletion attraction was dependent on the molecular weight and concentration. This compare well with the theoretical description of the depletion interaction. Polydispersity has been investigated. [221]

The surfaces and colloidal probes considered so far, although they have been shown that they can be made of a range of materials, have all been bare. Moving towards directly measuring the interactions between two supported bilayers would involve the coating of the colloidal sphere and flat surface. The most well studied coated sphere-plate interactions measured with the colloidal probe technique involve the coating of the sphere and surface with polymers or polyelectrolytes.

With uncharged but hydrophilic polymers such as PEO or PEG the forces between a coated colloidal sphere and coated surface have been investigated in several studies. [222–224] With PEO coated surfaces the measured interactions were generally repulsive on approach but adhesive forces were occasionally observed on retraction. It was argued that these adhesive interactions were caused by bridging interactions between the surface and the sphere. [223] Further studies of the bridging interaction with coated colloidal probes were performed by Biggs et al. [222] The degree of coating was related to the measured interactions. Where complete coverage was achieved the interactions were repulsive, with this repulsive force beginning at twice the radius of gyration of the polymer. Whereas when the surface coating was incomplete a weak attractive force was occasionally observed due to bridging of the polymer between the two surfaces. Generally the interactions on approach between coated colloidal probes and surfaces with uncharged polymers were dominated by electrical double layer and steric forces, the van der Waals forces were only observed to pay a minor role. With the addition of electrolytes the double layer forces diminished and at high electrolyte concentrations the interactions were dominated by steric repulsion. [224]

The coating of the surfaces with a charged polymer or polyelectrolyte exhibited similar interactions to those observed with the uncharged polymers. Hartley et al. observed the interactions to be similar to those predicted by the DLVO theory however they did not observe any significant steric interactions. [225] Others however have shown the repulsive interactions to exist down to contact between the surfaces with an additional short range steric interactions. Bridging interactions have also been observed as adhesion on retraction. [226, 227] Other studies have investigated polyelectrolytes and the impact of different colloidal spheres or surfaces on the measured interactions. Generally the measured interactions are dominated by long range double layer and short range steric repulsions. [227–230]

Bilayer - bilayer interactions have been sparsely studied by colloidal probe AFM with the main focus in this area being on the use of the SFA. One of the first papers using surfactants or lipids with the colloidal probe technique was published by Karaman et al. [231] However this was mostly focused on measuring the impact of a surfactant dispersion on interactions between polystyrene spheres. Johnson et al used the colloidal probe technique to directly measure the interactions between two supported cationic surfactant bilayers. [232] They showed a repulsive double layer interaction at larger separations and a small short range attractive interaction due to van der Waals forces. Pera et al. measured the interactions between two lipid bilayers using AFM however they used a sharp imaging probe as opposed to a colloidal probe. [233] Whilst they were able to measure the repulsive interactions between the bilayers the tip geometry is not as well defined and controlled as with the colloidal probe technique. Lorenz et al. used the colloidal probe technique to investigate the interaction between two lipid bilayers. [234] Whilst they did show some repulsive interactions on approach the main focus of this work was on the breaking of the bonds between ligands and receptors embedded into the bilayers on separation.

Whilst the impact of additives such as electrolytes, polymers, and polyelectrolytes on the interactions measured between uncoated colloidal particles, such as silica, have been investigated using the colloidal probe technique there is little literature available on the use of the colloidal probe technique for the direct measurement of the interactions between supported surfactant bilayers. In this work we

aim to develop methods that enable the direct measurement of interactions between double tailed cationic surfactant bilayers using the colloidal probe technique. From there the impact of different additives to the system such as electrolytes, polymers, and polyelectrolytes on the directly measured interactions between the bilayers will be investigated.

As these are soft, self-assembled systems, contrasted with hard spheres like silica, additives to the system can have a significant impact on the structure and behaviour of the surfactant bilayers. To gain a more complete understanding of the impact of these additives on the surfactant systems it is important to understand to what extent the additives mediate the interactions between bilayers and to what extent the changes in interaction are the result of changes to the properties of the surfactant bilayers. Finally the measured interactions are to be compared with the behaviour and stability of the bulk vesicle dispersions in order to validate the measured interactions and their correlation with the behaviour of the system as a whole.

Chapter 3

Tools and Techniques

3.1 Atomic Force Microscopy

3.1.1 Theoretical Principle

Atomic Force Microscopy (AFM) is a type of scanning probe microscopy. [187] It can be used to create an image of the topographical structure of a surface with resolutions down to the Angstrom level. It operates by measuring the interactions between a sharp tip attached to a cantilever and the sample surface as the tip is scanned across the surface. The interaction between the tip and sample are measured by monitoring the deflection of the cantilever using the optical lever technique. This involves reflecting a laser off the back of the cantilever and recording how the position of the reflected light changes as the cantilever bends. [188] The tip is scanned across the surface of the sample either by moving the sample under the probe, in sample driven systems, or by scanning the tip across a stationary surface in tip driven systems. There is no significant difference in the quality of images produced from sample drive or tip driven systems. Typical AFM shown in figure 3.1

There are three main imaging techniques, contact mode, tapping mode or non-contact mode, and quantitative imaging or peak force tapping mode. Some imaging

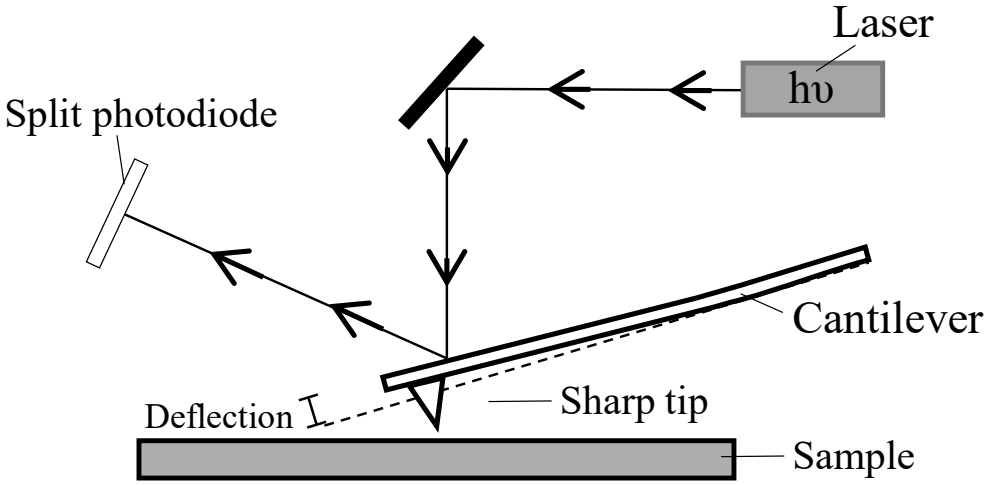


Figure 3.1: Simplified schematic of an atomic force microscope.

techniques are known by several names due to different instrument designers using different names, but the underlying principles are the same. Figure 3.2 illustrates these imaging modes.

Contact mode, one of the first imaging modes, involves imaging the surface with the probe in direct contact with the sample. [184] The probe is first lowered towards the surface, or the sample raised towards the probe, until deflection of the cantilever is observed. The probe is then scanned across the surface whilst attempting to keep the deflection constant. This is done via a feedback loop adjusting the height of the sample. These changes in the sample height are then converted to give a topographical map of the sample surface. The force applied to the surface can be varied by adjusting the set deflection with which the sample is imaged. This technique is good for hard surfaces but can be unsuitable for softer samples as the tip can damage the sample.

Tapping mode, or non-contact mode, in contrast with contact mode does not involve the direct contact between the probe and the sample. [235] Instead the cantilever is oscillated, using small piezo electric drivers, near to the surface of the sample. The surface is then scanned, as in contact mode, keeping the amplitude of the oscillation constant. Interactions between the probe and the surface, due to van der Waals forces, as the separation between the probe and the sample changes results in a dampening of the probe oscillation. A feedback loop is then used to adjust the

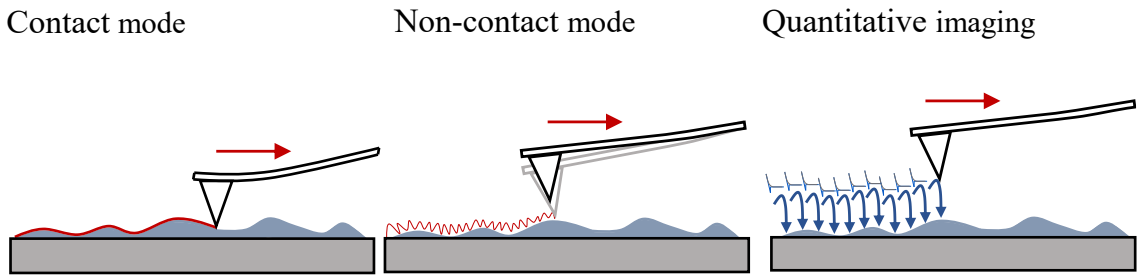


Figure 3.2: Diagram showing the three main AFM imaging modes: contact mode, non-contact mode, and quantitative imaging mode.

height of the surface to keep the amplitude constant as the surface is scanned. This is then used to create a topographical image of the sample surface. The major advantage of taping mode is that the probe does not come into contact with the sample which enables soft samples to be sampled without the risk of damaging them.

A more recent development in AFM imaging is the Quantitative Imaging (QI) technique. This technique combines force spectroscopy, discussed in section 3.2, and AFM imaging, giving more information about the sample surface as opposed to just the topographical data. The QI technique involves measuring and recording a force distance curve at each pixel. These force curves are then used to create topographical images by the piezo extension required to bring the tip into contact with the surface. The force distance curves provide other information about the properties of the sample which can be used to create images. These include the adhesion, force required to pull the tip off the surface, and the measured slope, which can be used to probe the nanomechanical properties of the surface. Images can be created to map the differences in properties across the sample surface.

3.1.2 Experimental protocol

All AFM imaging presented here was performed using a JPK Nanowizard 4, now owned by Brucker, using quantitative imaging (QI) mode. Imaging was performed using PNP-TR probes, square pyramidal tips on a 100 μm triangular pyrex-nitride cantilever with an optimal spring constant of 0.32 N/m, sourced from Windsor Scientific. For each sample multiple images were recorded in several location across

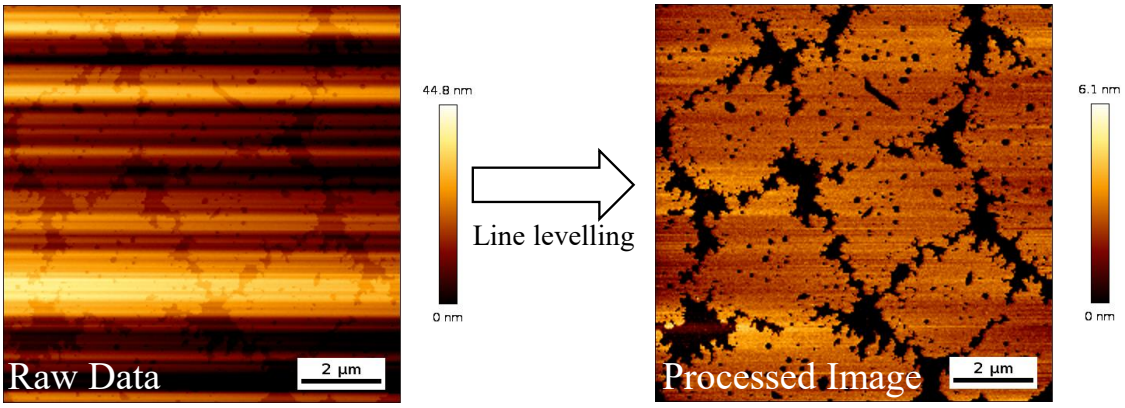


Figure 3.3: Impact of the line fitting algorithm on AFM images showing the raw data and the final processed image.

the surface. Probes were cleaned before use by placing them in a UV/ozone cleaner for 15 minutes.

Images were typically 524 x 524 pixels, the peakforce set point was kept between 1.5 and 2 nN, the pixel time was 6 s and the z-length was 80 nm. Unless otherwise stated all imaging was performed at 23 ± 2 °C. Cantilevers were calibrated using the thermal tuning method. Their spring constants were found to be within 10% of their stated value.

3.1.3 Image Processing

Images were processed using the JPK SPM Data Analysis software. Due to the relative flatness of the samples, the features of interest of only a few nanometres in height, the offset between scan lines, caused by sample tilt and piezo drift, is noticeable. The topographical images needed to be flattened by running a line fitting algorithm. This algorithm equalises the height of the scan lines enabling the surface topography to be more clearly presented, as shown in figure 3.3. The adhesion and measured slope maps did not need to be processed in this way.

The software was also used extract cross sections, showing the height variation of the surfaces, and to add scale bars and colour legends to the images.

3.2 Force Spectroscopy and the Colloidal Probe Technique

3.2.1 Theoretical Principle

Although the AFM was developed as an imaging technique, the forces between an AFM tip and the sample can be measured as a function of distance. This is performed by extending the peizo in the z direction towards the surface and then retracting it whilst measuring the cantilever deflection. As mentioned the cantilever deflection an be converted into force by Hookes law by equation 3.1, where K_s is the spring contestant of the cantilever and P is the cantilever deflection.

$$F = K_s P \tag{3.1}$$

The resultant force curves can be split into two regions. The non-contact region, the portion of the force curve before the tip comes into contact with the surface, and the contact region, the portion of the force curve after the probe has come into contact with the surface. The non-contact region can give information about the interactions between the AFM tip and sample surface. [183] A repulsive interaction would result in the deflection of the cantilever away from the surface, whilst an attractive force would result in the cantilever deflecting towards the surface with the potential of it jumping into contact with the surface. Once in contact with the surface the peizo continues to extend applying a force to the sample through the AFM tip. If the sample is not infinity stiff then it will be compressed and deformed as force is applied to it through the AFM tip. This can be used to probe the nanomechanical properties of the sample. [236]

The colloidal probe technique is a modified version of force spectroscopy. [199] It involves attaching a small colloidal sphere to the AFM cantilever. The forces between the colloidal sphere and the the sample are measured in same manner as standard force spectroscopy. The main advantage of the colloidal probe is that the

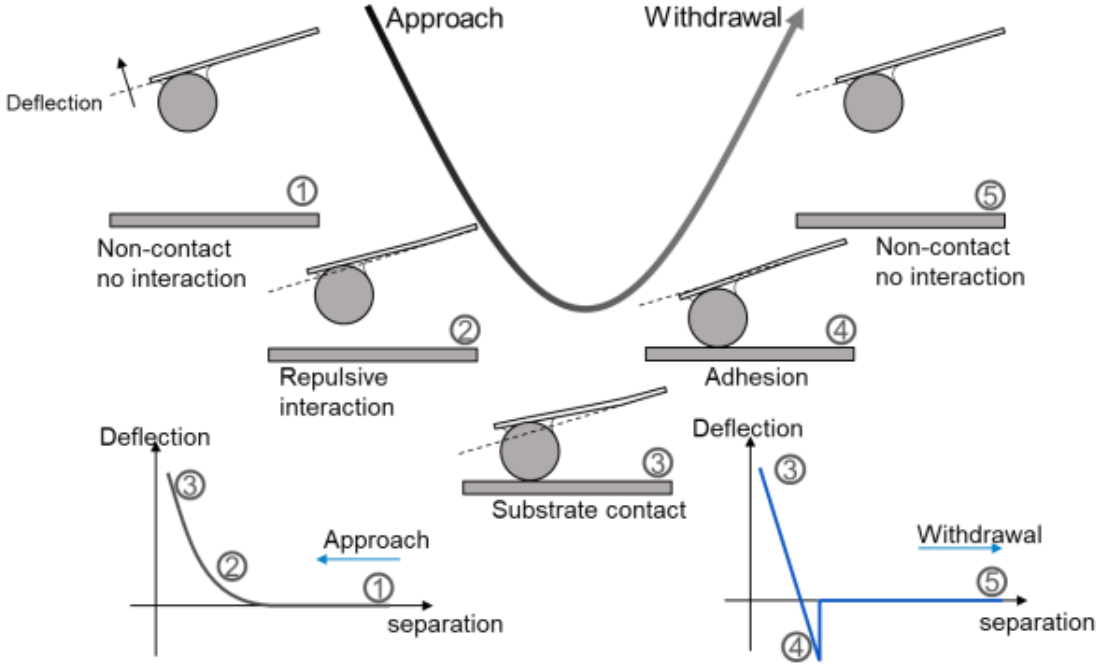


Figure 3.4: The operation of the colloidal probe force spectroscopy technique with theoretical force curves showing the types of interactions measured at different points in the force ramp.

geometry if tip is easier to control and the surface area interacting with the sample is larger and therefore more sensitive to small forces. The colloidal probe technique was discussed in detail in section 2.4. Figure 3.4 shows the operation of the colloidal probe force spectroscopy technique with theoretical force curves showing the types of interactions measured at different points in the force ramp.

3.2.2 Experimental protocol

Force Spectroscopy

All AFM force spectroscopy presented here was performed using a JPK Nanowizard 4, using PNP-TR probes, square pyramidal tips on a 100 μm triangular pyrex-nitride cantilever with an optimal spring constant of 0.32 N/m, sourced from Windsor Scientific. Force spectroscopy was performed after imaging so different areas of the surface could be targeted. Forces curves in each area of interest were collected in an 8 x 8 grid at a constant approach and withdrawal speed of 1 μm/s.

Colloidal Probe Technique

The colloidal probe force microscopy presented here was performed using a JPK Nanowizard 4. The probes used were CP-PNP-BSG and were obtained from Windsor Scientific. They consisted of a 20 ± 2 μm borosilicate glass sphere glued on a 100 μm triangular pyrex-nitride cantilever with an optimal spring constant of 0.32 N/m. Multiple force measurements were collected for each sample an 8 x 8 grid with a constant approach and withdrawal velocity of 1 μm/s. Probes were cleaned before use by placing them in a UV/ozone cleaner for 15 minutes. It was not possible to directly measure the spring constant of the colloidal probe cantilevers, however the equivalent imaging probes were measured to be with 10% of the optimal value.

3.2.3 Data processing

Force curves were analysed using the JPK SPM Data Analysis software. The raw data is in the format of piezo extension verses cantilever deflection. The cantilever deflection is converted into force by Hooke's law, as discussed above. This is done automatically by the software as it takes the spring constant from the data files.

Two processes need to be carried out to convert the raw data into useful force distance curves. Firstly the baseline needs to be set to zero deflection. This is due to drift where the initial laser reflection is not always at the centre of the split photodiode which registers this as a deflection. This is simply adjusted by setting the initial "deflection", where the probe is far from and not interacting with the sample, to zero.

Secondly, as the the tip-sample separation is not known, the contact point needs to be set. For an infinity stiff sample, where the sample is not deformed, the deflection will increase linearly with piezo extension, this is often referred to as the compliance region. This linear interaction is due to cantilever bending as it is pushed into the surface. By setting a contact point the peizo extension can be converted to tip sample separation and the the deflection due to piezo extension can be corrected for. For the infinity stiff sample the force distance curve will show the measured force

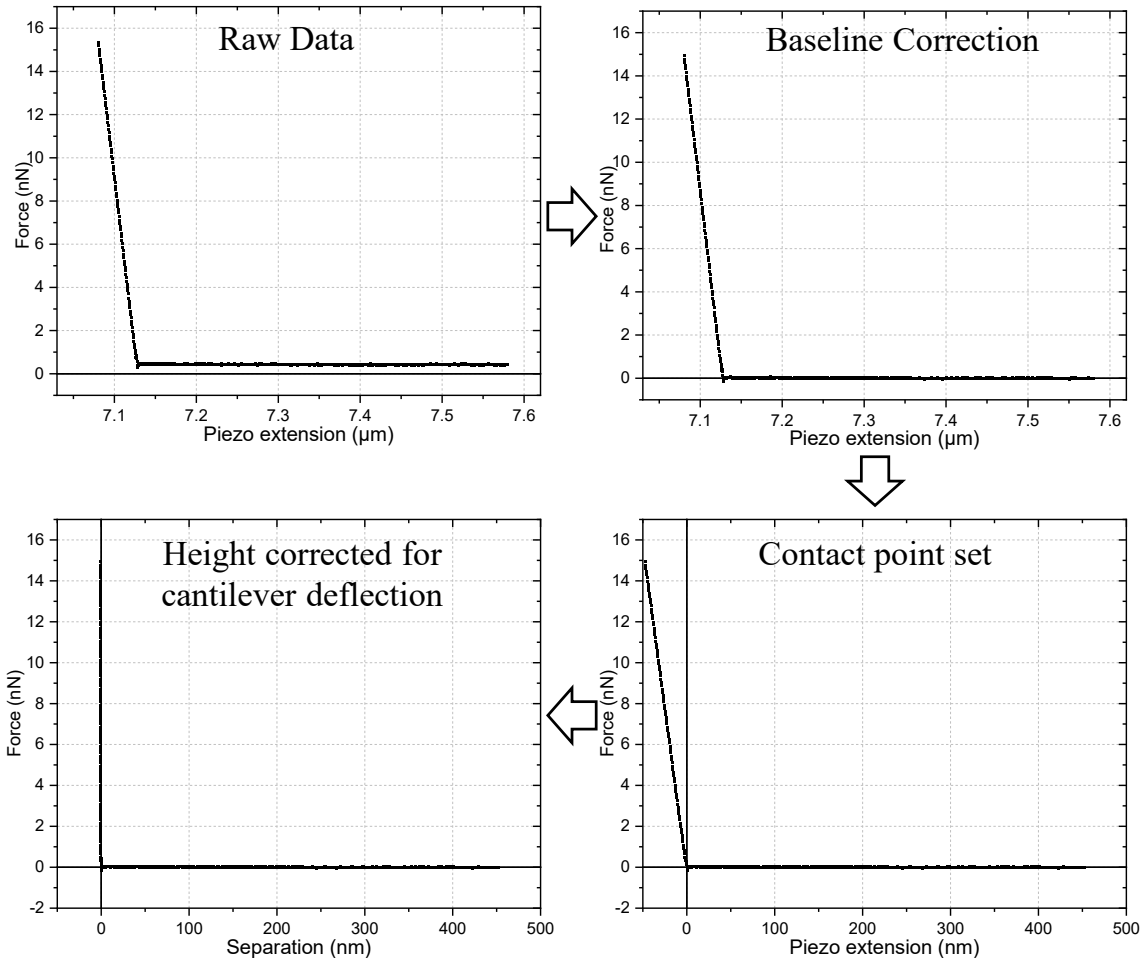


Figure 3.5: Preprocesses used in the data processing of force curves. Showing the impact of each process on the raw data.

increasing to infinity at the contact point. These processes are shown in figure 3.5.

3.3 Small and Wide Angle X-ray Scattering

3.3.1 Theoretical Principle

Small and wide angle x-ray scattering has been widely used to probe the structure of semi-ordered systems, such as those formed by amphiphile/water systems. [237] This is done looking at the elastic scattering behaviour of x-rays as they are passed through the sample. Recording the angle at which the X-rays are scattered. This

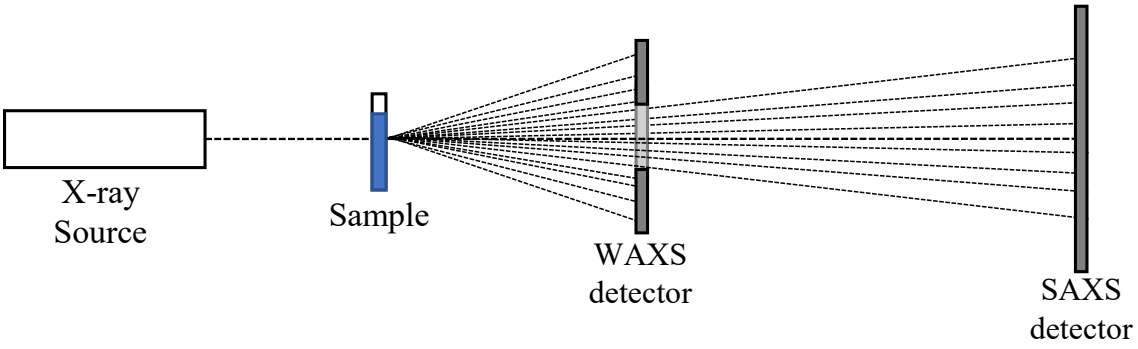


Figure 3.6: Simplified schematic of a combined SAXS/WAXS system similar to I22.

is typically up to a scattering angle of 1° for SAXS and 5 - 60° for WAXS. [238] Depending on the angular range that can be clearly resolved structural information from 1 to 100 nm and repeat distances of up to 150 nm can be resolved. Scattering at wide angles is caused by sub-nanometre structures and is often used to look at the phase of the alkyl chains in self assembled amphiphile systems. [239] A generalised set up involves an X-ray source, a sample holder, and a 2-D x-ray detector, as shown in figure 3.6.

The underlying theory of the scattering of he x-rays is Bragg diffraction. [240] The constructive interference of scattered radiation by an ordered system. Wavelength as to be comparable to the ordering hence x-rays for atomic systems. The waves are scattered by the repeating structures within the sample. When the difference in path length is an integer multiple of the wavelength the scattered waves remain in phase with one other resulting in constructive interference and appear as very intense points in the scattering pattern known as Bragg peaks. [241] Destructive interference occurs when the path length is not on integer of the incident wavelength. The impact of the constructive or destructive interference is intensifies due to the cumulative effect of scattering from successive ordered domains.

Bragg's law, equation 3.2, describes the conditions at which the constructive interference is the strongest. Where θ is the angle of incident, d is the distance between the repeating structures, and λ is the wavelength of the incident radiation. [240]

$$2d\sin\theta = n\lambda \tag{3.2}$$

From Bragg's law it is notable that the angle of incidence is one of the key parameters for determining constructive interference. Whilst this is important for crystalline samples, where the sample has to be rotated to investigate in which orientations and angles constructive scattering occurs, this is not required for relatively low ordered environments such as polymers, colloids, and self-assembled amphiphile/water systems. As these systems only have short range order structures are present within the in all spacial orientations. Meaning that part of the sample will be in the correct orientation to satisfy the Bragg condition. Due to these random orientation the x-rays are scattered is a cone leading to the Bragg peaks from SAXS appearing as a set of distinctive concentric rings.

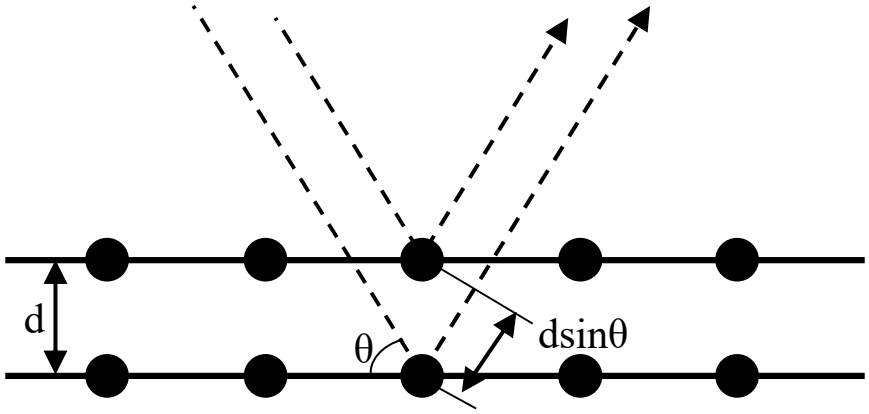


Figure 3.7: Diagrammatic representation of Bragg diffraction. Showing the elastic scattering of two incident beams by two different atoms within the sample.

Synchrotrons are often used as the X-ray source in SAXS experiments, all though bench top generators are also used. The main advantage of using synchrotron radiation is that the radiation produced is 10,000 times more intense than can be produced in a laboratory, enabling the study of very dilute or low scattering samples. [40] Synchrotron radiation is the electromagnetic radiation produced when produced when charged particles are accelerated radially. [242] To produce a practically continuous beam electrons are sped up to near relativistic speeds and kept circulating in a storage ring. The storage ring is not circular but a many sided polygon with bending magnets at each junction. The beam line used here had the additional benefit of

being able to measure both SAXS and WAXS simultaneously.

3.3.2 Experimental protocol

Diamond SAXS/WAXS

SAXS and WAXS were performed at the Diamond Light Source (Oxfordshire) on beamline I22. X-ray scattering patterns were collected at a fixed detector distance of 3 m, a fixed energy of 12.4 keV, and an exposure time of 3 s. The diffraction pattern of silver behenate was used to calibrate the detector. Samples were measured in glass capillaries. At each temperature the samples were allowed to equilibrate before scattering was performed.

BEDE SAXS

The BEDE system is a bench top x-ray scattering system. A fixed detector distance of 1 m, a fixed wavelength of 1.54 Å, and an exposure time of 10 s. The diffraction pattern of silver behenate was used to calibrate the detector. Samples were measured in glass capillaries. At each temperature the samples were allowed to equilibrate before scattering was performed.

3.3.3 Data processing

Data was analysed using the Dawn Diamond analysis software which enabled the importing and analysis of x-ray scattering patterns. The scattering patterns were radially integrated to produce linear intensity plots which could be used to assign scattering angles to the Bragg peaks.

3.4 Differential Scanning Calorimetry

3.4.1 Theoretical Principle

Differential scanning calorimetry (DSC) is a thermoanlaytical technique which measures the difference in energy required to heat a sample and a reference material as a function of temperature. [243] The heat flowing to the sample and reference is varied to keep them at the same temperature throughout the experiment. The reference sample needs to have a well defined heat capacity over the temperature ranges to be investigated. Here an empty sample pan is used as the reference material.

The underlying principle of the technique is that when a sample undergoes a physical transition, e.g. melting, more or less heat will need to flow to it to keep the sample and reference at the same temperature. For an endothermic process, such as melting, more heat must flow to the sample to keep it at the same temperature as the reference, due to the absorption of heat by the sample. Whereas for an exothermic process, such as crystallisation, less heat needs to flow to the sample compared with the reference to keep them at the same temperature due to the release of heat from the sample during the transition. By measuring the difference in heat flow between the sample and the reference as a function of temperature, the temperature range of transitions can be observed as well as the amount of heat absorbed or realised during them, the enthalpy of transition. [244]

DSC can be used to study a number of physical properties from melting and crystallisation of crystalline structures, to glass transition temperatures of polymers. Here the technique is used to investigate the gel-fluid transitions of self-assembled surfactant/water systems. Allowing the determination of transition temperatures for producing phase diagrams and to investigate the impact of additives on the physical properties of the system.

3.4.2 Experimental protocol

Experiments were performed using a Perkin-Elmer Diamond DSC. Sample mass of 3 - 5 mg using aluminium TZero pans from TA instruments. For each sample three cycles were run between 15 °C to 55 °C at a rate of 5 °C min^{-1}. Samples run against an empty sample pan for reference.

3.5 Dynamic Light Scattering and Zeta Potential

3.5.1 Theoretical Principle

Dynamic light scattering (DLS) is a tequnique used to determine the size distribution of small particles in suspension such as colloidal or polymer dispersions. The technique involves shining a laser through the sample and detecting the light scattered from the particles, measuring the fluctuation in the scattering intensity as a function of time. [245]

Information about the suspended particles is derived from an autocorrelation function of the intensity trace. Over a short amount of time the correlation is high as the particles have not moved much from their original position. As the time increases the correlation decays as the particles move from their original position. The decay is related to the motion of the particles and is used to provide the diffusion coefficient. The diffusion coefficient is related to the size of the particles.

The zeta potential is measured using the Electrophoretic Light Scattering (ELS) technique which is based on dynamic light scattering. [246] Whilst in DLS the particle motion is caused by Brownian motion, in ELS the particle motion is caused by an oscillating electric field. The particle velocity is determined by measuring the phase shift between the scattered light and the incident laser. This electrophoretic mobility is then used to calculate the zeta potential.

3.5.2 Experimental protocol

A Brookhaven zetaPALS was used for both particle sizing and zeta potential measurements. Zeta potential measurements were carried out using a field frequency of 2 Hz and a voltage of 4 V. Six runs were performed per sample with 10 cycles per run. Dynamic light scattering was performed at an angle of 90° using a 659 nm laser. Six runs were performed per sample. All measurements were performed at 25 °C.

3.6 Sample Preparation

3.6.1 Bulk surfactant/water systems

The required mass of surfactant and any additives were dissolved in the minimal volume of chloroform. The chloroform was allowed to evaporate under nitrogen re-precipitating the surfactant or surfactant mixture. This ensured that any any additives were dispersed throughout the surfactant phase. The samples were dried in a lyophiliser overnight before being hydrated with deionised water or the electrolyte solution of interest. Samples were freeze-thawed using liquid nitrogen until homogenous. Trapped air bubbles were removed by centrifugation.

3.6.2 Vesicle Dispersions

For stability studies

The surfactant was added to deionised water at a concentration of 10 mg/ml and vortex mixed until a homogenous dispersion had been achieved. The surfactant dispersion was then sonicated using a probe sonicator for 10 minutes to form a vesicle dispersion. The dispersions were then diluted to 1 mg/ml by the addition of an aqueous solution containing the additives of interest. The vesicle dispersions

were then allowed to equilibrate overnight before measurements were taken.

For supported bilayer formation

Pure surfactant vesicles were fabricated by dispersing 1 mg of the surfactant in 1 ml of deionised water by vortex mixing until homogenous. The surfactant dispersion was then placed in an ultrasonic bath for 20 minutes, until the turbidity had dissipated indicating the formation of vesicles.

For forming bilayers containing additives incorporated into the bilayers the required mass of surfactant and additives were dissolved in, and then re-precipitated from, the minimum volume of chloroform. The surfactant/additive mixture was then suspended in deionised water and vortex mixed until homogenous. Due the small masses of additives required, the dispersion were made up at 10 mg/ml. The surfactant dispersions were then diluted to 1 mg/ml and sonicated for 20 minutes in an ultrasonic bath to form small unilamellar vesicles.

3.6.3 Supported Bilayers

AFM substrates for supported bilayer studies were prepared by glueing a small disk of the desired substrate material to a 13 mm diameter steel disk. The substrates used where muscovite mica, borosilicate glass, and silicon. Muscovite mica was prepared for bilayer formation by cleaving and removing the top layer. Providing a clean surface for each sample. Borosilcate glass and silicon were cleaned by washing in ethanol followed by being placed in a UV/ozone cleaner for 15 minuets before use.

Supported surfactant bilayers were formed by the vesicle deposition technique. [247] 100 µl of the vesicle dispersion was pipetted onto a clean AFM substrate and allowed to equilibrate at either room temperature or at 60 °C for 20 minutes, depending on experimental protocol. The system was then flushed with 10 times volume of deionised water to remove any excess or undeposited vesicles from the system.

Chapter 4

The Self-Assembly Behaviour of Double Tailed Cationic Surfactants

4.1 Introduction

The surfactant system of interest in this study is the industrial surfactant di(alkyl iso-propyl ester) dimethyl ammonium methylsulfate (DIPEDMAMS). This is a doubled chained amphiphile with a quaternary ammonium head group, the aliphatic chains are attached to the head group by two ester bonds. These are often referred to in industry as ester "quats". As an industrial product the system is not a "pure" surfactant system. The raw material used to form the aliphatic tails of the surfactant is derived from a natural product. As such it contains a mixture of fatty acids, stearic, palmitic, and oleic acid in the approximate ratio of 14:26:47. This means that the tails of an individual DIPEDMAMS molecule are are statistical mixture of the three fatty acids. Figure 4.1 shows the skeletal structure of DIPEDMAMS. The system will also contain trace amounts of free fatty acids and single chained analogues.

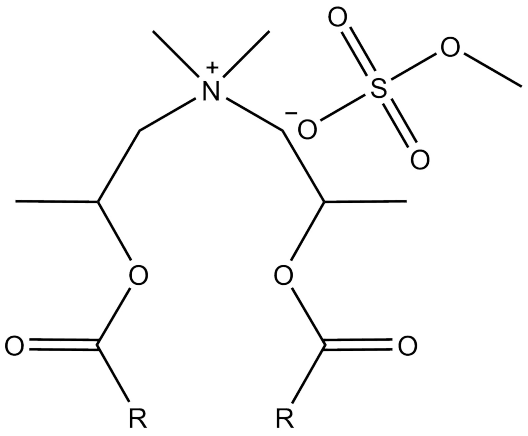


Figure 4.1: Structure of the DIPEDMAMS surfactant, were R is a fatty alkyl chain originating from a fatty acid mixture of C16, C18 and C18:1.

As mentioned the DIPEDMAMS surfactant is an industrial product. It is primary used in liquid fabric enhancers. These are generally sold in the form of concentrated surfactant vesicle dispersions. When added towards the end of a washing cycle the surfactants adhere to the surface of fabrics, due to attractive Coulombic interactions, creating a hydrophobic layer making the fabric feel "soft". These dispersions often contain additives such as salts, polyelectrolytes, polymers, and perfumes. As has been previously discussed, the main interest of this work is to understand the behaviour of the surfactant vesicle dispersion in relation to the interactions between the surfactant vesicles. In order to begin to understand these types of vesicle dispersions we must first understand the behaviour of the DIPEDMAMS surfactant in an aqueous environment.

As discussed in section 2.1, amphiphiles such as the surfactant DIPEDMAMS, spontaneously assemble into ordered or semi-ordered structures in an aqueous environment. In this chapter we try to understand the behaviour of DIPEDMAMS in an aqueous environment. The aqueous phase behaviour of similar surfactant systems have been studied previously and the general impact of the number of tails, their length, and the size of the head group is well studied, see section 2.1. [30, 248–250] However there is no literature available on the aqueous phase behaviour of DIPEDMAMS.

Small and wide angle x-ray scattering has been used extensively to investigate

the structure of lipid and surfactant self assembled structures. [251–253] Here SAXS is used to investigate the relationship between structures formed by the self-assembly behaviour of the DIPEDMAMS surfactant in surfactant/water systems and the concentration of surfactant within the system. This was followed by an investigation into the impact of temperature on the self-assembled structures including the use of WAXS to probe the state of the alkyl chains within the self-assembled structures. DSC was then used to further probe the thermal phase behaviour of the DIPEDMAMS/water systems.

Atomic force microscopy was then used to investigate the topographical structure of supported DIPEDMAMS bilayers. Enabling a comparison of the behaviour of the bulk surfactant/water system and the behaviour of the supported system. With the use of quantitative imaging mode information in the surface interactions and nano mechanics of the bilayers could be extracted.

4.2 Experimental

The cationic surfactant, di(alkyl iso-propyl ester) dimethyl ammonium methylsulfate (DIPEDMAMS) was provided by Procter and Gamble. Synthesised using an industrial fatty acid mixture of C18, C16 and C18:1 chains, therefore the aliphatic tails are a statistical mixture of the three fatty acids, see figure 4.1. All samples were prepared with deionised water, $< 18\,\mathrm{mS}$, filtered through an activated carbon filter to remove organic impurities

4.2.1 Preparation of DIPEDMAMS/water systems

DIPEDMAMS/water systems for x-ray scattering and DSC studies were prepared by the methods described in Chapter 3

4.2.2 Small and Wide Angle X-ray Scattering

Diamond SAXS/WAXS

SAXS and WAXS were performed at the Diamond Light Source (Oxfordshire) on beamline I22. X-ray scattering patterns were collected at a fixed detector distance of 3 m, a fixed energy of 12.4 keV, and an exposure time of 3 s as detailed in Chapter 3 At each temperature the samples were allowed to equilibrate for five minutes before scattering was performed.

BEDE SAXS

The BEDE system is a bench top x-ray scattering system. A fixed detector distance of 1 m, a fixed wavelength of 1.54 Å, and an exposure time of 10 s. As detailed in Chapter 3. At each temperature the samples were allowed to equilibrate for five minutes before scattering was performed.

4.2.3 Differential Scanning Calorimetry

Experiments were performed using a Perkin-Elmer Diamond DSC. Sample mass of 3 - 5 mg using aluminium TZero pans from TA instruments. For each sample three cycles were run between 15 to 55 °C at a rate of 5 °C min^{-1}. Samples run against an empty sample pan for reference, see Chapter 3.

4.2.4 Atomic Force Microscopy

All measurements were made using a JPK Nano wizard 4 AFM and analysed using the JPK data processing software as detailed in Chapter 3

Preparation of Supported Surfactant Bilayers

Supported surfactant bilayers were formed by the vesicle deposition technique from a vesicle dispersion containing 10 mol% perillyl alcohol as described in Chapter 3.

AFM Imaging

All imaging was performed in quantitative imaging (QI) mode. Multiple images of different areas of each supported bilayer were collected. The temperature was ramped from 25 to 65 °C then back to 25 °C imagining the supported bilayers at 10 °C intervals. Further details on QI mode and on the imaging protocols can be found in Chapter 3

4.3 Results and Discussion

4.3.1 SAXS/WAXS Study of the self-assembly behaviour of DIPEDMAMS/water systems

Small and wide angle x-ray scattering were used to probe the self assembly behaviour of the DIPEDMAMS surfactant in an aqueous system. The relationship between the surfactant concentration and the self assembled structures the surfactant molecules adopted was investigated.

Figure 4.2 shows the full SAXS image for a 20 wt % DIPEDMAMS/water system at 25 °C. The detector is a modular design comprised of several independent detectors, this can be seen in the check pattern where there is no detection between the detectors. At the centre of the scattering pattern is the beamstop. This is to prevent the mainbeam, non-scattered x-rays, from reaching the detector as this would saturate the image and possibly damage the detector, the wires suspending the beamstop can be observed in this image. The bright ring immediately around

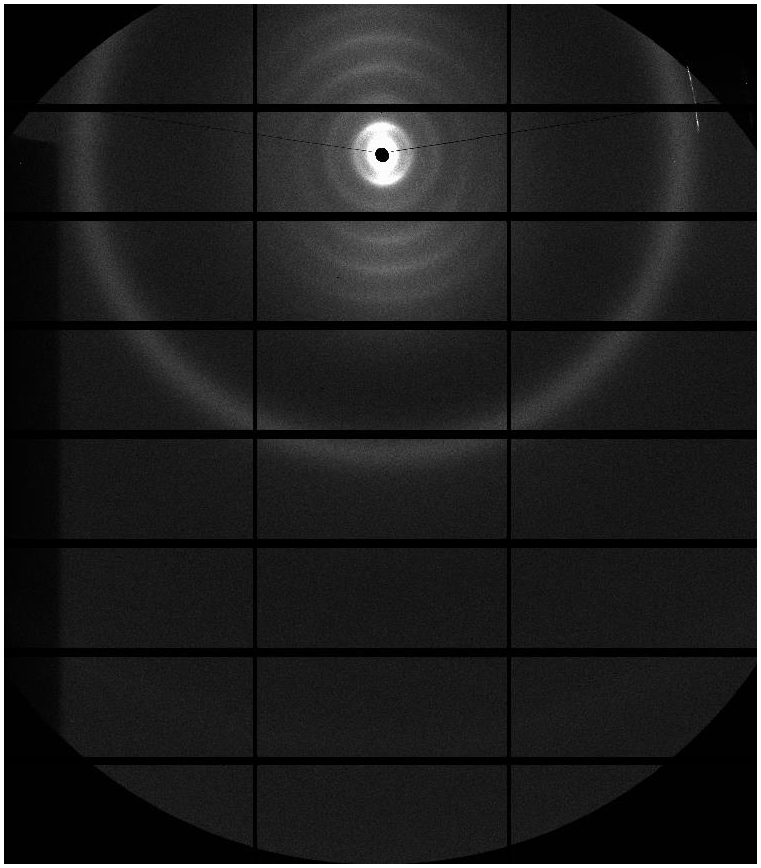


Figure 4.2: Full detector image of the SAXS pattern for a 20 wt% DIPEDMAMS/water system at 25 °C.

the beamstop is due to the mainbeam and not the result of scattering from the sample. The scattering pattern shows a series of distinct equally spaced rings showing that this sample has some form of long range order. The scattering pattern appears to be more intense in the vertical axis compared to the horizontal suggesting that there is some sample alignment. A broad ring further out is suggested to be caused by scattering from the glass capillary.

The radial integration of the SAXS image for 20 wt% DIPEDMAMS/water system at 25 °C gives the linear intensity plot shown in figure 4.3. The radial integration produces a symmetrical plot with the beamstop on the centre, here only one side of the linear intensity plot is shown. The integration enables us to resolve features that may not be resolvable by eye from the SAXS image and to assign values to the Bragg peaks. The large peak between 0 and 0.005 Å^{-1} is the mainbeam around the beamstop, the maximum of this peak is not shown on this scale. The scattering

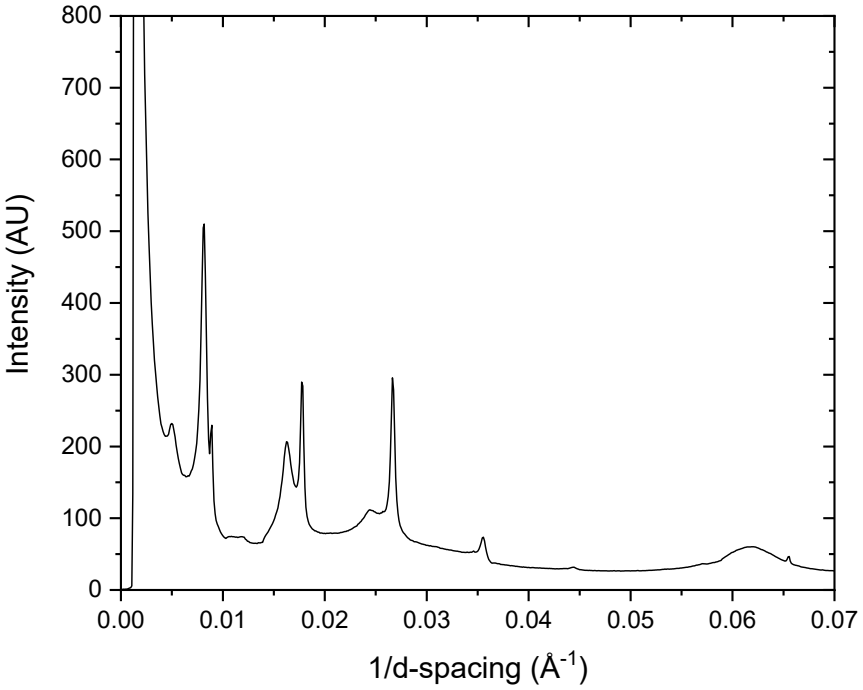


Figure 4.3: Linear intensity plot for the SAXS pattern of a 20 wt% DIPEDMAMS/water system produced by the radial integration of the raw SAXS image.

below 0.003 Å^{-1} is the defuse scattering due to large scale structures and not a Bragg peak. There then follows, between 0.005 and 0.05 Å^{-1}, two series of equally spaced Bragg peaks. The broad peak at 0.0625 Å^{-1} is not believed to be caused by scattering from the sample but from the glass capillary. The Bragg peaks from the sample show that it consists of two co-existing lamellar phases and from the peak separations the d-spacings can be determined.

Figure 4.4 shows cropped SAXS patterns, set to the same intensity/colour scale, for DIPEDMAMS/water systems from 1 - 50 wt%. 0.1 wt% is not shown as the scattering is too weak. As the surfactant concentration increases the intensity of the scattering patterns increases. No clear Bragg peaks are observed at 1 wt% and those at 5 wt% are difficult to resolve. Clear Bragg peaks are observed at 10 wt% surfactant and above. The scattering patterns appear to show two series of equally spaced concentric rings with the spacing between the rings increasing with increasing surfactant concentration. At 5 wt% and above there is an increased scattering intensity in the vertical plane suggesting some degree of sample alignment most likely caused by the glass capillary.

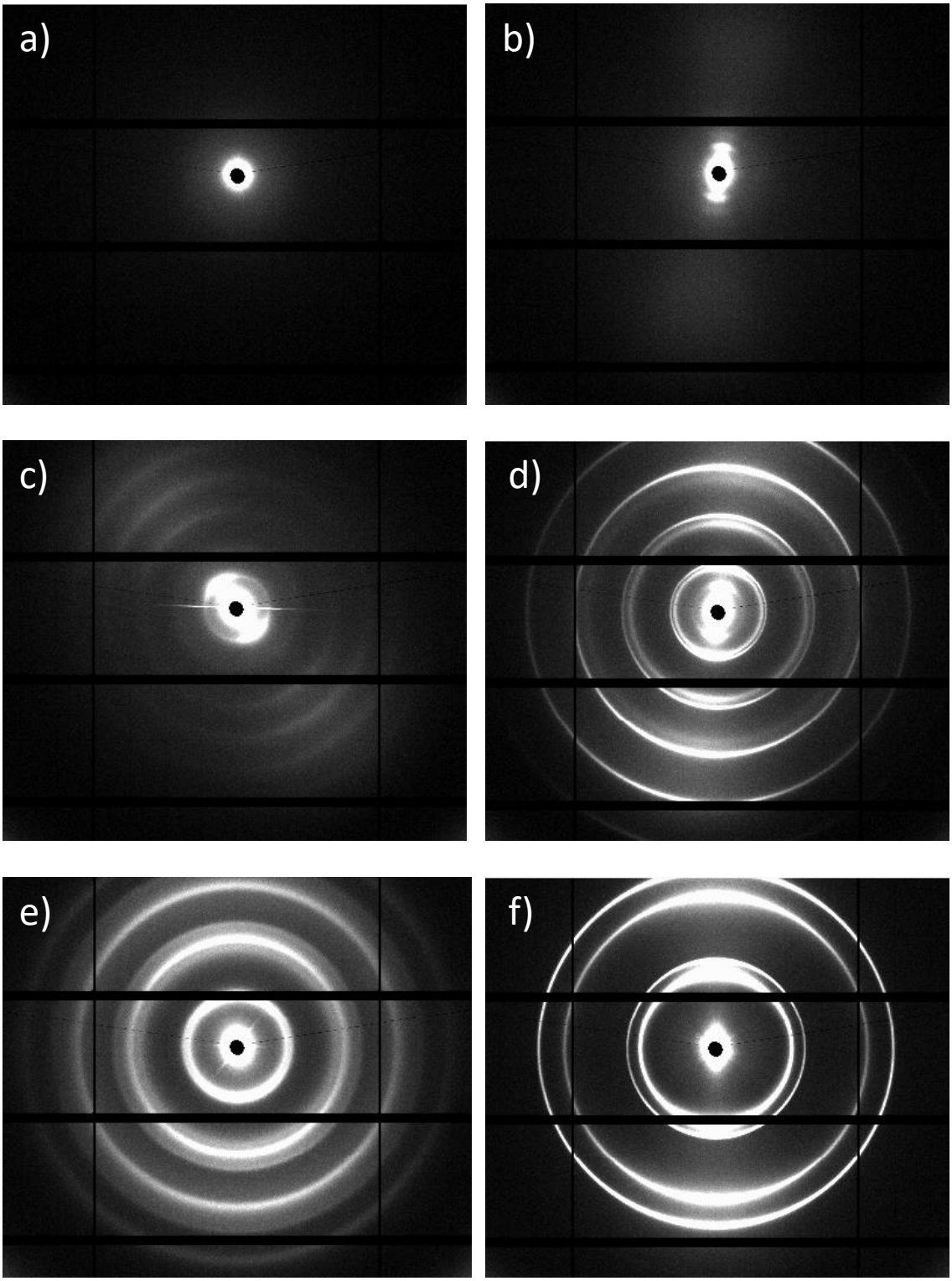


Figure 4.4: Cropped SAXS images of DIPEDMAMS/water systems at 25 °C at surfactant concentration a) 1 wt%, b) 5 wt% c) 10 wt%, d) 20 wt%, e) 30 wt%, f) 50 wt%.

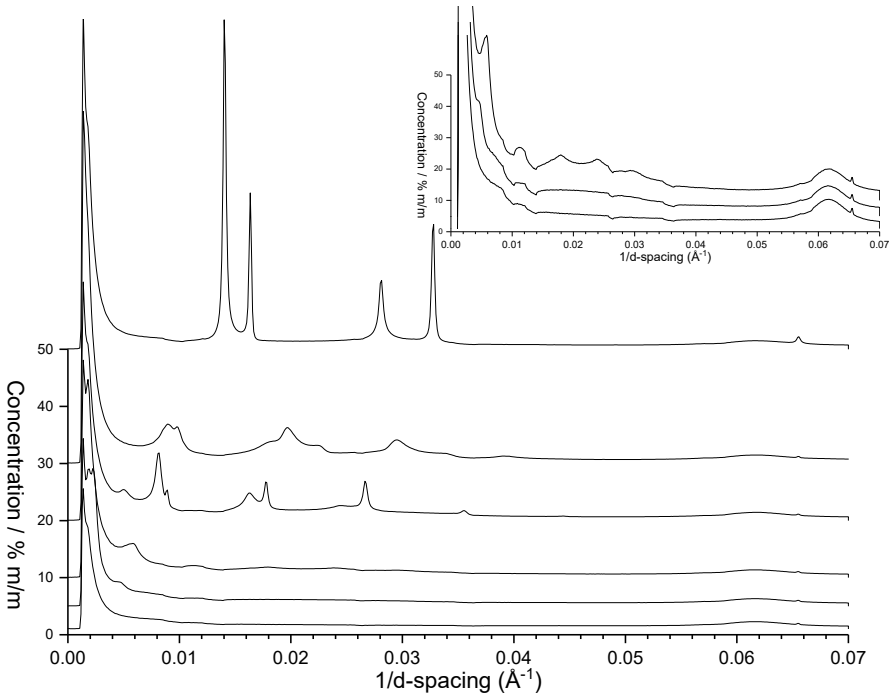


Figure 4.5: Linear intensity plots of the SAXS patterns of DIPEDMAMS/water systems, at 25 °C, and surfactant concentrations 1 - 50 wt%. The insert shows an enlarged section of the linear intensity plots focusing on the 1 - 10 wt% range.

Linear intensity plots from radial integration of the SAXS patterns at 25 °C for DIPEDMAMS/water systems from 1 - 50 wt% are shown in figure 4.5. At 0.1 - 1 wt% no obvious scattering pattern is observed and no Bragg peaks are resolvable. At 5 wt% two possible Bragg peaks can be observed as shoulders on the peak from the scattering around the beam stop. As the surfactant concentration is increased to 10 wt% a single set of equally spaced Bragg peaks can be observed. Surfactant concentrations from 20 to 50 wt% each show two sets of equally spaced Bragg peaks at room temperature. The intensity of the scattering patterns and Bragg peaks increases with increasing surfactant concentration. This increase in scattering intensity is a result of the system containing more material from which the x-rays are able to scatter. From the linear intensity plots it is observed that the Bragg peaks appear to shift to the right, to higher scattering angles, as the surfactant concentration increases. Peak intensities decrease as we move further from the centre. As the diffraction angle increases the intensity of the scattering decreases due to the smearing out of the structure (electron density) that is characteristic of mesophases. The linear intensity plots do not show the smooth decrease in intensity

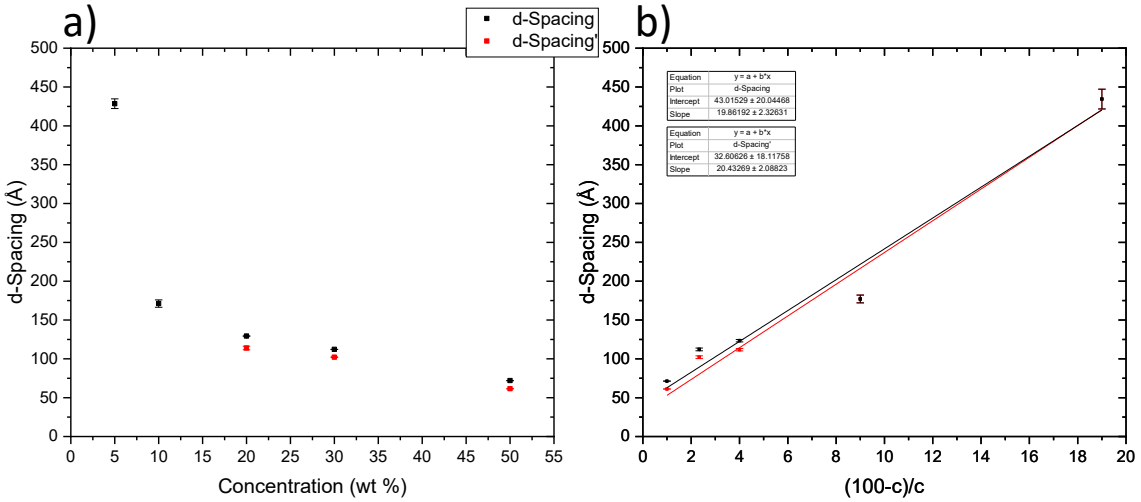


Figure 4.6: Plots of d-spacing as a function of a) DIPEDMAMS concentration and b) water to surfactant ratio including extrapolation to zero water content for a calculation of the intrinsic surfactant bilayer thickness.

as theory would predict. This is probably caused by a combination of directionality as observed by the intensities in different direction and by gaps between the detectors interfering with the radial integration.

A series of equally spaced rings or Bragg peaks is indicative of the lamellar phase. In the lamellar phase the surfactants are arranged into bilayers where the aliphatic tails are sequestered inside the bilayer and the hydrophilic head groups are on the outside of the bilayer exposed to the aqueous environment. [30] The bilayers are arranged in a stack separated from each other by a layer of water. From the distance between the lamellar Bragg peaks it is possible to calculate the d-spacing for the system. The d-spacing is the combined surfactant bilayer and water layer thickness. Figure 4.6 shows the d-spacing for each lamellar phase observed as a function of surfactant concentration, at 25 °C.

It is observed that the d-spacing decreases with increasing surfactant concentration. There appears to be a large decrease between 1 and 10 wt%. From 10 to 50 wt% the rate of decrease slows. Above 20 wt% the d-spacing for both lamellar phases is shown, at all concentrations showing two co-existing lamellar phases the difference in d-spacing is 1.2 ± 0.2 nm. The d-spacing can be viewed as a measure of three things: surfactant chain length, inclination, and water layer thickness. As

the surfactant concentration increases the water/surfactant ratio decreases causing a decrease in the water layer thickness. If the d-spacing is plotted as a function of water/surfactant ratio as opposed to surfactant concentration, the d-spacing can be extrapolated to zero water to give an estimate for the bilayer thickness. Using the larger d-spacing for each lamellar phase, this gave a bilayer thickness of 4.3 ± 1.8 nm. Assuming that a carbon-carbon bond has a length of 1 Å, DIPEDMAMS bilayers would be predicted to have a thickness of approximately 4.4 nm, assuming the surfactant molecules are oriented perpendicular to the plane of the bilayer; thus there is no interdigitation between the aliphatic tails; and an all trans chain configuration. Our experimental figure for bilayer thickness compares fairly well with the predicted thickness and falls within the error. However the error for the experimental values is rather large, as a result any minor interdigitation or inclination can not be resolved. Using the smaller d-spacing, when two lamellar phases are present, result in an experimental bilayer thickness of 3.3 ± 1.8 nm. Again this is reasonable when compared to the theoretical value for bilayer thickness.

Other than the differing d-spacing, the SAXS data do not offer any information on the structural difference or other causes between the two coexisting lamellar phases observed between 20 and 50 wt%. This is unlikely to be caused by poor or inconstant sample hydration or inhomogeneous samples. If the samples were inhomogeneous the SAXS patterns would be expected to show a broadening of the Bragg peaks as opposed to two clearly defined lamellar phases. As mentioned earlier the aliphatic tails of the surfactant system under investigation here are a statistical mixture of C18, C16 and C18:1. There is a possibility of phase separation within the bilayers forming regions enriched or depleted in certain chain ratios compared to the statistical whole. [254, 255] If it were simply separation by chain length then the predicted difference in bilayer thickness would be 2 Å, whereas the measured difference in d-spacing was around 1.2 nm and the difference in extrapolated bilayer thickness was 1.04 nm. The experimental differences in thickness are an order of magnitude larger than what would be expected from a variation in chain length. Another, more probable, explanation for the coexisting lamellar phases would be difference in the structure or order of the lamellar phases. It is possible that the thinner bilayers are a result of a tilting of the surfactant molecules within the bilayer with respect to the plane of the bilayer or from the interdigitation of the aliphatic

tails. These different bilayer sections could be the result of an area being enriched or depleted with respect to saturated or unsaturated aliphatic chains. However it is not possible to discern this from the SAXS data. [251]

WAXS scattering patterns provide information on the internal structure of the bilayers. As we are working in reciprocal space, scattering at wider angles is the result of shorter range ordering as opposed the the longer range order observed with SAXS. The WAXS patterns for the DIPEDMAMS/water systems from 1 - 50 wt% surfactant are shown in figure 4.7. The images are set to the same intensity/colour scale for ease of comparison. As discussed earlier the WAXS detector is L shaped to enable the main beam and scattering at smaller angles to pass. This accounts for the dark area in the lower right of each WAXS image. The dark lines crossing each image are due to the modular nature of the detector, as with the SAXS images. The WAXS patterns of all surfactant concentration investigated here exhibit a series of wide diffuse scattering bands. The position of these bands does not appear to be dependent on the surfactant concentration. From 5 wt% and above a single sharp ring is observed just inside the diffuse bands. The intensity of this ring increases with surfactant concentration whilst its position remains unaffected. This peak may be present at 1 wt% but the scattering intensity is too low for it to be easily observed by eye.

The radial integration of the WAXS images produce the linear intensity plots shown in figure 4.8. There is no scattering signal detected between 0 and 0.1 Å^{-1} due to the L shaped nature of the detector, scattering in this region passes through to the SAXS detector. At all surfactant concentrations investigated here, 1 - 50 wt%, a series of broad peaks were observed between 0.3 and 0.6 Å^{-1}, corresponding to the wide diffuse scattering bands observed in the WAXS images. The intensity of these peaks decreases with increasing surfactant concentration but their position remains constant. A sharp peak is observed at 0.24 Å^{-1} for all concentrations, corresponding to the single sharp ring in the WAXS images. The intensity of this peak increases with increasing surfactant concentration. For 50 wt% this peak as been cropped to fit within the plot. The valley observed at 0.88 Å^{-1} is believed to be caused by gaps between the detector plates and therefore not a feature of the wide angle scattering pattern.

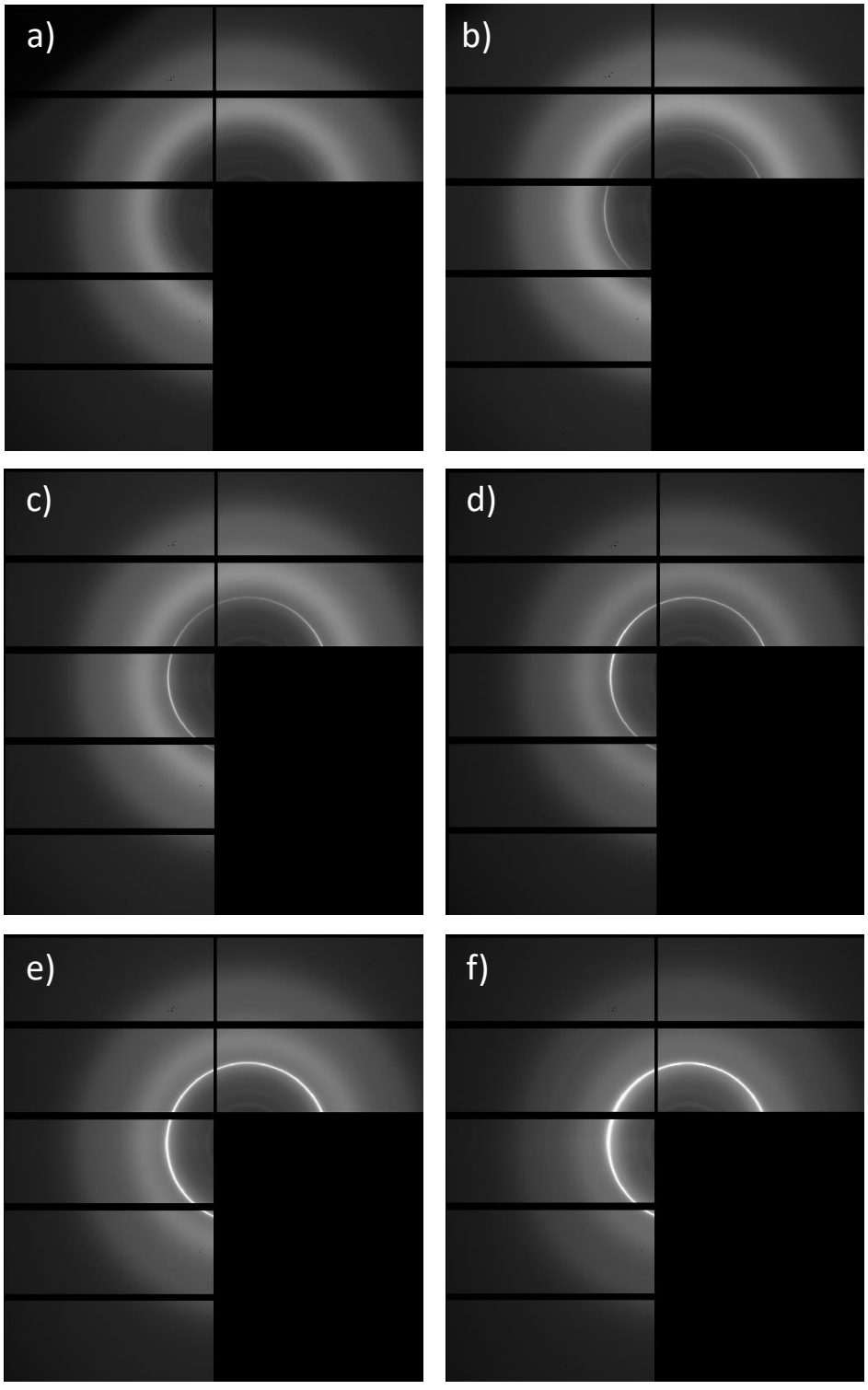


Figure 4.7: WAXS images of DIPEDMAMS/water systems at 25 °C at surfactant concentration a) 1 wt%, b) 5 wt% c) 10 wt%, d) 20 wt%, e) 30 wt%, f) 50 wt%.

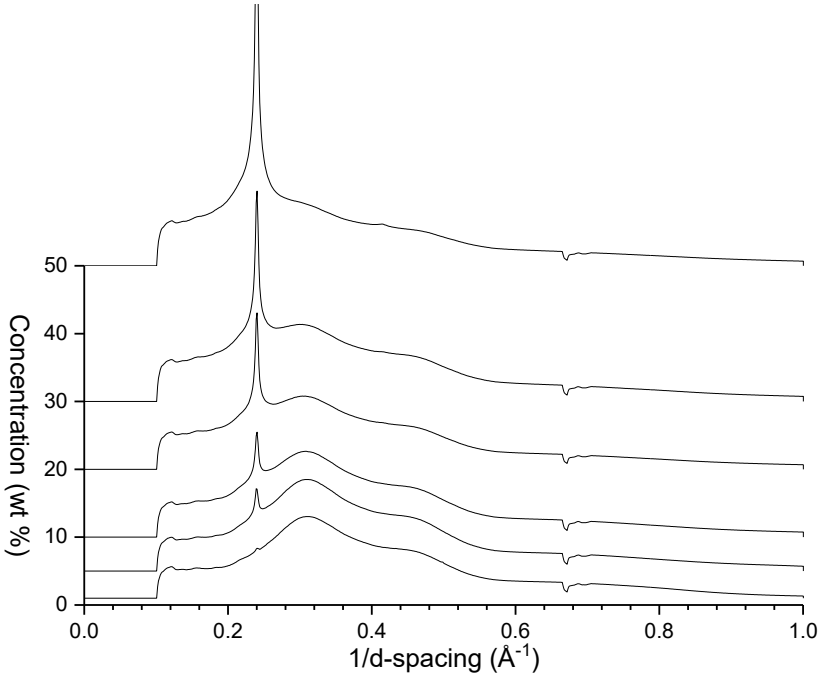


Figure 4.8: Linear intensity plots of the WAXS patterns of DIPEDMAMS/water systems, at 25 °C, and surfactant concentrations 1 - 50 wt%.

As previously mentioned the WAXS can provide information on the state of the surfactant molecules within the larger structure, in this case a bilayer. The sharp peak at $0.24\,\text{Å}^{-1}$ (d = 4.17 Å) is indicative that the lamellar phase is a lamellar gel phase,with a 2D-hexagonal packing of the surfactant molecules with an in-plane lattice parameter of a = 4.81 Å. This means that the surfactant molecules have rotational but not translational freedom within the bilayer as opposed to the crystalline phase where the molecules have neither freedom or the liquid phases where they have both, as described in section 2.1. The broad peaks observed between 0.3 and $0.6\,\text{Å}^{-1}$ are the result of scattering from the water within the system as water does have some degree of short range order. However the distances are more variable resulting in a broader peak than the scattering from the surfactant. An increase in the intensity of the $0.24\,\text{Å}^{-1}$ peak is observed as the surfactant concentration increases as there is more material for the x-rays to scatter from and there is a decrease in the intensity of the 0.3 and $0.6\,\text{Å}^{-1}$ peaks as the surfactant concentration increases as there is less water in the system from which the x-rays can scatter.

4.3.2 The effect of temperature on the self-assembly behaviour of DIPEDMAMS/water systems

Diamond Experiments

The spontaneous assembly of individual surfactant molecules into complex structures in an aqueous system is dependent not only on the surfactant concentration but also upon the temperature of the system, as discussed in section 2.1. The surfactant/water systems investigated above were first cooled to 15 °C then heated to 55 °C, SAXS and WAXS data were collected every 10 °C.

The SAXS images for the 20 wt% DIPEDMAMS/water system as it is heated from 15 to 55 °C are shown in figure 4.9. Between 15 and 35 °C the SAXS images show two series of equally spaced rings. At 45 °C and above only one series of equally spaced rings is observed. Some degree of alignment is observed at all temperatures, the x-rays appear to be scattered more intensely in the vertical axis as opposed to the horizontal suggesting that there is some alignment of the sample. This possibly increases with temperature but it is difficult to elucidate from the images alone. It may also be an effect of the two peaks combining so that they scatter more intensely.

Linear intensity plots for the SAXS of 1 to 50 wt% DIPEDMAMS/water systems heated from 15 to 55 °C are shown in figure 4.10. No Bragg peaks were observed for 1 wt% surfactant at any temperature. The 5 wt% surfactant system, between 15 and 25 °C exhibited a couple of Bragg peaks appearing as shoulders to the mainbeam. As the system is heated these peaks appear to contract towards the main beam and are resolvable as shoulders at 35 °C. Above 35 °C it is difficult to resolve any Bragg peaks. This may be due to the diffraction angle being so small that they are indistinguishable from the main beam or that there is an absence of ordered structures within the system. The 10 wt% system shows a single set of equally spaced Bragg peaks at all temperatures investigated. From 15 to 35 °C the peaks are observed to contract slightly towards the main beam. The biggest change is observed when heating from 35 to 45 °C, the peaks sharpen and the intensity dramatically increases although their positions remain unchanged. No further changes were observed when

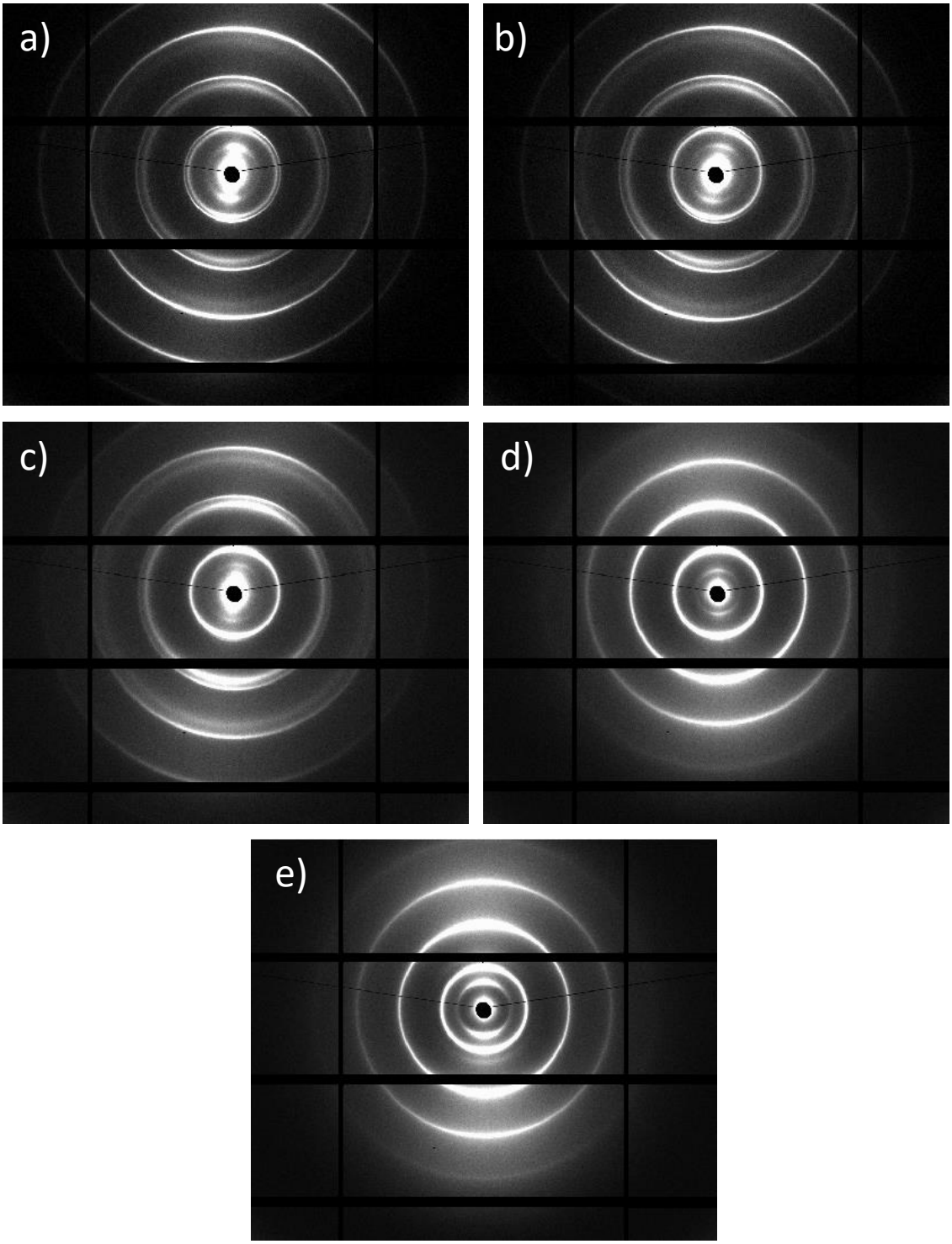


Figure 4.9: Cropped SAXS images of 20 wt% DIPEDMAMS/water systems at a) 15 °C, b) 25 °C, c) 35 °C, d) 45 °C, e) 55 °C.

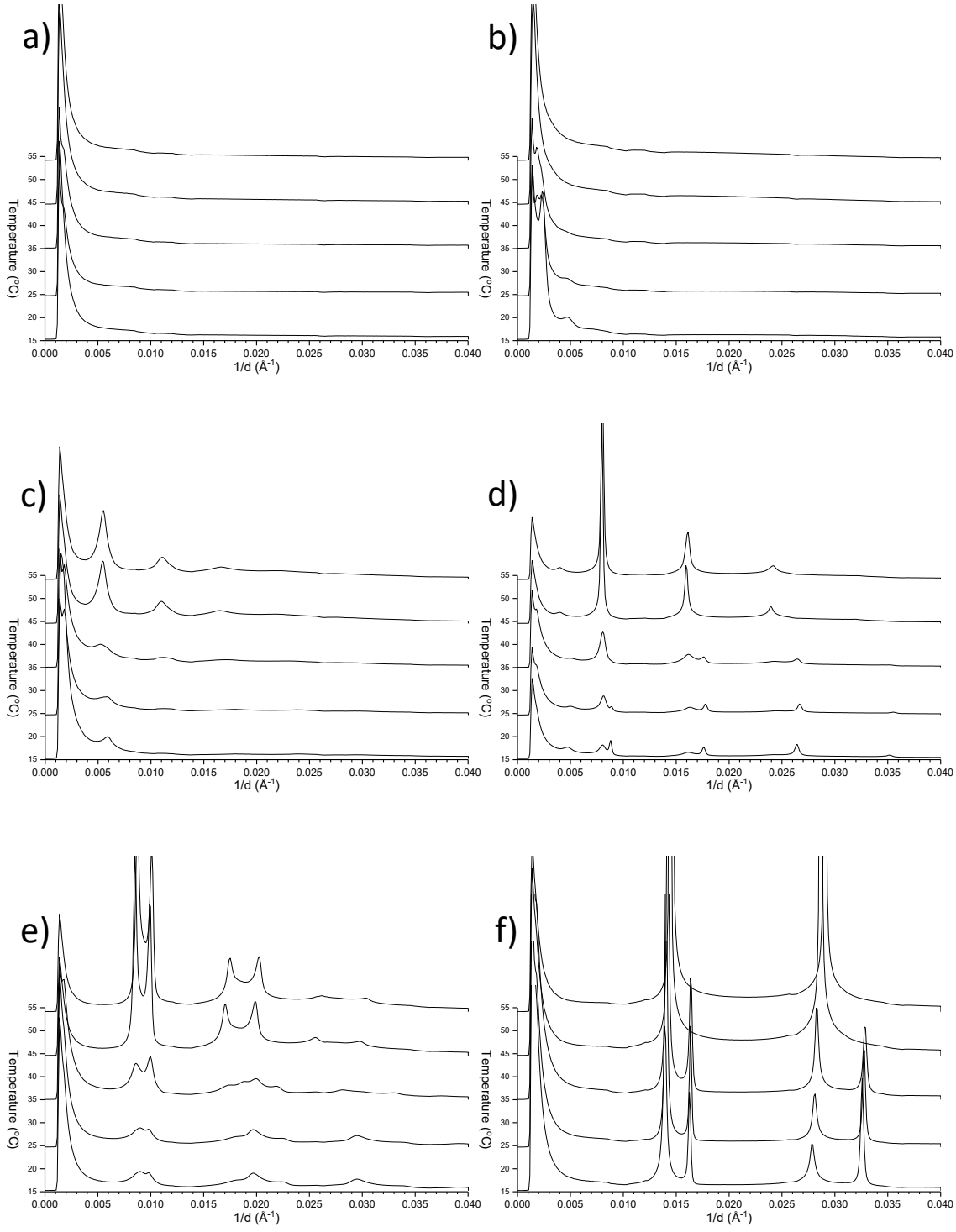


Figure 4.10: Linear intensity plots of the SAXS patterns of DIPEDMAMS/water systems with increasing temperature at surfactant concentrations a) 1 wt%, b) 5 wt% c) 10 wt%, d) 20 wt%, e) 30 wt%, f) 50 wt%.

heating to 55 °C. Surfactant/water systems at 20, 30 and 50 wt% all show two series of equally spaced Bragg peaks in ambient conditions, as discussed above. For all three systems on heating the Bragg peaks appear to sharpen and increase in intensity with the greatest change occurring between 35 and 45 °C. 20 and 50 wt% behave in a similar manner when heated. The positions of the Bragg peaks remain constant but the intensity of the peaks is affected. For both samples when heated from 15 to 35 °C the intensity of the equally spaced Bragg peaks at higher scattering angle decreases whilst the intensity of the set at slightly lower scattering angle increases. For 20 wt% at 35 °C the first peak of the wider Bragg peaks is hidden by the increased scattering of its counter part in the lower angle set. At 45 °C for both 20 and 50 wt% only one set of equally spaced Bragg peaks is observed, this is the pattern with the lower scattering angle. The 30 wt% surfactant sample displays different behaviour at 45 °C compared to the 20 and 50 wt% systems. At 30 wt% both sets of equally spaced Bragg peaks are observed at 45 °C and above. There is a sudden increase in the intensity of the scattering for both set between 35 and 45 °C but both set remain unlike 20 and 50 wt%. The scattering intensity is roughly the same for both sets of Bragg peaks.

The lack of Bragg peaks at 1 wt% DIPEDMAMS suggests that there is no long range order within the system at any of the temperatures investigated. At low concentrations the formation of ordered structures becomes increasing energetically unfavourable. The entropy cost to solvate or form micelles from the surfactant molecules is lower than that required for the formation of bilayers. At 5 wt% the system adopts a lamellar phase at 35 °C and below. As the temperature is increased from 15 to 35 °C the d-spacing increases, as the bilayers and or the water layers expand. It is not possible to assign a structure at 35 °C and above as the peaks are not identifiable, as mentioned above. It is possible that the d-spacing has increased to an extent where it can no longer be measured with this experimental set up or that the sample no longer has any long range order, potentially now a dispersion of vesicles or micelles. At 10 wt% and above the surfactant water system appears to adopt a lamellar phase at all temperatures investigated. The 10 wt% system adopts a single lamellar phase at all temperatures with the d-spacing increasing slightly as the sample was heated from 15 to 35 °C, it is then constant up to 55 °C. The 20 and 50 wt% surfactant systems adopt two co-existing lamellar phases between

15 and 35 °C. For both systems as the temperature is raised from 15 to 35 °C the scattering from the lamellar phase with the smaller d-spacing decreases and the intensity for the phase with the larger d-spacing increases. This suggests that the proportion of the bilayers adopting the phase with the smaller d-spacing is decreasing and the proportion in the phase with the higher d-spacing is increasing. As the temperature increases further to 45 °C only the lamellar phase with the larger d-spacing is observed. If the two phases observed below 35 °C are the result of differing structural arrangements, as discussed earlier, then it is possible that the increased temperature is causing the thinner bilayers to undergo reorganisation to resemble the structure of the thicker lamellar phase. The 30 wt% system exhibits similar behaviour to the 20 and 50 wt% systems below 35 °C however both lamellar phases are still present at 45 °C and above. It is not clear why the 30 wt% sample displays such different behaviour to the samples either side of it. the largest change in the scattering for all samples above 1 wt% appears to happen as the temperature increases from 35 to 45 °C. For 5 wt% this is when it is no longer possible to pick out a scattering pattern, for 10 to 50 wt% this temperature change results in a large increase in the scattering intensity along with, for 20 and 50 wt% the disappearance of the thinner co-existing lamellar phase. As this is a feature shared by all samples that scattered well it is possible that there is some form of transition taking place between 35 and 45 °C.

The WAXS data can be used to provide information on how the internal structure of the lamellar bilayers is affected by increasing temperature. Figure 4.11 shows the WAXS images for a 20 wt% DIPEDMAMS/water system as the temperature is increased from 15 to 55 °C. From 15 to 35 °C a sharp scattering ring is observed followed by a series of broad diffuse scattering rings. As the temperature increases from 35 to 45 °C the sharp scattering ring contracts and broadens whilst the the diffuse scattering rings remain constant in both intensity and position. There is no further change on heating to 55 °C. This pattern of a sharp intensely scattering peak contracting and broadening on heating above 35 °C is observable in the WAXS images for all concentrations from 1 to 50 wt% with only variation in the relative intensity of the peaks as the concentration is increased.

The WAXS linear intensity plots of 1 to 50 wt% DIPEDMAMS/water systems

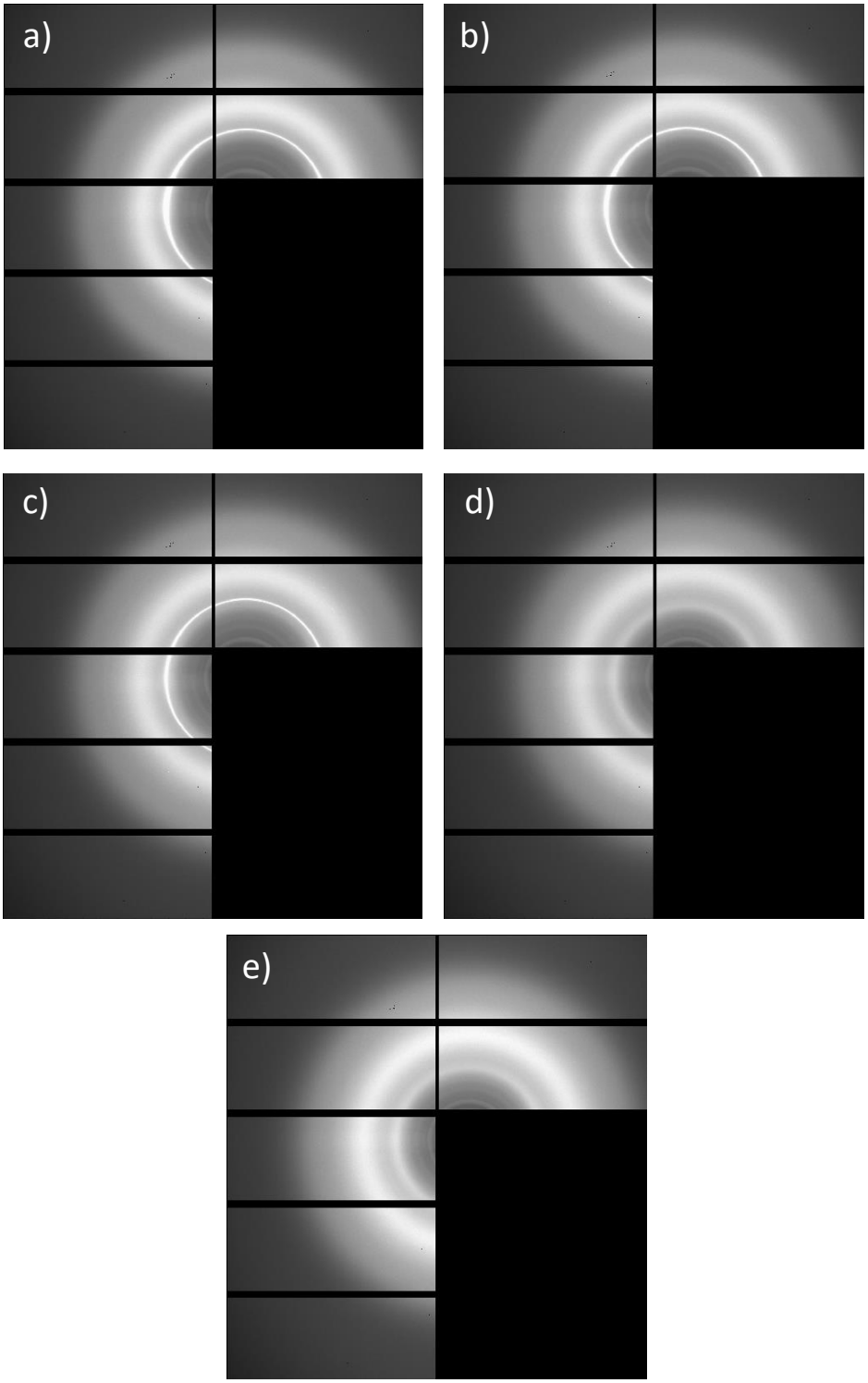


Figure 4.11: WAXS images of 20 wt% DIPEDMAMS/water systems at a) 15 °C, b) 25 °C, c) 35 °C, d) 45 °C, e) 55 °C.

heated from 15 to 55 °C are shown in figure 4.12. Broad peaks are observed between 0.3 and 0.6 Å^{-1} at all concentrations and temperatures. The intensity of these peaks decreases with increasing surfactant concentration but do not appear to be affected by temperature. A single sharp peak is observed at 0.24 Å^{-1} for all concentrations between 15 and 35 °C. The intensity of this peak increases with increasing surfactant concentration. At 35 °C the intensity of the 0.24 Å^{-1} peak has decreased and an additional broad scattering peak is observed at 0.22 Å^{-1}. This peak is difficult to observe at 1 wt% due to the low intensity of the scattering but is clearly observable from 5 wt% and above. As the temperature is increased above 35 °C the sharp peak at 0.24 Å^{-1} disappears and the intensity of the broad peak around 0.22 Å^{-1} increases but does not increase further above 45 °C. The intensity of the broad peak at 0.22 Å^{-1}, like the sharp peak at 0.24 Å^{-1}, is dependent on the surfactant concentration. The dip around 0.62 Å^{-1} is due to the detector mask and not scattering from the sample.

The broad peaks observed between 0.3 and 0.6 Å^{-1}, as mentioned above, are the result of the short range ordering of water, this accounts for the observation that their intensity decreases with increasing surfactant concentration. There is no observed change to these peaks with temperature which is to be expected as there are no known conformational changes for water within the temperature range investigated. As discussed earlier, the sharp peak observed at 0.24 Å^{-1} shows that the aliphatic chains within the bilayer are in a gel phase, with rotational but not translational freedom. As this scattering is due to structures formed by the surfactant it follows that as the surfactant concentration increases so does this scattering intensity. The scattering intensity of the broad peak around 0.22 Å^{-1} also shows dependence on the surfactant concentration as this peak is also the result of scattering from the surfactant bilayers. A broad peak around 0.22 Å^{-1} is indicative that the surfactant tails are in a fluid state, combined with the SAXS data, it can be concluded that a lamellar fluid phase is present. In the lamellar fluid phase the surfactant molecules within the bilayers have translational, rotational freedom, and and chain conformational as opposed to just rotational freedom in the lamellar gel phase, see section 2.1 for more details. Below 35 °C only the lamellar gel phase is observed for all surfactant concentrations. At 35 °C both the broad fluid peak, 0.22 Å^{-1}, and the sharp gel peak, 0.24 Å^{-1}, are present. As the intensity of the gel

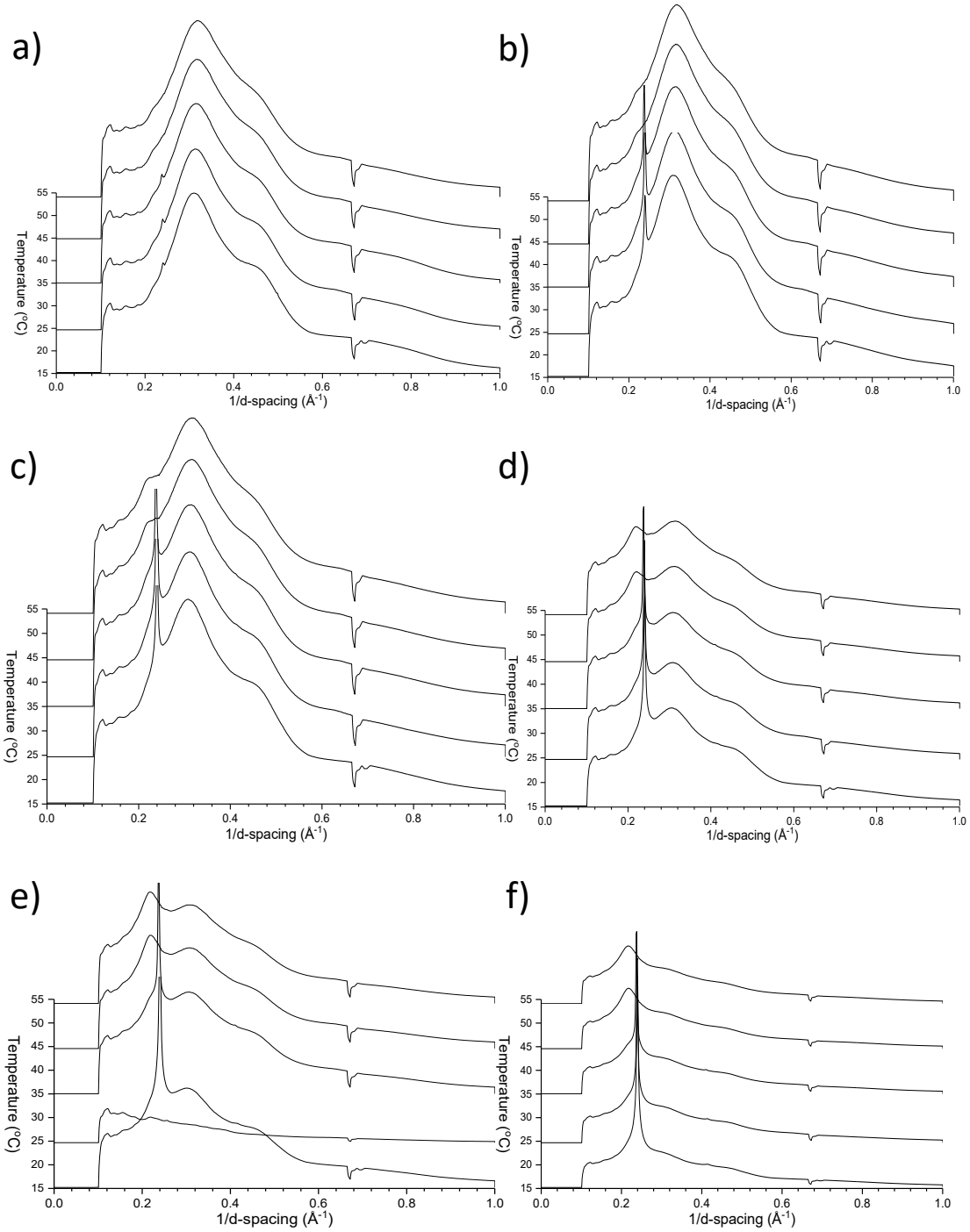


Figure 4.12: Linear intensity plots of the WAXS patterns of DIPEDMAMS/water systems with increasing temperature at surfactant concentrations a) 1 wt%, b) 5 wt% c) 10 wt%, d) 20 wt%, e) 30 wt%, f) 50 wt%. For clarity the y-axis has been offset by the temperature of the sample.

peak begins to decrease at this temperature it is suggested that the gel phase is beginning to transition to the fluid phase. It is possible that the lamellar gel and lamellar fluid phases are co-existent at 35 °C or that the samples have had insufficient time to transition from the gel phase to the fluid phases as they were only held at the set temperature for a few minutes. By 45 °C, at all surfactant concentrations, the whole sample has transitioned from the lamellar gel phase to the lamellar fluid phase as suggested by the absence of the sharp 0.24 $Å^{-1}$ peak and that the intensity of the fluid peak, 0.24 $Å^{-1}$, does not increase on further heating to 55 °C.

BEDE follow up Experiments

Due to time limitations it was not possible to investigate what happens when the samples were cooled again after heating them to 55 °C at the Diamond Light Source. Therefore it was decided to try and investigate this on a bench top set up. The samples were heated from 20 to 60 °C before being cooled back down to 20 °C at 5 °C increments.

Bench top x-ray generators are orders of magnitude less intense than those that can be generated at a synchrotron, see Chapter 3. Due to this only DIPEDMAMS/water systems of 30 wt% and above scattered sufficiently well for the SAXS patterns to be interpretable. Figure 4.13 shows the full linear intensity plot for the 50 wt% DIPEDMAMS/water system, at 25 °C. It is noticeable that the signal to noise ratio and the resolution of the scattering pattern are much lower compared to that taken at Diamond. The sample clearly shows two sets equally spaced Bragg peaks suggesting that the sample consists of two co-existing lamellar phases, as shown in the Diamond samples and discussed above. The beamstop in this system is slightly off centre, as a result the edge of the mainbeam can only be seen on the "left" hand side of the linear intensity plot. There is also a defect in the detector observed by a trough around 0.08 $Å^{-1}$. Due to these two issues the "left" side of the SAXS linear intensity plots will be used for ease of comparison with the Diamond scattering patterns.

SAXS linear intensity plots for 30 and 50 wt% surfactant samples being heated

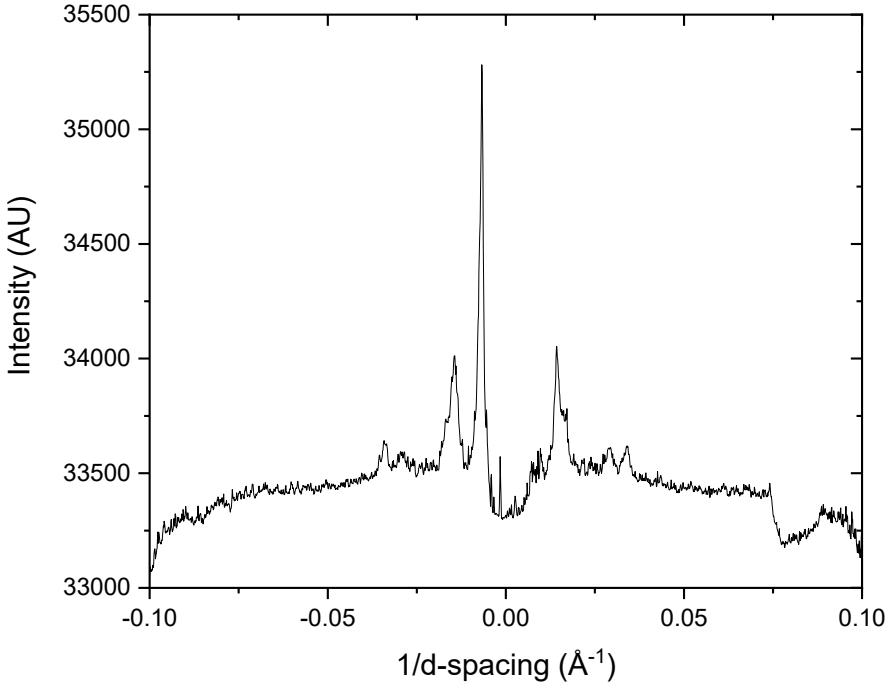


Figure 4.13: Structure of the DIPEDMAMS surfactant, where R is a fatty alkyl chain originating from a fatty acid mixture of C16, C18 and C18:1.

from 20 to 60 °C and then back to 20 °C are shown in figure 4.14. Immediately apparent from the BEDE SAXS data is that the peaks are less well defined than in the Diamond data. Not only is the intensity of the scattering lower, due to the lower intensity of the incident x-rays, but the peaks are much broader causing them to overlap to a greater degree than observed in the Diamond data. This is due to the poor collimation of the bench top beam in comparison to the synchrotron beam. On heating both samples show a similar pattern to what was observed in the Diamond data. Both show two sets of equally spaced Bragg peaks below 40 °C. These can be difficult to resolve due to the broadness of the peaks and the low the scattering intensity but the scattering. within error, is at the the same angle as observed in the Diamond data. On heating to 40 °C and above the 50 wt% surfactant sample exhibits only one set of equally spaced Bragg peaks whereas for the 30 wt% sample both sets of Bragg peaks are observable at all temperatures, as observed above. As with the Diamond scattering patterns the intensity of the scattering peaks increases and they sharpen as the temperature increases. The largest increase is between 35 and 40 °C similar to that observed before but the increased number of temperature intervals enables a narrowing of the temperature window in which this transition is observed.

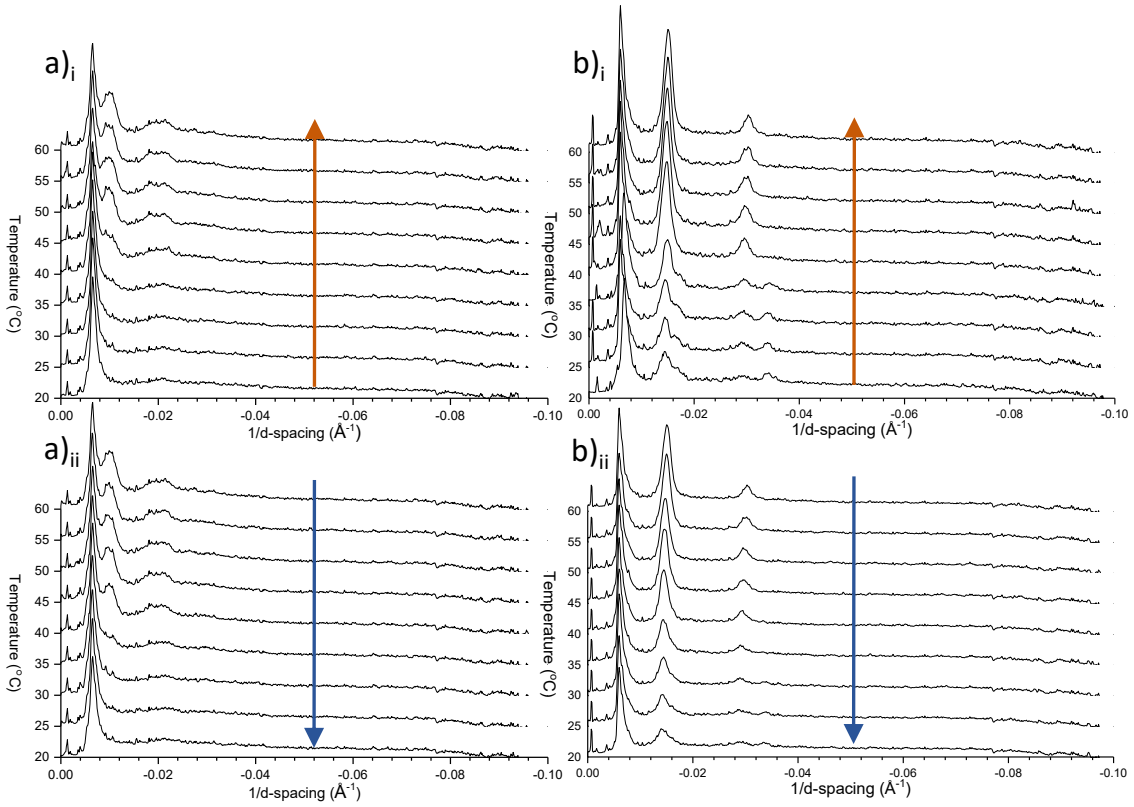


Figure 4.14: SAXS linear intensity plots of a) 30 wt% and b) 50 wt% DIPEDMAMS water systems with i) increasing and ii) decreasing temperature. Temperature range of 20 - 60 °C.

On cooling from 60 to 20 °C the intensity of the Bragg peaks decreases and the peaks broaden, for both samples. The 30 wt% surfactant sample shows two sets of equally spaced Bragg peaks at 60 °C which remain on cooling but become broader and less intense. The largest drop in intensity is observed when the sample is cooled from 45 to 40 °C. The 50 wt% surfactant sample shows a single set of equally spaced Bragg peaks at 60 °C reverting to two sets of equally spaced Bragg peaks on cooling. The transition from two sets to one set of Bragg peaks occurs between 40 and 35 °C, but due to the low scattering intensity it is difficult to resolve. As with the 30 wt% sample the peaks broaden and their intensity decreases on cooling with the greatest change observed between 40 and 45 °C.

This confirms some of the results seen in the Diamond data. Both 30 and 50 wt% form two co-existing lamellar phases before heating. On heating the 30 wt% surfactant system remains as two co-existing lamellar phases, whilst the 50 wt% system shows only one lamellar phase at and above 35 °C. Both samples appear to

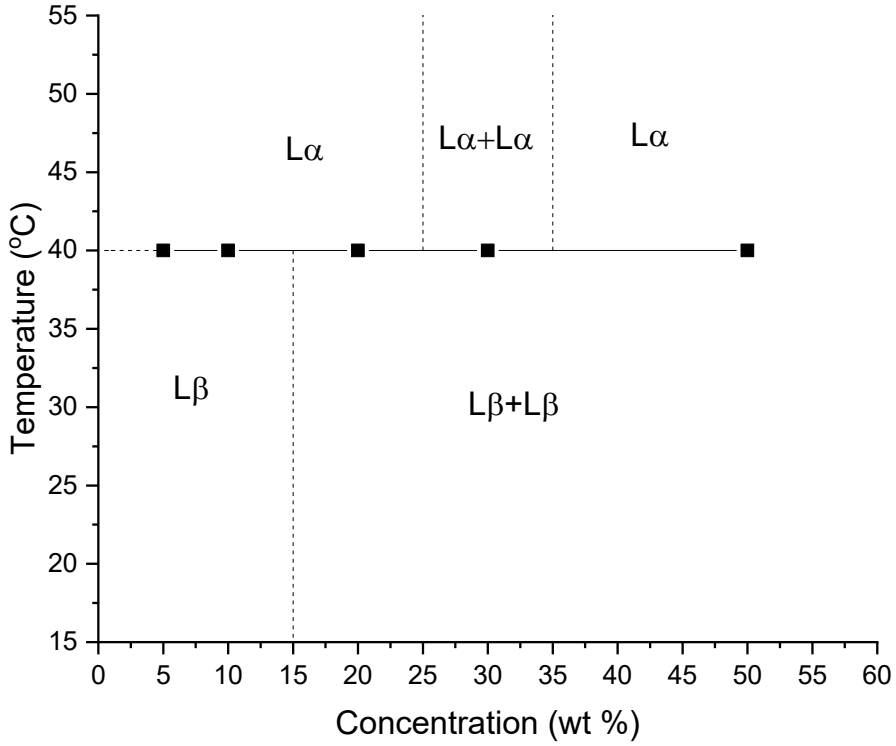


Figure 4.15: Proposed phase diagram for the DIPEDMAMS/water system as a function of surfactant concentration and temperature.

show some sort of transition between 30 and 35 °C where the peaks sharpen and the scattering intensity increases. This is also observed for the Diamond samples and is believed to be related to the transitions from the lamellar gel to lamellar fluid phase as indicated by the Diamond WAXS data. Once cooled back to 20 °C the samples exhibit an identical scattering pattern as to before heating, within error, revealing that the conformational changes caused by heating are reversible. The 50 wt% sample reverts to two co-existing lamellar phases. Unfortunately the WAXS data were not available with the bench top experimental set up but it is suggested that a similar pattern would be observed on cooling as on heating.

SAXS/WAXS Conclusions

Using the information obtained from both Diamond synchrotron experiments and the BEDE bench top experiments, it is possible to propose a phase diagram for the DIPEDMAMS/water system. From 5 to 50 wt% surfactant, and between 15 and

60 °C the system adopts one or two co-existing lamellar phases. Below 35 °C the lamellar phases adopted are the lamellar gel phase and when heated to 45 °C and above the system transitions into the lamellar fluid phase. Once cooled below 35 °C the system reverts back to the lamellar gel phase. There was no observed change in the transition temperature from the SAXS/WAXS data with changing surfactant concentration. At surfactant concentrations above 10 wt% two co-existing gel phases are observed up to 35 °C. Above 35 °C these are observed to melt forming a single continuous lamellar fluid phase except for the 30 wt% samples where two co-existent fluid lamellar phases are observed above 35 °C. On cooling the two lamellar gel phases reformed.

Due to low scattering intensity at low concentrations it is difficult to determine the ordered structures formed, if any, at these concentrations. An added difficulty is that if they do also form a lamellar phase the d-spacing would be so large as to push the Bragg peaks very close to the edge of the main beam. At 5 wt% the Bragg peaks are difficult to observe due to the factors mentioned but they are observable. Below 5 wt% there are no detectable SAXS peaks but the WAXS data does show the sharp gel peak at 0.24 Å^{-1} melting to a broad fluid peak, 0.22 Å^{-1}, as the temperature is increased over 35 °C. This suggests that there is some short range order between the surfactant molecules. Whether or not this corresponds to a lamellar phase with a large d-spacing is not known.

4.3.3 DSC of the DIPEDMAMS/water system

Differential Scanning Calorimetry was used to further probe the transition between the lamellar gel and lamellar fluid phases observed from the x-ray scattering experiments. DIPEDMAMS/water systems from 1 to 50 wt%, at the same surfactant concentrations as investigated in the x-ray scattering work, were studied. The samples were cycled between 15 and 55 °C for three cycles at a rate of 5 °C min^{-1}. No noticeable hysteresis was observed in any of the samples investigated.

On heating all samples show an endothermic transition between 35 and 45 °C and one or two endothermic transitions on cooling. From 5 to 10 wt% only one

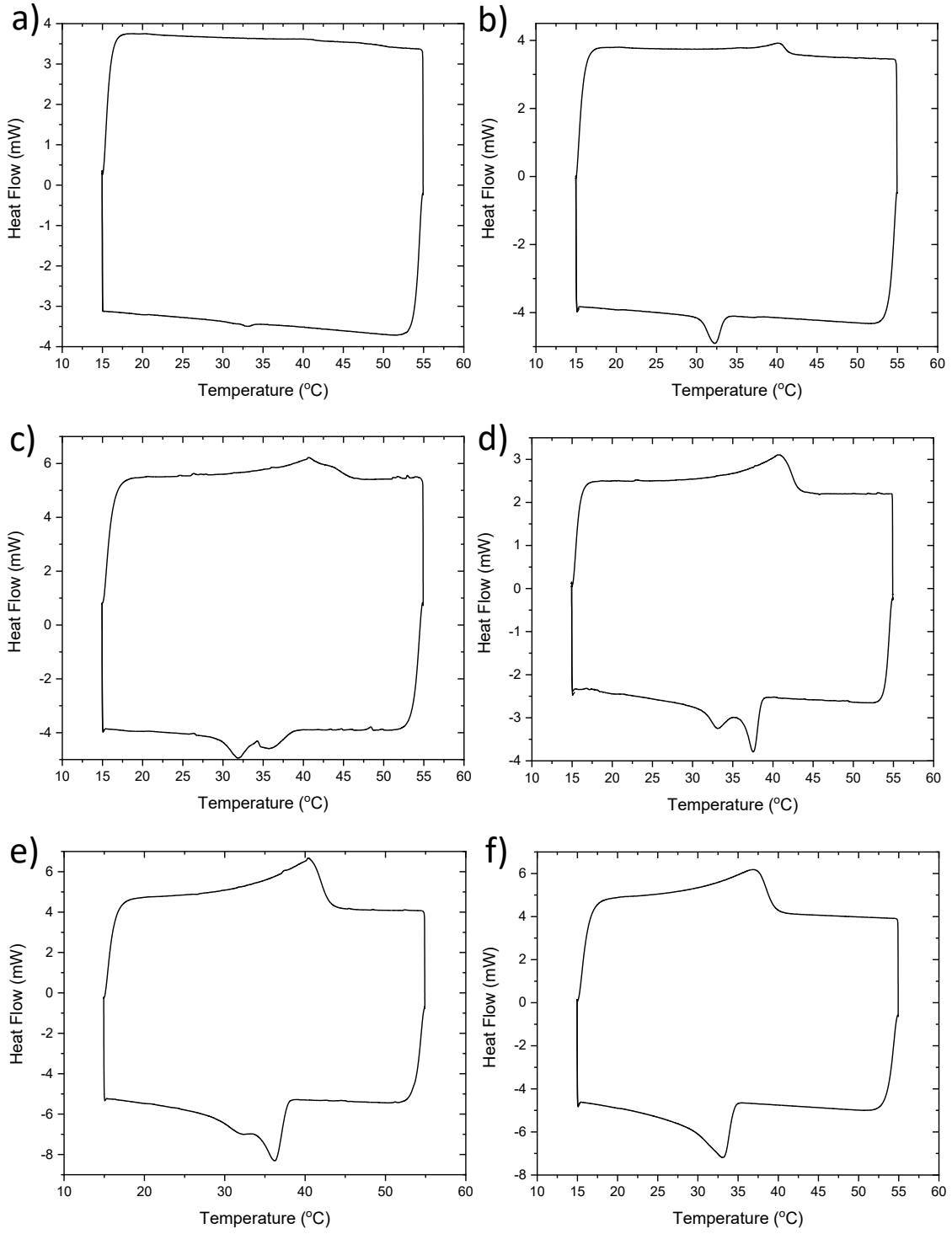


Figure 4.16: DSC curves for the DIPEDMAMS surfactant system at surfactant concentrations a) 1 wt%, b) 5 wt% c) 10 wt%, d) 20 wt%, e) 30 wt%, f) 50 wt%. Scan conducted at 5 °C min^{-1} between 15 and 55 °C. Scans shown are the second cycle.

transition is observed on both heating and cooling with the peak on heating being around 42 °C and the peak on cooling around 32 °C. The endothermic transition on heating has a rather gradual onset at all concentrations but becomes more noticeable as the surfactant concentration increases. At 1 and 5 wt% the transition on cooling is fairly symmetrical with the onset of the transition appearing to happen over similar temperature range as the end of the transition. Between 10 and 30 wt% two exothermic transitions are observed on cooling. One with a peak around 32 °C, possibly the same transition as observed for the 1 and 5 wt% samples, and the other with a peak around 37 °C. The height of both peaks increases as the surfactant concentration is increased from 10 to 30 wt% however the increase of the 37 °C transition is greater than that observed for the 32 °C transition. Whilst the onset of the 37 °C transition is comparative sharp, the end of the transition is poorly defined and very broad. This becomes more noticeable as the concentration increases. As a result of this, the 32 °C transition is observed only as a shoulder on the 37 °C peak at 30 wt%. As at 1 and 5 wt% a single endothermic transition is observed on heating for 10 to 30 wt% surfactant systems. The only notable observable change in this transition as the surfactant concentration is increased from 10 to 30 wt% is that intensity of the signal increases, the shape and position of the transition remains, within error, unchanged. At 50 wt% the endothermic transition on heating retains the distinctive shape observed at all other concentration of having a very gradual onset compared to the end of the transition, but the whole peak has shifted from 45 °C, as observed at lower concentrations, to 38 °C. On cooling, a single large exothermic transition is observed with a sharp onset with the end of the transition being very broad and difficult to define, similar to the transition at 37 °C observed between 10 and 30 wt%. A second exothermic transition, as observed between 10 and 30 wt%, is not observed. However this could be present but hidden by the larger transition as at 30 wt% the second transition is only just observable as a shoulder on the larger 37 °C transition. As with the endothermic transition on heating for 50 wt%, the endothermic transition is observed at a slightly lower temperature of 33 °C compared to the transition at lower surfactant concentrations.

The endothermic transition observed on heating corresponds to the lamellar gel to lamellar fluid transition observed in the x-ray scattering data. The x-ray scattering data placed this transition between 35 and 45 °C the DSC data supports

this observation with the gel to fluid transition occurring at 42 °C. At 35 °C the WAXS showed the lamellar gel and fluid phases co-existing it is likely that this is linked to the broad onset of the transition observed in the DSC data. The sample has begun transitioning from the gel phase to the liquid phase but will not be completed until the temperature is raised above 42 °C. Broad DSC transitions are usually indicative of an impure sample, as the aliphatic tails of the DIPEDMAMS surfactant system are a statistical mix of C18, C18:1, and C16 the samples are inherently a mixture.

The observed increase in the size of the exothermic transition on heating, with increasing surfactant concentration is related to the mass of surfactant present in the system. DSC, as discussed in section 3.5, measures the difference in energy required to heat the sample and a reference pan at the same rate. As the transitions observed here are the result of the melting of the surfactant tails the amount of energy required for the sample to transition from the gel phase to the liquid phase is dependent on the mass of surfactant present. The decrease in the transition temperature observed in the DSC curve for the 50 wt% DIPEDMAMS/water system was not observed in the Diamond data as the transition still falls within the 35 to 45 °C window. However the BEDE data does provide some corroborating evidence. From figure 4.14 it is noted that the largest change for the 30 wt% surfactant sample occurs between 40 and 45 °C whereas at 50 wt% the melting from two lamellar phases to one lamellar phase takes place between 35 and 40 °C. Unfortunately, as mentioned before, the WAXS was unavailable for the BEDE experiments. The cause of the change in the transition temperature at 50 wt% is not understood as there are no obvious changes in the lamellar structure as observed in the small and wide angle scattering data.

The exothermic transitions observed on cooling are believed to be caused by the transition from the lamellar fluid back to the lamellar gel phase. At low surfactant concentrations, < 10 wt%, only one transition is observed at 32 °C and is generally symmetrical in comparison to the endothermic transition on heating suggesting the transition from fluid to gel is more homogenous than the melting from gel to lamellar. The second exothermic transitions observed for surfactant concentrations 10 and 30 wt% suggests that either, the transition from fluid to gel is a two step process, or there are two transition from the fluid to the gel phase. From the SAXS studies 20

wt% and above DIPEDMAMS/water system adopt two co-existing lamellar phases it is proposed that the two transitions could be for each lamellar gel phase however only one lamellar gel phase at room temperature was observed at 10 wt%. It is however possible that the 10 wt% samples do form two co-existing lamellar phases but are not distinguishable in in the SAXS due to the low intensity of the scattering. The increase in the intensity of the 37 °C peak at the expense of the 32 °C peak is potentially caused by one gel phase dominating over the other with increasing concentration hence this transition is dominant in the DSC curves. As the 50 wt% samples clearly show two co-existing lamellar gel phases which have been shown to re-emerge on cooling it is suggested that both transitions are present but the broad nature of the 37 °C transition means that the 42 °C transition is difficult to observe.

4.3.4 Effect of Temperature on supported bilayers

Later in the project the facility became available to controllably heat the AFM sample stage. This allowed the supported surfactant bilayers to be imaged as a function of temperature. This facilitated the investigation of the structure of the supported bilayers as a function of temperature enabling the comparison of the phase behaviour of the supported bilayers with the bulk lamellar system.

Mica supported DIPEDMAMS surfactant bilayers were formed by the vesicle deposition method as discussed in Chapter 3. For each bilayer the same area of the surface was imaged at each temperature. Two image sizes were used; one measuring 20 x 20 µm, and the other measuring 5 x 5 µm. The drift between images made the 20 x 20 µm images more consistent as the temperature was increased.

Topographical AFM images, 20 x 20 µm are shown along side maps of the tip-sample adhesion and measured slope of mica supported DIPEDMAMS bilayers are shown in figure 4.17 for increasing temperature and figure 4.18 with decreasing temperature. Figures 4.19 and 4.20 show 5 x 5 µm topographical images with associated cross sections with increasing and decreasing temperature.

At 25 °C the DIPEDMAMS bilayers show two regions differing in height by 1 -

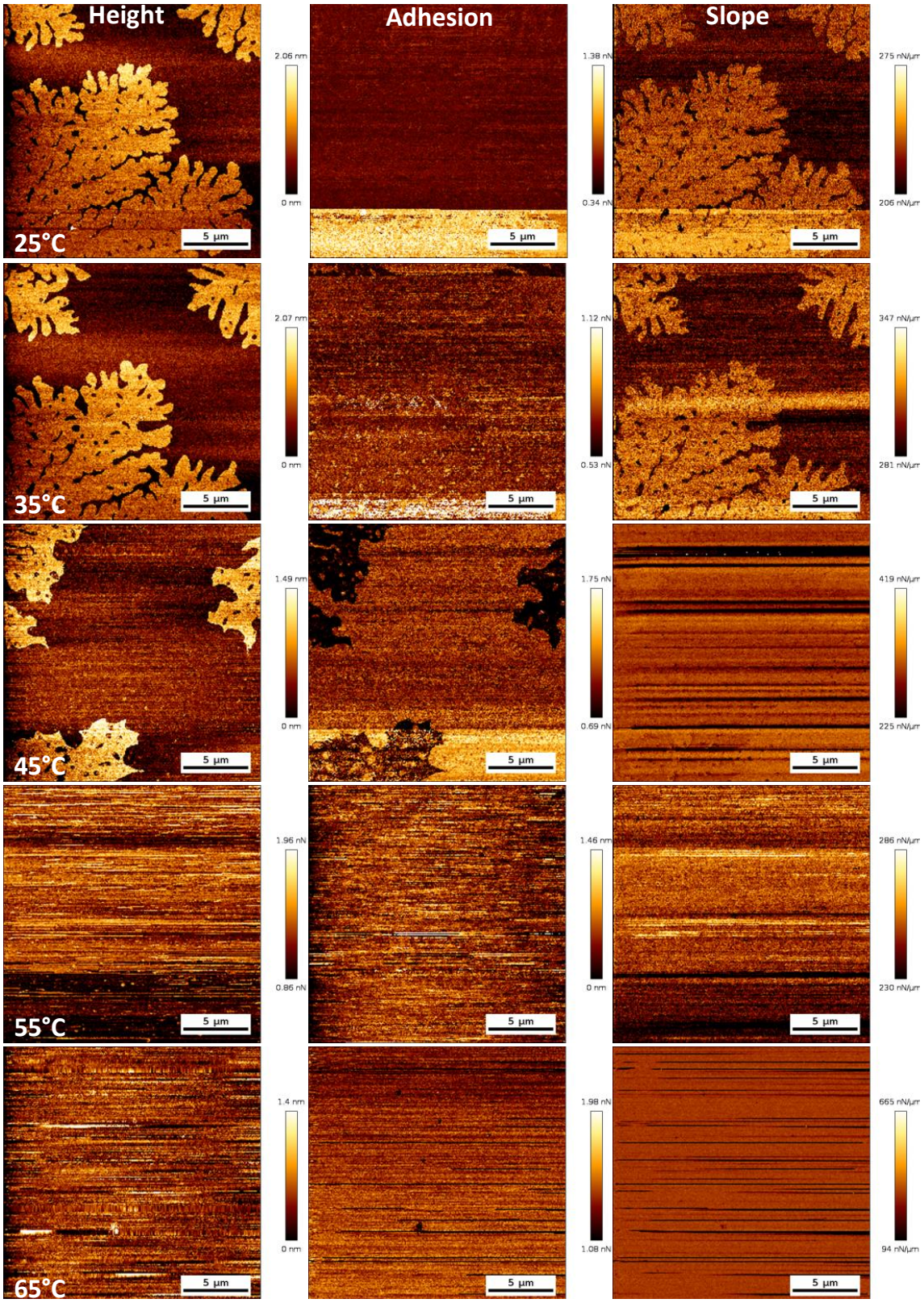


Figure 4.17: Typical QI AFM topographical images, with associated typical maps of surface adhesion and measured slope, for DIPEDMAMS bilayers on mica with increasing temperature from 25 - 65 °C.

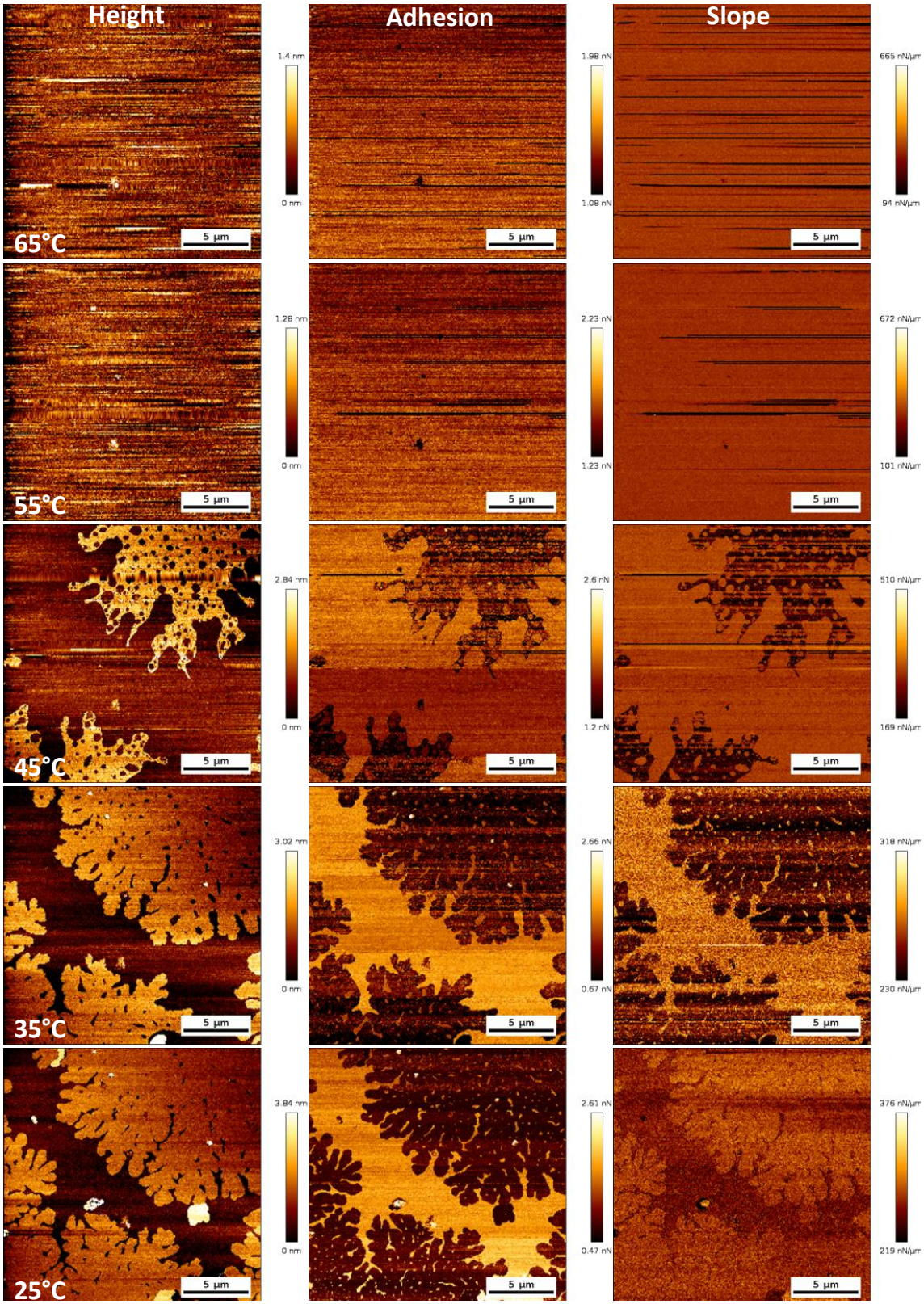


Figure 4.18: Typical QI AFM topographical images, with associated typical maps of surface adhesion and measured slope, for DIPEDMAMS bilayers on mica with decreasing temperature from 65 - 25 °C.

1.5 nm. This is suggested to be the result of the supported bilayers adopting two different structural confirmations or phases. This is supported by the SAXS/WAXS data which show the co-existence of two lamellar phases in the bulk system. The adhesion image has not resolved well due to the probe picking up some form of contaminate during the scan. The 5 x 5 µm image for this temperature however does show that the thicker region is less adhesive than the thinner regions as discussed earlier. The measured slope maps, analogous for the local relative stiffness of the sample, show the thicker regions as stiffer than the lower regions, as previously discussed.

As the temperature increases to 25 °C there is a possible reduction in size of the thicker region but this is difficult to judge due to drift between images. Adhesion maps are still plagued by the probe picking up contaminants as it images, however the 5 x 5 µm images show no significant change between the relative adhesion of the different phases compared with the images taken at 25 °C. No significant change is observed from the measured slope images as the temperature is increased from 25 to 35 °C.

At 45 °C whilst the samples still exhibit two distinct bilayer phases the area covered by the thicker phase has reduced significantly leaving the majority of the mica covered by the thinner bilayer phase. No significant changes are observed in the adhesion maps at 45 °C, the thinner bilayer still exhibits a higher tip to sample adhesion than the thicker phase. The slope map for this image is comparatively poor quality however it does suggest that the relative stiffness of the thicker phase has decreased and is now lower than the thinner phase. This is supported by complimentary 5 x 5 µm images that show the thinner phase as having a higher measured slope than the thicker phase.

Above 55 °C the supported bilayers appear to be rather featureless. It is suggested that this is due to the surfactant bilayers adopting a single continuous lamellar phase. The surface does however appear to be rougher compared to either of the bilayer phases at room temperature. It is not certain if this is a real effect or if it due to the increased thermal noise at these elevated temperatures. No significant changes were observed on further heating to 65 °C.

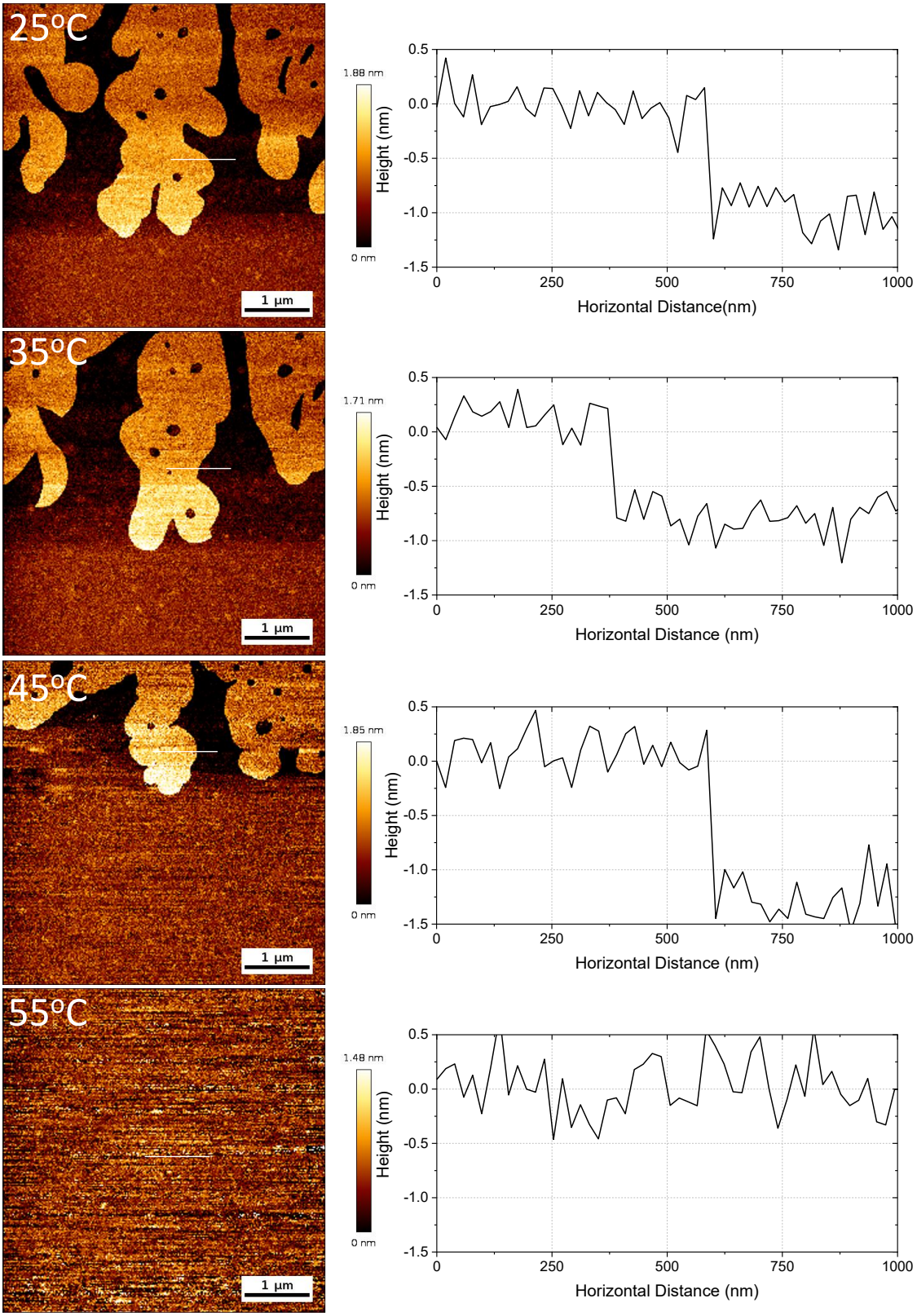


Figure 4.19: Typical 5 x 5 µm QI AFM topographical images, with associated cross-sections, for DIPEDMAMS bilayers on mica with increasing temperature from 25 - 55 °C.

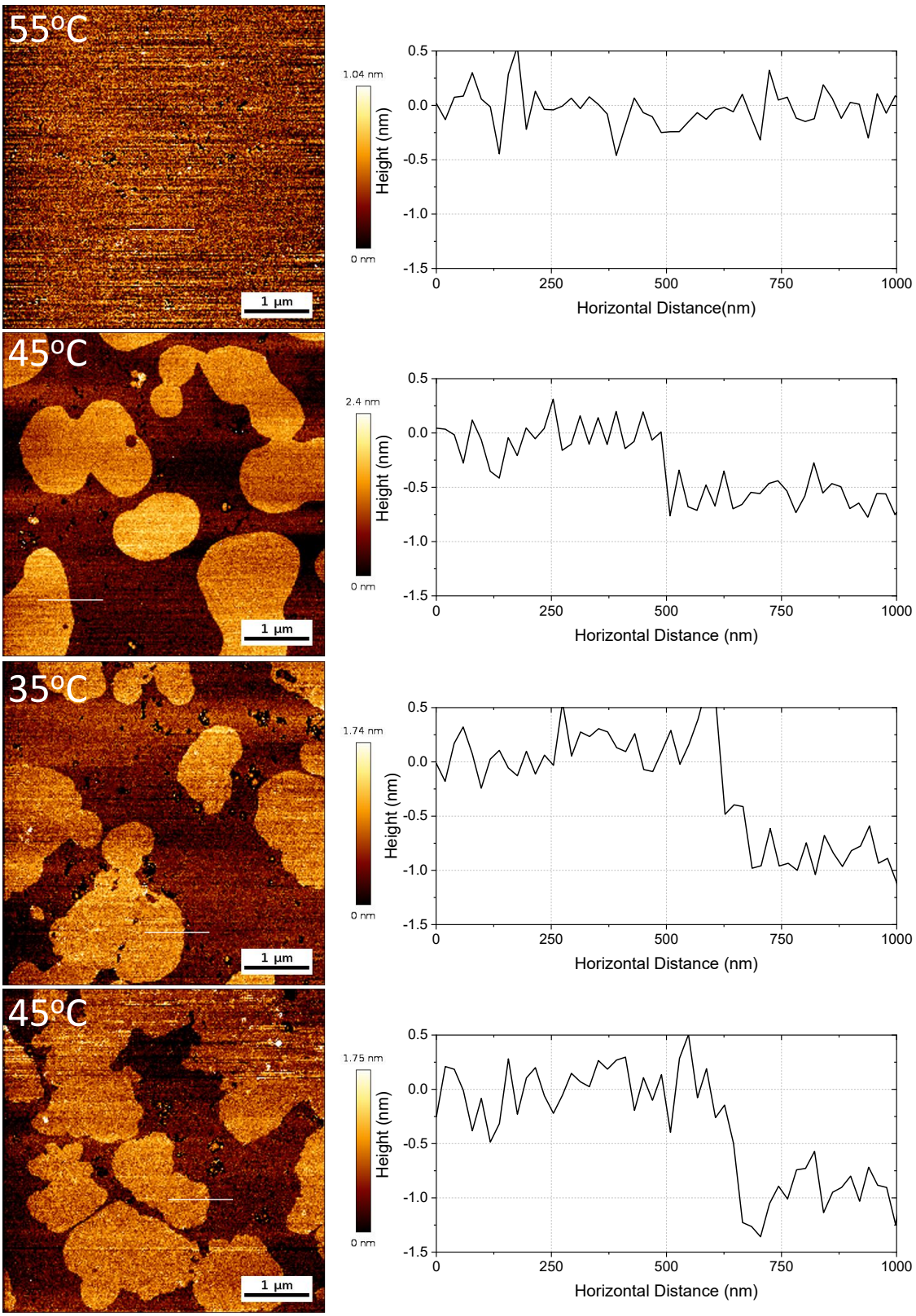


Figure 4.20: Typical 5 x 5 µm QI AFM topographical images, with associated cross-sections, for DIPEDMAMS bilayers on mica with decreasing temperature from 25 - 55 °C.

On cooling to 45 °C, shown in figure 4.18 the bilayer is once again observed to separate into two distinct bilayer phases differing in thickness by 1 - 1.5 nm. Once again it is observed that the adhesion is lower for the thicker phase than the thinner phase. However the maps of the measured slope show the thicker phase to be less stiff than the thinner phase. This was observed on heating at 45 °C but not at room temperature before heating.

The area covered by the thicker bilayer phase has increased on cooling to 35 °C. The adhesion remains as before, being higher for the thinner phase than the thicker. The measured slope shows the thicker phase as softer than the thinner. As with the samples on both heating and cooling at 45 °C but in contrast to the sample at 35 °C before heating.

Once cooled back down to 25 °C the area covered by the thicker region has increased slightly in comparison to the sample at 35 °C. The adhesion properties remain unchanged with the thicker region being less adhesive than the lower. The measured slope maps now show a similar relationship between the two phases as observed before heating at 25 °C where the thicker region has a higher measured slope, comparative stiffness, than the lower region.

The observation of two bilayer phases at room temperature which rearrange to form a single continuous bilayer phase at elevated temperature and reverting to a two phase configuration after cooling fits well with the observation from the SAXS/WAXS data of the bulk lamellar samples at concentrations above 20 mol%. The onset of this transition, on heating, for the supported bilayers appears to be between 35 and 45 °C and is completed between 45 and 55 °C. For the bulk lamellar system appears to transition between 35 and 45 °C with only one lamellar phase observed at 45 °C.

On cooling the onset clearly lies between 55 and 45 °C however it is not clear if the transition has been completed between 45 and 35 °C or 35 and 25 °C. Whilst little further change in the topography is observed between 35 and 25 °C on cooling the relative stiffness of the two phases suggests that the transition has only been completed after further cooling to 25 °C. In contrast the SAXS/WAXS data only

shows the reappearance of the two bilayer phases between 35 and 25 °C. Looking at the slope maps it is possible to suggest that the temperature does need to be lower than the initial onset of transition on heating for the two phases to fully re-appear and have the same properties as before heating. The transition does appear to happen over a much broader temperature range and at a slightly increased temperature compared to the bulk lamellar phase.

It is likely that the substrate of the supported surfactant bilayers does have some impact on the structure and therefore the transition and transition temperature of the DIPEDMAMS bilayers. Interactions between the surfactant head groups and the substrate may affect the electrostatic repulsion between the head groups impacting the overall packing order of the supported bilayers compared with bilayers in the bulk system. A change in the packing of the bilayers may result in changes to the physical properties of the system such as the transition temperature. However, the supported bilayers do exhibit very similar temperature dependent behaviour to that observed in the SAXS/WAXS studies of the bulk system. Whilst the behaviour of the supported bilayers in response to changes in temperature was not identical to that observed for the bulk lamellar samples it never the less follows a very similar behaviour. Therefore it is suggested that the supported surfactant bilayers are a good facsimile for understanding DIPEDMAMS bilayers, it must be noted that the exact temperatures and ranges of any thermally induced transitions will be affected by the supported nature of these bilayers.

On heating to 45 °C a change in the relative stiffness of the thicker bilayer phase is observed. The thicker phase appears to be softer than the thinner phase. This is also observed on cooling. One possible explanation for this observation is that the thicker phase has undergone a change in its internal packing or arrangement resulting in a decrease in the stiffness of the bilayer. This change in arrangement then result in the decrease in the bilayer thickness as the once thicker phase appears to merge with the thinner phase as the temperature continues to increase. It is unclear whether or not the thinner phase is also going through a transition which the thicker one also goes through with them both adopting the same phase and configuration at high temperature or if the thicker phase is melting to join the thinner phase with the thinner phase remaining unchanged.

The force data do however show a softening of the thinner phase at higher temperatures suggesting that it also goes through a transition from most likely the gel phase to the fluid phase, as suggested by the SAXS/WAXS data. It is not possible to determine if there is a change in the thickness of this bilayer phase with the transition from gel to fluid but the SAXS/WAXS data suggests that if there were a change this change would be minimal.

Conclusions of the effect of temperature on supported bilayers

In conclusion the AFM imaging data of the supported DIPEDMAMS bilayers with temperature shows that the supported bilayers behave in a similar manner as the bulk lamellar phases as observed by small and wide angle x-ray scattering. The supported bilayers under go a similar structural re-arrangement as a function of temperature as the bulk samples. However the transition temperature and the breadth of the transition are subtly different for the supported bilayers when compared with the bulk samples. Whilst this suggests that the mica substrate has some effect on the structure of the bilayers it does not appear to impact on the overall pattern enabling the conclusion that supported surfactant bilayers are a good analogue for isolated lamellar bilayers.

4.4 Conclusions

At room temperature DIPEDMAMS/water systems adopt a lamellar gel phase from 5 to 50 wt% concentration. At 20 wt% and above two co-existent lamellar gel phases are observed. These phases differ in d-spacing by 1.2 ± 0.2 nm. The d-spacing for both of these phases decreases with increasing surfactant concentration.

An experimental value for bilayer thickness was obtained by plotting d-spacing against water concentration, as opposed to surfactant concentration and extrapolating to zero water content. This gives an experimentally determined bilayer thickness of 4.3 ± 1.8 nm. This compared well with a theoretical value of 4.4 nm and with

literature values for similar surfactant systems.

On heating the system under goes a phase transition from a lamellar gel to a fluid lamellar phase around 35 °C. This is observed for all concentrations from 5 wt%. The samples showing two co-existing lamellar phases at room temperature tend to only show one lamellar fluid phase above the transition temperature, with the 30 wt% samples showing two lamellar fluid phases at high temperature. On cooling the two lamellar gel phases reappear.

AFM imaging of supported DIPEDMAMS bilayers was used the compare the structure of the supported bilayers with the observations from the bulk surfactant/water systems as studied by SAXS/WAXS. Supported bilayers of DIPEDMAMS exhibited some form of phase separation. They formed two distinct bilayer phases separated by a height difference of 1 - 1.5 nm, suggesting one phase to be thicker than the other. This was observed on both glass and mica. As QI mode enabled maps of the surface adhesion and relative stiffness to be acquired alongside the standard topographical AFM images. These images suggested that the thicker bilayer phase was stiffer in comparison to the thinner phase and was less adhesive on retraction than the thinner phase. This two phase expression is consistent with the SAXS/WAXS data which show, at higher concentrations, two co-existing lamellar gel phases with a difference in d-spacing of 1.2 ± 0.2 nm. This difference in d-spacing being similar to the difference in thickness of the two supported bilayer phases.

On heating the supported DIPEDMAMS bilayers a transition from two co-existing lamellar phases to a single continuous lamellar phase was observed around 40 °C. On cooling the sample was observed to transition back into two discrete bilayer phases. Overall this observation from the supported bilayers fits well with the overall trend observed from the SAXS/WAXS data. However the transition temperature and the range over which the transitions occur does appear to be subtly different between the support bilayers and the bulk surfactant/water systems. Whilst the exact temperatures of the transition may show some variation between the supported and bulk samples the over all behaviour and trends compare well. It is therefore concluded that supported DIPEDMAMS bilayers on mica are a good facsimile for DIPEDMAMS bilayers.

Chapter 5

Measuring the Interactions between Supported Cationic Surfactant Bilayers

5.1 Introduction

As discussed in section 2.4 supported amphilphile bilayers have been used with both the SFA and the colloidal probe AFM technique to study the interactions between lipid and surfactant bilayers as model systems for the interactions between vesicles within an aqueous dispersion. [203, 234, 256–259] This has enabled the direct measurement of DLVO forces, depletion, steric and other interactions between bilayers. [172, 177, 260] This requires the formation of stable surfactant bilayers, with good surface coverage, on both mica sheets, for the SFA, or on both the colloidal probe and the mica substrate for the colloidal probe technique.

Supported bilayers have been used through out the literature as models for both lipid and surfactant membranes. [144, 261–267] They are generally formed by one of two methods, the Langmuir-Blodgett trough, and the vesicle deposition technique. [268, 269] Whilst Langmuir-Blodgett deposition could be used to form sup-

ported bilayers on mica sheets, the technique is not well suited for forming bilayers on colloidal probes, therefore the vesicle deposition method was the most suitable method for forming bilayers on both mica substrate and colloidal probe for CP-AFM studies. Bilayers are generally formed from vesicle dispersions where the vesicles are above their transition temperature. [270] The bilayers are in the fluid phase. Most natural lipid systems are fluid at room temperature, but when T_m is above ambient the samples are general incubated at a temperature above their melting point to form the supported bilayers. As discussed in Chapter 4 the chain melting temperature of the DIPEDMAMS surfactant system is between 35 and 40 °C, with the facility to heat the AFM stage only becoming available later in the project, surfactant bilayers for colloidal probe AFM had to be formed at room temperature.

In this chapter we begin to develop methodologies to measure the interactions between the supported cationic surfactant bilayers formed at the end of the previous chapter. These bilayers need to be formed not only on a flat substrate but also on a glass bead as part of a colloidal AFM probe. The temperature at which bilayers are formed is identified as a key issue with the formation of DIPEDMAMS bilayers on both the substrate and the colloidal probe.

Below the transition temperature only patchy bilayers could be formed therefore an investigation into methods to reduce the transition temperature of the surfactant system by the addition of alkyl alcohols was carried out. Whilst the main objective of this investigation was to form supported surfactant bilayers with good surface coverage at room temperature, the impact of the alkyl alcohol additives on other properties of the system was also investigated. The bulk phase behaviour of alkyl alcohol/surfactant/water system was investigated by small and wide angle x-ray scattering was investigated and the nanomechanical properties of the supported bilayers were also investigated by force spectroscopy. Enabling the comparison of the room temperature formed systems with the pure DIPEDMAMS bilayers formed at 65 °C to judge the technique's suitability as a method for forming bilayers at room temperature.

Finally DIPEDMAMS bilayers were formed on both the probe and the flat substrate simultaneously at room temperature enabling the measurement of interactions

between supported cationic vesicles. Both mica and glass were investigated as the flat substrate for use in colloidal probe force spectroscopy studies.

5.2 Experimental

5.2.1 Preparation of Alkyl Alcohol Modified DIPEDMAMS Systems

DIPEDMAMS/alkyl alcohol/water systems for x-ray scattering and DSC studies were prepared by the methods described in Chapter 3. Samples were hydrated to 20 wt% by mass.

5.2.2 Differential Scanning Calorimetry

Experiments were performed using a Perkin-Elmer Diamond DSC. Sample mass of 3 - 5 mg using aluminium TZero pans from TA instruments. For each sample three cycles were run between 15 to 55 °C at a rate of 5 °C min^{-1}. Samples run against an empty sample pan for reference, see Chapter 3.

5.2.3 Small and Wide Angle X-ray Scattering

SAXS and WAXS were performed at the Diamond Light Source (Oxfordshire) on beamline I22, as detailed in Chapter 3.

5.2.4 Atomic Force Microscopy

All measurements were made using a JPK Nano wizard 4 AFM and analysed using the JPK data processing software as detailed in Chapter 3

Preparation of Supported Surfactant Bilayers

Supported surfactant bilayers were formed by the vesicle deposition technique from a DIPEDMAMS/alkyl alcohol vesicle dispersion as described in Chapter 3.

AFM Imaging

All imaging was performed in quantitative imaging (QI) mode. Multiple images of different areas of each supported bilayer were collected. Further details on QI mode and on the imaging protocols can be found in Chapter 3.

Force Spectroscopy

Multiple force measurements were performed against the supported bilayer samples using sharp imaging probes. Forces were measured against each of the different areas of the samples observed during imaging. Further details on the force spectroscopy protocols can be found in Chapter 3.

Bilayer-Bilayer Interactions by Colloidal Probe Force Spectroscopy

Multiple force measurements were collected for each sample in an 8 x 8 grid with a constant approach and withdrawal velocity of 1 µm s^{-1}, as detailed in Chapter 3. Force curves were collected both before and after the formation of supported DIPEDMAMS bilayers.

5.3 Results and Discussion

5.3.1 Issues with formation of bilayers on probe

Bilayers have shown to be easy to form on several well known substrates. However until now they have all been formed at 60 °C, above the gel to fluid transition temperature of the system. Bilayers can be formed on the substrate with ease by placing the sample in the oven, allowing to cool then washing to remove any unadhered vesicles. This kept the bilayers hydrated at all times, as dehydration is likely to damage or destroy them. [271] This is difficult if not impossible to achieve when the probe has to cross the water-air boundary on mounting, as this damages the bilayer.

It was decided that the best way to form bilayers on both a colloidal probe and a flat substrate was to form the bilayers in situ within the aqueous AFM imaging environment. This would remove the possibility of the bilayers dehydrating and ensure symmetry of the bilayer formation for the probe and the substrate. Initially the ability to heat the liquid AFM environment was not available. (The facility to heat the sample stage was available towards the end of the project) Therefore DIPEDMAMS bilayers needed to be formed at room temperature.

DIPEDMAMS bilayers can be formed at room temperature but unlike the bilayers formed at temperature they tend to be patchy and the surface coverage is almost always incomplete. Figure 5.1 shows a DIPEDMAMS bilayer formed on mica at room temperature. Two clear domains are observed similar to the 60 °C formed bilayers in figure 5.1 however as can be seen from the cross-section the height difference is 3.5 - 4 nm. As this is roughly the theoretical bilayer thickness as calculated from the SAXS data it is believed that the lower domain is bare mica and the higher domain is the bilayer. This is further supported by the stiffness and adhesion maps showing the lower phase as much stiffer than the higher phase. The QI force curves for the lower section also bear much more of a similarity to those for bare mica and the curves for the upper phase showing similar features to those for the bilayers formed at temperature. It is argued that raising the vesicles above

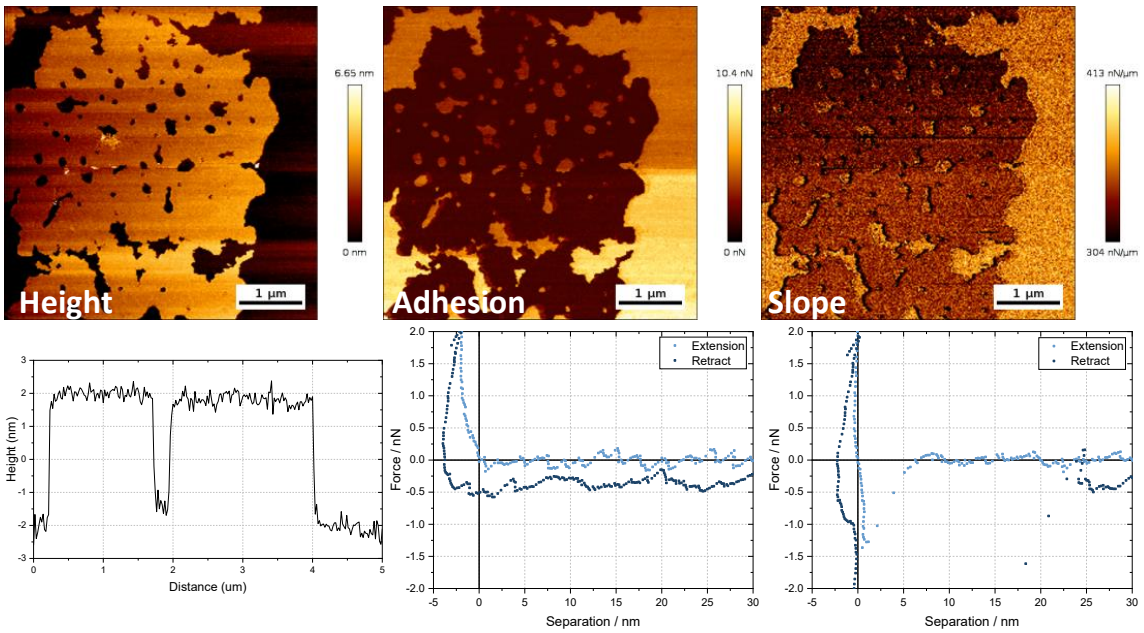


Figure 5.1: DIPEDMAMS bilayer formed at room temperature on freshly cleaved mica. Imaging was done in QI mode and the topographical, adhesion and measured slope maps are shown. A crossection of the topographical image is included as well as an example of the QI force curves for upper (left) and lower (right) regions.

the transition temperature aids bilayer formation. [272–275]

Even though the bilayers were patchy the surface coverage was always greater than 50%. If this were achieved on the probe as it was on the mica substrate it maybe be possible to measure the interaction between the bilayers if averaged over an area of the surface to avoid mica bilayer interactions. Formation of DIPEDMAMS surfactant bilayers on both the mica substrate and the glass colloidal probe in situ at room temperature was not successful. As can be seen in figure 5.2, the forces measured between the clean glass colloidal probe and freshly cleaved mica in DI water are repulsive. This is as predicted. The surface of mica in an aqueous environment has an intrinsic negative charge, glass also has a slight negative surface charge at neutral pH. [276, 277] Therefore a repulsive Coulombic interaction is observed as the surfaces approach one another. If DIPEDMAMS bilayers were successfully formed on both the substrate and the probe a repulsive interaction would be expected on approach. However as observed in figure 5.2 the forces are attractive. These attractive interactions are fairly long range, the onset observed at separations between 60 and 80 nm. This is too long range for the van der Waal's forces so it is

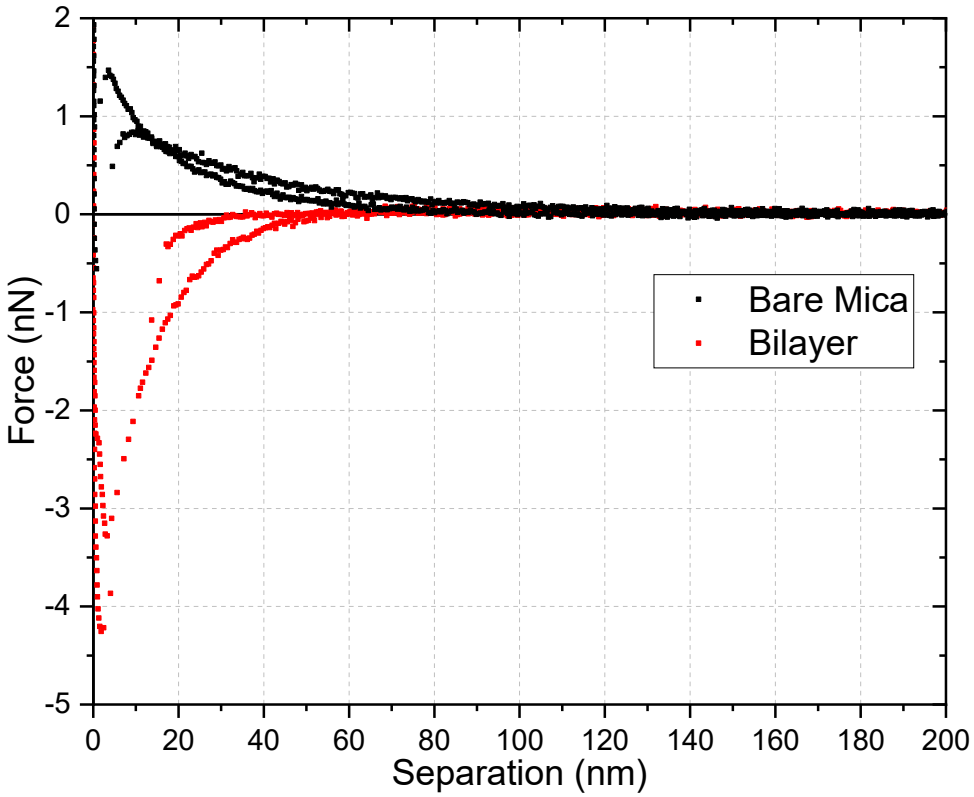


Figure 5.2: Approach force distance plots of the interaction measure between a glass colloidal probe and mica both before and after incubation with a DIPEDMAMS vesicle dispersion at room temperature.

believed to be due to attractive Coulombic interactions suggesting that the probe and and mica are oppositely charged. Either a bilayer has not been formed on the probe but a patchy one has been formed on the mica, as shown in figure 5.1, or ratio of covered to bare surface is sufficiently different on the two surfaces to result in an overall attractive interaction. This holds as the probe is moved to different points on the surface.

These attractive interactions suggest that bilayers can not be successfully formed on both probe and substrate below the transition temperature. As the facility to heat both probe and sample in situ did not exist at this time it was hypothesised that if the transition temperature could be lowered to room temperature then bilayers could be formed in situ on both probe at substrate at room temperature.

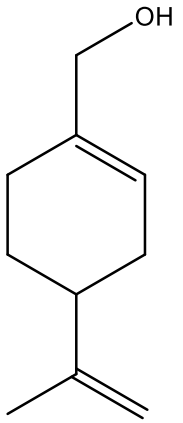


Figure 5.3: Structure of perillyl alcohol.

5.3.2 Alkyl Alcohol Modification

In an attempt to control the transition temperature of the DIPEDMAMS/water system the role of alkyl alcohols on the properties of lipid bilayers was considered. It is well known that saturated long chain alkyl alcohols will insert into a lipid or surfactant bilayer creating more ordered regions and structures which causes an increase in the gel to fluid transition temperature [278, 279] Whereas unsaturated long chain alkyl alcohols, once inserted into the membrane, can disrupt the local packing of a bilayer, fluidising it and reducing the transition temperature. [280, 281]

Small chain alkyl alcohols conversely have been demonstrated to decrease the transition temperature of lipid and surfactant bilayers. The small chain alkyl alcohols neither penetrate nor become incorporated in the bilayers they remain in the aqueous phase acting as a co-solvent or solvatrope. [282–284] The short chain alkyl alcohols decrease the dielectric constant of water essentially making the water more hydrophobic. This decreases the interfacial tension between the aqueous phase and the aliphatic chains ultimately decreasing the ordering of the hydrocarbon tails. [285, 286] This results in a decrease of the transition temperature. It was proposed that, as the short chain alkyl alcohols resided in the water, when the supported bilayers were washed to remove any excess vesicles that the alcohol would be removed restoring the bilayer ordering. It was hypothesised that this would result in similar bilayers to those formed above the transition temperature then allowed to

cool back into the gel phase before imaging.

Another potential method for reducing the transition temperature of the DIPED-MAMS/water system would be to use a hydrotrope. A hydrotrope is a compound that increases the aqueous solubility of a second poorly soluble component. [287] It is predicted that the addition of a hydrotrope to this system would result in a similar affect to the addition of a solvatrope. However the hydrotrope would act upon the surfactant bilayers decreasing the hydrophobicity of the alkyl chains as opposed to a solvotrope which acts upon the solvent making it more hydrophobic. This results in a weakening of the alkyl chain interactions, increasing their thermal motion and ultimately resulting in a reduction of the transition temperature. [288]

The alkyl alcohols investigated were hexadecanol, decanol, 9-decenol, pentanol, ethanol, and perillyl alcohol. The structure of perillyl alcohol is shown in figure 5.3. Hexadecanol was likely to insert into the bilayers, stiffening them and increasing the transitions temperature this having no practical use for the method development it was useful to observe if long chained alkyl alcohols affected the system as predicted. Decanol and 9-decenol were also predicted to reside in the bilayer but enabling us to look at the effect of chain length and unsaturation as a potential path to explore. Pentanol and ethanol, examples of short chained alkyl alcohols, are hypothesised to act as co-solvents or solvatropes increasing the fluidity of the bilayers and reducing the transition temperature. Perillyl alcohol is believed to act as a hydrotrope and provide another method to reducing the transition temperature.

The alkyl alcohol ratio was initially set at 10 mol% with respect to the surfactant with the overall surfactant and alkyl alcohol concentration at 10 wt% in D.I. water. This allowed an investigation into the impact of each of the alkyl alcohol and to give an idea of their efficacy. It would then be possible to further investigate any alkyl alcohol which appeared promising in reducing the transition temperature towards room temperature.

Alkyl Alcohol Modification: DSC

The DSC curves of 10 wt% DIPEDMAMS/water systems containing 10 mol% alkyl alcohol are shown in figure 5.4. It is observed that the addition of the alkyl alcohols does have an effect on the transition temperature of the surfactant system. All samples show a large broad onset of the transition temperature due to the mixed nature of the surfactant sample. As expected, the hexadecanol doped sample shows a large increase in the transition temperature of the system. The gel to fluid transition increased from 35 - 40 °C to 45 - 50 °C. Samples with 10 mol% pentanol and ethanol exhibited no significant change in the transition temperature with the transition temperature for both samples being between 35 and 40 °C. The surfactant samples doped with n-decenol, decanol, and perillyl alcohol all exhibited a significant decrease in the gel to fluid transition temperature. Decanol and 9-decenol appear to be similarly effective reducing the transition temperature down to between 25 and 30 °C. Perillyl alcohol appear to be the most effective in reducing the transition temperature down to 20 - 25 °C.

The increase in the transition temperature with the addition of hexadecanol was predicted and serves to show that the longer alkyl alcohols are successfully being incorporated into the bilayer. As discussed above this is due to the stiffening of the bilayer by the insertion of the long chain alkyl alcohol. Due to increased van der Waal's and hydrophobic interactions between the alkyl chains.

Pentanol and ethanol were both predicted to exist in the aqueous phase between the bilayers and act as a co-solvent or a solvatrope. This was predicted to reduce the transition temperature. However this was not observed. Instead the transition temperature remained virtually unchanged. It is not known whether this is due to the effect of these being minimal in comparison to other alkyl alcohols or if the effect requires a much greater fraction of these alcohols to be effective. [289–291]

Decanol and 9-decenol similarly did not behave as expected but did have an effect on the transition temperature. It was predicted that the decanol would increase the transition temperature whilst the predicted impact of 9-decenol was uncertain. The data show that both caused a similar decrease in the transition temperature. Due

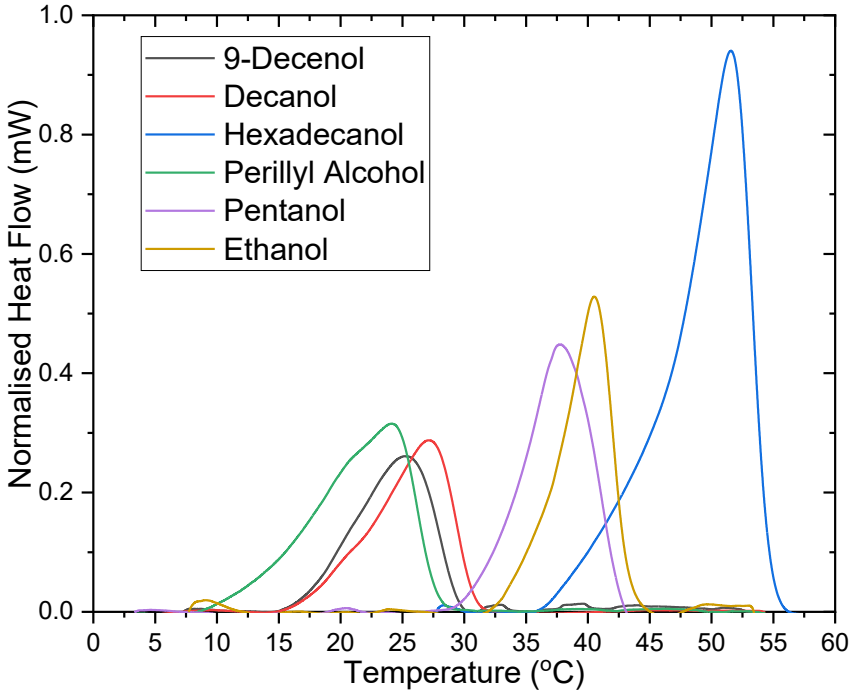


Figure 5.4: Second heating cycle of normalised DSC curves for DIPEDMAMS/water systems containing 10 mol% alkyl alcohol.

to the length of these alkyl alcohols they are expected to insert into the bilayer and for the decanol to act in a similar if less effective manner to hexadecanol. 9-decenol's predicted behaviour was uncertain due to the unsaturation however a single unsaturation in the trans configuration was not expected to have a large disrupting effect on the packing of the hydrocarbon tails. Perhaps the decanol being much shorter than the hydrocarbon tails in the surfactant means that the decanol has a more disrupting influence than an ordering one.

Perillyl alcohol whilst having the effect of decreasing the transition temperature as predicted has decreased the transition temperature to room temperature. Hydrotropes increase the solubility of the surfactant phase by inserting into the bilayer and disrupting the alkyl chain interactions, increasing the thermal motion of the chains and loosening the packing. [292] This appears to be a sufficient method for reducing the transition temperature of the surfactant system to room temperature for bilayer formation. Whilst some of the results as discussed above did not yield the predicted behaviour the purpose of this investigation was to find a method of reducing the transition temperature for ambient bilayer formation. Therefore fur-

ther DSC investigations into the other alkyl alcohols and the effect of changing the alkyl alcohol concentration was not pursued at this time particularly in the light of the observation that 10 mol% Perillyl alcohol was sufficient to reduce the transition temperature to the exact range required. Thus this alcohol was used in all further experiments to lower the transition temperature of the system to room temperature.

Alkyl Alcohol Modification: SAXS/WAXS

Small and wide angle x-ray scattering of the alkyl alcohol doped surfactant system was used to confirm that the addition of the alkyl alcohols was having the affect on the bilayer packing as suggested by the DSC data. The SAXS linear intensity plots for all alkyl alcohols at 25 °C is shown in figure 5.5. An ethanol doped sample is not shown as the sample was damaged during transport.

Minimal difference is observed between the scattering pattern of the undoped DIPEDMAMS/water system and the system containing 10 mol% pentanol. Both show a single series of equally spaced Bragg peaks corresponding to the lamellar phase as discussed in Chapter 4. The SAXS pattern for surfactant samples with 10 mol% decanol, 9-decenol, and perillyl alcohol all show a strongly scattering series of equally spaced Bragg peaks shifted slightly to the left, lower scattering angle, compared with the undoped system. The scattering peaks for these systems are significantly sharper than those for the pentanol doped and undoped systems. The scattering peaks for the 10 mol% hexadecanol samples show, what is believed to be, two co-existing lamellar phases. One of the phases has a lower scattering intensity and a similar d-spacing to that observed for the undoped sample. The peaks for the other phase are more intense and scatter at lower angle corresponding to a larger d-spacing.

The WAXS linear intensity plots for the alkyl alcohol doped DIPEDMAMS/water systems, at 25 °C, is shown in figure 5.6. The undoped sample shows a single sharp peak at $0.24\,\text{Å}^{-1}$ corresponding to the gel phase. [293] The 10 mol% pentanol and hexadecanol samples similarly exhibit only a single sharp peak at $0.24\,\text{Å}^{-1}$. Decanol and 9-decenol exhibit both a single sharp peak at $0.24\,\text{Å}^{-1}$ and a broad peak at

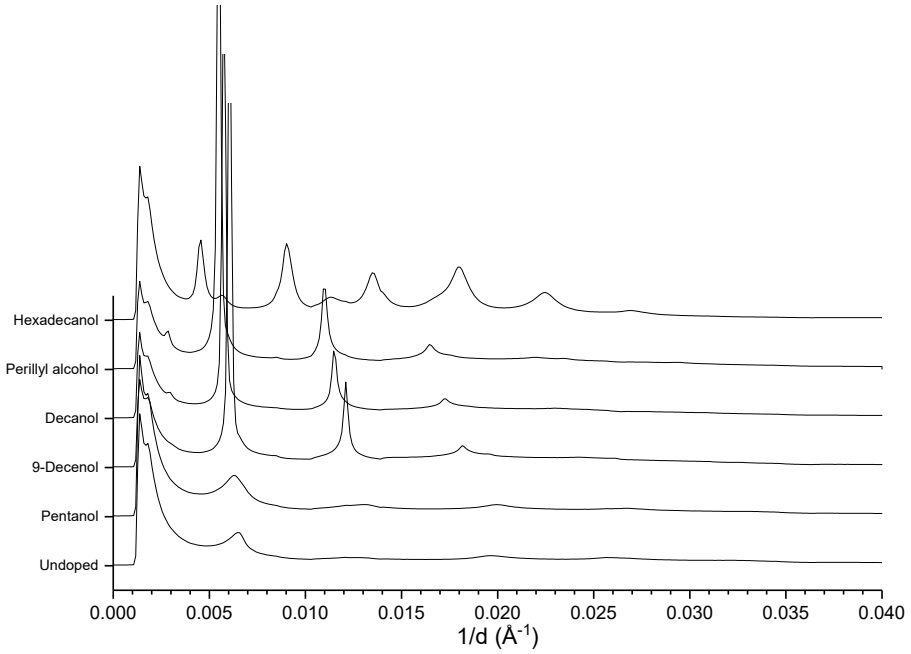


Figure 5.5: Linear intensity plots of the SAXS patterns of DIPEDMAMS/water systems, at 25 °C, containing 10 mol% alkyl alcohols.

$0.22\,\text{Å}^{-1}$, corresponding to the gel and fluid phases respectively. Suggesting phase separation and co-existence of the lamellar gel and fluid phases. The 10 mol% perillyl alcohol doped sample shows only the broad fluid peak at $0.22\,\text{Å}^{-1}$. All WAXS patterns show a series of broad peaks between 0.26 and $0.6\,\text{Å}^{-1}$ which corresponds to the short range order inherent in water, this was discussed in Chapter 4.

No significant change in the x-ray scattering pattern of the DIPEDMAMS/ water system is observed whit the addition of pentanol at a concentration of 10 mol% in relation to the surfactant. Both samples exhibit a single lamellar gel phase at 25 °C. The addition of decanol or 9-decenol appear to have a similar affect on the bulk structure of the DIPEDMAMS/water system. The surfactant system with the addition of either of these alkyl alcohols adopts a codependent lamellar gel and lamellar fluid phase at 25 °C compared with just a gel phase without the addition of the alkyl alcohols. The addition of perillyl alcohol at 10 mol% solids appears to have reduced the transition temperature far enough that the sample adopts a single lamellar fluid phase at 25 °C. With the addition of hexadecanol the samples adopt the gel phase at 25 °C as predicted from the DSC data. The scattering intensity of the decanol, 9-decenol, and perillyl alcohol samples appears more intense and the

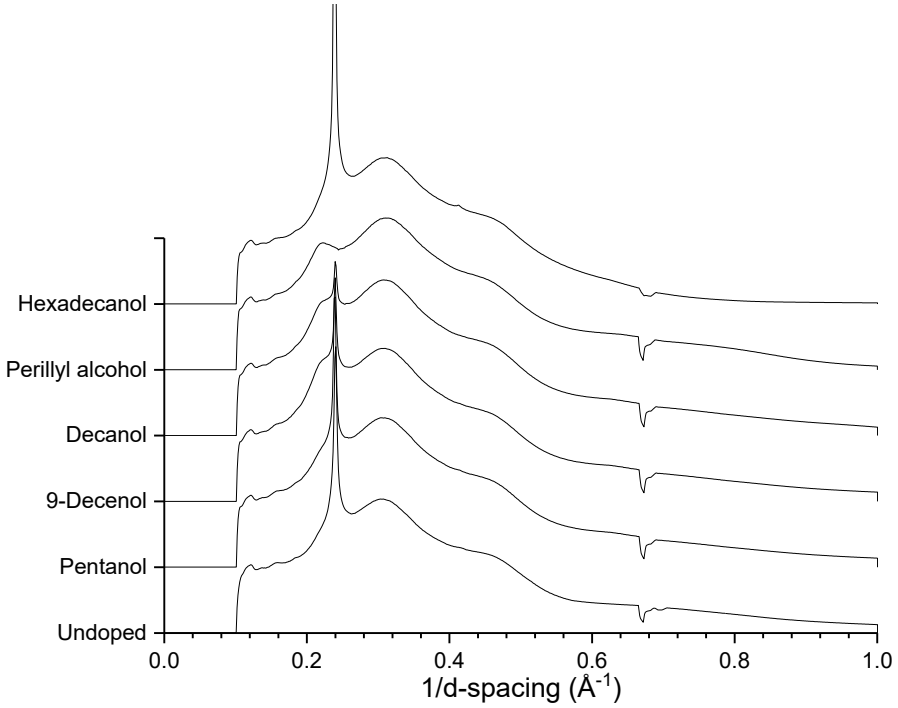


Figure 5.6: Linear intensity plots of the WAXS patterns of DIPEDMAMS/water systems, at 25 °C, containing 10 mol% alkyl alcohols.

peaks sharper than the undoped, pentanol, and hexadecanol samples. It is suggested that the scattering from samples in the fluid phase or partially in the fluid phase is more intense than that from the gel phase samples. This is commented upon further in Chapter 4 where this increased scattering intensity was observed on heating the lamellar phase above the transition temperature and further supports the belief in the success of this method in decreasing the transition temperature of the surfactant system.

Alkyl Alcohol Modification: AFM Imaging

With the confirmation that the addition of alkyl alcohols can lower the transition temperature of the DIPEDMAMAS surfactant system far enough to ensure that the bilayers are in the fluid phase at room temperature. It was necessary to confirm that this was a potential solution to the room temperature supported bilayer formation issue.

Using freshly cleaved mica as the substrate, supported surfactant bilayers were formed at room temperature from the alkyl alcohol doped systems investigated above. The main focus was on the 10 mol% perillyl alcohol doped system as this appeared, from the DSC and x-ray scattering data, to be the best candidate for the formation of complete surfactant bilayers at room temperature The other alkyl alcohol enriched samples were investigated to provide contrast as well as an opportunity to compare bulk structural data provided by the SAXS experiments with the structure of the supported surfactant bilayers. As well as an opportunity to further investigate the impact of the addition of the alkyl alcohols to the surfactant system.

Supported DIPEDMAMS bilayers formed by incubating a DIPEDMAMS vesicle dispersion at 65 °C for 15 - 20 minutes achieved complete coverage of the substrate. These bilayers show two distinct regions differing in thickness by 1 - 1.5 nm. Bilayers formed by incubation at room temperature failed to completely cover the substrate leaving regions of bare mica and bilayer patches with a height difference of 3.5 to 4 nm. The bilayers formed at room temperature from addition of ethanol and pentanol at 10 mol% both produce samples of two clear topographical regions. A featureless lower region with a higher tip to sample adhesion on retraction and a higher measured slope or stiffness. Multiple holes are observed in the upper layer which penetrate down to the lower region. The boundary between the two regions is fairly rough. The upper regions show less adhesion on separation and measured slope is significantly lower and therefore less stiff than the lower regions.

The decanol and 9-decenol doped samples also show a similar pattern to the undoped bilayers formed at room temperature and the pentanol and ethanol systems. The AFM images of these bilayers show two clear regions differing in height by 3.5 - 4 nm. The upper region has a lower tip to sample adhesion than the lower region and the measured slope is higher for the lower region than the upper region. There are holes in the upper regions with a depth similar to the average upper to lower region height difference. These holes appear to be less numerous than the with the sample containing ethanol or pentanol. The decenol sample shows smaller regions scattered across the lower region with similar properties to the upper region but forming much smaller regions. This is not observed with the other alkyl alcohol enriched samples.

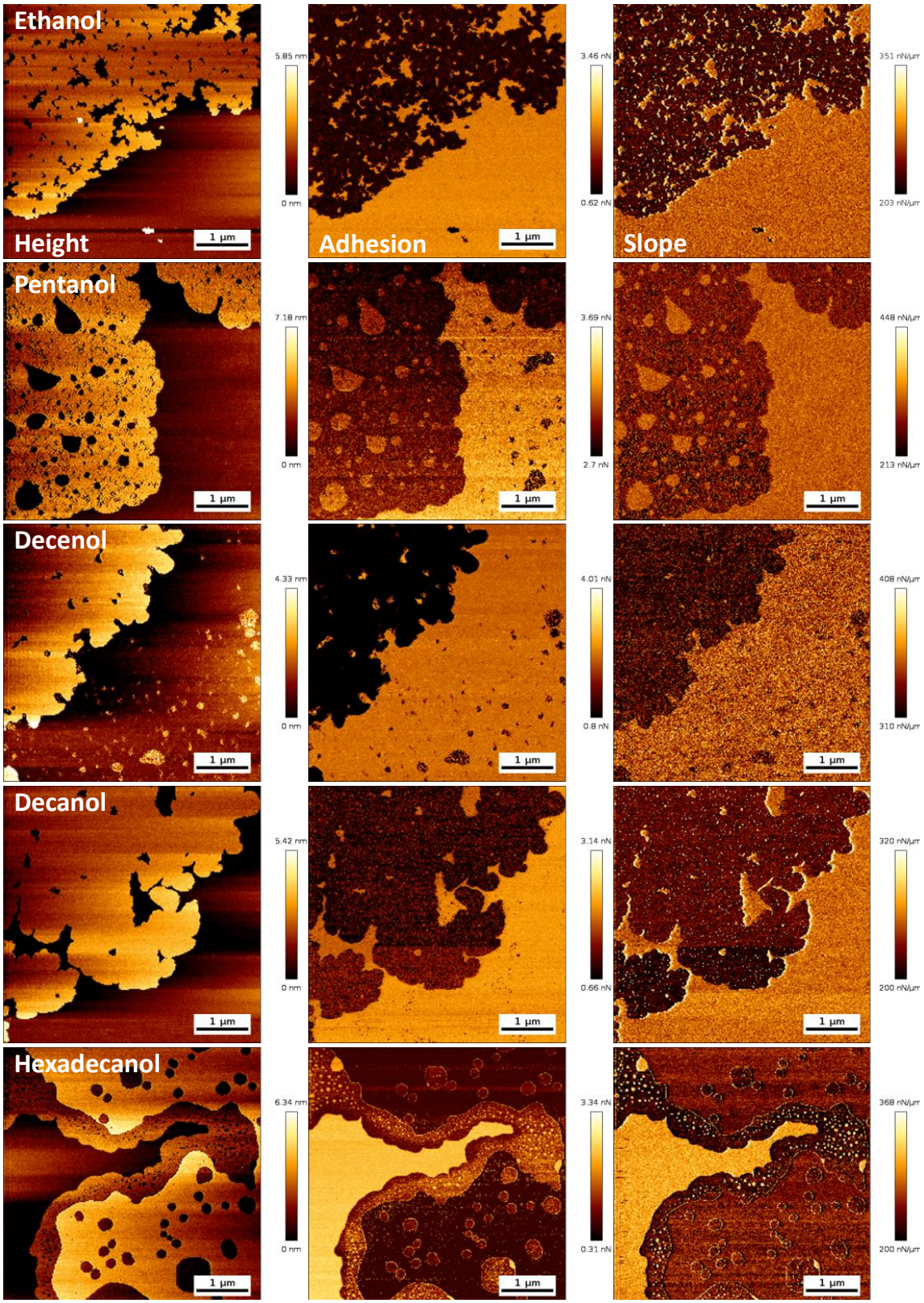


Figure 5.7: Typical QI AFM topographical images, with associated typical maps of surface adhesion and measured slope, for DIPEDMAMS bilayers on mica containing 10 mol% alkyl alcohol. All bilayers formed and imaged at room temperature.

Ethanol and pentanol showed no change in DSC nor SAXS/WAXS data so we do not expect to see any change here. The supported bilayers containing ethanol and pentanol appear almost identical to the undoped room temperature formed samples. Incomplete bilayer coverage. Upper phase is the bilayer judging by the height difference and the difference in interactions. The lower region is bare mica deduced from a combination of the height difference and the measured slope images showing that this area is much stiffer than the upper layer. The adhesion doesn't quite match predictions. Looking at the earlier figure for bare mica they suggest that the tip sample adhesion is rather low but here it is higher than the bilayer tip adhesion. This will be discussed further later in a comparison of the force spectroscopy data from these images.

The addition of decanol and 9-decenol did show a decrease in the transition temperature from the DSC data and co-existing lamellar gel and fluid phases in the SAXS/WAXS. However the samples show only minor difference from the undoped room temperature formed samples. For reasons stated above it is suggested that these samples produce patchy bilayer coverage when formed at room temperature. It is noteworthy however that these bilayer patches do appear to have fewer holes within them than the ethanol, pentanol, and undoped samples potentially suggesting that the bilayers are more fluid than the previous samples. This however can not be confirmed by the measured slope images as these only provide a measure of relative stiffness within the images.

The AFM images of the hexadecanol doped samples show three clear topographical regions. An upper region and middle region and a lower region, the height difference between these different regions is 3 and 4 nm respectively. The lower phase is relatively flat and featureless and bares a similarity to bare mica. It has the highest tip to sample adhesion and the highest measured slope of all three regions. The middle phase is mostly observed around the edges of the upper phase and within holes in the upper phase. This phase appears to have the lowest measured slope of the three phases and the second highest tip to sample adhesion. There are multiple small holes in the middle phase, approximately 1 to 10 nm in diameter, which appear to penetrate down to the lower region. The holes appear to have an increased adhesion and measured slope and are more comparable with the lower

region. The upper region is mostly surrounded by the middle region and contains several holes of varying size, 10 to 500 nm in diameter, which penetrate down to the middle layer. The upper region has the lowest adhesion on retraction and whilst the measured slope is slightly higher than the middle region it still appears significantly softer than the lower phase.

The DSC curves and the SAXS/WAXS data all showed a significant effect of adding hexadecanol at 10 mol% to the surfactant/water system. The transition temperature was observed to increase significantly and the bulk system appeared to separate into two co-existing lamellar gel phases. It is suggested, as with the other alky alcohol systems, that the lower phase is bare mica. Based on the measured slope and featureless topography. As with the other samples this suggests that the bilayer coverage is incomplete. It is suggested that the upper and middle regions are both surfactant bilayers but separated into two distinct lamellar phases as suggested by the SAXS/WAXS data. The SAXS/WAXS data suggests a difference in bilayer spacing of 4.2 nm which compares favourably with the difference in thickness of 3.8 nm observed from the AFM imaging. The similarity in the relative stiffness of the middle and upper phases compared with the lower phase further suggests that the top two regions are surfactant bilayers. The difference in relative stiffness of the two bilayer phases suggests that there is a difference in the internal structure or ordering of the different phases. However it is not certain why this would lead to a difference in the tip sample adhesion on retraction.

AFM images of supported surfactant bilayers formed by incubating a 10 mol% Perillyl alcohol/DIPEDMAMS vesicle dispersion at room temperature on mica are shown in figure 5.8 alongside images of DIPEDMAMS bilayers formed at room temperature and 60 °C for comparison.

Two clear regions differing in height by 1 - 1.5 nm are observed in the AFM images of supported 10 mol% Perillyl alcohol/DIPEDMAMS bilayers. The topography of the 10 mol% perillyl alcohol DIPEDMAMS bilayers is very similar to the topography of the bilayers formed at 60 °C from the unmodified surfactant system which also show two clear regions differing in height by 1 - 1.5 nm. In contrast the systems without perillyl alcohol formed at room temperature show a height differ-

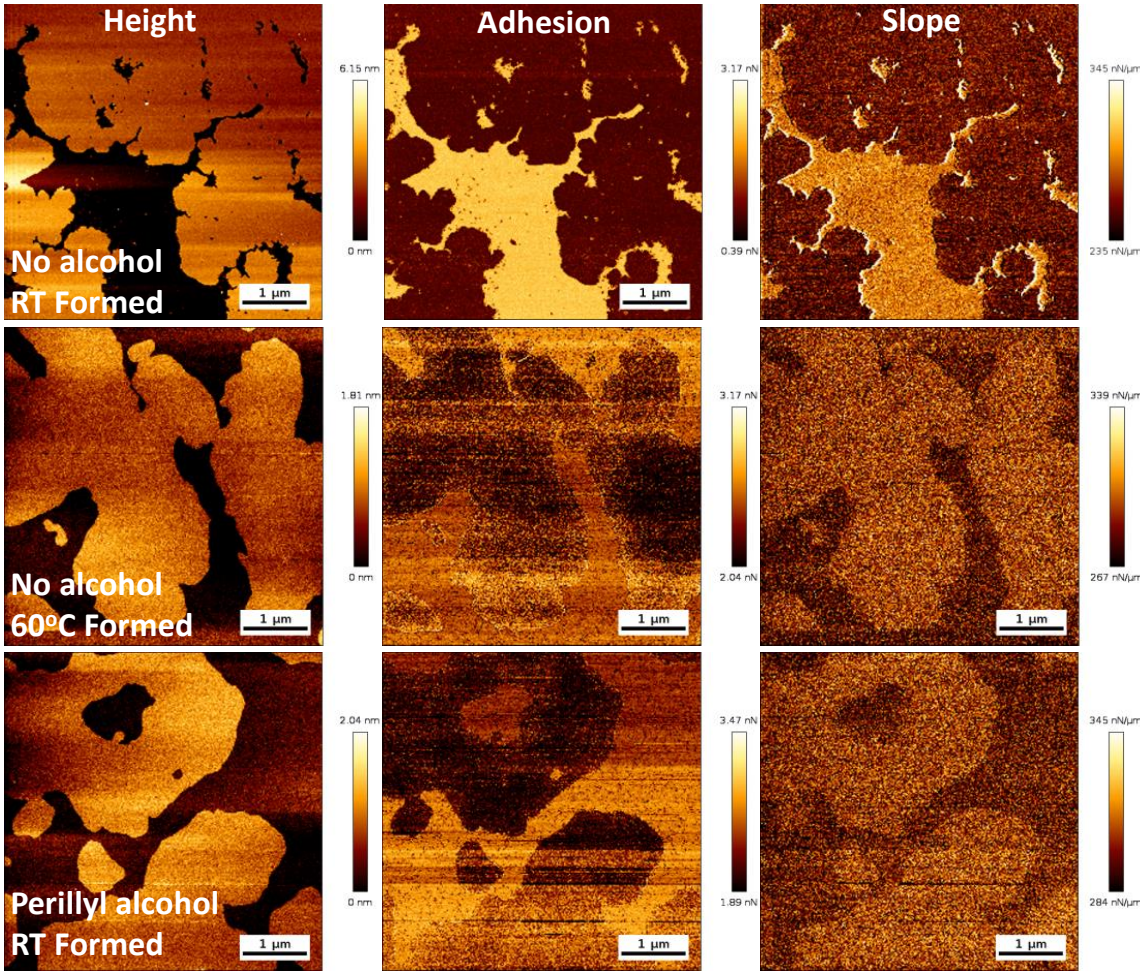


Figure 5.8: Typical QI AFM topographical images, with associated typical maps of surface adhesion and measured slope, for DIPEDMAMS bilayers on mica. Top row show images of bilayers containing only DIPEDMAMS formed at room temperature, the middle row show pure DIPEMAMS bilayers formed at 60 °C and the bottom row shows bilayers contain 10 mol% perillyl alcohol formed at room temperature.

ence of 3 - 4 nm. The measured slope of the 10 mol% perillyl alcohol samples is higher for the upper regions than the lower regions but the tip to sample adhesion is lower for the upper regions than the higher regions. The DIPEDMAMS bilayers formed at 65 °C with no added alkyl alcohol show the same pattern of higher measured slope and lower adhesion for the upper regions than the lower regions. For DIPEDMAMS bilayers formed at room temperature however the measured slope is higher for the lower regions with a larger difference between the the measured slope for the different regions. The adhesion shows a higher adhesion for the lower region than the upper region, similar to the 10 mol% perillyl samples, but with a greater difference between the adhesion in these two regions than for the perillyl or 65 °C

incubated samples.

As discussed earlier the DIPEDMAMS bilayers formed by incubation at 60 °C form a continuous bilayer on all substrates investigated and show that the bilayers adopt two different bilayer phases differing in thickness by 1 - 1.5 nm. Formed at room temperature only patchy bilayers were formed. Bilayers formed at room temperature with the addition of perillyl alcohol at 10 mol% show complete coverage. The bilayer does however separate into two distinct phases differing in thickness by 1 - 1.5 nm, almost identical to the undoped bilayers formed at 65 °C. The adhesion and measured slope plots also show a good agreement between the perillyl doped samples and the 60 °C samples.

As observed from the DSC curves and further confirmed by the SAXS/WAXS data the addition of perillyl alcohol at 10 mol% reduced the transition temperature to below room temperate such that the system was observed to be completely in the the lamellar fluid phase at 25 °C. As opposed to a mixed fluid and gel phases as observed for other alkyl alcohols. It is suggested that successful complete supported bilayer coverage can only be achieved when the surfactant system is in a fluid phase.

There is however some disagreement between the structure of the bilayers on the mica and the structure observed in the bulk samples by SAXS/WAXS. The pure DIPEDMAMS supported bilayers formed at 60 °C show two different bilayer phases this is shown in the SAXS/WAXS of this system, at 25 °C, as discussed in Chapter 4. The 10 mol% perillyl doped supported bilayers also shows two distinct phases and appear, at least topographically, indistinguishable from the pure DIPEDMAMS bilayers samples formed at 60 °C. However the SAXS/WAXS patterns of the perillyl samples, at 25 °C, show only a single fluid lamellar phase. However this does compare favourably with the SAXS/WAXS patterns of the pure DIPEDMAMS system above the transition temperature. This suggests that whilst the addition of perillyl alcohol is clearly aiding the formation of supported bilayers at room temperature it does not appear to have an effect on the topography of the bilayers once they are formed. One possibility is that the perillyl alcohol occupies the aqueous phase and is removed on washing, as discussed above with the idea of solvotropes. However this is unlikely due to the alcohol's structure. Another possible cause lies in the na-

ture of supported surfactant bilayers in that they are supported by a solid substrate which is absent in the bulk samples observed by x-ray scattering. It is possible that the binding to the mica changes the packing and structure of the surfactant bilayers perhaps having a similar effect as decreasing the temperature for the bulk system, causing the bilayers containing 10 mol% perillyl alcohol to appear similar to the pure DIPEDMAMS bilayers. [294]

In order to more carefully compare the bilayers the force spectroscopy between the bilayers and the probe was investigated in more detail.

5.3.3 Alkyl Alcohol Modification: Force Spectroscopy

Force spectroscopy can be used to investigate the interactions between the AFM probe and the sample. As part of this investigation it was used to probe the difference in interaction between the different regions observed from the AFM imaging in more detail than is possible from the QI data. The nanomechanical properties of the supported bilayers can also be investigated with this technique. Whilst it was of interest to investigate the effect of added alkyl alcohols on the nanomechanics of the DIPEDMAMS bilayers, the main focus here was to compare pure DIPEDMAMS bilayers formed at 60 °C and those formed at room temperature with the addition of 10 mol% perillyl alcohol.

A comparison of typical force curves measured between the sharp AFM tips and the DIPEDMAMS bilayers containing 10 mol% alkyl alcohol are shown in figure 5.9. As these samples are believed to form patchy bilayers, force curves are shown for both the upper region, the bilayers, and the lower regions, bare mica (see figure 5.7). Zero separation is set relative to the mica substrate.

The force curves measured between the probe and the upper regions of the alkyl alcohol doped bilayers all show a similar pattern. On approaching the surface no interaction is observed until approximately 7 nm from the hard mica substrate for all samples shown except hexadecanol. At this point a small attraction is noted between the probe and the surface. As the probe continues to approach the surface

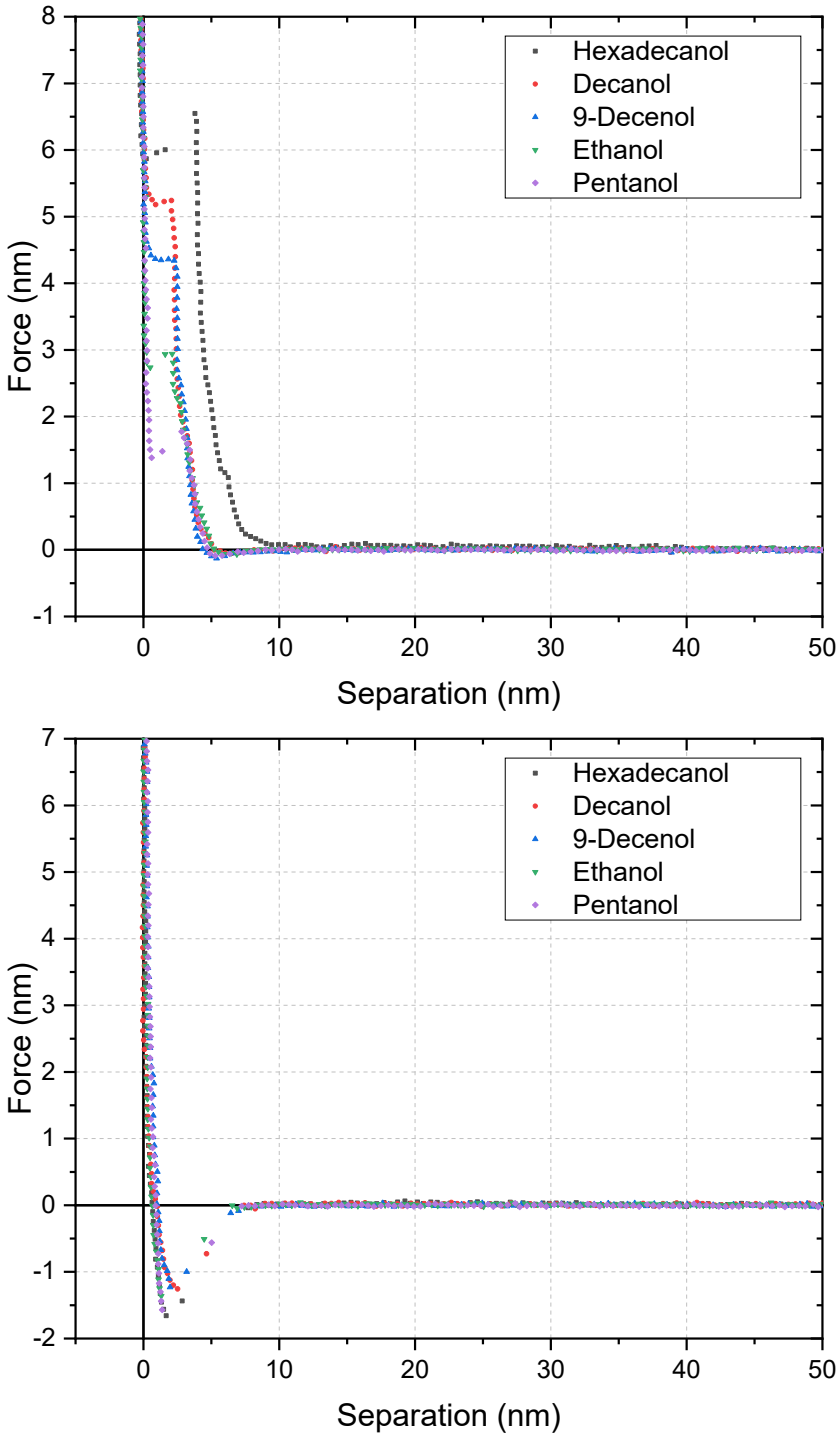


Figure 5.9: Approach force distance curves measured between a sharp AFM probe and DIPEDMAMS bilayers containing 10 mol% alkyl alcohol. The top plot shows forces measured against the higher areas and the bottom figure those measured against the lower areas.

the force increases rapidly until the probe is observed to jump to the surface 2.5 and 3 nm of separation. The force then appears to increase indefinitely as hard contact with the surface is achieved. For the bilayers containing 10 mol% hexadecanol the initial interactions begin approximately 10 nm from the mica substrate and the jump to the surface occurs around 5 nm.

The forces measured between the probe and the lower regions of the DIPID-MAMS/alkyl alcohol samples, suggested to be bare mica, are significantly different from those observed for the upper region. On approach no interaction is measured until a separation of approximately 7 nm where the probe is observed to jump to the surface. This indicates a significant attractive force between the probe and the sample. No significant difference in the forces was observed for samples containing different alkyl alcohols.

On withdrawal (not shown here) the probe remained on the surface before jumping away as the applied force increased. There was no significant difference in the withdrawal force except the amount of force required to pull the probe from the surface.

For the upper region this is further confirmation that this is a bilayer. The initial attraction is most probably due to van der Waal's forces rather than being coulombic in nature as it short ranged and rather weak. The initial increase in force is caused by compression of the surfactant bilayer before the probe then punches through the bilayer to the surface. From the compression of the bilayer it is possible to draw conclusions on the nanomechanical properties of the bilayers. [295, 296] In terms of compressibility there appears little change apart from hexadecanol. There is however a change in the break through forces. The break through force for the upper region, assumed to be a surfactant bilayer, for the pure DIPEDMAMS system formed at room temperature was between 3 and 4 nN, shown in figure 5.10. The break through force for the ethanol containing systems was also shown to be within this range. The systems with pentanol show a lowered break though force of between 1 and 2 nN whilst 9-decenol, decanol and hexadecanol, all showed an increase in the force required to breakthrough the bilayers to the mica substrate. Due to the large element of probability and variation when looking at break through forces. [297] It

is problematic to draw too much from these breakthough events without a large statistical analysis, requiring a far greater number of force curves to be collected, which is beyond the scope of this investigation. However it is notable that the thickness of the bilayers, measured from the initial contact point to contact with the substrate, does show an increase for the hexadecanol containing bilayers but significant difference for the other bilayers. Supporting the observations form the topographical imaging.

The lower region shows an attraction on approach which is quite possibly Coulombic in nature as it is relatively long ranged. There is however a small compression after attraction before the hard "wall" of the solid substrate is reached, but no evidence of a break through event and the compression is far to small to be a bilayer. The attraction, if this were bare mica, is confusing as it is not observed for actual bare mica, the interaction should be minimal. Mica should be anioinic under these condition as should the silicon nitride of the probe. It is suggested that the probe picks up or is some how coated by monomers of the surfactant giving the probe a slight positive charge. This is possibly unavoidable and happens on first contact with the surface. (This doesn't appear to have too much of an impact on the interpretation of the results as it is obviously very reproducible one just needs to be aware of this effect when interpreting force curves.)

Figure 5.10 shows typical sharp probe force spectroscopy approach curves for 10 mol% perillyl doped DIPEDMAMS bilayers, pure DIPEDMAMS bilayers formed at 65 °C, and pure DIPEDMAMS bilayers formed at room temperature. Force curves for the lower and upper regions of each sample are shown. For ease of comparison zero separation has been defined as compliance region of the force curves, see Chapter 3, where the probe is in hard contact with the substrate. For the upper regions of these samples the force curves are very similar until a separation of approximately 2.5 nm. No long range interactions are observed between the probe the samples on approach. Around 5 nm a weak attraction is observed for all samples followed by a rapid increase in the measured force between the probe and the surface which has approached a gradient similar to the compliance region by approximately 3 nm. At a separation of 2.5 nm or an applied force of approximately 3.5 nN the force curves diverge.

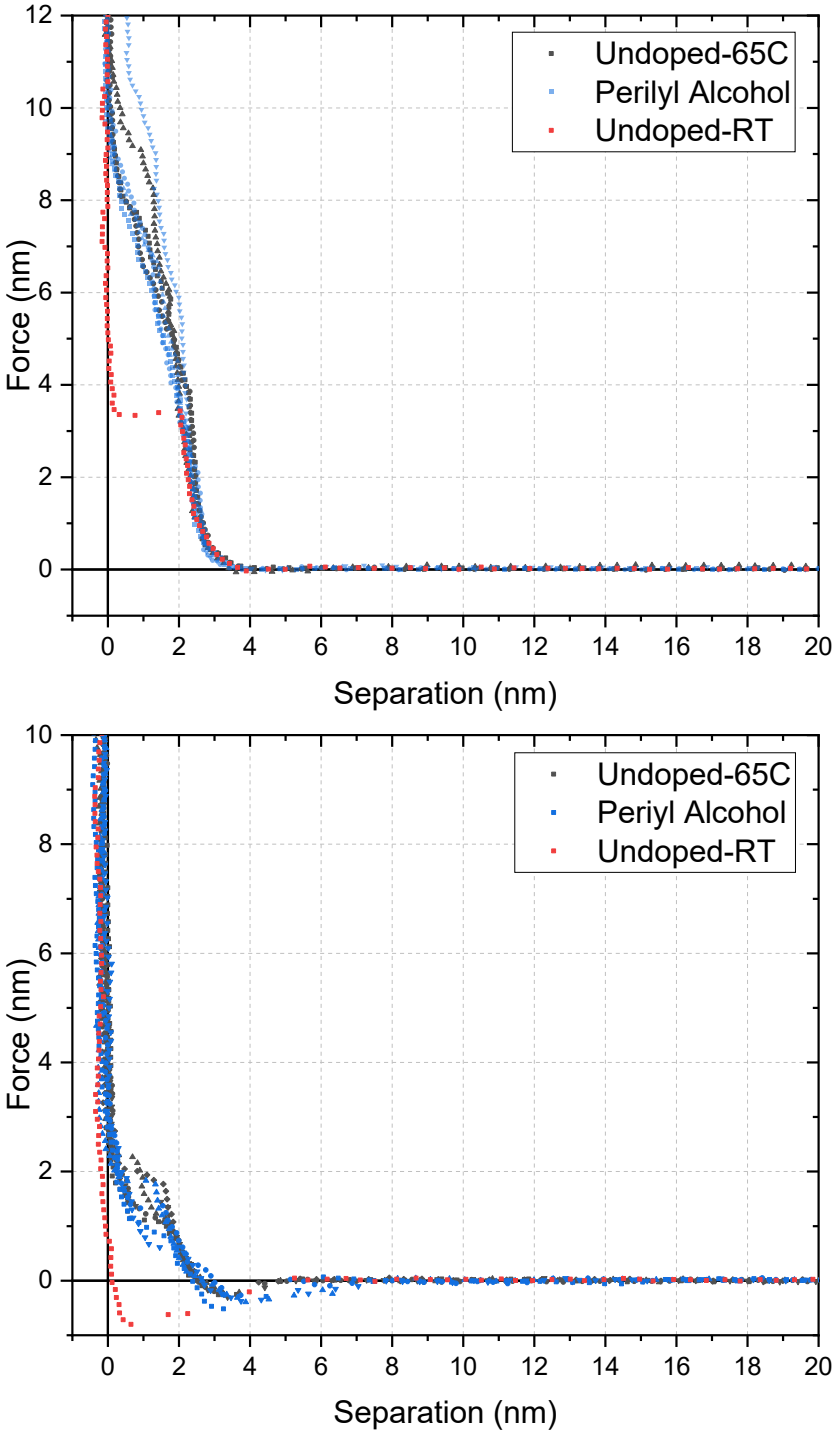


Figure 5.10: Approach force distance curves measured between a sharp AFM probe and DIPEDMAMS bilayers. The top and bottom plots show the forces measured against the higher areas and lower areas of the bilayers respectively.

The force curves for the pure DIPEDMAMS samples formed at room temperature show a jump to hard contact at an approximate separation of 2.5 nm and an applied force of 3.5 nN. This jump to hard contact is not observed for the DIPEDMAMS sample formed at 60 °C nor for the sample containing 10 mol% perillyl alcohol formed at room temperature. At a separation of approximately 2.5 nm and an applied force of 4 nN the gradient of the force curve decreases until hard contact is achieved and the gradient tends to infinity. There is some variation in the applied force at which compliance is reached with it ranging from 8 - 10 nN. No significant difference is observed between the sample containing perillyl alcohol and the sample formed at 60 °C.

The force spectroscopy curves of the lower regions show a similarity in the interactions with DIPEDMAMS samples containing 10 mol% perillyl alcohol formed at room temperature and pure DIPEDMAMS samples formed at 60 °C. The interaction with the lower regions of the pure DIPEDMAMS bilayers formed at room temperature are significantly different from the other two samples.

On approaching the lower regions of the samples there is no observed interaction between the probe and the samples until a separation of 5 - 7 nm. At this separation an attraction is observed. For the pure DIPEDMAMS samples formed at room temperature this attraction results in a jump to hard contact. The perillyl alcohol containing and the 60 °C incubated samples both show an increasing measured force below a separation of 3 or 4 nm. The measured force increase with decreasing separation but less steeply than observed for the upper regions of these samples. Events leading to hard contact are observed to occur after an applied force of between 1 and 2 nN for both samples and a separation of around 2 nm. Some of these show a jump to hard contact whilst others exhibit a decrease in the gradient until reaching the compliance region, similar to events observed for the upper regions of these samples.

As discussed above, the small attraction observed on approaching the upper regions of these samples is most likely the result of attractive van der Waals forces; the initial increase in the measured force is due to contact with and the the subsequent compression of a surfactant bilayer. As the load applied to the bilayers increases

the probe eventually pushes through the bilayers. This is a sudden event for all room temperature formed bilayers with and without the addition of 10 mol% alkyl alcohols except for those containing perillyl alcohol. The force curves for the upper regions of the pure DIPEDMAMS bilayers formed at 60 °C and those containing 10 mol% perillyl alcohol formed at room temperature do not show the probe suddenly breaking through the bilayers after a certain applied force. Two possible explanations for the observed force curves are further compression of the bilayer with increasing applied force or a more gradual process of the probe pushing into and through the bilayer to the mica substrate below. Of these possible phenomenon the latter is more probable is more likely as the bilayer thickness, measured from first contact to the start of the compliance region, is not significantly different for all three samples shown here suggesting that the tip has traversed the whole bilayer. A potential explanation for difference in the break through behaviour is that the partially covered surfaces the surfactant molecules can moved laterally whereas this would cause them to be compressed in the completely covered bilayers.

The similarities between the force curves for the lower regions of the 10 mol% perillyl alcohol samples and the pure DIPEDMAMS samples formed at 60 °C and their contrast with the force curves for the lower regions of the pure DIPEDMAMS samples formed at room temperature provide further support for the claim that lower regions of the first two are covered by a supported surfactant bilayer whilst the later is bare mica. It was suggested above that the observed attraction, at least for the areas considered to be bare mica, could be the result of the probe picking up some or possibly being coated by surfactant monomers giving the probe a slight positive charge. However this would not account for the attraction observed for perillyl alcohol or 60 °C formed samples. For the room temperature pure DEPEDMAMS samples the increase in measured force after the initial attraction is believed to be contact with the hard mica substrate as evidenced by hard contact. For the perillyl alcohol containing and 60 °C incubated samples, the initial increase in measured force after attraction is suggested to be contact with, and then the compression of, a surfactant bilayer as the force applied increases. Whilst the indentation of these bilayer regions appear comparable to each other. The indentation per applied force is greater for the lower regions than the upper regions of these samples. Suggesting that the lower bilayer regions are softer and therefore more compressible than the

upper regions. The force required to push through or break through these bilayers to the mica substrate below is also lower than required for the upper regions. The observation of these break through or push through events further supports the claim that a surfactant bilayer is present. The difference in the relative stiffness of these two regions as observed from the force spectroscopy backs up the observations from the imaging data.

The difference in thickness of the bilayers in the two regions for the 10 mol% perillyl alcohol samples and the pure DIPEDMAMS samples formed at 60 °C as observed from the AFM imaging is also reflected in the force curves by measuring the distance between first contact with the bilayer and hard contact with the substrate.

The 10 mol% perillyl alcohol samples incubated at room temperature and the pure DIPEDMAMS samples formed at 60 °C form topographically similar bilayers consisting of distinct thicker and thinner regions. These samples, when investigated by atomic force spectroscopy, also exhibited no significant differences. Therefore it is concluded that the addition of 10 mol% perillyl alcohol not only enables complete DIPEDMAMS bilayers to be formed at room temperature on mica but also form bilayers that exhibit significantly similar force interactions and nanomechanical properties as those formed from pure DIPEDMAMS by incubation at 65 °C.

5.3.4 Measurement of Bilayer-Bilayer interactions by Colloidal Probe Atomic Force Spectroscopy

With the ability to now form complete DEPEDMAMS bilayers at room temperature on mica. The next step was to test if this would lead to the formation of surfactant bilayers on the probe as well. Figure 5.11 shows a series of colloidal probe force spectroscopy curves measured between the clean probe and a freshly cleaved bare mica surface in D.I. water and those measured after incubating the system with a vesicle dispersion containing 10 mol% perillyl alcohol at room temperature.

From figure 5.11 it is observed that there is variation in the forces measured between the colloidal probe and the mica surface. This variation is observed be-

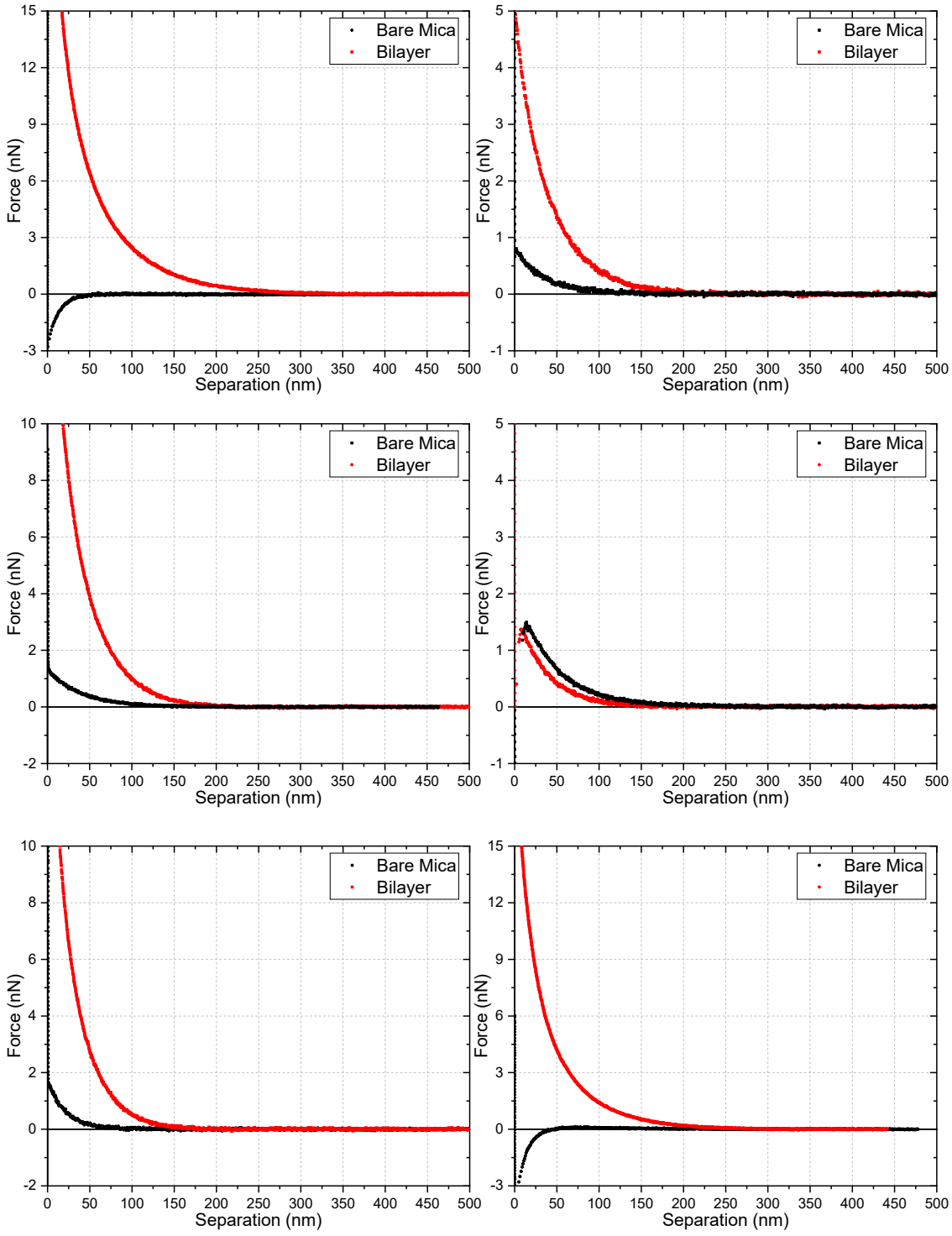


Figure 5.11: Colloidal probe AFM force distance curves measured on approach between a glass colloidal probe and a mica surface. Each plot shows the measured force both before and after bilayer formation.

tween different probes, different mica surfaces, and repeat experiments. However within a single experimental run the forces measured across different regions of the surface are consistent. As the colloidal probe approaches the surface no interaction between the glass sphere and the mica surface until a separation of between 80 and 120 nm. Between these separations the probe is observed to bend towards or away from the surface resulting in an increase or decrease in the measured force between the surfaces, corresponding to a repulsive or attractive interaction respectively. For the samples exhibiting a repulsive interaction the measured force appears to increase exponentially as the separation decreases. Eventually the relationship between the force measured and separation becomes linear, this is assumed to hard contact between the probe and surface and was set as zero separation. In the attractive regime the force measured does initially appear to decrease exponentially as the separation decreases but then appears to decrease linearly before increasing as the probe is assumed to come into contact with the surface. The majority of the measured interactions fit into the repulsive category with only a few examples exhibiting an attractive interaction.

After incubation at room temperature with a 10 mol% perillyl alcohol DIPED-MAMS vesicle dispersion the system was washed with DI water to remove any deposited vesicles and the forces between the colloidal probe and the surface were measured again. After vesicle deposition, and subsequent bilayer formation, the measured interactions all show similar interactions. On approach no interaction is observed until a separation of 200 to 250 nm where the measured force begins to increase, however there is some variation between samples. For all measurements, as the separation decreases the force measured increases exponentially. At small separation < 10 nm some samples show a sudden decrease in the measured force before hard contact is achieved. The majority of samples however do not exhibit this short range attraction and the forces remain repulsive up to hard contact. There is some variation between samples, similar to that observed for the interactions between the bare probe and substrate, but the measurements are generally in good agreement especially between those using the same probe. No obvious difference was observed between different mica samples. This is not surprising considering that the mica is cleaved each time before use and the uniformity of the bare mica surfaces. Forces measured in several different regions across each surface were extremely consistent.

The interactions between the sphere and bare mica the interactions are suggested to be due to electric double layer forces, for the repulsive interactions at least. Due to the surface structure and charge suggest for the glass and the mica at neutral pH. -OH dissociation for glass resulting in a net negative charge and ion disassociation of the mica resulting in a net negative charge. The attractive interactions are surprising and as mentioned above they are comparatively rare compared to the repulsive interactions. It is suggested that this is simply due to some form of contamination. Probably from the imaging buffer or attached to the colloidal probe as it is the most difficult to clean not likely mica as it can be freshly cleaved each time before use.

Variation between the strength of the repulsion can come from various sources. Variation in the size and roughness of the colloidal glass sphere which are outside of our control, although size does have upper and lower limits. The spring constant of the cantilever will vary and unlike the sharp tip probes for imaging this is difficult to measure for the colloidal sphere due to the added weight of the glass sphere. However this doesn't vary too much for the type of probe used here and can be assumed to be within 10% of the nominal force constant. The positioning of the sphere on the cantilever will also effect the measured force, but is difficult to control so must just be factored in to the experimental results. The surface is not considered to have a significant effect on the variability of the measurement as they are fairly uniform and freshly cleaved as mentioned before.

The repulsive interaction between the probe and surface after vesicle deposition is due to electrical double layer forces. This is suggested by the exponential increase in measured force as the separation decreases. As demonstrated earlier vesicle deposition at room temperature with a pure DIPEDMAMS vesicle dispersion resulted in attractive interactions which were suggested to be caused by patchy bilayer formation on the mica substrate and no bilayer formation on the colloidal probe. Confident that vesicle deposition with a 10 mol% perillyl alcohol DIPEDMAMS vesicle dispersion forms complete bilayers on mica at room temperature, it is suggested that a bilayer is also formed on the glass colloidal probe. Therefore the long range repulsion observed for these system is caused by the electrostatic repulsion between the two supported cationic bilayers.

As mentioned above a minority, of experimental runs do show a strong short range attraction around a separation of < 20 nm. A short range attraction in this type of system would most likely be attributed to Van der Waal's interactions, as discussed in section 2.3.1. This combination of electrostatic repulsion and van der Waal's attraction has been widely studied and measured and is known as the DLVO theory, for more information please see section 2.3.3. If this short range attraction was the result of the van der Waal's forces, this attraction would be expected to be observed for all properly formed bilayers. It is suggested that this attraction could be the result of the incomplete or improper formation of the surfactant bilayers. Another possible theory is that if some adhered vesicles or bilayer fragments are present during force measurements then these contaminants may induce a depletion interaction as they are forced out from between the bilayers as the separation decreases. The depletion interaction is explored in Chapter 7 and discussed in section 2.3.7.

As with the force measurements between the colloidal probe and the mica substrate before the deposition of the surfactant bilayers, there is some variation in the strength of the forces measured between the cationic surfactant bilayers. Variations in the experimental set up between probes and between runs as discussed above in relation to the variability in the forces measured between a clean probe and bare mica are equally sources of error for the measurement of forces between the supported bilayers. There are additional factors that need to be considered with the addition of the supported bilayers.

As the surfactant bilayers are formed in situ with the colloidal probe already in place it is not possible to confirm the presence or condition of the supported bilayers by imaging. As removing the probe will damage the bilayer. Therefore it can only be assumed for each experimental run that the bilayers have been formed. This adds an additional source of variability to the force measurements as there is no direct conformation that the bilayers have been formed and whether or not they have been formed with good surface coverage. Unruptured vesicles adhered to the surface, or free vesicles left within the system due to insufficient washing, may further add to the variability of the force measurements.

Although there was variation in the strength of the measured interaction between

the supported cationic bilayers between experimental runs, there was little variation within each run as the interactions were measured across different regions and areas of the sample. This is noteworthy, as two different regions are observed in the imaging. suggesting that either the interaction between the these different areas are not sufficient to lead to significant differences in the measured interactions or that there is no difference in the interaction or the are the forces are acting over a large area so averages out these different regions.

Whilst mica was demonstrated to be the most practical substrate for use in AFM imaging experiments of supported surfactant bilayers the difference in surface structure, charge, and more complex surface chemistry compared with the glass probe could not be ignored. Figure 5.12 shows the interactions between clean glass substrate and probe in DI water and the interactions measured after incubating the system, at room temperature, with a DIPEDMAMS vesicle dispersion containing 10 mol% perillyl alcohol.

The interactions between a glass colloidal probe and a glass surface in D.I. water are generally repulsive however a few samples do show an attractive interaction, see figure 5.12. As with the mica there is some variation in the strength and range of the forces measured. Across the surface these force appear to be consistent but the variation is observed between runs and probes.

After incubation with the vesicle dispersion and washing with D.I. water the forces were measured again, to determine the interactions between supported DIPED-MAMS bilayers on glass. The interactions were generally repulsive and compare well with the interactions measured using mica as the substrate. However there does appear to be a greater variation in the observed forces between experimental runs compared with mica. There is also more variation across the surface when using glass as the substrate when compared to mica.

As discussed above for mica the main source of uncertainty and variation within the system lies with the probe. This was discussed in terms of manufacturing tolerances, the surface roughness and size of the colloidal sphere, and contamination of the system. The substrate was believed to have a minimal impact on the variation

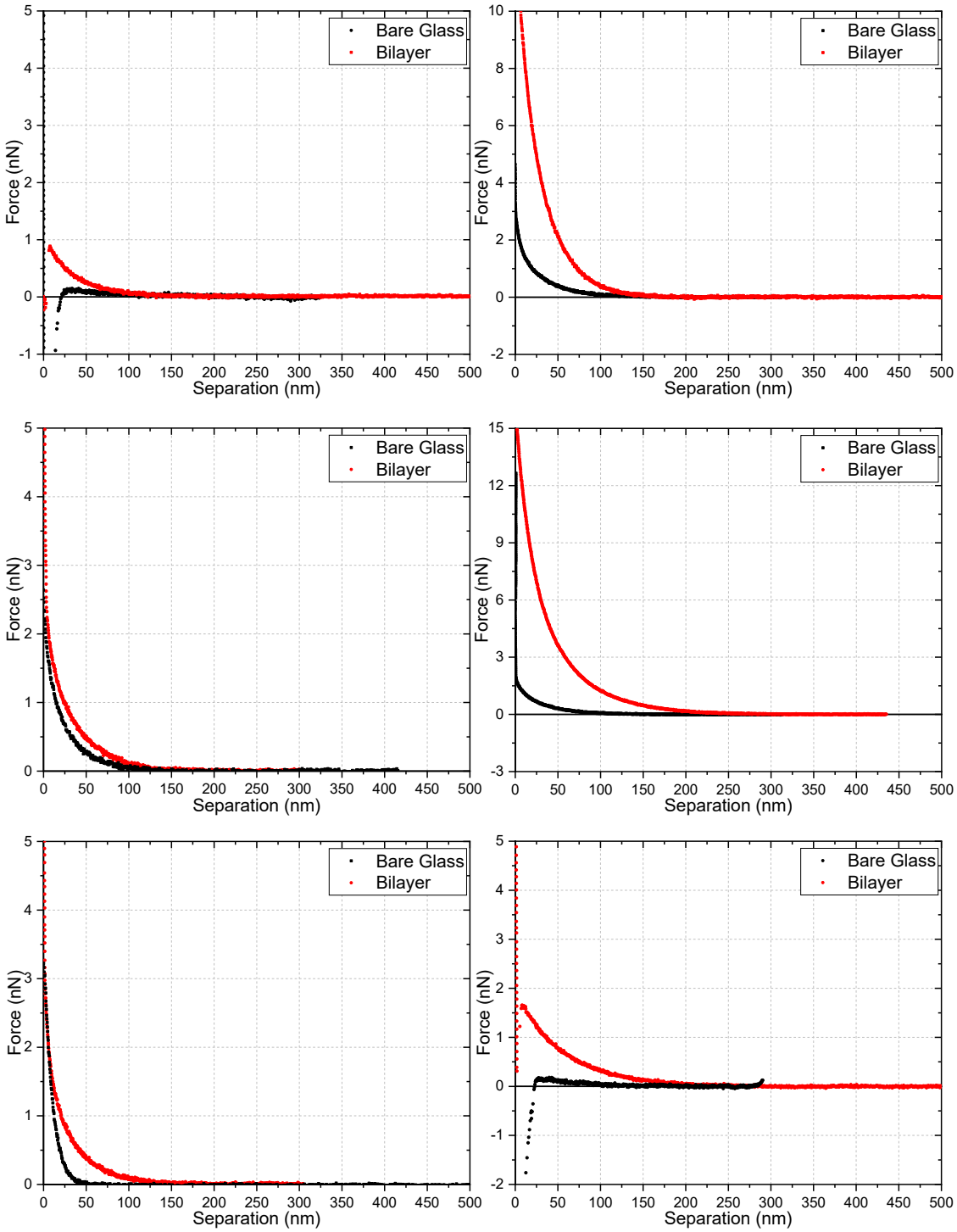


Figure 5.12: Colloidal probe AFM force distance curves measured on approach between a glass colloidal probe and a glass surface. Each plot shows the measured force both before and after bilayer formation.

due to its uniformity and method of cleaning. The glass substrate however introduces a greater surface roughness to the system, which has been shown to have an impact on the measured forces.

Another consideration when using glass instead of mica is the cleaning and preparation of the substrate. Whilst mica is relatively facile to prepare via cleavage, glass requires cleaning. This is was performed here by UV-ozone plasma. This has been used in other studies but some still suggest the use of Piranha solution. Whilst UV-Ozone plasma cleaning appeared to be sufficient, this may account for some of the additional variation observed for the glass system.

The difficulty in reliably cleaning the glass substrate compared with the mica means that contamination with this system was much more common. This is believed to be the cause of some of the complex interactions observed for the glass based bilayer bilayer interactions.

Whilst the use of a glass substrate had the potential to simplify the surface chemistry considerations, and reduce the impact of any asymmetrical affects, when analysing the interactions between supported surfactant bilayers. The difficulties in reproducibility suggested to be a result of the combination of the cleaning method's affect on the surface charge and the difficulty of ensuring that the substrate was completely free of contamination lead to the decision to use mica as the substrate for colloidal probe force microscopy and directly measuring the interactions between supported cationic surfactant bilayers.

5.4 Conclusions

Supported surfactant bilayers needed to be formed in the presence of both the colloidal probe and flat substrate in order to begin to measure the interactions between the surfactant bilayers. To form complete surfactant bilayers the system needed to be above the fluid to gel transition temperature for the surfactant vesicle system. The facility to heat samples on the AFM stage was not initially available therefore

a method to form complete surfactant bilayers at room temperature was required.

Various alkyl alcohols were investigated for their ability to affect the packing density and therefore the transition temperature. At a fixed molar ration of 10 mol%, pentanol and ethanol was not observed to have a significant impact on the bulk lamellar phase nor the structure of the supported bilayers compared with those of pure DIPEDMAMS. Decanol, 9-decenol, and perillyl alcohol were all shown to decrease the transition temperature with perillyl lowering the transition temperature below room temperature. As a result the bulk systems containing decanol and 9-decenol were found to form a co-existing lamellar gel and lamellar fluid system. The perillyl alcohol containing sample was observed to be entirely lamellar fluid at room temperature.

Only samples containing perillyl alcohol at 10 mol% formed complete surfactant bilayers at room temperature from a vesicle dispersion. Vesicle dispersions containing the other alkyl alcohols that were investigated or of pure DIPEDMAMS only formed patchy bilayers at room temperature where large areas of the the mica substrate were not covered by a surfactant bilayer.

The supported surfactant bilayers formed at room temperature with the addition of perillyl alcohol were topologically indistinguishable from those formed at 65 °C from a pure DIPEDMAMS vesicle dispersion. They were both shown to achieve complete coverage of the mica substrate and the supported bilayers separated into two distinct regions differing in bilayer thickness by 1 - 1.5 nm.

The nanomechanical properties of these bilayers, investigated by force spectroscopy, were significantly different for the thicker and thinner bilayer regions, further supporting that these areas have different structural conformation. Comparing the thicker phases to thicker phase and thinner phase to thinner phase there is a significant similarity between room temperature formed perillyl alcohol containing samples and the pure DIPEDMAMS bilayers formed at 65 °C.

The force spectroscopy of the room temperature formed bilayers containing the other alkyl alcohols or pure DIPEDMAMS provided further evidence that they only

formed bilayers with partial coverage. The areas covered by a surfactant bilayer exhibited different nanomechanical behaviour from the room temperature formed perillyl alcohol containing samples and the pure DIPEDMAMS bilayers formed at 65 °C

Finally, by using a DIPEDMAMS vesicle dispersion containing 10 mol% perillyl alcohol surfactant bilayers were able to be formed on both the substrate and the colloidal probe in situ at room temperature. The interaction between the supported cationic surfactant bilayers was then measured as the probe was brought towards the surface. The interactions between the bilayers were observed to be repulsive and the repulsion was suggested to be the result of coulombic interactions. Whilst there was some variation in the strength and range of the interactions there were generally reproducible within error.

Glass was briefly investigated as an alternative flat substrate to mica as this could simplify the surface chemistry and reduce the asymmetry of the system. However increased variation in the measured forces and the unreliability of cleaning methods for the glass substrate lead to the conclusion that mica was the substrate of choice for measuring the interactions between supported cationic surfactant bilayers going forward.

Chapter 6

Impact of Halide Salts on the Structure of, and Interactions between, Supported Cationic Surfactant Bilayers

6.1 Introduction

Surfactant vesicle dispersions have many industrial applications and are widely used in several sectors, including healthcare, cosmetics, homecare, food and other commercial products. The majority of these products are complex colloidal dispersions composed of multiple components, and additives to fine tune the physical and the commercial properties of the dispersion. The formulation of these products requires precise control of the colloidal properties and an understanding of the stability of the colloidal system. The addition of perfumes, salts, polymers, dyes and polyelectrolytes to these systems in commercial products makes the stability of these systems difficult to predict and to control. With the increasing awareness of the impact of plastic waste on our environment, and recent initiatives to reduce its use, there have been movements within industry towards the use of more highly concentrated vesi-

cle dispersions. This makes the understanding and prediction of the stability and phase behaviour of these systems evermore important. To be able to predict the stability of these systems the interactions between the surfactant vesicles must be understood.

Vesicle dispersion can be considered as colloidal dispersions. As discussed in section 2.2, the stability of colloidal dispersions is determined by the interactions between the colloidal particles, in the case of vesicle dispersions the interactions between the vesicles. If the interactions between the vesicles are not sufficiently repulsive this can lead to the flocculation, if reversible, or coagulation, if not, of the vesicles. This can lead to the phase separation of the vesicle dispersion if the aggregated vesicles begin to sediment or cream out of the aqueous phase. [76] Vesicles system also offer additional routes to instability such as vesicle fusion, or the transformation of the vesicles into lamellar sheets, not possible with hard sphere vesicle systems. [298]

Considering an uncharged hard sphere colloidal dispersion, two colloidal spheres in solution will not interact with each other at long range but the short range interactions will be dominated by the born repulsion and the attractive van der Waals forces. [92] To counteract this, and to aid in stabilising the colloidal dispersion, charged colloidal particles can be used. For surfactant vesicle systems ionic surfactants are employed. At the surface of the resulting charged vesicles an electrical double layer at the surfactant water interface forms. As two charged vesicles approach one another in the dispersion their electrical double layers overlap creating a repulsive interaction, as described in detail in section 2.3.2. EDL interactions are generally longer range than the van der Waals interactions and dominate the interactions at large separations. The DLVO theory combines the EDL forces and van der Waals forces to describe and understand the stability of simple colloidal systems, as discussed in section 2.3.3. [113, 114]

The DLVO theory is generally good enough to describe the interactions between particles within a simple colloidal system and to predict the stability of the dispersion. [299] However for more complex multicomponent systems additional interactions have been observed which can not be accounted for by the DLVO theory alone.

These non-DLVO interactions include such interactions as depletion attraction, depletion stabilisation, polymer bridging, hydration effects, and steric interactions, as well as any ion specific effects. [126, 222, 300, 301] As the DLVO theory mostly considers the colloidal particles to be hard spheres additional interactions or behaviour not predicted by the DLVO theory may impact the stability of vesicle dispersions. With vesicle system we must consider how additives not only effect the interaction between the vesicles but how they may effect the structure of the vesicles themselves. Additives acting on the bilayer or interacting with he surfactant monomers themselves may play a role not depicted by the DLVO theory. There has also been a push towards more highly concentrated vesicle dispersions were the vesicle's elasticity and deformation may also play a role in the intervesicle forces. [302, 303]

In this chapter the interactions between two supported bilayers of the cationic surfactant DIPEDMAMS were directly measured using colloidal probe atomic force microscopy, as shown in figure 4.1. The impact of increasing NaCl concentrations on the interactions and how different sodium halide salts affect the bilayer bilayer interactions were investigated. Atomic force microscopy was used to investigate the impact of the halide ions ions and their concentration in the topography and nanomechanical properties of the supported surfactant bilayers to try and differentiate between the impact of the salts on the interactions between the bilayer and changes in the interactions caused by the impact of the salts on the bilayers themselves. SAXS and WAXS were used to compare the impact of the salts on supported bilayers and on the bulk lamellar phase as supported bilayers may impact on the behaviour of the bilayers. Finally the behaviour of bulk vesicle dispersion in the presence of the halide salts investigated was studied by particle sizing and zeta potential. Enabling the comparison of the measured interactions and the behaviour of the vesicle dispersion.

The interaction between the supported bilayers was observed to decrease with increasing salt concentration as the electrolyte screened the vesicles' electrical charges from each other. This screening effect was observed to increase for halide salts further down the periodic table with lower atomic number halides being less effective at reducing the repulsion between bilayers. As the standard DLVO model does not account for ion specific effect other models of the electrical double layer are discussed

in an attempt to explain this observation. This effect of larger halide ions having a greater impact on the behaviour of the system compared with smaller halide ions at the same concentration was also reflect in the AFM imaging, x-ray scattering, and the stability of the bulk vesicle dispersions. A large portion of the work presented in this chapter has been adapted from a paper published by the author. [304]

6.2 Experimental

The cationic surfactant, di(alkyl iso-propyl ester) dimethyl ammonium methylsulfate (DIPEDMAMS) was provided by Procter and Gamble. Synthesised using an industrial fatty acid mixture of C18, C16 and C18:1 chains, therefore the aliphatic tails are a statistical mixture of the three fatty acids see Chapter 4. NaCl, NaBr, NaI and $CaCl_2$ were obtained from Sigma-Aldrich. All solutions were prepared with deionised water, $<$ 18 mS, filtered through an activated carbon filter to remove organic impurities.

6.2.1 Preparation of supported lipid bilayers

Supported surfactant bilayers were formed by the vesicle deposition technique from a vesicle dispersion containing 10 mol% perillyl alcohol as described in Chapter 3. Bilayers were formed on both mica and the glass colloidal probe in situ at room temperature as described in Chapters 3 and 5.

6.2.2 Atomic Force Microscopy

All measurements were made using a JPK Nano wizard 4 AFM and analysed using the JPK data processing software as detailed in Chapter 3

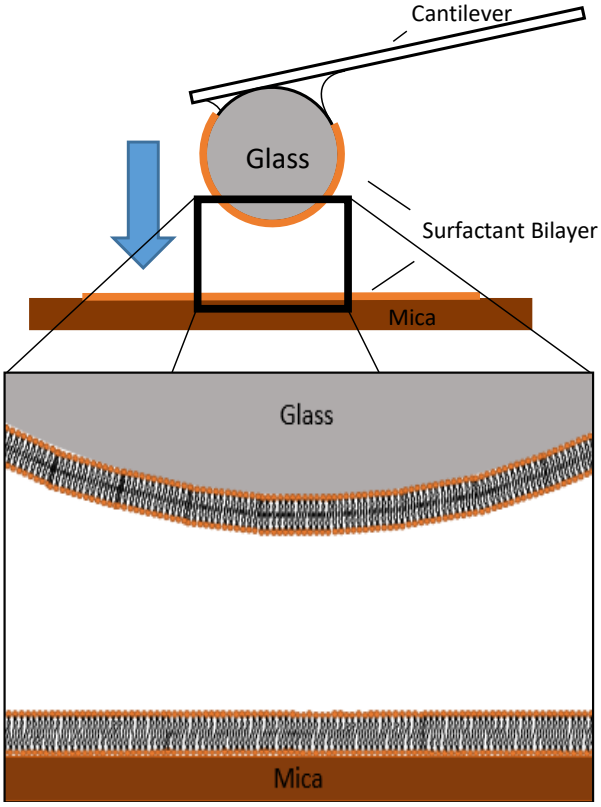


Figure 6.1: Schematic of the colloidal probe experimental set up used for the direct measurement of interactions between two cationic surfactant bilayers.

Colloid Probe Atomic Force Spectroscopy

Colloidal probe force spectroscopy was used to measure force distance curves between a colloidal sphere, attached to an AFM probe, and a flat substrate, as shown in figure 6.1. By forming a supported cationic surfactant bilayer on both surfaces the interactions between the bilayers could be investigated. The aqueous environment was changed by flushing the system with the electrolyte solution of interest. Force curves were collected in multiple positions across the surface for each electrolyte solution. For more details please see Chapter 3

AFM Imaging

All imaging was performed in quantitative imaging (QI) mode. The aqueous environment was changed by flushing the system with the electrolyte solution of interest.

Multiple images of different areas of each supported bilayer in the electrolyte solutions were collected. All imaging was performed at 23 ± 2 °C. Further details on QI mode and on the imaging protocols can be found in Chapter 3

6.2.3 Small Angle X-ray Scattering (SAXS)

Sample Preparation

DIPEDMAMS/water systems were fabricated according to the protocols discussed in Chapter 3. Samples were hydrated at 20 wt% by mass.

Beamline set up

SAXS was performed at the Diamond Light Source (Oxfordshire) on beamline I22, as detailed in Chapter 3 Samples were measured in glass capillaries at 25 °C.

6.2.4 Dynamic Light Scattering and Zeta Potential

Sample Preparation

DIPEDMAMS vesicle dispersions with the electrolyte concentration and composition of interest were fabricated according to the protocols described in Chapter 3.

Particle sizing and zeta potential measurements

Particle sizing and zeta measurements were performed using a A Brookhaven zeta-PALS as detailed in Chapter 3. All measurements were performed at 25 °C.

6.3 Results and Discussion

6.3.1 Interaction between supported cationic surfactant bilayers with increasing NaCl concentration

Supported cationic surfactant bilayers were formed on freshly cleaved mica and the borosilicate glass sphere of a colloidal AFM probe at room temperature. Perillyl alcohol was added at 10 mol% to the DEPEDMAMS vesicle dispersion in order to form good surfactant bilayers at room temperature, as discussed in Chapter 5. The interactions between the bilayers could then be measured as the colloidal probe was moved towards the mica supported bilayer at a constant piezo extension velocity of $1\,\mu m\,s^{-1}$. On contact the peizo continued to move towards the surface until an applied force of 20 nN had been reached. The probe was then withdrawn at the same rate of $1\,\mu m\,s^{-1}$. The interaction between the bilayers on approach and withdrawal will result in the deflection of the cantilever which can be used to determine the interaction forces between the bilayer on the probe and substrate at a given separation.

The interactions were measured at multiple locations to ensure reproducibility and to look for any variation across the supported bilayer. The electrolyte concentration was then increased, and the system allowed to equilibrate, before the interactions were measured again. As discussed in section 5.3.4 there is some variation in the forces measured between supported DIPEDMAMS bilayers between experimental set ups. This method of changing the electrolyte concentration enable the effect of the concentration to be investigated within the same experimental set up.

Figure 6.2 shows the forces measured between two supported cationic surfactant bilayers, on approach, as the NaCl concentration is increased from 0.01 mM to 100 mM. At all concentrations the interactions between the bilayers were repulsive, indicated by the deflection of the cantilever away from the surface on approach. The repulsive interaction appears to increase exponentially with decreasing probe substrate separation. As the separation decreases the probe eventually comes into

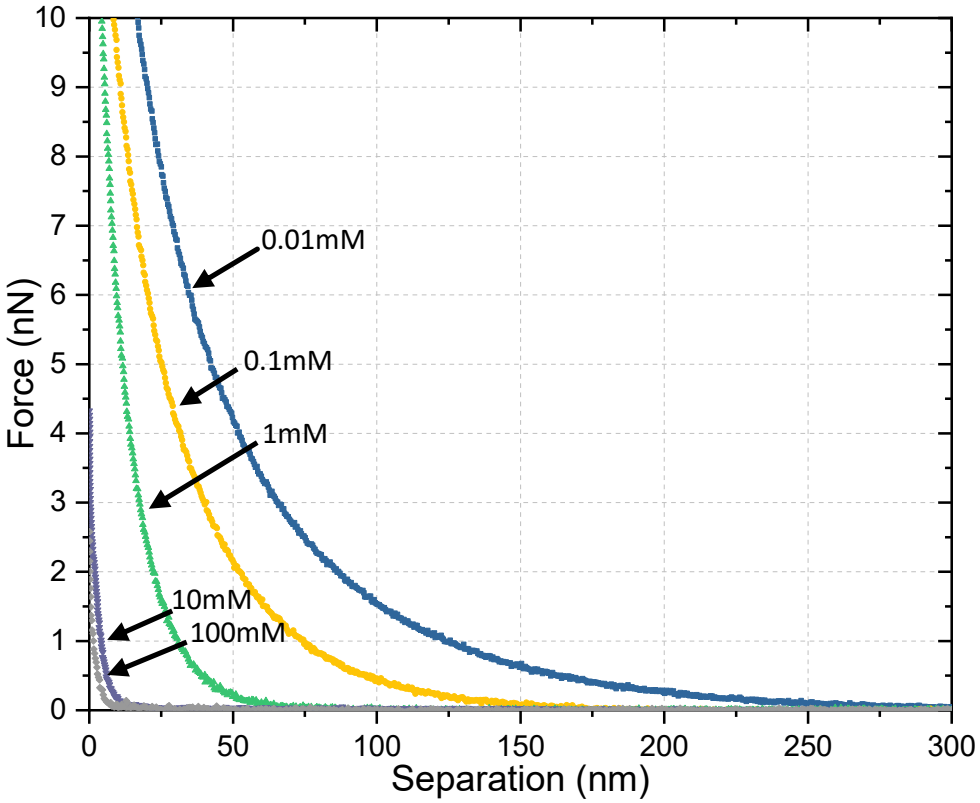


Figure 6.2: Forces measured between DIPEDMAMS on approach in solutions of increasing NaCl concentration.

hard contact with the surface, typically between 15 nN to 25 nN. The separation at which the onset of the repulsive interaction was observed decreased with increasing salt concentration and the applied force at which the cantilever deflection became compliant with the piezo extension also decreased. On withdrawing the bilayers, the observed interactions were, within error identical, to the forces on approach. The force curves shown for each salt concentration are typical of those observed across the surface at that concentration.

To further interpret and understand the bilayer bilayer interactions and the impact of salt on the forces, the data were compared to the DLVO theory. The DLVO theory combines the attractive van der Waals forces with the repulsive interactions arising form the electrical double layer. This is discussed in detail in section 2.3.2. As the system studied here involves a colloidal sphere and a flat substrate the DLVO theory will be discussed for a sphere-plate geometry.

The van der Waals interactions for the sphere-plate geometry can be described

as:

$$W_{vdw} = -\frac{AR}{6D^2} \tag{6.1}$$

Where A is the Hamaker constant, R is the radius of the sphere, and D is the surface to surface distance. [35] The literature value of 1.3×10^{-21}J for the Hamaker constant was taken. [178]

The electrical double layer interactions for the sphere-plate geometry at constant surface potential can be described as:

$$W_{edl} = \frac{128\pi n k_B T \gamma^2}{\kappa} R \exp^{-\kappa D} \tag{6.2}$$

Where n is the bulk electrolyte ion concentration in m^{-3}, k_B is the Boltzmann constant, $\gamma = \tanh(ze\psi/4k_BT)$, where e is the elementary charge, z is the valence, and ψ is the surface potential. κ is the Debye-Huckle coefficient given by equation 6.3. [305]

$$\kappa = \sqrt{\frac{2e^2 N_A I}{\epsilon_0 \epsilon_r k_B T}} \tag{6.3}$$

Where k_B is the Boltzman constant, N_A is Avogadro's number, and I is the electrolyte concentration in $mole/m^3$. The total interaction W_{DLVO} is then the sum of the van der Waals and electrical double layer (EDL) interactions, as shown in equation 6.4. [35, 305]

$$W_{DLVO} = W_{vdw} + W_{edl} \tag{6.4}$$

The DLVO theory was compared to the experimental data using the Debye length (κ^{-1}) and the surface potential (ψ) as fitting parameters for the electrical

interactions. The van der Waals interactions were assumed to be constant and the Hamaker constant was set to the literature value for this system.

The DLVO model suggested that the interactions between the two bilayers should be repulsive at long range before becoming attractive at a separations between 2 nm to 4 nm. This is in contrast with the experimental data which shows the interactions between the bilayers to be increasingly repulsive up until the surfaces come into contact. Previous surface force apparatus (SFA) experiments by Anderson et al [182] and others for surfactant and lipid bilayers, formed using a Langmuir-Blodgett trough, but is in agreement with Horn et al, [179] where the bilayers were formed by the vesicle deposition technique.

As the salt concentration for the model is increased, the range and strength of the repulsive interactions decreases. Whilst this pattern is similar to the experimental data, at concentrations above 10 mM the model suggest that the repulsive interactions should be shorter ranged and weaker than those observed in the experimental data.

A comparison of the experimental data, the DLVO model, and the model electrical double layer forces are shown in figure 6.3. That data has been plotted on a semi-log scale in order to emphasise the exponential nature of the repulsive interactions. As mentioned the short range attraction, due to the attractive van der Waals interactions, predicted by the DLVO theory, is not observed in the experimental. This is most likely due to the repulsive effect of short range hydration forces or due to steric repulsion caused by the surfactant's large head group. Therefore, in the discussion of the measured bilayer-bilayer interaction the focus will be on the electrical double layer forces component of the DLVO theory.

The experimental data and the theoretical EDL interaction generally compare well. There is a very good agreement between the experimental data and the theoretical for the initial repulsive interactions. As the separation is further decreased the two begin to diverge. The experimental data show a greater repulsion at shorter separations than predicted by the EDL model. The separation at which the experimental data begins to diverge from the theoretical model is dependent on the NaCl

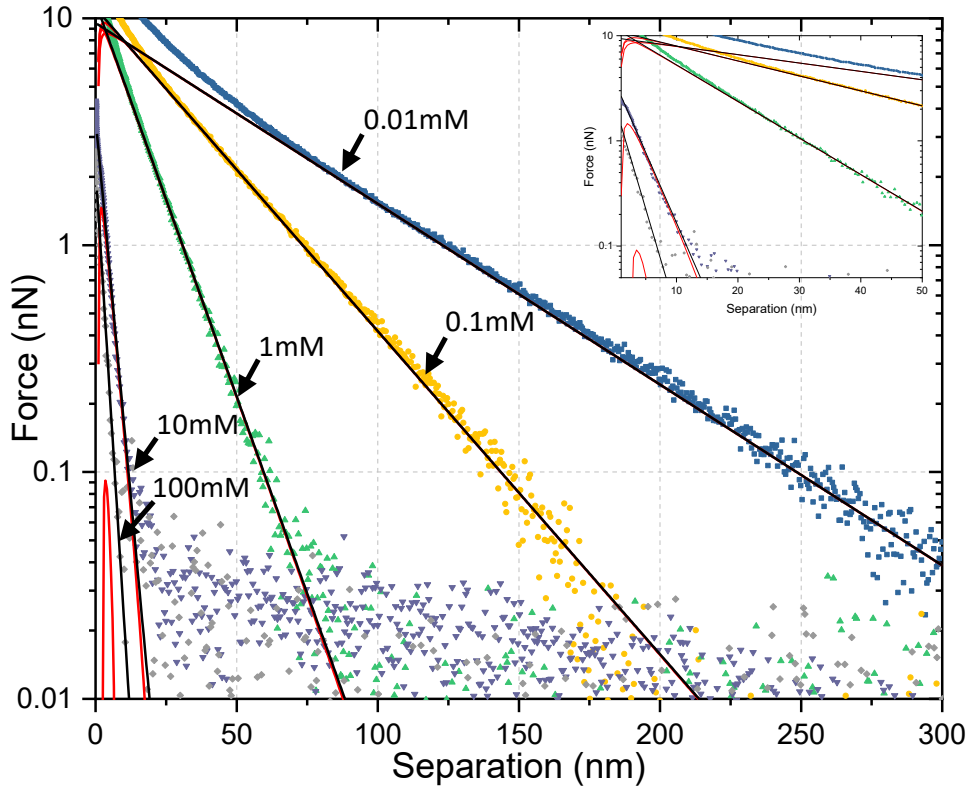


Figure 6.3: Forces measured between DIPEDMAMS on approach in solutions of increasing NaCl concentration, on a semi-log scale. Solid red lines show the theoretical DLVO fitting for each electrolyte environment and the solid black lines show the theoretical EDL forces. See table 6.1 for fitting parameters.

concentration. The data diverge at a separation of around 60 nm for 0.01 mM, 10 nm for 1 mM and less than 2 nm for 10 mM NaCl.

Looking at the combined DLVO theory with regards to the experimental data. At lower salt concentrations, $\leq$ 10 mM, the theoretical DLVO forces fit the data rather well at long range. In this region the model is dominated by contributions from the EDL interactions. At short range the combined model predicts an attraction not observed in the experimental data as discussed earlier. At NaCl concentrations $\geq$ 10 mM the combined DLVO is poor due to the influence of the attractive forces in the model which predicts that the force between the bilayers should be less repulsive than shown in the experimental data. However the experimental data at these concentrations fit well with the theoretical EDL interactions.

At low NaCl concentrations it is suggested that the attraction due to van der

Table 6.1: Fitting parameters used in DLVO and EDL fits to the CP-AFM data in figure 6.3

	Debye length/κ^{-1}		Fitted Surface Potential	
[NaCl]/mM	Theoretical/nm	Fitted/nm	ψ/mV	Normalised ψ
0.01	97	54.5±1	60±2	1
0.1	30	30.5±1	48±2	0.80
1	10	12.5±0.5	29.5±1	0.49
10	3	3±0.5	11±1	0.18
100	1	2.2±0.5	5.5±0.5	0.09

Waals forces, as predicted by the DLVO theory, is not observable due to its short range and weak nature compared to the EDL forces at these concentrations. Due to the relatively large head groups of the surfactant, steric effects are also likely to be a factor. The increased repulsion observed at short range in the experimental data, which was not predicted by the model EDL interactions may also contribute to the absence of measured short range attraction. This increased repulsion, compared with the theoretical model, may be due to a combination of hydration and steric forces or be due to charge regulation between the two bilayers. These are not accounted for by the DLVO theory.

The model interactions due to the electrical double layer are shown in equation 6.3. This model uses several approximation and assumption that need to be considered when comparing the experimental to the theoretical data. It assumes symmetry within the system with the surface potential ψ of both surfaces taken to be identical. This equation is the low potential solution to the Poisson-Boltzmann equation and assumes that the surface potential remains constant as a function of separation. Ducker et al, used a numerical solution to the Poisson-Boltzmann equation, with a constant surface charge regime. Using a constant surface charge assumption as opposed to a constant surface potential the theoretical showed a sharp increase in the repulsion at small separation. [200]

A comparison of the DLVO theory parameters and experimentally derived values are shown in table 6.1. The experimental and the theoretical Debye lengths decrease with increasing NaCl concentration. Apart from at 0.01 mM NaCl the experimental values compare well with the theoretical values. The experimental values for the Debye length at 0.01 mM is significantly lower, only 55%, of the theoretical value.

The Debye length can be considered as a measure of the range of the EDL interactions. As the electrolyte concentration is increased the number of charged species between the bilayers increases. These additional charged species act to screen the electrical interaction between the charged bilayers, which is predicted by the theoretical model and observed from the experimental data. The discrepancy between the theoretical and experimental data at low NaCl concentrations is suggested to be due to impurities in the deionised water which would have a greater effect on the Debye length in samples containing low NaCl concentrations.

The measured values for the surface potential are observed to decrease with increasing NaCl concentration. As discussed in Chapter 5 there is some variation in the strength of the observed repulsion between experiments. This translates into a variation in the experimentally derived values for the surface potential, these were generally within the range of $\sim$ 55 - 70 mV at 0.01mM NaCl. Due to this variation in terms of the initially measured surface potential the decrease in surface potential is best viewed in relation to the measured value at 0.01 mM. The normalised surface potential is included in the table for ease of comparison between experimental runs. The measured surface potential values are lower than those measured for similar surfactant systems using the surface force apparatus but generally in good agreement with the initial zeta potential measurements of 60 - 70 mV for the vesicle system at 0.01mM NaCl. Decreasing surface potential with increasing salt concentration has been observed for other surfactant systems and hard sphere colloidal systems such as silica. [181, 306] In hard sphere systems the increasing salt concentration is considered to increase the surface charge density but decreases the surface and zeta potentials. With surfactant and other soft matter systems the impact of salt concentration on the local packing and organisation within the bilayer must also be considered. [307]

6.3.2 Role of Counterion in Bilayer-Bilayer Interactions

The interactions between two supported DIPEDMAMS bilayers on approach were measured in solutions of NaI, NaBr, and $CaCl_2$. For each of the salts the interactions were measured as the halide concentration was increased from 0.01 mM to 100 mM.

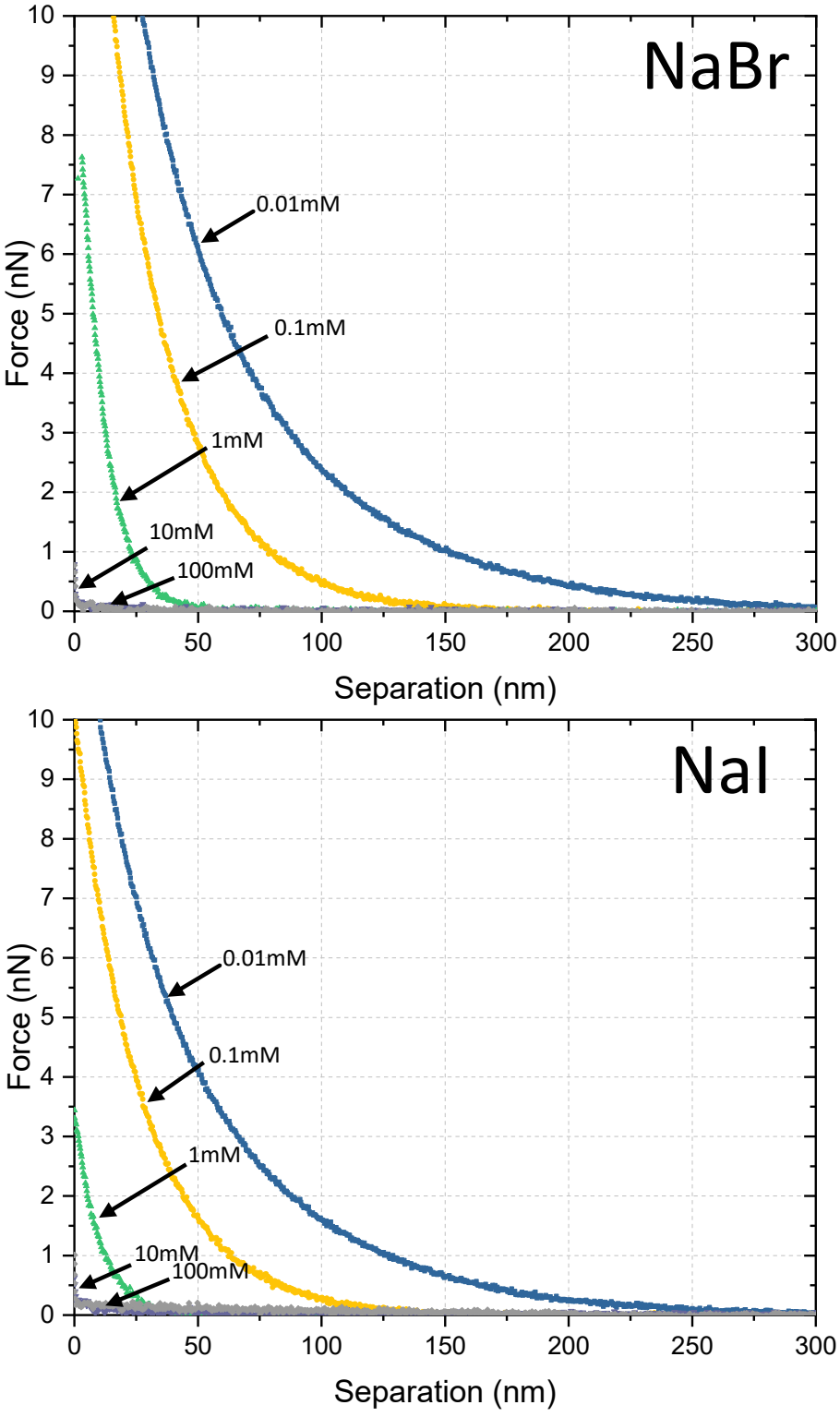


Figure 6.4: Forces measured between DIPEDMAMS bilayers on approach in electrolyte solutions with increasing concentration.. Halide concentrations and salt identity are shown in the figure.

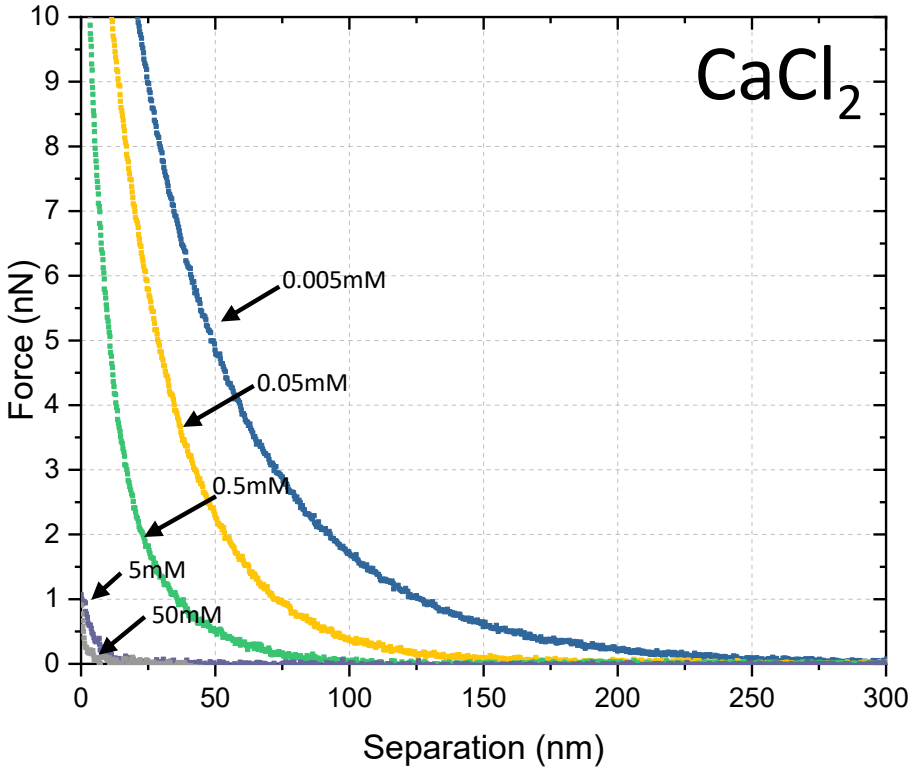


Figure 6.5: Forces measured between DIPEDMAMS bilayers on approach in electrolyte solutions with increasing concentration. Halide concentrations and salt identity are shown in the figure.

At least 64 force profiles were collected at each salt concentration and each experiment was repeated with different probes. NaBr and NaI were used to investigate the impact of different counterions on the surfactant system with $CaCl_2$ probing the impact of the co-ion and polyvalent cations. Figure 6.4 and 6.5 show the measured interactions between the supported surfactant bilayers in increasing concentrations of NaI and NaBr, and $CaCl_2$ respectively. The force curves shown here are typical of those collected at each salt concentration.

At 0.01 mM halide concentration, for all salts, the measured forces were solely repulsive. At separations above 300 nm no interactions were observed but as the separation was decreased and the two bilayers brought into contact a repulsive interaction was measured between 300 and 250 nm. As the separation was further decreased the repulsive force measured between the surfaces increased exponentially. At very small separation the repulsion became indistinguishable from the compliance region of a force curve and hard contact between the two bilayers was assumed.

No significant difference between the forces measured in deionised water and in a 0.01 mM salt solutions were observed, forces in deionised water omitted for clarity.

As the salt concentration is increased from 0.01 mM to 1 mM the interactions remain repulsive however the range and strength of the repulsive interaction appears to decrease. Whilst this trend of decreasing repulsion is observed for all salts investigated the extent to which the interactions decrease appears to be dependent on the halide counter ion. The NaI containing system shows a larger decrease in the repulsive interactions than the NaBr systems, which in turn show a larger effect on the interaction than NaCl. The $CaCl_2$ system appears to have a similar impact on the measured repulsive interactions as the NaCl systems discussed earlier.

Increasing the halide concentration further to 10 mM results in a further decrease to the range and strength of the repulsive interactions. For NaBr and NaI the measured interactions are so small that they are difficult to differentiate from the background thermal noise. Whereas the interactions for the $CaCl_2$ and NaCl systems are still resolvable. As the measured forces for NaBr and NaI are so low at 10 mM it is difficult to resolve, on this scale, any further changes to the interactions on increasing the salt concentration to 100 mM. In $CaCl_2$ an increase in the halide concentration to 100 mM does result in a further decrease in the range and strength of the repulsive interactions. However this change appears small compared with the decrease observed over lower salt concentrations.

Figures 6.6 and 6.7 show theoretical model interactions for the interactions between two charged surfaces on approach alongside the measured interactions between the cationic surfactant bilayers in increasing concentrations of NaI, NaBr, and $CaCl_2$ on semi-log scales. Comparing the DLVO and EDL fits the attractive van der Waals component of the DLVO model appears to be absent. This may be explained by the presence of short range repulsive interactions not accounted for by the DLVO theory, as discussed earlier. For clarity only the EDL interactions have been shown.

From the semi-log plots it is clear that the the majority of the the repulsive interaction is exponential in nature. However at small separation the forces do deviate from a purely exponential relationship with the rate of increase in repulsion

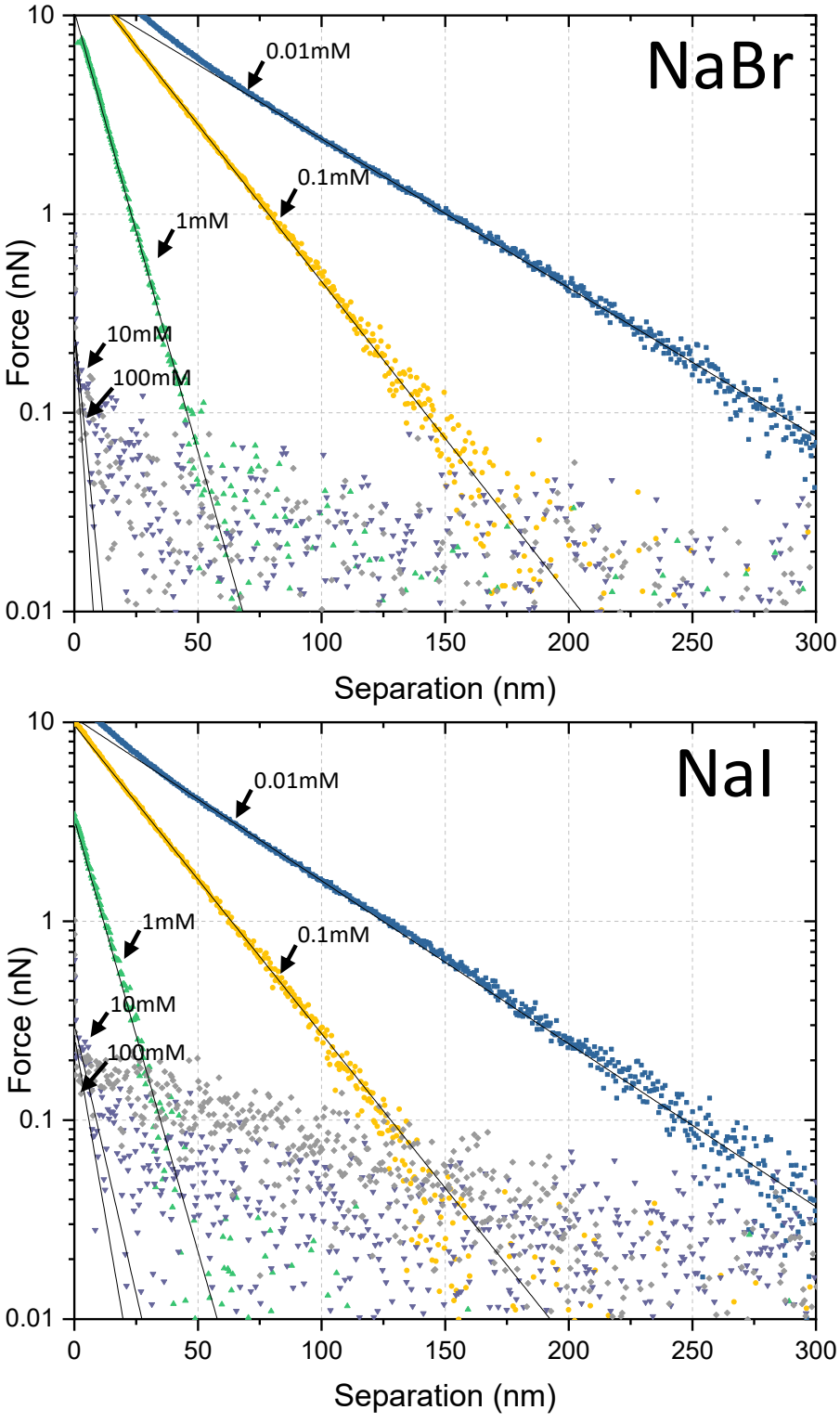


Figure 6.6: Forces measured between DIPEDMAMS bilayers on approach in electrolyte solutions with increasing concentration, on a semi-log scale. Solid black lines show the theoretical model EDL interactions interactions for each environment. Halide concentrations and salt identity are shown in the figure. See table 6.2 for fitting parameters.

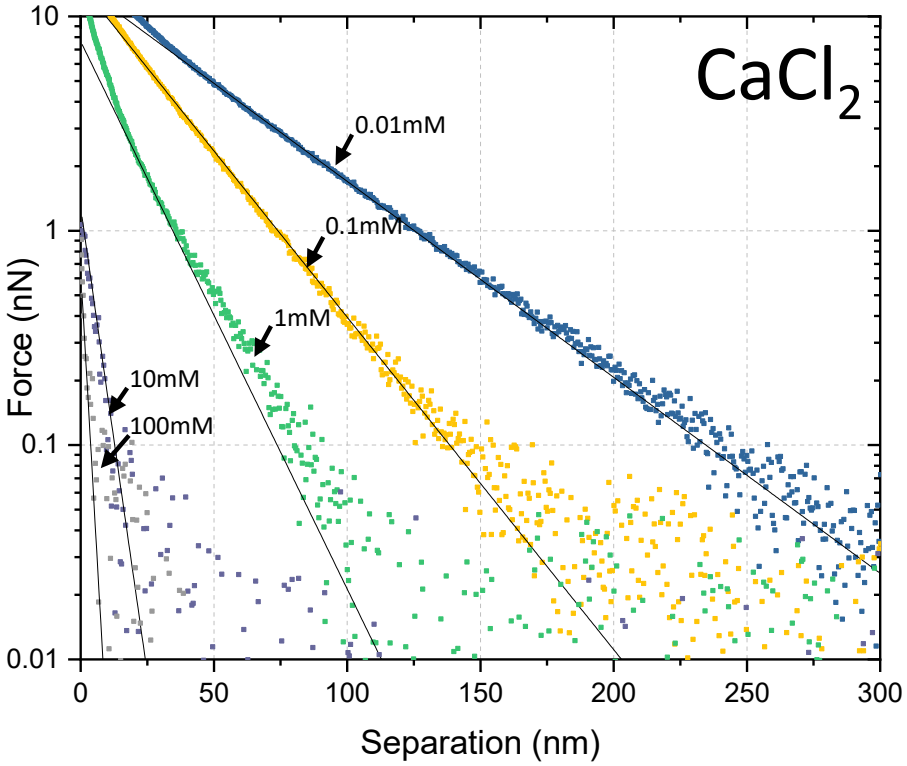


Figure 6.7: Forces measured between DIPEDMAMS bilayers on approach in electrolyte solutions with increasing concentration, on a semi-log scale. Solid black lines show the theoretical model EDL interactions interactions for each environment. Halide concentrations and salt identity are shown in the figure. See table 6.2 for fitting parameters.

increasing with shortening separation. The model EDL forces fit the experimental data well with some divergence between the model and the data at short separations at the lower salt concentrations. From the plots it is observed that the theoretical model EDL forces generally fit the experimental data well for all halide salts investigated. There are however some divergences at very low salt concentrations and at the higher salt concentrations. At 0.01 and 0.1 mM halide concentrations the model fits the initial interaction well but diverges from the experimental data as the separation decreases. At smaller separation the experimental data are more repulsive than the model predicts, this is more pronounced at at lower salt concentrations than higher. The fitting at high halide concentrations, $\leq$ 10 mM, is problematic due to the short range and weak nature of the forces at these concentrations especially in the NaBr and NaI environments.

On a semi-log scale the model forces show a linear relationship between sepa-

Table 6.2: Fitting parameters used in DLVO and EDL fits to the CP-AFM data in figure 6.6 and 6.7

	Debye length/κ^{-1}		Fitted Surface Potential	
[NaBr]/mM	Theoretical/nm	Fitted/nm	ψ/mV	Normalised ψ
0.01	97	58±2	73±10	1
0.1	30	28±1	51±4	0.69
1	10	9.4±0.6	21.5±1	0.29
10	3	2.5±1	5.6±0.5	0.07
100	1	2±1.5	3.8±2	0.05
[NaI]/mM				
0.01	97	54±1	63±3	1
0.1	30	28±1	41±1	0.66
1	10	10±0.5	14±1	0.22
10	3	3±2.5	3±2	0.06
100	1	1±0.5	2.5±2	0.04
[CaCl2]/mM				
0.005	79	47±2	66±5	1
0.05	25	26±2	52±2	0.78
0.5	8	14±4	25±4	0.38
5	2.5	4.5±0.5	7.5±1	0.17
50	0.8	2±0.5	3±0.5	0.05

ration and the force between the bilayers. The absolute value of the gradient is inversely proportional to the Debye length whilst the intercept is directly related to the surface potential. From the plots it can be observed that the absolute gradient increases and the intercept of the model plots decrease with increasing salt concentration. The increase in gradient with the increasing salt concentration does not appear to be dependent on the identity of the salt but the decrease in intercept does appear to be dependent. The increasing $CaCl_2$ appears to have the least effect on the intercept whilst NaI is observed to have the largest effect on the decreasing intercept.

Table 6.2 shows the results of the DLVO fitting operation for all concentrations of NaBr, NaI and $CaCl_2$, giving theoretical and experimental values for the Debye length and experimental values for the surface potential. As there is some variation in the initial experimental surface potentials a column normalising these values at 0.01 mM has been included for ease of comparison.

The experimental Debye lengths for all salts decrease with increasing salt con-

centration. This coincides with the qualitative observation from the experimental data that the range of the interaction decreases with increasing salt concentration. Comparing the Debye lengths of the different sodium salts at similar concentrations shows no significant difference between them, the higher concentration of NaI do appear to have a longer Debye length than their chloride and bromide counterparts, however this is believed to be due to the difficulty of fitting with the small distances observed in these environments. The experimental Debye lengths of $CaCl_2$ are not significantly different to those in NaCl.

There is a good agreement between the theoretical Debye lengths, and the experimental Debye lengths, for all sodium salts at most concentrations however they do begin to diverge at low and high concentrations. At the lowest concentration, 0.01mM, the experimental Debye lengths are shorter than predicted by the calculations, most likely a result of impurities in the deionised water or ions from dissolved CO_2, and at the highest concentration of 100mM the experimental Debye lengths are typically longer. The experimental Debye lengths for the $CaCl_2$ concentrations bear more of a similarity to the theoretical sodium chloride Debye lengths than to the theoretical $CaCl_2$ Debye lengths. At the lowest concentration, 0.005 mM $CaCl_2$, the Debye length is shorter than predicted, as with the sodium salts, the experimental lengths for the remainder of the concentrations are longer than predicted.

The surface potentials extracted from the fitting of the DLVO forces to the experimental data, shown in table 6.2, show that for all electrolytes the surface potential decreases with increasing salt halide concentration. The decrease in surface potential appears to be related to the halide counter-ion. $CaCl_2$ and NaCl have a very similar effect on the surface potential when compared by chloride concentration as opposed to absolute electrolyte concentration, taking into account that $CaCl_2$ provides two chloride ions per molecule compared to NaCl. NaBr and NaI exhibit a much stronger effect on the surface potential as a function of concentration compared to the chloride salts, with NaI being more effective at reducing the surface potential than NaBr. It is worthwhile to point out that a direct comparison of the surface potentials at each salt concentration is hindered by variation in the initial surface potentials, measured at 0.01mM for sodium salts, and 0.005 mM for $CaCl_2$. This is attributed to variations in the surface roughness of the probe, the position of the

sphere on the probe, and by variations in the spring constant of the cantilever. These are difficult to fully control as the probes are manufactured off site and tuning the cantilevers by thermal motion is not possible due the dampening effect of the glass sphere. However when similar imaging probes were used, the spring constants were found to be within 10% of the stated value To help mitigate some of this uncertainty and for ease of comparison, an additional column, normalising the fitted surface potential to the fitted potential at 0.01 mM halide has been included in table 6.2.

There is a clear trend with regards to the electrolytes' efficacy to decrease the surface potential. In order of least potent to most this is as follows $CaCl_2$ = NaCl < NaBr < NaI. Exhibiting a clear correlation between potency and the position of the halides within the periodic table, potency increases as one moves down the halide group. In contrast to the Debye length values which are independent of the halide type.

The trend, or lack thereof, with regards to the electrolyte composition and the experimental Debye lengths can be explained by equation 6.3. The Debye length is a measure of the distance over which a charged species electrical effect can persist. As the distance from the charged species increases the charge becomes increasingly electrically screened. With each Debye length from the charge the electrical potential will decrease by $1/e$. From equation 6.3 it is noted that the Debye length is dependent on the relative permittivity of the solvent, ϵ_r, and the electrolyte concentration, I. Suggesting that the nature of the charge, in this case the bilayers, and the identity of the electrolyte are not important, which is what has been observed in the experimental data.

Simple electrical double layer models such as the Gouy-Chapman and Stern models can be used to begin to understand the role of the increased electrolyte concentration on the measured surface potential. [107] Assuming the bilayer acts as a charged surface the models suggest that there would be a layer of strongly adsorbed couterions at the surface, the Helmholtz layer, and then a diffuse layer enriched in the halide counter ions but not strongly held to the surface, the concentration decreases exponentially with distance from the Helmholtz layer until it is equal to the concentration of the bulk solution. [35,305] This model would suggest that as the

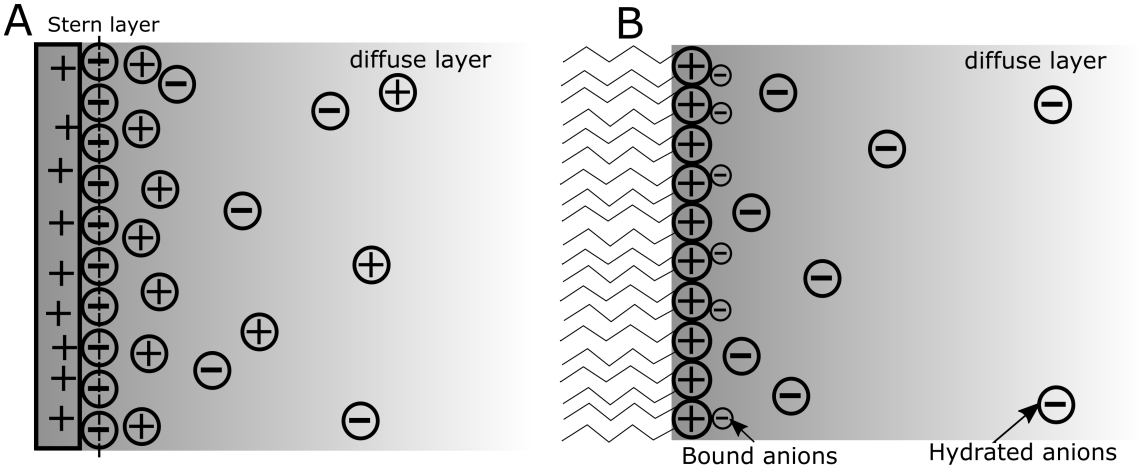


Figure 6.8: Schematic showing a) a classic EDL with stern layer and diffuse layer b) ionic pair model for a surfactant bilayer.

electrolyte concentration increased the Helmholtz layer would be largely unaffected but would shorten the diffuse layer. This leads to a decrease in the potential between the Helmhotz layer and the diffuse layer, lowering the measured surface potential. However, these models can not account for ion specific effects, the only property of the charged species they account for is their charge and concentration.

A potential explanation for the observed trend comes from the trend's similarity to the Hofmeister series. [308, 309]. The Hoffmeister series was originally developed to describe an ion's ability to salt in or salt out proteins. That is where the solubility of the protein increased or decreases with increasing electrolyte concentration. With respect to surfactant systems salting in generally refers to a decrease in the surfactant packing order whilst salting out results in an increase in the packing order. This is generally considered to be the result of how strongly the counterion binds to the surfactant head group and is dependent on the size and degree of hydration of the ion. The Hoffmeister series for anions is typically ordered $SO_4{}^{2-} < HPO_4{}^{2-} < Cl^- < NO_3{}^- < Br^- < I^-$. This compares well to the trend observed for halide salts here. Salts on the left hand side of the series are typically described as kosmotropes. They are strongly hydrated, have a small ionic radius and have a high charge density. The right hand side, in contrast, are considered chaotropes. They are weakly hydrated, have a large ionic radius and a low charge density. The halides can not truly be separated into kosmotropes and chaotropes but take on a more chaotropic properties as they move down the periodic table. It is suggested that this weakening hydration

sphere of the halide ions plays a role in their observed ability to decrease the surface potential of the surfactant bilayer.

Kalinin and Radke proposed an ionic binding model to describe the species specific effects of counter ions on surfactant monolayers. [310] Using the surfactant bilayers, monolayers in their model, as the charged surface; the model proposes an inner Helmholtz plane of partially dehydrated counterions forming ionic pairs with the surfactant head groups. The counter ions in the diffuse layer, as in classic EDL models, are fully hydrated and range from the Helmholtz layer to the bulk electrolyte solution, as shown in figure 6.8. The surface potential in this model is determined by the number of unpaired ionic surfactant head groups and the electrolyte concentration in the bulk solution.

Using this model it is possible to qualitatively explain the trend observed in the experimental surface potentials in relation to the halide counter ions. As discussed above, the strength of the hydration sphere around a halide ions decreases moving down the periodic table. Using the ion binding model, shown in figure 6.8 it can be argued that weakly hydrated ions are better able to and more likely to bind to the surfactant head groups, than strongly hydrated ions. Therefore at any given electrolyte concentration the number of halide counter ions bound to the surfactant head groups depends on the identity of the counter ion. As the surface potential is dependent on the number of unbound surfactant head groups, it is expected that the surface potential will be lower with the addition of NaI compared to NaBr, and lower in NaBr compared with NaCl or $CaCl_2$, which, taking only the Cl concentration, should behave in a similar manner. This is in good agreement with the experimental observations discussed above which show that the declining surface potential with increasing electrolyte concentration is dependent on the identity of the halide counter ion.

6.3.3 AFM Imaging

It is suggested that there are two main ways in which the halide salts can impact the forces between the surfactant bilayers. One is to change the way the interactions are

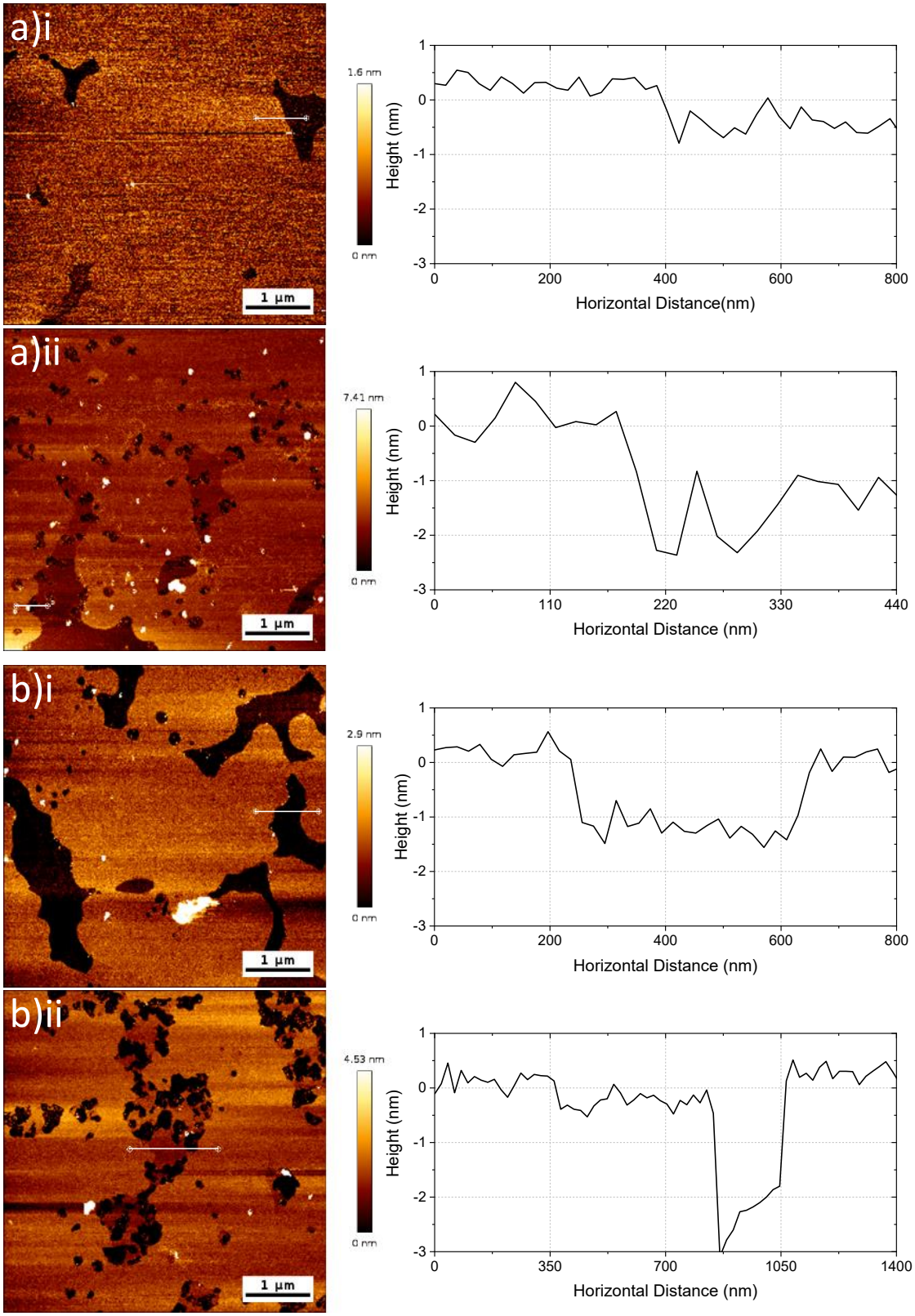


Figure 6.9: AFM images, 5 x 5 μm and associated cross-sections for a)i0.01 mM NaCl a)ii 100 mM NaCl b)i 0.01 mM NaBr b)ii 100 mM NaBr.

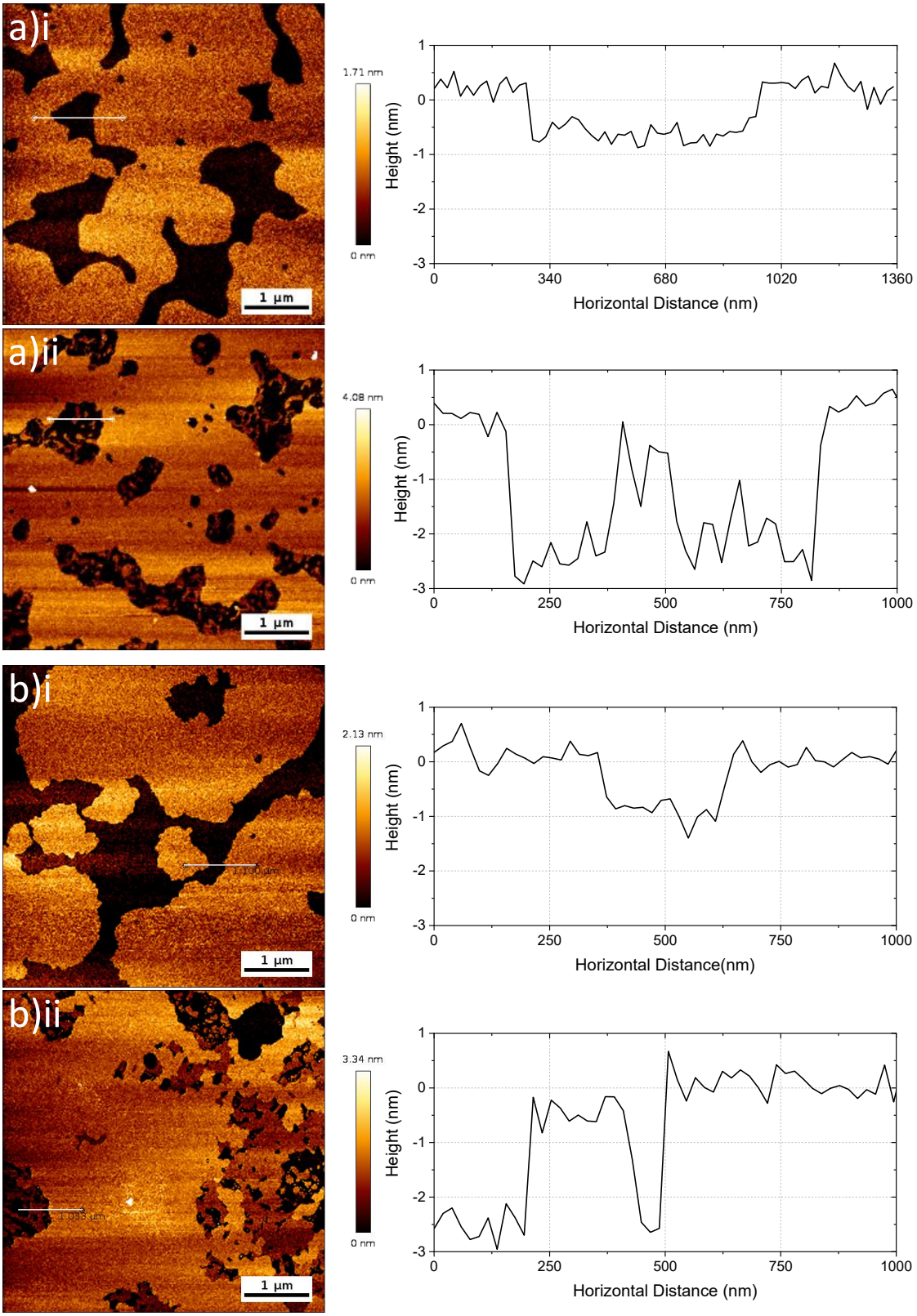


Figure 6.10: AFM images, 5 x 5 μm and associated cross-sections for a)i0.01 mM NaI a)ii 100 mM NaI b)i 0.005 mM $CaCl_2$ b)ii 50 mM $CaCl_2$.

transmitted through the medium between the surfaces and the other is to affect the surfaces themselves thus changing the interactions between them. A combination of the two is most probable. To compliment the colloidal probe measurements of the interactions between surfactant bilayers the impact of halide salts on the topography and properties of the supported surfactant bilayers was investigated by AFM.

Supported DIPEMDMAMS bilayers, containing 10 mol% perillyl alcohol, were formed by the vesicle deposition technique at room temperature. In the same manner as those formed for the colloidal probe force spectroscopy. The bilayers were then imaged in increasing concentrations of NaCl, NaBr, NaI, or $CaCl_2$. Several bilayers were investigated for each electrolyte series.

Figure 6.9 and 6.10 show typical topographical AFM images of DIEPDMAMS bilayers in 0.01mM and 100mM NaCl, NaBr, NaI, and 0.005 mM and 50 mM $CaCl_2$ along with cross-sections of each image. Formed in deionised water the bilayers all show complete coverage of the mica substrate. The bilayers show two clearly defined regions differing in thickness by 1 - 1.5 nm which have been attributed to bilayer adopting different phases or structural arrangements in these areas. Occasionally bilayer fragments or vesicles were observed on top on the supported bilayers but these are believed to have had minimal impact on the force measurements.

At low salts concentrations < 0.1 mM, no significant change in the topography of the bilayers is observed for all salts investigated. The bilayers still show complete coverage of the mica substrate and exhibit the phase separation behaviour discussed above. As the salt concentration is raised above 0.1 mM (0.05 mM for $CaCl_2$) holes are observed in the bilayer. These appear to be concentrated in the thinner regions of the bilayers. These holes are typically 3 to 4 nm in depth. The number and size of these holes increases with increasing electrolyte concentration. There is also a change in the height difference measured between the thicker and thinner phases as the electrolyte concentration increases. The difference in thickness is generally 1 - 1.5 nm at low salt concentrations but decreases to approximately 0.5 nm at higher salt concentrations. The height difference between the two bilayer phases is observed to decrease gradually from 1 - 1.5 nm at low salt concentrations, to be between 0.5 and 1 nm at high salt concentrations.

All electrolytes investigated had the same general impact on the topography of the surfactant bilayers. However, the number and size of the holes formed in the surfactant bilayers not only exhibited a dependency on the electrolyte concentration but also on the identity of the halide salt. At a given halide salt concentration, it was observed that the system containing NaI will have more holes and larger holes in the bilayer than systems containing NaBr or NaCl; and the system with NaCl will show small holes and a fewer number of holes than the other sodium salts. Comparing systems containing NaCl and $CaCl_2$, at equivalent concentrations of chloride ions as opposed to total molarity, show little significant difference between them in terms of the bilayer topography.

The formation of holes in the surfactant bilayers with increasing electrolyte concentration offers an additional explantation for the observation that the measured surface potential decreases with increasing salt concentration. It is suggested that as more holes form in the supported bilayers and the surface coverage decreases the charge density and the overall surface potential decrease. The formation of holes in the supported surfactant bilayers also show a similar dependence on the identity of the halide salts as the experimental surface potentials from the colloidal probe experiments. Assuming the behaviour of the surfactant bilayers on the colloidal probe is similar to that on the flat mica this would also go some way in explaining why the repulsive interaction between the bilayers does not fully recover on decreasing the electrolyte concentration.

Figure 6.11 shows the height, adhesion, and measured slope maps for supported DIPEDMAMS bilayers at all NaBr concentration investigated. As discussed before the supported DIPEDMAMS bilayers form two different bilayer phases. These phases have different surface properties and nano-mechanics. The adhesion and measured slope maps show that there is a grater tip-sample adhesion on retraction for the thinner bilayer phase and that the thicker phase has a greater measured slope or relative stiffness than the thinner bilayer phase. As mentioned above, no change in the structure of the bilayers was observed between deionised water and 0.01 mM electrolyte concentration. As the NaBr concentration is increased holes are observed to form in the supported bilayers as mentioned. These holes appear to increase in size and number as the concentration increases. Overall the addition of

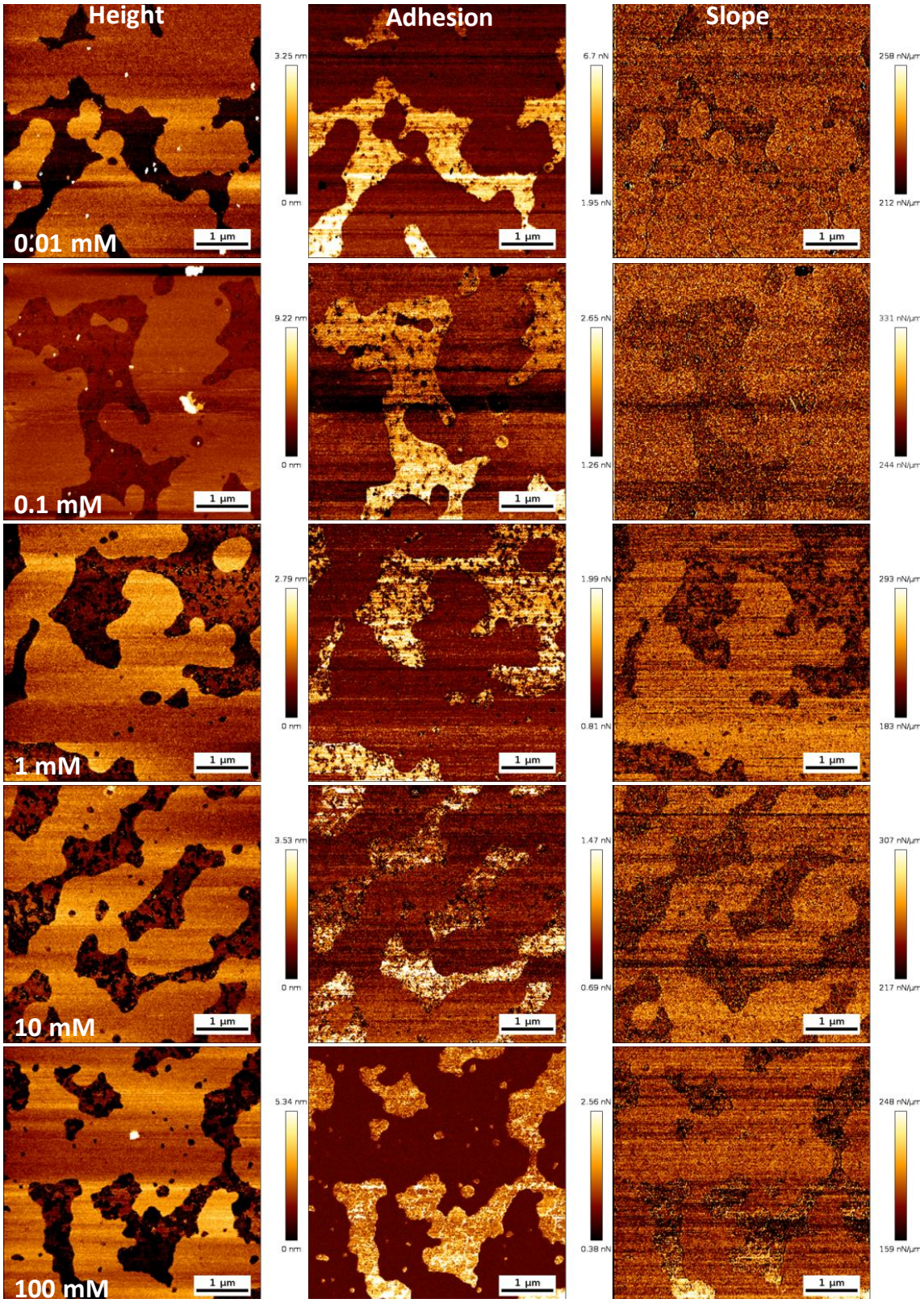


Figure 6.11: Typical QI AFM topographical images, with associated typical maps of surface adhesion and measured slope, for supported DIPEDMAMS bilayers imaged in increasing concentrations of NaBr. Concentrations shown in figure.

the electrolyte into the system does not appear to have an significant impact on the adhesion difference between the two bilayer phases nor are any significant changes observed in the relative stiffness of the two phases. Commenting on the impact of the holes on the nano-mechanics of the bilayers is problematic. In the adhesion maps some images show a decrease in the adhesion in those areas where holes are observed whereas other images or sections of images show an increase in the measured adhesion in those areas where the holes are observed in the topographical images. This is similarly true for the measured slope maps, with some showing a decrease in the measured slope in the areas where holes are observed, others showing no significant differences whilst others showed an increase in the measured stiffness in these areas.

The differing activity between the halide salts to affect the topography of the bilayer follow the same trend as observed with the bilayer interactions and the decreasing surface potential. That is chloride being the least effective and iodide being the most effective. As discussed above as the halide counter ion is changed from chloride to bromide to iodide the ionic radius increases, the charge density decreases, the binding strength of the hydration shell decreases, leading to an increase in the binding affinity to the surfactant head group. As a consequence of the increased degree of counter ion binding, the charge on the surfactant head group is increasingly delocalised. This results in a decreased repulsion between the surfactant head groups within the bilayer. In a bulk dispersion this may result in the better packing of the surfactants, a decreased radius of curvature resulting in larger self-assembled structures. [311, 312]

6.3.4 Small Angle X-ray Scattering

Small angle x-ray scattering was used to investigate the effect of halides salts on the structure of the bulk surfactant lamellar system. Bulk surfactant water systems were fabricated in the same manner as in previous chapters with the deionised water replaced with the halide salt solution of interest. The experiments into the effect of temperature on the bulk system and the supported bilayers and into the addition of alkyl alcohols into the system both showed the complementary behaviour of the bulk samples and the supported bilayers. It was proposed that the SAXS of the bulk

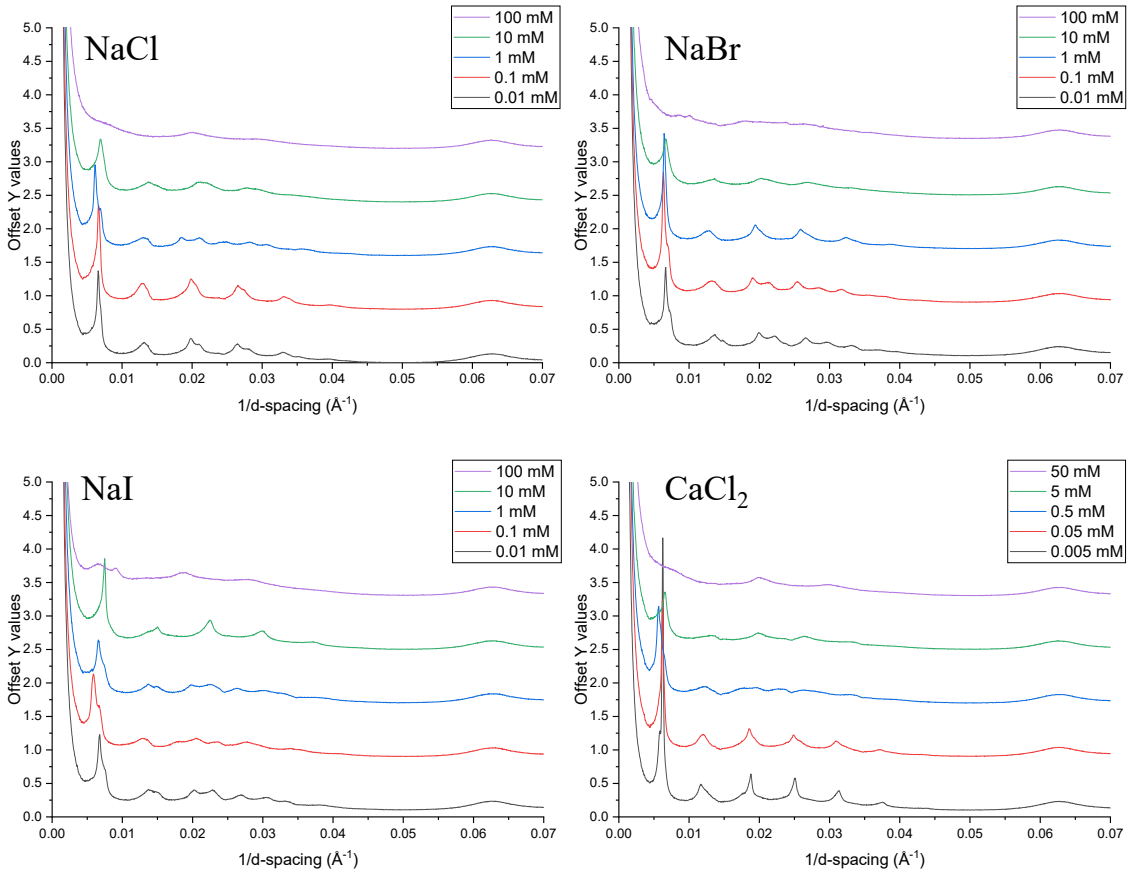


Figure 6.12: Linear intensity plots of the SAXS patterns of DIPEDMAMS/water systems with varying electrolyte concentrations. Electrolyte concentrations and identity are shown in the figure.

system with halide salts might help to elucidate the nature of the change observed in the supported bilayers.

The radially integrated linear intensity plots of the SAXS patterns for bulk DEPEDMAMS/water systems, 20 wt% surfactant with 0.01 - 100 mM; NaCl, NaBr and NaI, and 0.005 - 50 mM $CaCl_2$ are shown in figure 6.12. At 0.01 mM NaCl two series of equally spaced Bragg peaks were observed. At low scattering angles it is often problematic to differentiate the two peaks due to significant overlap but they do become more resolvable at larger scattering angles. As the salt concentration increases there is a slight shift in the peaks towards the y-axis. This applies to both sets of peaks. As the salt concentration increases to 10 mM NaCl the peaks shift back towards the right, an increase in the scattering angle. This shift does appear to apply to both sets of peaks however it is accompanied by a broadening of the peaks

making the assigning of the two sets of peaks difficult due to the increasing overlap of the peaks. Increasing the salt concentration to 100 mM results in a significant increase in the scattering angle, rightward shift in the Bragg peaks, along with a significant broadening of the peaks. At 100 mM only one set of Bragg peaks are resolvable. It is uncertain whether only one set are present, or if the second set observed at lower salt concentrations are present, but obscured by the broadening of the peaks.

The addition of NaBr to DIPEMAMS/water systems has a similar effect on the bulk surfactant lamellar structure as NaCl. From 0.01 mM to 1 mM the system exhibits two series of equally spaced Bragg peaks with a slight compression of the scattering angle as the salt concentration increases. A broadening of the peaks is also observed making the differentiation for the two sets of peaks more problematic as the concentration increases. At 10 mM NaBr the scattering angle and peak spacing increases slightly then increases significantly at 100 mM. As with NaCl there is also a significant broadening of the peaks at these concentrations. It is uncertain whether one or two sets of peaks are present at these concentrations due to broadness of these peaks.

With NaI, at low salt concentrations, the pattern is again similar. Two sets of equally spaced Bragg peaks with decreasing angle or scattering and separation with increasing salt concentration. However, whilst NaCl and NaBr showed a decrease in peak separation up to 1 mM salt concentration followed by an increase as the concentration increased further. With NaI the peak separation and scattering angle increases between 0.1 mM and 1 mM NaI. A further slight increase is observed at 10 mM followed by a significant increase in the peak spacing at 100 mM NaI. Two sets of equally spaced Bragg peaks are easily observable up to 1 mM NaI but with the broadening of the peaks from 10 mM to 100 mM it is increasing difficult to resolve the two sets of peaks. It is uncertain whether one or two sets of peaks are present at these concentrations due to broadness of these peaks.

The SAXS of samples containing increasing concentrations of $CaCl_2$ show a similar pattern to the other salts investigated. Two sets of equally spaced Bragg peaks which show decreasing angle of scattering and separation as the salt concentration

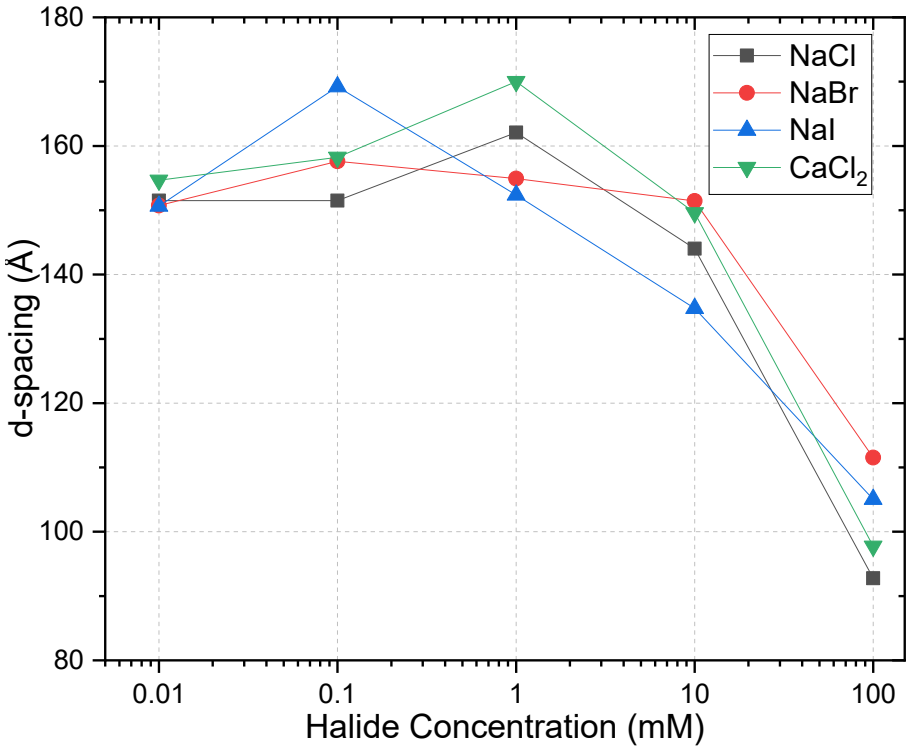


Figure 6.13: Plot of the d-spacing of DIPEDMAMS lamellar phases as a function of halide concentration for all electrolytes investigated.

increases from 0.05 to 0.5 mM (halide concentration equivalent to 0.01 to 1 mM for the monovalent salts investigated) followed by a small and a significant increases at 5 and 50 mM (10 and 100 mM mono-halide equivalent). This increase is accompanied by a broadening of the peaks, as observed with the other salts. The samples containing $CaCl_2$ exhibit the smallest separation between the two sets of Bragg peaks compared with the other halide salt containing samples, with the secondary peaks only appear as shoulders on the main Bragg peaks at most concentrations.

As previously discussed, equally spaced Bragg peaks refer to the lamellar phase, where the d-spacing, bilayer thickness plus water layer thickness, is inversely proportional to the separation of the Bragg peaks. The two sets of equally spaced Bragg peaks observed for most samples in figure 6.12 correspond to two co-existing lamellar phases with differing d-spacings. This was observed and discussed when investigating the temperature dependent phase behaviour of the surfactant system in section 4.3.4. The difference between d-spacings is 1 - 2 nm, with no significant trend. Similar to that observed in Chapter 4.

The d-spacings for each sample are shown in figure 6.13, where the lines are included to guide the eye only. The samples with increasing concentrations of NaCl, and $CaCl_2$ both show an increase in the d-spacing as the salt concentration increases from 0.01 to 1 mM. This is followed by a decrease at 10 mM then by a sharp decrease in the d-spacing as the concentration rises to 100mM.

The d-spacings of the samples containing NaBr and NaI show an increase from 0.01 to 0.1 mM with the d-spacing decreasing from 1 to 100 mM. The d-spacing of the NaBr samples appear to decrease slowly between 0.1 and 10 mM before sharply decreasing at 100 mM. The d-spacing of the NaI samples, by comparison, decrease rapidly from 0.1 to 100 mM. The d-spacing for the NaBr samples appears to show the smallest increase in the d-spacing followed by a smaller decrease at higher concentrations than the other halide salts. NaCl, NaI, and $CaCl_2$ all show a similarly large range in d-spacings.

At each salt concentration there does appear to be some degree of variation in the measured d-spacings making direct comparison at each concentration problematic and although the variation in d-spacing at 0.01 mM halide concentration is not large there is a more significant range in the d-spacings at 100 mM halide concentration. There are various sources of error for this but the main source is believed to be the broadening of the peaks increasing the error in the d-spacing measurement.

The d-spacing is a measure of the length of the repeating unit within the lamellar phase. It is the sum of the bilayer thickness and the thickness of the aqueous layer separating the surfactant bilayers. Therefore changes in the d-spacing can only be the result of changes to the thickness of the bilayer, the aqueous phase, or both. Changes to the water layer would not be observable by AFM imaging of supported bilayers however changes to the bilayer itself may show some correlation.

The two co-existing lamellar phases observed from the SAXS patterns are believed to correspond to the two bilayers phases observed from the AFM images of the supported surfactant bilayers, as discussed in Chapters 4 and 5. The SAXS patterns for all halide salts investigated potentially show a merger of the two co-existing lamellar phases into a single phase at high salt concentrations. This however

is not observed in the AFM images of the supported bilayers. However, due to the broadening of the Bragg peaks at high salt concentration it is possible that the two phase behaviour is not resolvable from the SAXS patterns. The cause of the broadening of the Bragg peaks at higher salt concentrations is not clear. A broadening of Bragg peaks is normally indicative of an increase on the variation in the d-spacing. The formation of holes in the supported bilayers does not appear to be reflected in any conformational changes observed from the SAXS patterns of the bulk lamellar system.

The declining in the d-spacing at higher salt concentrations is easiest to understand in comparison with the force spectroscopy data. The force spectroscopy data suggested that the increasing salt concentration decreased the repulsive interactions between the bilayers. It also suggested a dependency on the identity of the halide ion, with Cl^- having a the least effect and I^- decreasing the repulsive interaction the quickest. A similar pattern is observed in the d-spacings from the SAXS patterns. The d-spacing for NaCl and $CaCl_2$ behave in a very similar manner, both show a decrease in the d-spacing only above 1 mM halide equivalent concentration. Whilst the d-spacing of the samples containing NaI, in comparison, are shown to decrease sharply above 0.1 mM. Assuming that the two phenomena are linked, it is likely that the decreasing d-spacing is due to the shrinking water layer as the decreased repulsion between the bilayers forces them closure together. However, the increase in the d-spacing observed up to 1 or 0.1 mM, depending on the salt, would contradict this to some degree or suggest that there are other factors and interaction that need to be considered.

The Hofmeister series was discussed earlier in a bid to help explain the observation that the surface potential was dependent on both the electrolyte concentration and the identity of the halide counter ion. In this application it was used to describe the counter ion's binding affinity to the head group as part of the ion pair model for charged surfaces. For looking at the behaviour of the bulk surfactant system it is better to discuss the ions by their ability to "salt in" or to "salt out" surfactant systems. Salting in generally refers to a decrease in the packing order of the surfactant system whilst salting out generally refers to an increase in the packing order of the surfactant system. This is related to the ideas of kosmotropes and chaotropes

as discussed earlier. The halide ions can generally be considered chaotropes, having weakly hydrated, large ionic radius, and a low charge density. Chaotropes are considered to lower the polarity of water making organic molecules more soluble in an aqueous environment. This reduces the packing density of the surfactant system potentially leading to a swelling of the surfactant bilayers.

It is suggested that the addition of halide salts at low concentrations results in an increase in the bilayer thickness and therefore the d-spacing due to the salting in effect of the halide counter ions. As the concentration is increased further the d-spacing begins to collapse due to the reduction in the repulsion between the bilayers resulting in the compression of the water layer.

6.3.5 Particle sizing and Zeta Potential of Vesicles

The colloidal probe force spectroscopy data showed how the forces measured between the surfactant bilayers changed with increasing salt concentration and the effect of different salts. However it is not clear from those experiments at what point the system would become unstable. To further explore the relationship between the measured forces and the stability of vesicle dispersions the effect of electrolyte concentration and halide ion identity on the mean particle size and zetapotential of DIPEMAMS vesicle dispersions were investigated.

The effect of increasing salt concentration and the effect of different halide salts on the size and zeta potential of DIPEDMAMS vesicle dispersions are shown in figure 6.14. For clarity, the electrolyte concentration has been plotted on a $\log_{10}$ scale The initial particle size, and vesicle diameter was 82 ± 4 nm There was little observed change in the particle size as the salt concentration was increased from 0.01 mM to 1 mM. Increasing the salt concentration to 10 mM results in a five fold increase of the the mean particle diameter for the NaI containing dispersions. No significant change was observed in the particle size for the NaCl or NaBr containing dispersions. At 100 mM salt concentration all salt show a large increase in the mean particle diameter. A 10 times increase in the mean particle size of rthe NaCl and NaBr containing dispersion and a 100 fold increase was observed for the NaI

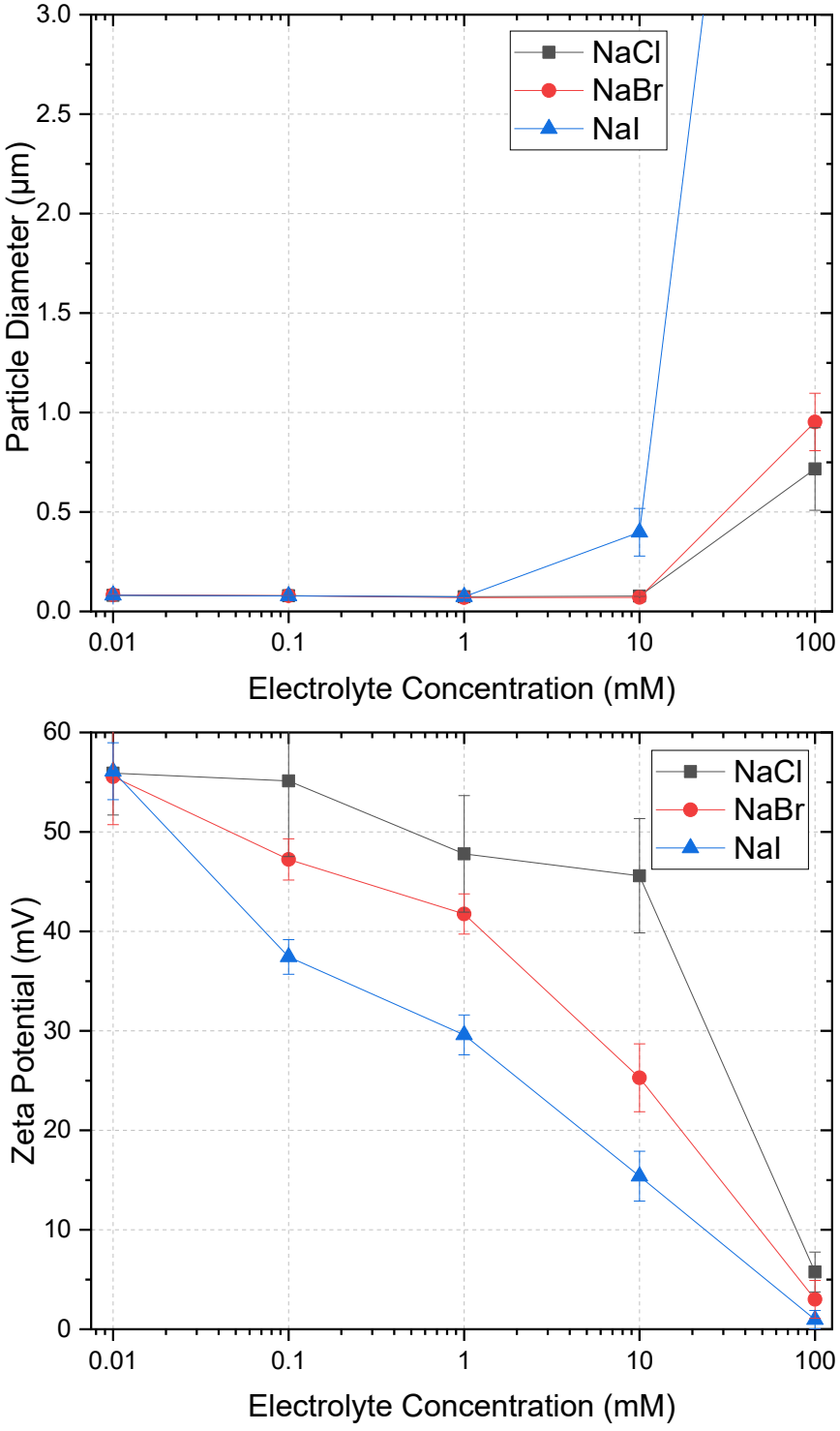


Figure 6.14: Plots of the mean particle diameter and zeta potential of a DIPED-MAMS vesicle dispersion as a function of increasing electrolyte concentration.

containing samples.

The initial zeta potential at 0.01 mM halide salt was measured as 56 ± 6 mV for all salts investigated. As the salt concentration was increased all salts showed a decrease in the zeta potential. From 0.01 mM to 10 mM the NaCl containing samples exhibited a steady decline in the zeta potential from 55 to 46 mV. Further increasing the concentration to 100 mM resulted in a large decrease in the zeta potential down to 5.6 mV. With NaBr there is a steady decrease of the zeta potential from 0.01 to 1 mM. Above 1 mM the zeta reduces more rapidly decreasing to 3.2 mV at 100 mM. The addition of NaI to the DIPEDMAMS vesicle dispersion results in the largest fall in the zeta potential compared with the other halide salts and does not appear to show a change in the rate of change at higher salt concentrations as with the other salts. At all salt concentration, above 0.01 mM, the zeta potential for the NaCl containing system was the highest and the the NaI containing system was the lowest.

The increase in the average particle diameter observed at high salt concentration is suggested to be caused by vesicle aggregation. These aggregates are suggested to form when the repulsive interaction between the vesicles decrease enabling them to come into contact where the attractive van der Waals interaction cause the vesicle to adhere to one another. The merging and engulfing of vesicles in close contact are also possible. The colloidal probe force microscopy showed the repulsive interactions between the bilayers decreasing with increasing salt concentration. However it was not able to comment on when the this would result in destabilising the vesicle dispersion. The colloidal probe microscopy also showed that the interactions where dependent on the identity of the halide ion and not just on the salt concentration. This was also observed in the vesicle stability measure by the mean particle diameter.

The zeta potential measurements showing a decreasing potential with increasing electrolyte concentration and showing a dependency on the identity of the halide counter ion compliment the observations of the the calculated surface potential from the colloidal probe experiments. However the two measurements, zeta potential and surface potential, are not identical and should not be mistaken as being equivalent. Whilst the surface potential is the potential difference between the colloidal surface

and the bulk dispersion. The zeta potential is the potential difference from the edge of the stationary ion phase around the colloidal and the bulk dispersion. As with the surface potential a higher zeta potential is associated with more stable colloidal dispersions.

An increase in the electrolyte concentration would generally decrease the zeta potential by increasing the charge concentration in the bulk dispersion phase resulting in a lower potential. Whilst most models of the electrical double layer would explain the impact of the electrolyte concentration in the the measured zeta potential they would not account for nor explain any ion specific effects. The ion specificity observed here and the from the colloidal probe data requires the consideration of the role of the halide counterion. It has been suggested that the chloride anions exhibited the weakest binding to the surfactant head groups whilst iodine anions exhibit the strongest binding. The reasons for this have been discussed earlier. Using the ionic pair model of electrical double layers, figure 6.8, it can be understood that increased counterion binding at the head group of the surfactant bilayers can decrease the surface potential and therefore the measured zeta potential.

6.4 Conclusions

Direct force measurements between two supported DIPEDMAMS bilayers show that the electrical double layer forces decay at rates in agreement with theoretical Debye lengths with some deviation at extremes of electrolyte concentrations. The measured surface potentials of the bilayers decreased with increasing electrolyte concentration, the potency of this effect was observed to be dependent on the the identity of the halide anion, with chloride being the least effective and iodide being the most effective. It is proposed that the weakening strength of the halide ion's hydration shell and therefore their increasing affinity for binding to the cationic surfactant head groups offers an explanation for this observation.

It was noted that the electrical double layer's dependency on the ion species present can not be explained by simple Gouy-Chapmen or Stern models of the EDL.

It has been discussed that models which treat the surface potential as being dependent on the unpaired cationic surfactant head groups and account for hydration effects can be better used to describe the relationships observed in this work.

Imaging of the supported surfactant bilayers was used to investigate the impact of the added salts on the bilayers themselves to differentiate between their impact on the bilayers and on the forces between them. The topographical atomic force microscopy images of the supported surfactant bilayers in the presence of increasing electrolyte concentrations showed the formation of holes in the bilayer penetrating down to the mica substrate. The size and number of these holes increased with increasing salt concentration. The hole formation was also dependent on the identity of the halide counter ion. The potency of the halide ions to form holes in the bilayer increased as one moves down the periodic table. Supporting the trend observed from the colloidal probe force microscopy. The observation of hole formation also provided an alternative explanation for the observation that the surface potential fell with increasing salt concentration.

Small angle x-ray scattering of the bulk lamellar system was used to investigate the impact of different salts and electrolyte concentration on the structure of the surfactant bilayers. The scattering patterns showed the two phase behaviour observed in the topographical images of the supported bilayers. The SAXS data showed changes in the d-spacing of the lamellar phase but there was no clear impact on the bilayers themselves. The d-spacing was observed to initially increase then decrease with increasing salt concentrations. Again there was a dependency on the identity of the halide counter ion. The salt concentration above which the d-spacing stopped increasing and started decreasing decreased with increasing ionic radius of the halide counter ion. The impact of the electrolyte on the d-spacing was suggested to be a combination of the halide ions ability to salt in the surfactant system and the decrease in the repulsion between the bilayers as the Debye length decreased.

Finally the impact of the halide salts on the mean particle diameter and zeta potential of DIPEDMAMS vesicle dispersions was investigated in order to compare the force measurements to the bulk vesicle systems. The mean particle diameter, as measured by dynamic light scattering showed, vesicle aggregation at higher salt

concentrations. The electrolyte concentration at which the system becomes unstable was dependent on the identity of the halide anion. The dispersion containing NaI saw vesicle aggregation at 10 mM whilst NaBr and NaCl were stable up to 10 mM. The zeta potential decreased with increasing salt concentration, which supports the observations from the colloidal probe microscopy. As with the measured surface potential from the force curves, NaI was observed to have the greatest impact on the zeta potential and NaCl had a least impact.

Chapter 7

Impact of Polymers and Polyelectrolytes on Bilayer-Bilayer Interactions

7.1 Introduction

Polymers and polyelectrolytes are well known additives to colloidal dispersions, used control various properties of the system from its rheology and commercial properties to the stability of the dispersion. The impact of polymers on hard sphere colloidal systems such as silica spheres, or nanoparticle dispersions has been widely studied. [313–315] The majority of work on such colloidal systems has focused on their bulk behaviour as opposed to the direct impact of the polymer additives on the interactions between the colloidal particles or in theoretical models of the interactions. [316–321]

Several key interactions between colloidal particles in polymer solution, not accounted for by the DLVO theory, are known. These interactions include the depletion attraction, oscillatory forces, depletion stabilisation, and the steric stabilisation by adsorbed polymers. [35,127,128] The depletion attraction, discussed in detail in sec-

tion 2.3.7, is an attractive interaction caused by the depletion of the polymer coils in the region between the colloidal particles when their separation is smaller than the radius of gyration of the polymer coils. This results in an osmotic gradient between inter-particle region and the bulk aqueous phase. The osmotic gradient results in an attractive force between the colloidal particles. This phenomenon is well known and the impact of polymers on the bulk behaviour of colloidal dispersions has been well studied. [322, 323] Oscillatory forces arise due to the ordering of particles between the surfaces, such as colloidal spheres, liquid crystals or polymer coils. [324, 325] As the separation is decreased a steric repulsion between the ordered coils and the surfaces is observed. When enough force as been applied one layer of the ordered phase is forced out resulting in an attractive force caused by the depletion interaction. Depending on the polymer properties and concentration several oscillation can be observed on approach as progressive layers of polymer coils are disrupted. [155, 326]

At high polymer concentrations the depletion attraction has been observed to give way to a depletion stabilisation. This arises when it becomes energetically unfavourable to demix the polymer chains in the inter-particle region as the colloidal particles are brought close enough together for the depletion attraction to operate. The work required to force the polymer coils from the inter-particle region is observed as a repulsive interaction which can lead to the stabilisation of the colloidal dispersion. [5]

Adsorbing polymers are often used to stabilise colloidal dispersions through steric stabilisation. This often involves the adsorbing or grafting of long chained polymers to the surface of the colloidal particles, although grafting is generally more effective. [5] As the polymer coated surfaces approach one another the outer polymer segments begin to overlap. This compression of the polymer chains is entropically unfavourable and leads to a repulsive entropic force. This steric repulsion is used and observed in many colloidal systems. [35] The force is dependent on the surface coverage of the polymer and whether the polymer is grafted onto the surface or merely adsorbed. At low surface coverage the polymers tend to sit as individual coils on the surface whereas at high coverage the chains are forced to extend away from the surface. This increases the range of the steric interaction much further than the radius of gyration of the polymer coils. [327]

The SFA has been used to investigate the forces between two mica sheets in various polymer solutions and melts. [158] The majority of this work has focused on the interactions between surfaces coated with a polymer or polyelectrolyte layer as opposed to the impact of the polymers on the interactions between the surfaces. [159–162] This may be due to the nature of the SFA, measuring the forces between two curved mica sheets. The SFA may not be ideal for directly measuring the interactions between colloidal particles in the presence of polymer solutions due to the difficulty in using surfaces other than mica and the high radius of curvature of the crossed cylinder geometry.

The invention of colloidal probe AFM enabled the direct measurement of the forces between a colloidal sphere and a flat substrate, and later between two colloidal spheres. [199–201] The main advantages over the SFA being the ability to directly measure the interactions between a variety of materials and to vary the radius of curvature by using different sized colloidal spheres. As with the SFA, the colloidal probe technique has been used to investigate the interactions between polymer coated particles. Directly measuring the steric, hydration, and electric double layer interactions between such coated surfaces as measured with the SFA. [227–230] The colloidal probe technique has also been used to directly measure the impact of non-adsorbing polymers and polyelectrolytes on the interactions between hard spheres. [264, 328–336]

The interactions within colloidal dispersion made up of "soft" spheres such as surfactant or lipid vesicles and micelles in aqueous polymer and polyelectrolyte solutions are of particular industrial relevance. There has been a good amount of work looking at the impact of polymers on the bulk properties and behaviour on these colloidal dispersions. [337–341] However there has been little literature on the direct measurement of the interactions between surfactant or lipid bilayers or monolayers that make up these systems in polymer solutions. In recent years some SFA experiments measuring the interactions between cationic surfactant bilayers in the presence of both adsorbing and non-adsorbing polymers have been published. [181,182] However it is believed that due to the relatively low curvature of the SFA system some non-DLVO forces, such as the depletion attraction, can not be measured with this technique but have been measured for bare probe systems with the colloidal probe

technique

In this chapter the impact of the cationic polyelectrolyte poly-dimethyldiallylammonium chloride (poly-DADMAC) and the uncharged polymer poly-ethylene oxide (PEO) on DIPEDMAMS vesicle systems were investigated. This was investigated in terms of polymer concentrations and molecular weight. Colloidal probe force microscopy was used to measure the effect of polymer addition on the forces between two supported cationic surfactant bilayers. Topographical AFM imaging was employed to investigate the impact of the polymer addition on the structure of the supported bilayers. This was in an attempt to decouple the impact of the polymers on the forces between the bilayers and changes to bilayers themselves. Finally the impact of these polymers on bulk DIPEDMAMS vesicle dispersions was investigated by measuring the zeta potential and mean particle diameter of these systems.

7.2 Experimental

The cationic surfactant, di(alkyl iso-propyl ester) dimethyl ammonium methylsulfate (DIPEDMAMS) was provided by Procter and Gamble. Synthesised using an industrial fatty acid mixture of C18, C16 and C18:1 chains, therefore the aliphatic tails are a statistical mixture of the three fatty acids see Chapter 3. Poly-dimethyldiallylammonium chloride (poly-DADMAC) poly-ethylene oxide (PEO), were obtained from Sigma-Aldrich in the following molecular weights, Poly-DADMAC: 100,000 - 200,000 Mw, 300,000 - 400,000 Mw, and 500,000 - 600,000 Mw; PEO: 400,000 Mw, 600,000 Mw, and 900,000 Mw. All solutions were prepared with deionised water, < 18 mS, filtered through an activated carbon filter to remove organic impurities.

7.2.1 Preparation of supported lipid bilayers

Supported surfactant bilayers were formed by the vesicle deposition technique from a vesicle dispersion containing 10 mol% perillyl alcohol as described in Chapter 3. Bilayers were formed on both mica and the glass colloidal probe in situ at room

temperature as described in Chapters 3 and 5.

7.2.2 Atomic Force Microscopy

All measurements were made using a JPK Nano wizard 4 AFM and analysed using the JPK data processing software as detailed in Chapter 3

Colloid Probe Atomic Force Spectroscopy

Colloidal probe force spectroscopy was used to measure force distance curves between a colloidal sphere, attached to an AFM probe, and a flat substrate. By forming a supported cationic surfactant bilayer on both surfaces the interactions between the bilayers could be investigated. The aqueous environment was changed by flushing the system with the polymer solution of interest. Force curves were collected in multiple positions across the surface for each polymer solution. For more details please see Chapter 3

AFM Imaging

All imaging was performed in quantitative imaging (QI) mode. The aqueous environment was changed by flushing the system with the polymer solution of interest. Multiple images of different areas of each supported bilayer in the polymer solutions were collected. All imaging was performed at 23 ± 2 °C. Further details on QI mode and on the imaging protocols can be found in Chapter 3

7.2.3 Dynamic Light Scattering and Zeta Potential

Sample Preparation

DIPEDMAMS vesicle dispersions with the polymer or polyelectrolyte concentration and molecular weight of interest were fabricated according to the protocols described in Chapter 3.

Particle sizing and zeta potential measurements

Particle sizing and zeta measurements were performed using a A Brookhaven zeta-PALS as detailed in Chapter 3. All measurements were performed at 25 °C.

7.3 Results and Discussion

7.3.1 The impact of polyelectrolytes on the measured interactions between supported cationic bilayers

The interactions between two supported DIPEDMAMS bilayers as they are brought into contact with each other were measured using colloidal probe force spectroscopy, as has been discussed in earlier chapters. As these measurements are performed in an aqueous environment poly-DADMAC was then added to the system by flushing the system with the polymer dispersion of interest. The polymer concentration could be increased incrementally without having to re-form the supported bilayers for each experimental environment. Enabling a more direct comparison of the effect of polymer addition in the measured interactions. This was desired as there is some variation in measured interaction between the bilayers between experimental runs.

The interaction between supported DIPEDMAMS bilayers in increasing concentrations of poly-DADMAC are shown in figures 7.1 to 7.3, for the three different

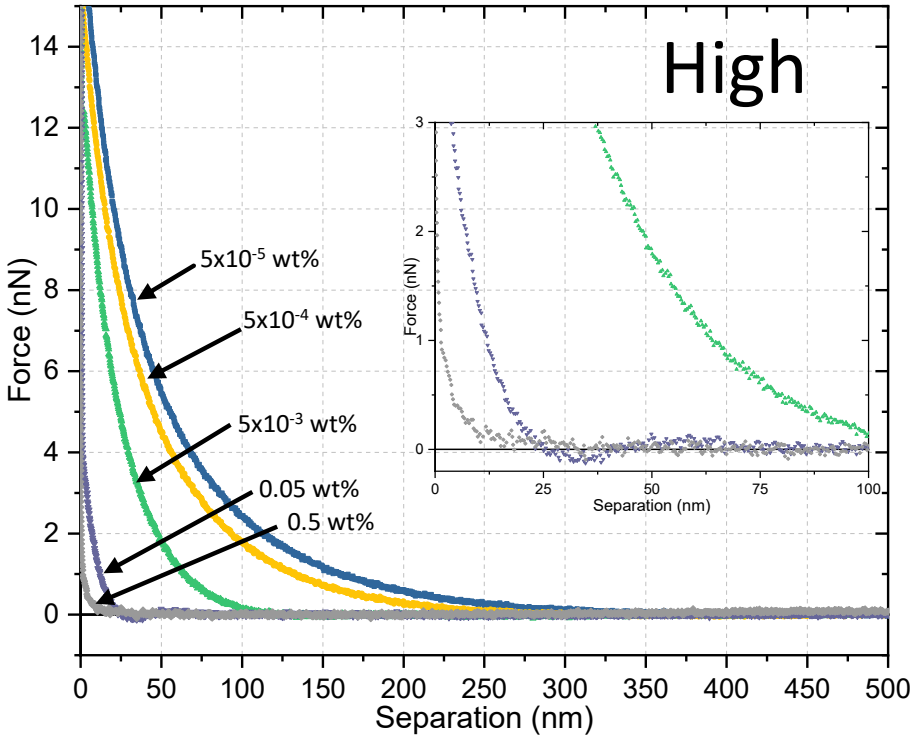


Figure 7.1: Forces measured between DIPEDMAMS bilayers on approach in increasing concentrations of high molecular weight poly-DADMAC. Polyelectrolyte concentrations are shown in figure. Insert shows the forces from 5×10^{-3} to 0.05 wt% poly-DADMAC on a smaller scale.

polymer molecular weights. For clarity the interactions in deionised water have not been included as no change was observed between the interactions in deionised water and the interactions in 5×10^{-5} wt% poly-DADMAC. This was true for all molecular weights investigated. At all polymer concentrations and for all molecular weights the forces on withdrawal were not significantly different from those on approach.

At 5×10^{-5} wt% poly-DADMAC and in deionised water the interactions on approach were solely repulsive. At these low polymer concentrations no interactions were observed until the surfaces were 300 nm apart but as the separation was decreased initial repulsive interactions were observed between 250 and 300 nm. As the separation was decreased the repulsive forces appeared to increase exponentially. At shorter separations the repulsive interactions appear to deviate from the roughly exponential relationship as the forces become more repulsive than the previous trend would have suggested. Further decreases in the separation between the bilayers resulted in one of two behaviours. Most commonly the repulsive interactions would

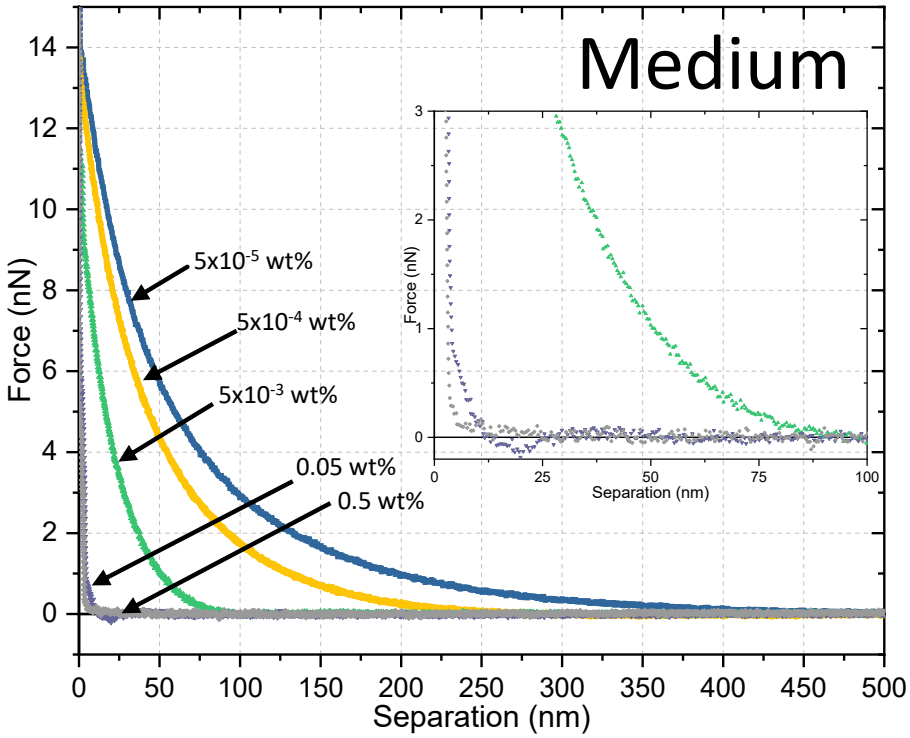


Figure 7.2: Forces measured between DIPEDMAMS bilayers on approach in increasing concentrations of medium molecular weight poly-DADMAC. Polyelectrolyte concentrations are shown in figure. Insert shows the forces from 5×10^{-3} to 0.05 wt% poly-DADMAC on a smaller scale.

increase beyond that expected if the relationship between the separation and repulsion was exponential until the relationship became indistinguishable from the compliance region and hard contact between the two bilayers was assumed. In a minority of force curves a small attractive force was observed just before contact at a separation between 2 and 5 nm and with an attractive force of < 0.5 nN.

As the concentration of the polyelectrolyte is increased from 5×10^{-5} wt% up to 5×10^{-3} wt% the interactions remain repulsive however the range and strength of the repulsive interactions are observed to decrease with increasing poly-DADMAC concentration. The decrease in the repulsive interactions appears to be independent of the molecular weight of the polymer dispersion. At a polyelectrolyte concentration of 5×10^{-2} wt% the measured interaction between the supported DIPEDMAMS bilayers are no longer solely repulsive. A small but significant attractive interaction is observed for all poly-DADMAC molecular weights. The range and strength of this attractive force however does appear to be dependent on the molecular weight of the

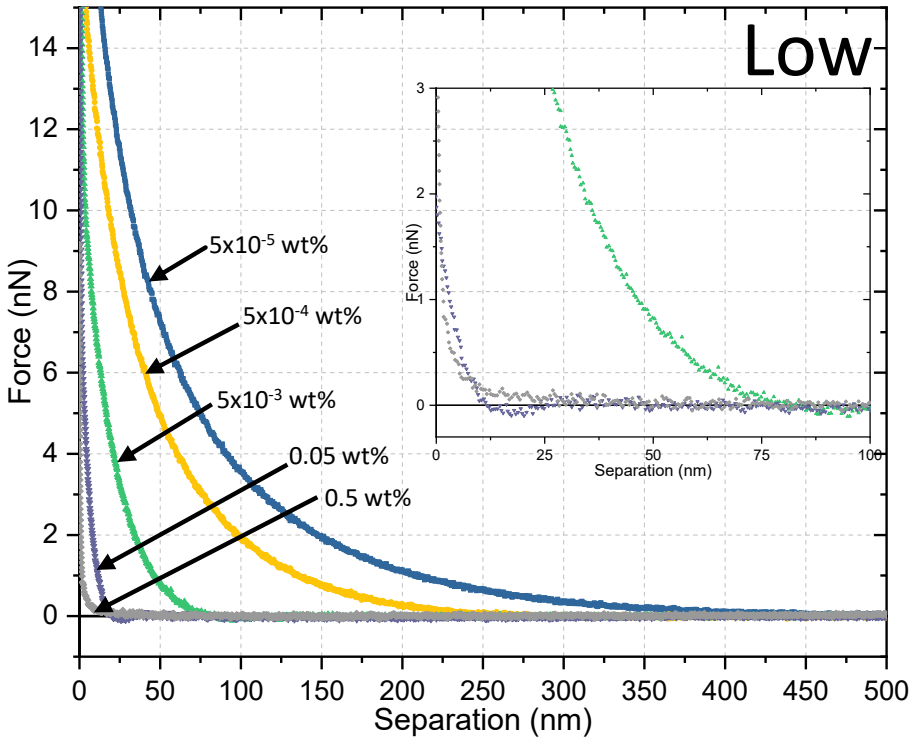


Figure 7.3: Forces measured between DIPEDMAMS bilayers on approach in increasing concentrations of low molecular weight poly-DADMAC. Polyelectrolyte concentrations are shown in figure. Insert shows the forces from 5×10^{-3} to 0.05 wt% poly-DADMAC on a smaller scale.

polymer. The onset of this attractive interaction appears to increase from around 30 nm, for the low molecular weight poly-DADMAC, to around 60 nm with the highest molecular weight poly-DADMAC. The strength of this attractive interaction also appears to increase with increasing molecular weight. This attractive force however does not lead to hard contact between the bilayers. The attraction is only observed down to a separation of between 10 to 20 nm. As the separation is further decreased the interactions become repulsive and increase in an exponential fashion until hard contact between the surfaces is achieved. At a polymer concentration of 5×10^{-1} wt% no long range attractive nor repulsive interactions are observed. Only a small repulsive interaction starting at a separation of < 10 nm and leading to hard contact is observed. There does not appear to be any significant differences between the measured forces at this concentration for the different poly-DADMAC molecular weights.

The experimental interactions between the supported surfactant bilayer in in-

creasing poly-DADMAC concentrations and the theoretical model EDL interactions are shown in figure 7.4 and 7.5 on a semi-log scale. Only the EDL model has been used here as the attractive van der Waal's component of the DLVO theory is not observed, as discussed in Chapter 6.

From the semi-log plots it is clear that the repulsive interactions observed from 1×10^{-5} wt% up to 1×10^{-3} wt% are exponential in nature, for all molecular weights, except at shorter separations. At small separation there is an additional increase in the repulsive interactions. This was also observed in the electrolyte experiments was suggested that this deviation from exponential behaviour at short separation was the result of additional short range repulsive interactions not accounted for by the DLVO theory such as hydration effects or steric interactions, or the result of charge regulating interactions between the two bilayers in close proximity. At these concentrations the EDL model for the interaction fit the data well. The model and the data did however diverge at short separations, where the data showed a greater repulsion, as discussed above. At a poly-DADMAC concentration of 1×10^{-3} wt% and above this deviation from the model and exponential behaviour was not observed at short separations.

At 1×10^{-2} wt% all poly-DADMAC molecular weights showed an attractive interaction followed by a repulsive interaction up until hard contact. For these environments the EDL interactions have been fitted to the repulsive interactions after the initial attractive forces. On the semi-log scale one can see that the repulsive interactions following the attractive interactions are exponential in nature. There is a good agreement between the model forces and the experimentally observed repulsive interactions.

As with the interactions observed with increasing electrolyte concentrations the absolute gradient of the model interaction increases whilst the intercept decreases with increasing polyelectrolyte concentration. This suggests that the range and strength of the inter-bilayer interactions decrease as the polyelectrolyte concentration increases.

Table 7.1 shows the results of the EDL fitting operation for all concentrations

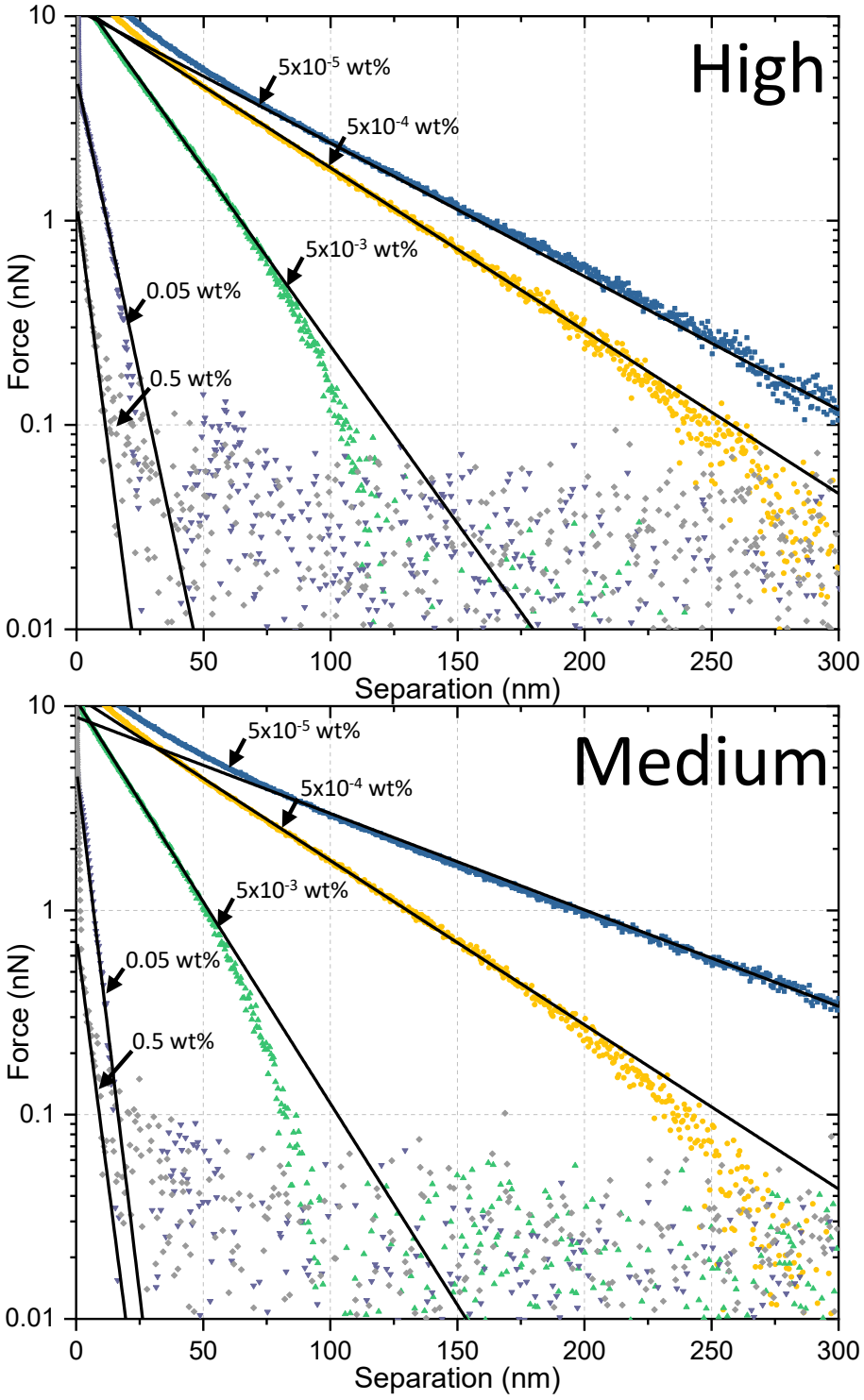


Figure 7.4: Forces measured between DIPEDMAMS bilayers on approach in increasing concentrations of different molecular weights of poly-DADMAC, on a semi-log scale. Solid black lines show the theoretical model EDL interactions interactions for each environment. Polyelectrolyte concentrations and molecular weights shown in figure.

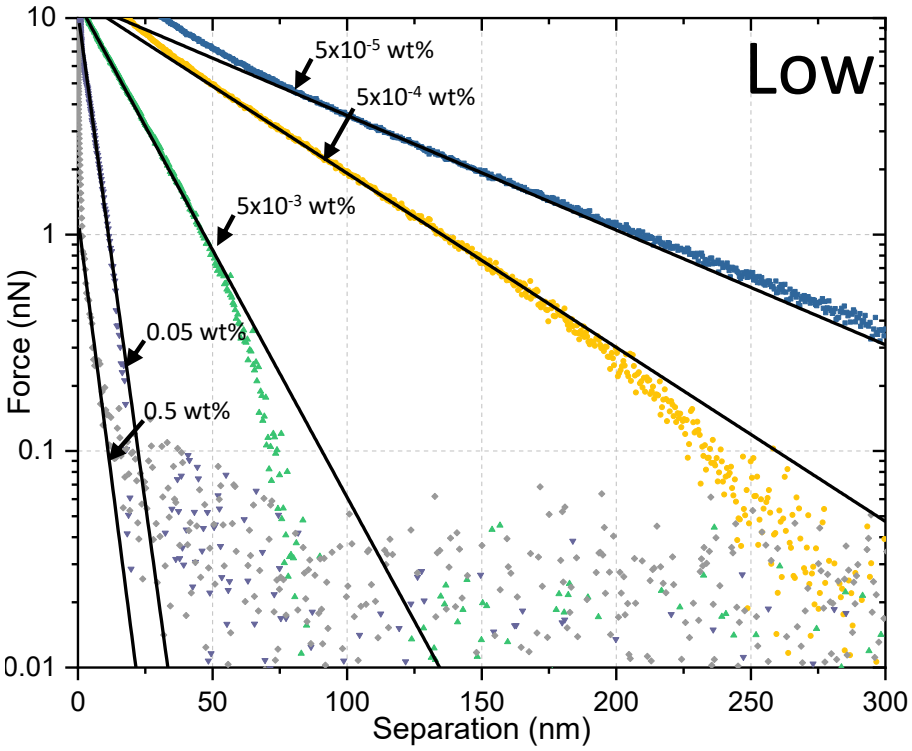


Figure 7.5: Forces measured between DIPEDMAMS bilayers on approach in increasing concentrations of different molecular weights of poly-DADMAC, on a semi-log scale. Solid black lines show the theoretical model EDL interactions interactions for each environment. Polyelectrolyte concentrations and molecular weights shown in figure.

and molecular weights of poly-DADMAC. The table gives theoretical and experimental values for the Debye length and experimentally determined values for the surface potential. As discussed previously there is some variation in the initial experimental surface potentials therefore a column normalising the surface potential at the 5×10^{-5} wt% values has been included for ease of comparison.

The experimental Debye lengths and surface potentials, for all poly-DADMAC molecular weights, decrease with increasing polymer concentrations. This reinforces the qualitative observations from the experimental plots that the range and strength of the interactions decreases with increasing concentration. The Debye lengths are independent of the molecular weight of the polyelectrolyte, as would be expected as the counter ion concentration is independent of the molecular weight of the polymer. No significant difference is observed between the experimental Debye lengths at a concentrations above 5×10^{-5} wt%. There is a significant variation between the

Table 7.1: Fitting parameters used in DLVO and EDL fits to the CP-AFM data in figure 7.4 and 7.5

	Debye length/κ^{-1}		Fitted Surface Potential	
[High]/wt%	Theoretical/nm	Fitted/nm	ψ/mV	Normalised ψ
5×10^{-5}	177	71±2	74±5	1
5×10^{-4}	56	54.5±2	67±3	0.91
5×10^{-3}	17	25±2	46±3	0.62
0.05	5	7.4±1.2	14.5±2	0.20
0.5	1.7	4.5±0.5	5.6±0.5	0.08
[Medium]/wt%				
5×10^{-5}	177	92±4	81±6	1
5×10^{-4}	56	54±2	66±4	0.81
5×10^{-3}	17	22±1	38±2	0.47
0.05	5	4.2±0.5	11±1	0.14
0.5	1.7	4.5±0.5	4.4±0.5	0.05
[Low]/wt%				
5×10^{-5}	177	82±3	94±9	1
5×10^{-4}	56	54±2	70±4	0.82
5×10^{-3}	17	19±1	37±2	0.44
0.05	5	4.8±0.5	17±1	0.20
0.5	1.7	4.5±0.5	5.5±0.5	0.06

Debye lengths at 5×10^{-5} wt% but due to the very low polymer concentration this is suggested to be due to the impact of impurities in the deionised water having a greater impact than the polymer concentration.

There is generally good agreement between the experimental and the theoretical Debye lengths except at the highest and lowest polyelectrolyte concentrations. At the lowest poly-DADMAC concentration of 5×10^{-5} wt% there is not only significant variation in the experimental values but they are significantly lower, $\sim$ 70 - 90 nm, than the theoretical value of 177 nm. This is most probably the result of impurities in the deionised water such as ions or dissolved CO_2 which would have a greater impact on the Debye length at these low polymer concentrations than the polyelectrolyte itself. At the highest poly-DADMAC concentration of 0.5 wt% the experimental Debye lengths are longer than predicted by the EDL model suggesting another force may be present.

The experimental surface potential extracted from the fitting of the EDL interactions to the experimental data, as shown in table 7.1, are observed to decrease as

the polyelectrolyte concentration increases. This decrease in the surface potential with increasing poly-DADMAC concentration is again independent of the molecular weight of the polymer. It is important to note here that a direct comparison of the experimental surface potential between different environments is hindered by the variation in the initial measured surface potentials. This has been put down to the several factors which are difficult to control such as the roughness of the colloidal probe, the position of the probe on the cantilever, and the exact spring constant of the cantilevers. These factors have been discussed in more detail in Chapter 5.

The declining experimental surface potentials observed with increasing polyelectrolyte concentration are similar to those observed with increasing concentrations of halide salts. As discussed in Chapter 6 the decreasing surface potential was attributed to the binding of the halide counter ions to the head groups of the supported cationic surfactant bilayers. If the cause of the declining surface potential with increasing concentration of poly-DADMAC is attributed to same mechanisms then one would expect that the experimental surface potential would be dependent on the chloride ion concentration and here the monomer concentration of the poly-DADMAC and independent of the molecular weight of the polyelectrolyte. This fits with the experimental observation that there is not dependence on the molecular weight of the polyelectrolyte.

The model used for the theoretical Debye lengths in poly-DADMAC is the same as that used for calculation of the Debye length for the salt solution discussed in Chapter 6, with some minor modifications. The electrolyte concentration parameters were modified to view the polyelectrolyte in terms of the concentration of monomers present as opposed to standard molarity. This approach appears to have been a good predictor of the experimental Debye lengths with the exception of the highest and lowest concentrations investigated. With the deviations between the experimental and theoretical data at low polymer concentrations explained by impurities in the deionised water having a greater impact on the experimental data than the electrolytes, as previously discussed. It could be argued that treating the addition of a polyelectrolyte to the system in the same manner as a normal salt solution with regards to the Debye length appears to be adequate and provides an explanation for both the dependence on the polyelectrolyte concentrations and the

independence from the molecular weight. However the higher than predicted experimental Debye lengths at 0.5 wt% poly-DADMAC however can not be explained so simply and neither can the attractive interactions observed at 0.05 wt%.

So far the polymer has only been considered as a series of charged monomers and we have treated it in a similar manner to a standard electrolyte in an attempt to understand its impact on the interactions between the supported cationic bilayers. The impact of the polymer chains themselves needs to be considered. At these concentrations the polymer chains would most likely be present as individual polymer coils. Whilst these most likely do not impact on the bilayer directly due to them both having a similar charge, it is suggested that they can play an important role in the interactions between the supported bilayers.

If the polyelectrolyte coils are considered as hard spheres much smaller than the radius of the colloidal probe then we can consider three different scenarios as the probe approaches the surface. Firstly where the the separation between the probe and the surface is greater than the diameter of the polymer coils, secondly where the separation is similar to the diameter of the coils, and thirdly where the separation between the bilayers is smaller than the diameter of the polyelectrolyte.

In the first regime, where the separation is larger than the polymer diameter, there is no expected difference in the expected bilayer-bilayer interactions with the addition of a polyelectrolyte in comparison to a traditional salt. However as the separation decreases and one moves through to the third scenario where the separation is less than the diameter of the polymer coils the situation arises where the polymer coils are excluded due to steric interactions from the region between the bilayers. This sets up two regions. The bulk dispersion containing the polyelectrolyte coils and hydrated halide counter ions and the region between the bilayers, containing the halide counter ions but depleted of the polyelectrolyte. This sets up an osmotic gradient between the two regions. The resultant osmotic pressure creates an attractive interaction between the bilayers. This is known as the depletion interaction.

It is suggested that the attractive interactions observed for all molecular weights at 0.05 wt% poly-DADMAC is caused by this depletion interaction. The strength

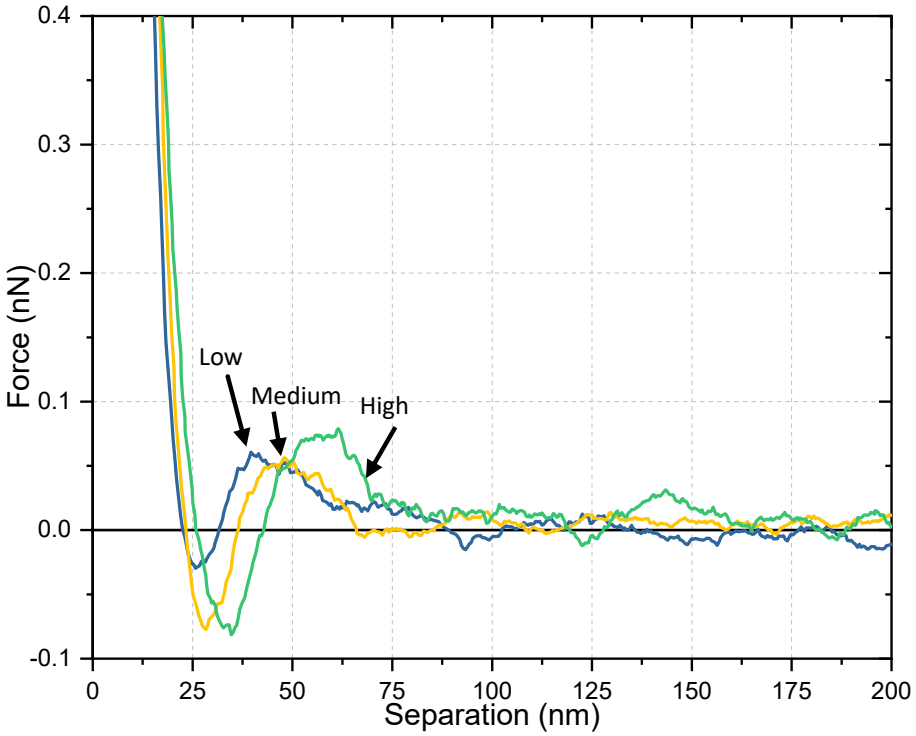


Figure 7.6: Forces measured between DIPEDMAMS bilayers on approach in 0.05 wt% poly-DADMAC at different molecular weights. Molecular weights shown in figure.

of the depletion interaction is generally considered to be dependent on the concentration of the depletant, in this case the polymer coils. As the addition of polyelectrolyte also decreases the repulsive interactions between the supported bilayers it is suggested that any depletion interaction is either too weak to be observed or masked by the dominating repulsive EDL interactions, at lower polymer concentrations. At the highest polyelectrolyte concentrations investigated the depletion attraction is also not observed. This could be due to several factors including stearic hindrance caused by the crowding of the colloidal probe by the polymer coils or the beginnings of chain overlap such that the polymer is no longer present in the dispersion as discrete spherical coils.

Whilst the over all trend in the forces between the bilayers showed no dependency on the molecular weight of the poly-DADMAC there does appear to be some difference observed between the measured depletion attraction at 0.05 wt%. Figure 7.6 shows the interactions measured on approach between supported cationic surfactant bilayers in the presence of 0.05 wt% poly-DADMAC for the three differ-

ent molecular weights investigated. For ease of comparison a smoothing function has been applied to the data. For all three molecular weights an initial repulsive interaction is observed before the depletion attraction. This has been observed for other system investigating the depletion interaction and is often ascribed to oscillatory interactions observed in some systems. [217,218,328] It is not certain if the repulsive interaction observed here is due to the double layer repulsion observed at higher poly-DADMAC concentrations between the two cationic bilayers or if the repulsion is due to steric interactions due to the ordering of the polymer coils between the bilayers. The steric interactions are related to the oscillatory forces as an applied force is required to force the ordered coils from the inter-bilayer region giving rise to a repulsive interaction. [219]

The Depletion interactions appear to show some dependence on the molecular weight of the polyelectrolyte. The range and strength of the attraction increases with the molecular weight. This can be understood by considering the dimensions of the polymer coils. Polymers of a higher molecular weight have a longer chain length which corresponds to an increased radius of gyration. The onset of the attractive depletion interactions are in some agreement with literature values for the radius of gyration for poly-DADMAC. [342, 343]

It is of note that, for all molecular weights investigated, the depletion attraction does not lead to hard contact between the supported bilayers. Instead an exponential repulsive interaction is observed. This could be attributed to the repulsive EDL forces or be caused by the structuring of polymer coils at the bilayer surfaces resulting in a depletion repulsion. This suggests that the overall interactions can only be understood as a combination of DLVO theory and depletion interactions. One model alone would not be sufficient to understand the interactions between supported cationic surfactant bilayers in polyelectrolyte dispersions

7.3.2 The impact of PEO on the measured interactions between supported cationic bilayers

Colloidal probe AFM force spectroscopy was used to measure the interactions between two supported DIPEDMAMS bilayers as a function of separation, with increasing concentrations of the neutral polymer polyethyleneoxide (PEO). All measurements were performed in an aqueous environment which enabled the polymer concentration to be increased by flushing the system with the PEO dispersion at the concentration of interest. By performing the experiments in this manner the effect of the polymer concentration on the interactions between the bilayers can be measured without having to re-form the bilayers between concentrations. This enables the effect of the polymers to be compared to the initial forces between the bilayers in deionised water minimising the impact of some of the variation observed measured interaction between the bilayers between experimental runs.

The interactions between supported DIPEDMAMS bilayers in increasing concentrations of PEO measured by colloidal probe force microscopy are shown in figure 7.7 and 7.8 for three different molecular weights. Forces shown are the forces measured on approach, there was no significant difference between the forces on approach and those on withdrawal. For clarity the interactions in deionised water have not been included as no change was observed between the interactions in deionised water and the interactions in 5×10^{-5} wt% PEO. This was true for all molecular weights investigated.

In deionised water and at 5×10^{-5} wt% PEO the interactions measured between the two supported surfactant bilayers were almost solely repulsive. At long range no interactions were observed but as the separation decreased initial repulsive interactions were observed ranging from 350 to 450 nm separation. As the separation was reduced further the repulsive interaction appeared in increase exponentially. At short separations, relative to the separation at which the initial interactions were observed, the repulsive forces appear to increase beyond what would be expected of an exponential relationship. Further decreases in separation resulted in the relationship between measured force and separation becoming indistinguishable from

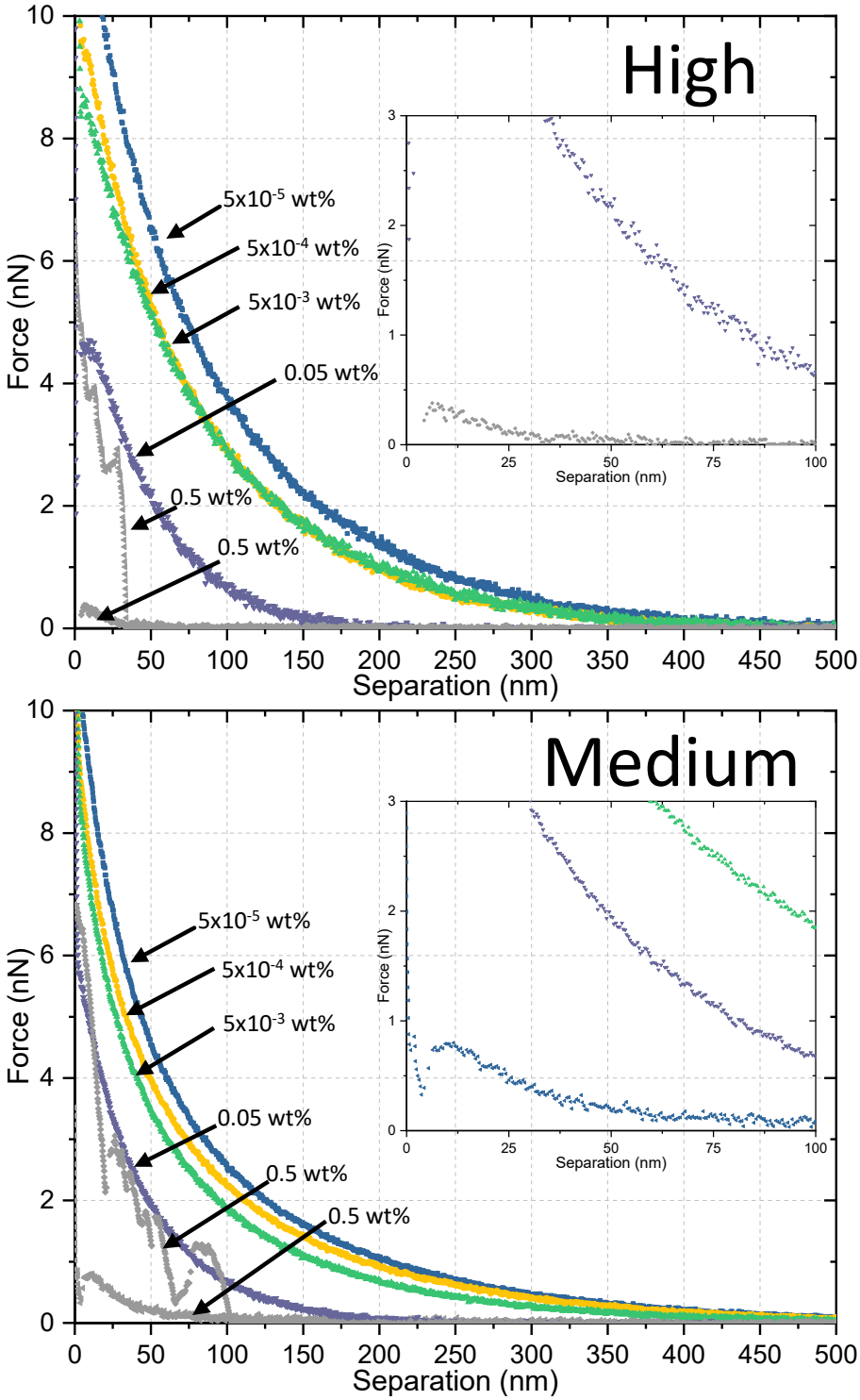


Figure 7.7: Forces measured between DIPEDMAMS bilayers on approach in increasing concentrations of different molecular weights of PEO. Polymer concentrations and molecular weights shown in figure. Inserts show the forces from 5×10^{-3} to 0.05 wt% PEO on a smaller scale.

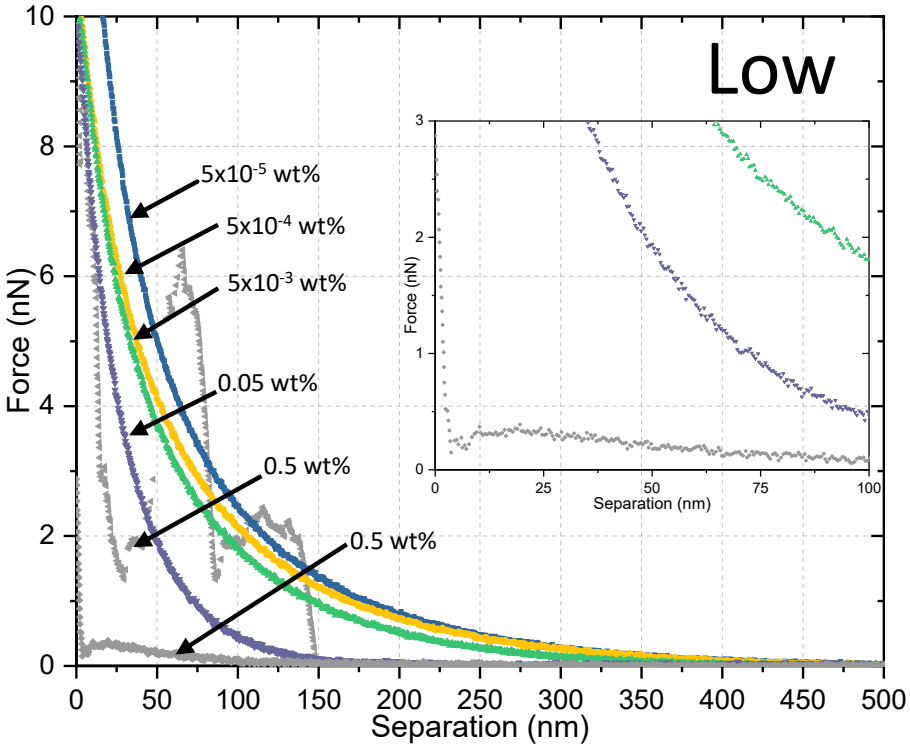


Figure 7.8: Forces measured between DIPEDMAMS bilayers on approach in increasing concentrations of different molecular weights of PEO. Polymer concentrations and molecular weights shown in figure. Insert shows the forces from 5×10^{-3} to 0.05 wt% PEO on a smaller scale.

the compliance region and hard contact between the two bilayers was assumed. For some runs and at some points across the surface a small attractive force was observed just before contact at a separation between 2 and 5 nm and with an attractive force of < 0.5 nN

The interactions remained repulsive as the concentration of PEO was increased from 5×10^{-5} wt% up to 5×10^{-2} wt%, although the range and strength of the repulsive interaction was impacted by the polymer concentration. Increasing the concentration from 5×10^{-5} to 5×10^{-3} wt% resulted in a relatively small decrease in the strength of the repulsive interaction and no significant change in its range. No significant dependency on the molecular weight of the polymer was observed at these concentrations. At 0.05 wt% a more significant decrease in both the range and strength of the measured repulsive interactions was observed, the separation at which the initial interactions were observed dropped to between 150 and 200 nm, the interactions still remained significantly strong. There is a possible dependency on

the molecular weight at this concentration. The high molecular weight does appear to show the largest decrease in the the interactions and the lightest PEO shows the least. However it is not certain if this is a real trend or just down to variation between experimental runs.

So far the measured interactions have been, to all intents and purposes, identical and constant across the surface for each experimental environment. However, at a PEO concentration of 0.5 wt% significantly different force profiles are measured across different areas of the mica supported surfactant bilayer surface. These forces generally fall into three categories. A weak and relativity short range repulsive interaction followed by attraction between 5 and 10 nm leading to hard contact. Solely attractive interactions, similar to those just mentioned but only showing an attraction leading to hard contact at a range of 5 to 10 nm. The third type show an almost a hard contact like interaction which rises and falls in a series of steps with an overall trend of increasing repulsive force leading up to what is possibly hard contact. These forces are very irregular between different areas of the surface with no two force curves being identical. The separation at which these forces are first observed ranges from 50 to over 400 nm however due to the irregular nature of these interactions the point of zero separation can be problematic to define. Of these "types" of interactions the repulsion followed by a short range attraction and the irregular forces were dominant. With these two types being roughly equally common. As such, typical examples of both of these types have been shown in figure 7.7 and 7.8.

The experimental interactions between the supported surfactant bilayer in increasing concentrations of PEO and the theoretical model EDL interactions are shown in figure 7.9 and 7.10 on a semi-log scale. Only the EDL model has been used here as the attractive van der Waal's component of the DLVO theory is not observed, as discussed in Chapter 6. Not shown are the step like forces that are observed at 0.5 wt%.

It is clear, from the semi-log plots that the observed repulsive interactions from 5×10^{-5} wt% up to 5×10^{-3} wt% PEO are exponential in nature for all molecular weights. At these concentrations the repulsive interactions are observed to increase

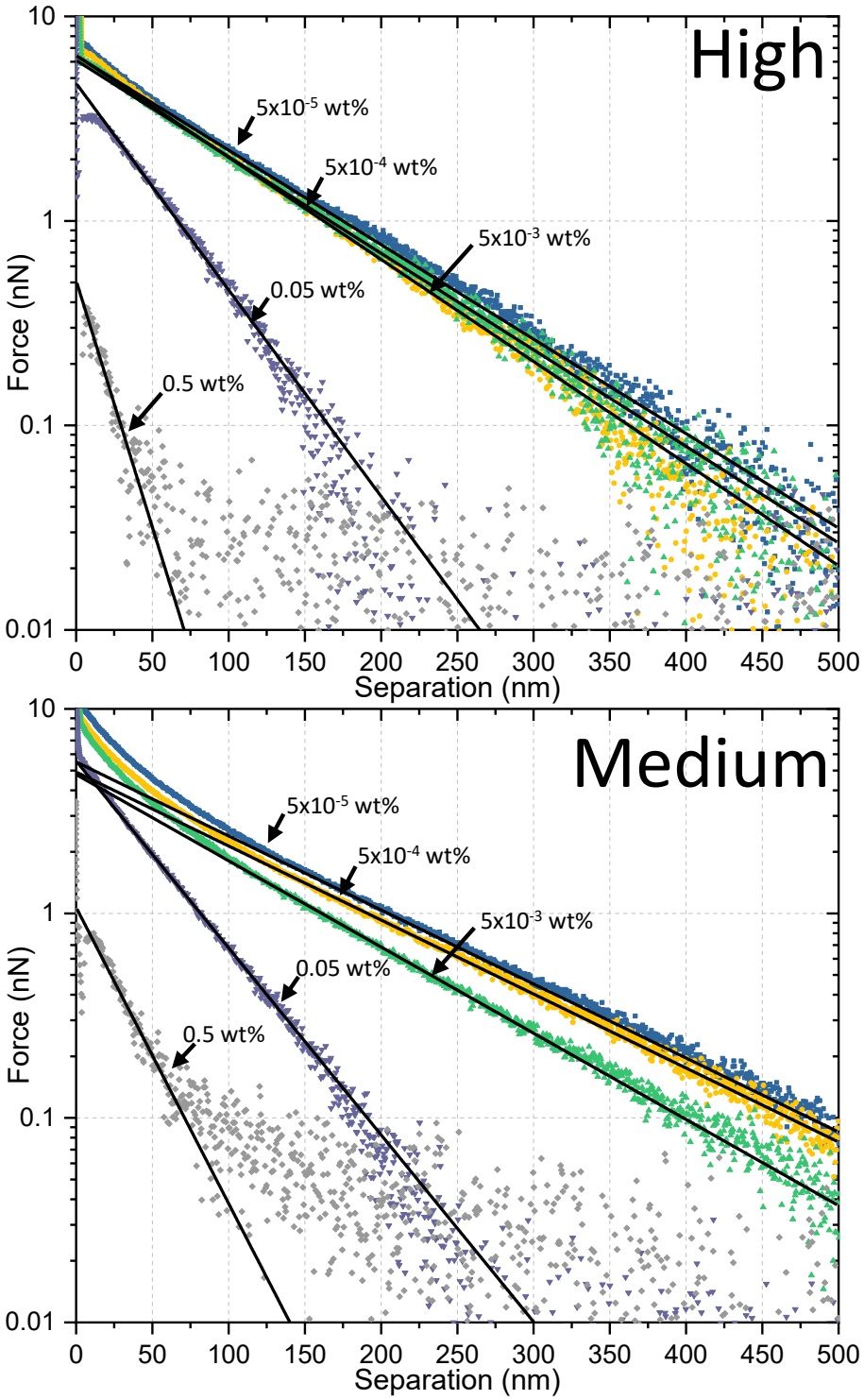


Figure 7.9: Forces measured between DIPEDMAMS bilayers on approach in increasing concentrations of different molecular weights of PEO, on a semi-log scale. Solid black lines show the theoretical model EDL interactions interactions for each environment. Polymer concentrations and molecular weights shown in figure.

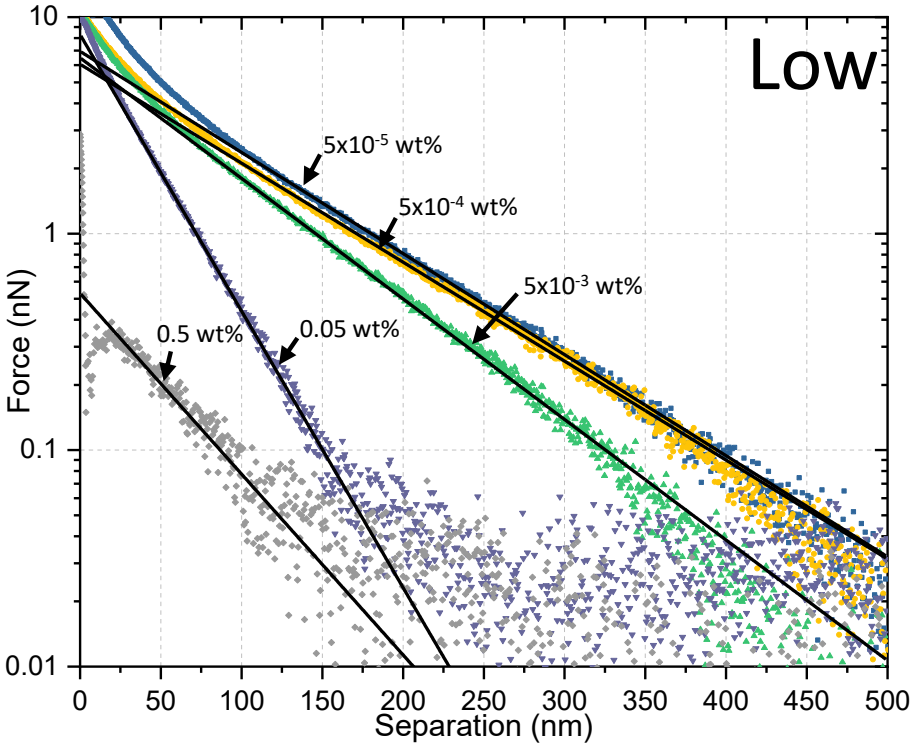


Figure 7.10: Forces measured between DIPEDMAMS bilayers on approach in increasing concentrations of different molecular weights of PEO, on a semi-log scale. Solid black lines show the theoretical model EDL interactions interactions for each environment. Polymer concentrations and molecular weights shown in figure.

further, at small separations, than an exponential relationship would suggest. This has been observed for almost all other bilayer-bilayer interactions measured using this technique and can be attributed to additional short range repulsive interactions not accounted for by the DLVO theory such as hydration effects, steric interactions, or the result of charge regulating interactions between the two bilayers in close proximity. At all concentrations and molecular weights the model EDL interactions generally fit the data well. However they do diverge at short separations where, as discussed, the experimental data show greater repulsive interactions than predicted. As the concentration of PEO increases from 5×10^{-5} wt% up to 5×10^{-3} wt% the separation at which this deviation is observed appears to decrease slightly with a larger decrease observed as the concentration is increased to 0.05 wt%.

At 0.5 wt% PEO the interactions shown, and compared to the theoretical model EDL interactions in figure 7.9 and 7.10 are those which exhibited a repulsive interaction followed by a short range attraction. This is for both clarity and the observation

that these are the only interactions at this concentrations that can be compared to the theoretical EDL model.

From the semi-log plots of the interactions at 0.5 wt% PEO the initial repulsive interactions are observed to be exponential in nature for all molecular weights. The theoretical EDL model does appear to fit these repulsive interactions well suggesting that the repulsive part of these interactions is the result of of the interactions between the electrical double layers of the supported surfactant bilayers.The addition repulsion observed at short separations is not observed at 0.5 wt%.

As the PEO concentration increases from 5×10^{-5} to 5×10^{-3} wt% very little change is observed in the absolute gradient of the model interactions nor is a significant change observed in the intercept of the model forces. This suggests that at these concentration the PEO has a minimal, almost negligible, impact on the interaction measured between the supported surfactant bilayers. At 0.05 wt% a decrease in the absolute gradient is observed but the intercept remains almost unchanged whilst at 0.5 wt% no obvious trend in the intercept is observed in the change from 0.05 wt% but there is a clear fall in the intercept

The results of the EDL fitting operation are shown in table 7.2 for all concentration and molecular weights of PEO. The table shows experimental values for the Debye length and experimentally determined values for the surface potential at each concentration an molecular weight. As discussed previously there is some variation in the initial experimental surface potentials therefore a column normalising the surface potential at the 5×10^{-5} wt% values has been included for ease of comparison.

Overall the experimentally derived Debye lengths and surface potentials, for all PEO molecular weights, are observed to decrease as the polymer concentration is increased from 5×10^{-5} to 0.5 wt%. However this change is not uniform. Very little change is observed between 5×10^{-5} and 5×10^{-3} wt% PEO whilst there is a significant decrease in both the Debye lengths and surface potentials on increasing the concentration to 0.05 wt% and again on increasing the concentration to 0.5 wt%. Neither the Debye lengths nor the surface potential show a dependency on the

Table 7.2: Fitting parameters used in DLVO and EDL fits to the CP-AFM data in figure 7.9 and 7.10

	Debye length/κ^{-1}	Fitted Surface Potential	
[High]/wt%	Fitted/nm	ψ/mV	Normalised ψ
5×10^{-5}	94±2	66±6	1
5×10^{-4}	87±2	63±5	0.95
5×10^{-3}	92±3	62±5	0.93
0.05	43±1	35±2	0.53
0.5	18±2	7.2±0.5	0.11
[Medium]/wt%			
5×10^{-5}	92±2	70±9	1
5×10^{-4}	94±2	65±4	0.93
5×10^{-3}	84±2	58±3	0.83
0.05	47.5±1	40.5±2	0.58
0.5	30±1	13.5±1	0.19
[Low]/wt%			
5×10^{-5}	93±3	69±7	1
5×10^{-4}	95±3	64±4	0.93
5×10^{-3}	78±1	59±2	0.86
0.05	34±1	42±2	0.61
0.5	52±1.5	12.5±0.5	0.18

molecular weight of the polymer. There are no theoretical models for the impact of uncharged polymers on the distance over which a charge can be "felt" in an aqueous environment. Therefore there are no theoretical Debye lengths for comparison.

At 5×10^{-5} wt% the Debye lengths for all PEO molecular weights are observed to be between 85 and 100 nm, this corresponds to an electrolyte concentration of approximately 5×10^{-5} M. As the concentration of PEO increases from 5×10^{-5} wt% to 5×10^{-3} wt% there is some variation in the measured Debye lengths but no significant or systemic change. This is true for all molecular weights investigated. Increasing the concentration to 5×10^{-2} wt% however did result in a drop in the experimental Debye lengths, again for all molecular weights. The Debye length drops by between one half to two thirds. At 0.5 wt% the behaviour of the Debye lengths is mixed. It appears to increase for lowest molecular weight PEO, decrease slightly for the medium weight and decrease further for the highest molecular weight investigated. As mentioned there is significant variation in the surface forces measured at this concentration therefore it uncertain whether this is a dependency on the molecular weight or an consequence of that variation.

The experimental surface potentials from the fitting of the EDL model to the experiential data are of the range 65 to 75 mV at 5×10^{-5} wt% PEO for all molecular weights. There does appear to be a slight decrease in the surface potential as the concentration is increased from 5×10^{-5} to 5×10^{-3} wt% however this change is small and within error of the initial surface potentials, this holds true for all molecular weights. A significant decrease in the surface potentials is observed on increasing the PEO concentration to 0.05 wt% with the values falling by between one half and third. At 0.5 wt% the surface potentials decrease further. The decrease in the surface potentials observed at higher polymer concentrations do not appear to show any significant dependency on the molecular weight of the polymer.

As previously discussed the decreasing surface potential was understood to be dependent on the concentration of halide anions within the system. These were understood to bind to the head groups of the supported surfactant bilayers reducing the surface potential. If this was the only factor affecting the measured surface potentials then one would expect PEO not to influence the surface potential. Up to 5×10^{-3} wt% PEO this holds true as there is little significant change in the measured surface potentials. The decrease in the surface potentials above 5×10^{-3} wt% must be caused by another mechanism. Proposed causes include, impact on the way forces are transmitted through the aqueous medium, salt impurities in the the PEO, adsorption to the surface of the supported bilayers or another form of interaction with the bilayers.

The Debye length as previously discussed can be viewed as a measure over which a change can be "felt" in an aqueous environment. It is mostly understood by the impact of electrolytes on shielding charges from one another. PEO is not charged and therefore can not be view in the same manner as an electrolyte or polyelectrolyte therefore it was not possible to predict its impact on the Debye lengths. However as the concentration of PEO increases above 5×10^{-3} wt% there is a clear decrease in the Debye lengths. Whilst it is not possible to explain this observation from the EDL model, it is possible to suggest a cause more descriptively. It is argued that at higher polymer concentrations the polymer acts either in a similar manner to an electrolyte shielding charge or it impacts upon the the ability of the charge to be transmitted through the aqueous media changing the permittivity of the the

environment.

The interactions at 0.5 wt% PEO, as discussed above, are variable showing three different types of interaction. One of the dominant force profiles show an repulsion followed by an attractive interaction at sort range. As the initial repulsive interaction fit well with the EDL model it is proposed that these forces are caused by the double layer repulsion between the supported cationic bilayers. The short range attraction could be attributed to two interactions. Either the van der Waal's interaction, as part of the DLVO theory, or a depletion interaction. The van der Waals interaction has not been observed constantly with the measurements of the interactions between the DIPEDMAMS bilayers in a variety of environments. This has be put down to repulsive steric and hydration interactions at short separations. For the van der Waals interactions to be observed here it is would require the PEO to cause a break down or a rearrangement of the hydration shell around the bilayers. The other explanation for this short range attraction is the depletion interaction. This would fit with observation of the depletion interaction of PEO between other cationic surfactant bilayers measured using SFA. The range of the interaction is also of the order suggested by other literature measurements. However there is too much variation between the force profiles to compare this potential depletion interaction as a function of polymer molecular weight.

The other dominant type of interactions observed at 0.5 wt% are characterised by a rapidly increasing measured force, similar to hard contact, starting at separation between 50 to over 400 nm. As the separation is further reduced it results in a series of sharply increasing and decreasing peaks in the measured force. These forces are clearly not the result of van der Waals, electrical double layer, or depletion interactions. It is suggested that they are not the result of interaction between the supported cationic surfactant bilayers but the result of interactions with something on the surface of the mica supported bilayer. A proposed explanation for these interactions involves the adsorption of PEO polymers to the surface of the supported bilayers. As the separation is decreased contact is made with the polymers which are compressed and deformed as the separation is decreased further resulting in a force plot showing repeat loading and yielding of the polymer coils. Assuming that the initial repulsive interaction is contact between the probe bilayer and the polymer

coils suggests that the direct interaction between the polymers and the bilayers is minimal as there are no long range forces observed. If the polymer is adsorbing onto the supported bilayers than the small attractive force observed in some force curves can not be due to the depletion interaction and must have another cause such as the van der Waals interaction as the adsorbing polymer may break up the hydration layer causing the strong short range repulsion.

7.3.3 AFM Imaging

The impact of PEO on supported cationic bilayers

In an attempt to gain a more complete understanding of the interactions measured between the supported DIPEDMAS bilayers and the impact of the addition of poly-DADMAC and PEO on them, supported bilayers of DIPEDMAMS were imaged in increasing concentrations of the polymers, using AFM imaging. This was performed for all of the molecular weights investigated in the colloidal probe work.

DIPEDMAMS bilayers were formed using the same vesicle deposition technique as used for the colloidal probe force microscopy. The vesicle dispersion contained 10 mol% perillyl alcohol and the bilayers were formed at room temperature. The polymer concentration was increased by washing the samples with the polymer solution of interest. Several images of the bilayers in each environment were taken.

Figure 7.11 shows typical height, adhesion, and measured slope maps of the supported DIPEDMAMS bilayers in increasing concentrations of the light weight PEO. As has been discussed before the supported DIPEDMAMS bilayers form two different bilayer phases. These phases have different surface properties and nano-mechanics. The adhesion and measured slope maps show that there is a greater tip-sample adhesion on retraction for the thinner bilayer phase and that the thicker phase has a steeper measured slope or relative stiffness than the thinner bilayer phase. No discernable change was observed from the bilayers formed in deionised water to those observed at 5×10^{-5} wt% PEO. This is also true for 5×10^{-4} wt% PEO where no significant changes were observed to either the topography, the sur-

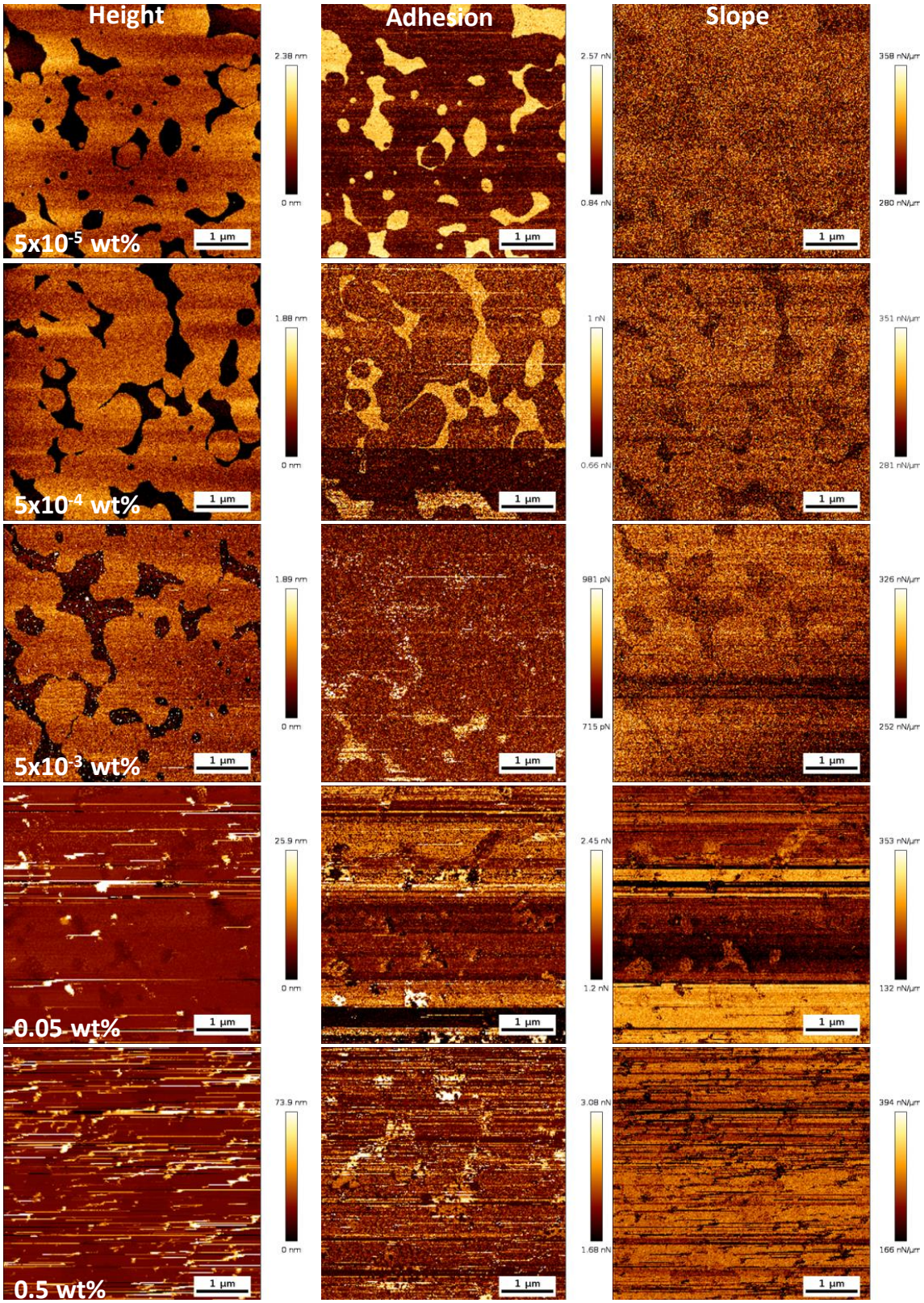


Figure 7.11: Typical QI AFM topographical images, with associated typical maps of surface adhesion and measured slope, for supported DIPEDMAMS bilayers imaged in increasing concentrations of 400,000 Mw PEO. Concentrations shown in figure.

face interaction or the nano-mechanical properties. At 5×10^{-3} wt% small, almost spherical like, features are observed in the height images. These range from less than 10 to over 100 nm in diameter with a height of between 80 and 120 nm. These are observed across the surface. They appear to have some impact on the tip to sample adhesion but do not appear to have a significant impact on the maps of the measured slope. The number and size of these sphere like features increases as the concentration is increased to 0.05 wt%. These appear to also introduce a number of line artefacts into the images making resolving the image more difficult. These line artefacts along with the striated changes observed in the adhesion and slope maps suggest that at least some of these particles are mobile and most likely being picked up by the AFM tip and moved during imaging. This makes drawing any conclusions from the slope and adhesion maps problematic as it is uncertain whether they are measuring the tip bilayer interaction or particle bilayer interactions. Increasing the concentration further to 0.5 wt% results in a further increase in the number of these particles and hence the number of line artefacts making the images difficult to resolve. This also negatively impacts on the adhesion and slope maps making them too busy to interpret in any meaningful way

This pattern is to the most part repeated across the other two molecular weights. However the concentration at which the particles first appear for the other molecular weights is 0.05 wt% where they are observed in lower numbers compared with the low molecular weight PEO. These again cause line artefacts due to the proposed mobility of these particles and render the adhesion and slope maps problematic to interpret.

Height images and corresponding cross-sections of the highest and lowest PEO concentrations for all molecular weights are shown in figure 7.12, 7.13, and 7.14. At 5×10^{-5} wt% there is no discernable difference in the topography of the supported bilayers. All show the expected two phase configuration with the two phases differing in thickness by 1 - 1.5 nm. At 0.5 wt% all samples show the appearance of particles or aggregates on the surface which induce a number of line artefacts. As briefly mentioned above the concentration at which the particles start to appear does appear to increase with increasing molecular weight. However from the figure one can clearly see how the number of these aggregates at 0.5 wt% appears to be inversely

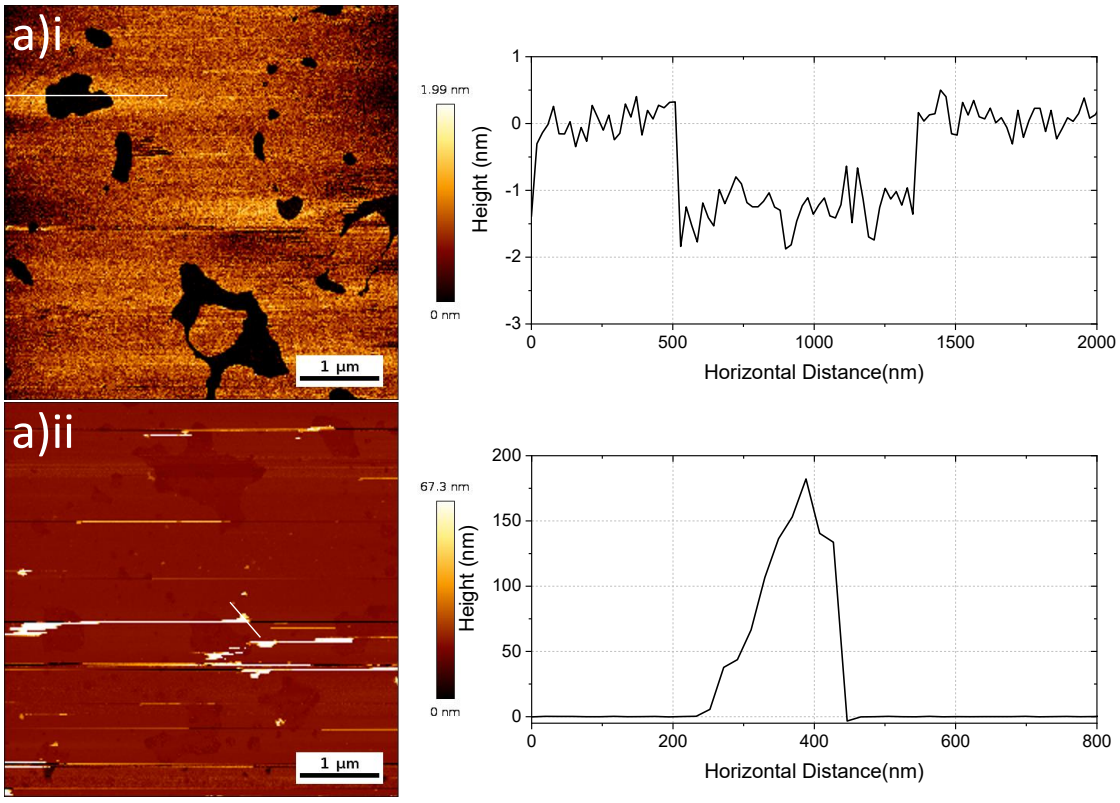


Figure 7.12: AFM images, 5 x 5 μm and associated cross-sections in PEO solutions a)i 5×10^{-5} wt% high molecular weight a)ii 0.5 wt% high molecular weight.

proportional to the molecular weight of the PEO dispersion present. The size, in terms of height as the diameter can be difficult to determine due to the line artefacts, appears to increase with increasing molecular weight.

It is suggested that the particles or aggregates observed on the surface on the supported bilayers are the the result of PEO polymer coils adsorbing to the surface of the bilayer. The adsorption of the polymer to the surface of the bilayers at higher polymer concentrations would offer an explanation for the observed forces. It is proposed that the force profiles showing rapidly increasing measured force, similar to hard contact followed by a series of sharply increasing and decreasing peaks in the measured force as the separation is further reduced are the result of interactions between the adsorbed polymers and the bilayer on the probe. The series of peaks observed in the force profile as the separation is decreased are explained by the compression and deformation of these polymer coils.

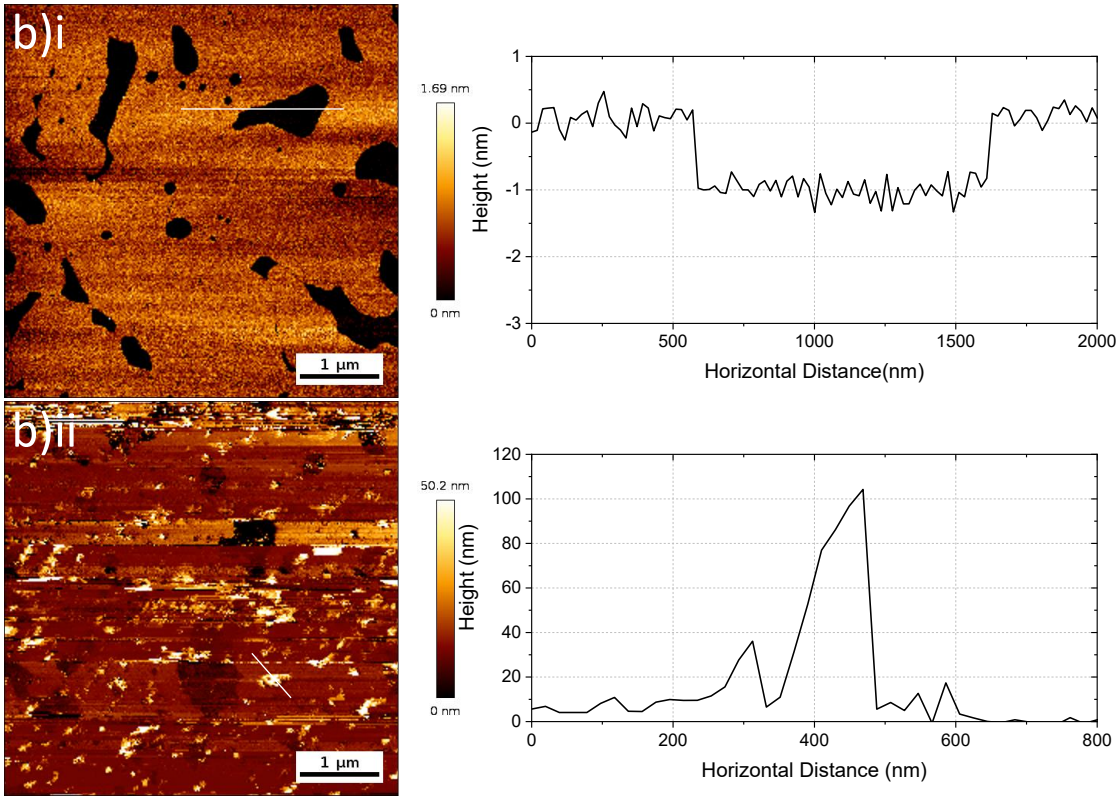


Figure 7.13: AFM images, 5 x 5 μm and associated cross-sections in PEO solutions b)i 5×10^{-5} wt% medium molecular weight b)ii 0.5 wt% medium molecular weight.

The features on the surface are not uniform in shape or size and whilst the polymer samples are polydisperse this can not account for the amount of variation observed. These are attributed to polymer aggregates made up of more than one polymer coil. The number of polymer aggregates and coils observed on the bilayer surfaces at 0.5 wt% show a dependency on the molecular weight of the polymer used. The images suggest that as the polymer molecular weight increases, fewer features are observed on the surface. Whilst the number of monomers in the samples is kept constant the number of coils will decrease as their size increases with the molecular weight. This observation therefore may be put down simply to the number of polymer coils present in the system. The size and height of these aggregates also appears to increase with increasing molecular weight. Which could be explained by the increasing size of the individual polymer coils. However the observed variation in size with the additional complication of the line artefacts make it difficult to comment too strongly on this.

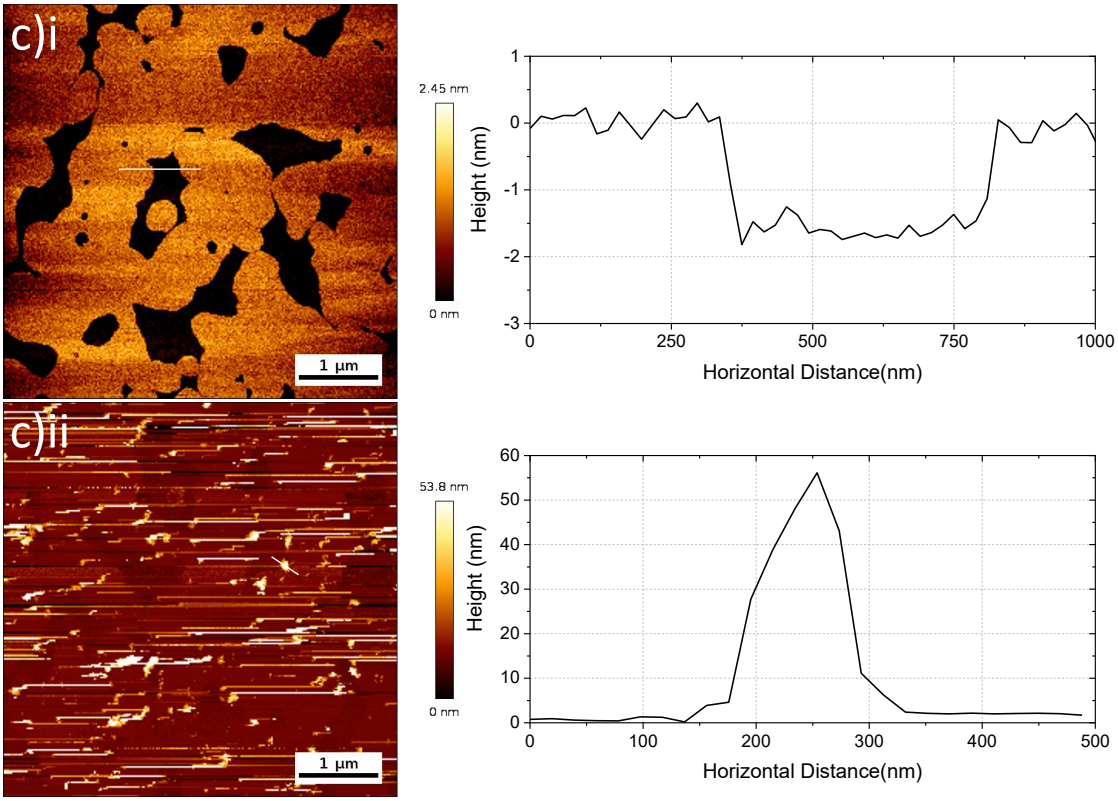


Figure 7.14: AFM images, 5 x 5 μm and associated cross-sections in PEO solutions a)i 5×10^{-5} wt% low molecular weight a)ii 0.5 wt% low molecular weight.

Due to the adsorption of the polymer coils onto the surfaces at higher PEO concentration and the induction of line artefacts into the images it is difficult to comment on the state of the supported surfactant bilayer underneath. However it is still possible to see the two phase configuration of the surfactant bilayer system in some areas of the images suggesting that the adsorption of the polymer to the bilayers does not have a significant impact on the structure of the bilayers.

The impact of Poly-DADMAC on supported cationic bilayers

Figure 7.15 shows typical height, adhesion, and measured slope maps of the supported DIPEDMAMS bilayers in increasing concentrations of the medium weight poly-DADMAC. In deioinsed water and in low poly-DADMAC concentration the bilayers adopt the two phase configuration with the different phases showing different surface properties and nano-mechanics. No significant changes were observed

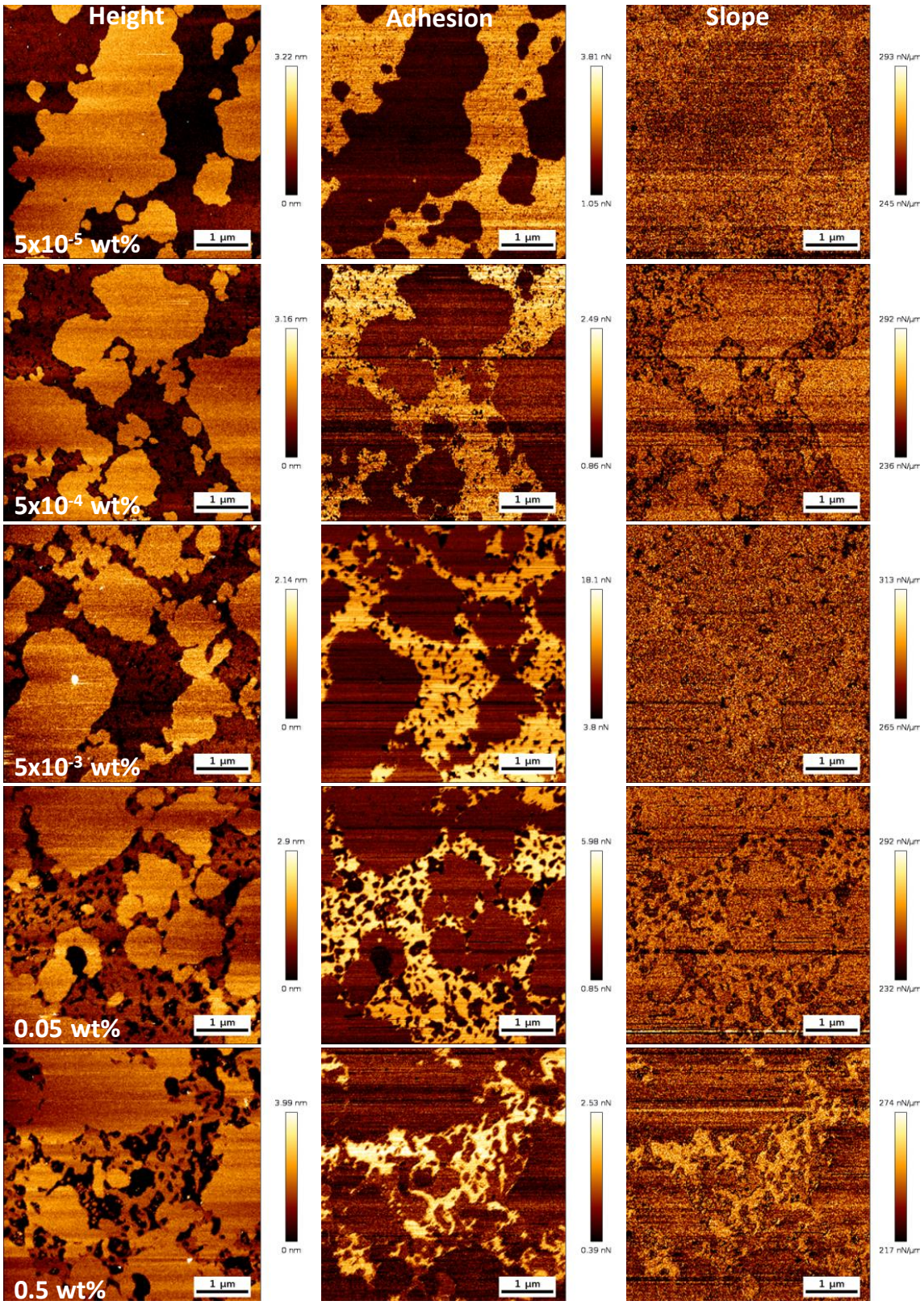


Figure 7.15: Typical QI AFM topographical images, with associated typical maps of surface adhesion and measured slope, for supported DIPEDMAMS bilayers imaged in increasing concentrations of medium poly-DADMAC. Concentrations shown in figure.

between the system in deionised water and 5×10^{-5} wt%. As the poly-DADMAC concentration is increased holes are observed to form in the supported surfactant bilayers. The size and number of these holes increases with increasing polyelectrolyte concentration. The addition of the polyelectrolyte does not appear to have a significant impact on the tip to sample adhesion of the two different surfactant phases. However it does appear to show a change on the contrast of the measured slope between the the two phases. However this does vary to some degree between different samples. It is difficult to comment on the adhesion and measured slope maps for the holes as some images show a decrease in the adhesion or measured slope in those areas where holes are observed whereas other images or sections of images can show an increase.

There were no significant differences in the bilayer images between the different poly-DADMAC molecular weights. They all suggested an equally potent effect on the bilayer at each concentration. All showed a steady increase in the number and size of the holes appearing in the bilayers as the poly-DADMAC concentration was increased.

Topographical Height images and their corresponding cross-sections at the highest and lowest concentration of poly-DADMAC for the light and heavy molecular weight systems are shown in figure 7.16. In 5×10^{-5} wt% poly-DADMAC both molecular weights show the two phase configuration expected for the DIPEDMAMS system. The height difference between the two phases being measured as 1 - 1.5 nm as expected. This is identical to the images in deionised water. At 0.5 wt% poly-DADMAC holes have been formed in the bilayers. There does not appear to be any dependence on the molecular weight of the polyelectrolyte on the size nor the number of these holes. These holes are typically 3 to 4 nm in depth. A change in the height difference between the thicker and thinner bilayer phases is observed as the electrolyte concentration increases. The difference is typically 1 - 1.5 nm at low salt concentrations but decreases to 0.5 - 1 nm at higher salt concentrations.

The observation of the formation of holes in the surfactant bilayers with increasing polyelectrolyte concentration is very similar to those observed with the addition of halide salts in Chapter 6. It was argued that the formation of holes in the bilay-

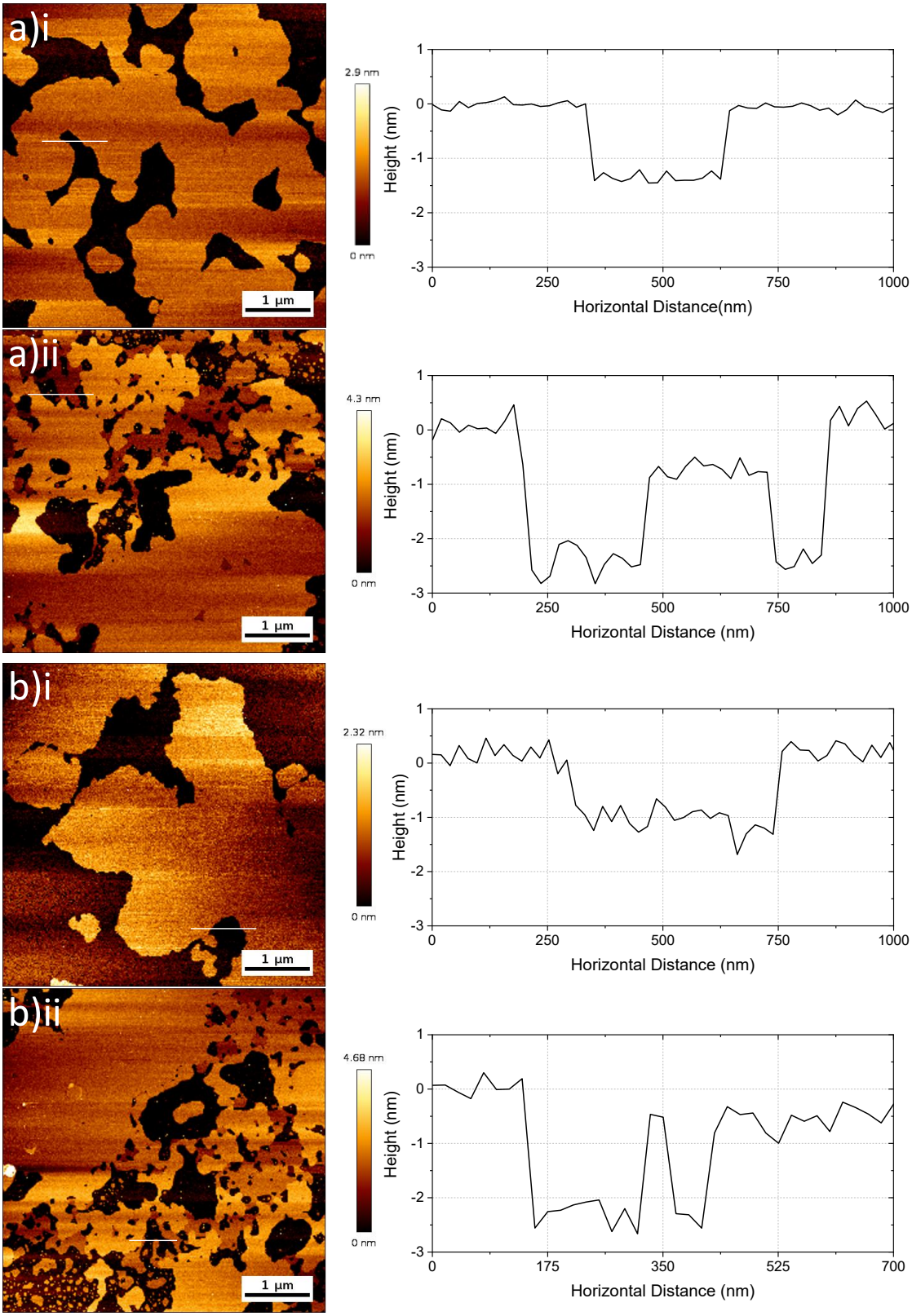


Figure 7.16: AFM images, 5 x 5 μm and associated cross-sections in poly-DADMAC solutions a)i 5×10^{-5} wt% high Mw a)ii 0.5 wt% high Mw b)i 5×10^{-5} wt% low Mw b)ii 0.5 wt% low Mw.

ers offered an additional explantation for the observation that the measured surface potential decreased with increasing salt concentration and it was suggested that as more holes form in the supported bilayer, the surface coverage decreased the charge density and the overall surface potential decrease. This aided in explaining some of the observations form the colloidal probe force spectroscopy. It was also proposed that the binding of the halide counter ions to the surfactant head groups disrupting the local hydration sphere and change the charge localization was a potential cause for the break up of the bilayer. If that holds true then the observations of the independence of the holes formation from the polymer molecular weight as the number of monomers and hence the chloride concentration was constant between samples at the same wt%. This does however suggest that the polyelectrolyte coils themselves have a negligible impact on the surfactant bilayers and only act to modify the forces between them.

7.3.4 Particle sizing and Zeta Potential of Surfactant Vesicles

Whilst the colloidal probe force spectroscopy data shows how the measured forces between the surfactant bilayers are impacted by the addition of polymers and polyelectrolytes it is not clear whether the decreasing strength of the repulsive interactions, or the appearance of small attractive interactions, are enough to induce the flocculation and instabilities into a bulk vesicle dispersion. To explore this relationship, the mean particle size and the zeta potential of DIPEDMAMS vesicle dispersions containing increasing concentrations of PEO and poly-DADMAC were investigated.

The effect of increasing concentrations and molecular weights of poly-DADMAC on the mean particle size and zeta potential of DIPEDMAMS vesicle dispersion are shown in figure 7.17. For clarity, the poly-DADMAC concentration has been plotted on a $\log_{10}$ scale. The initial particle size and therefore vesicle diameter was measured as 82 ± 4 nm. No significant change in the mean particle diameter was observed as the polyelectrolyte concentration was increased form 5×10^{-5} to 5×10^{-3} wt%. At

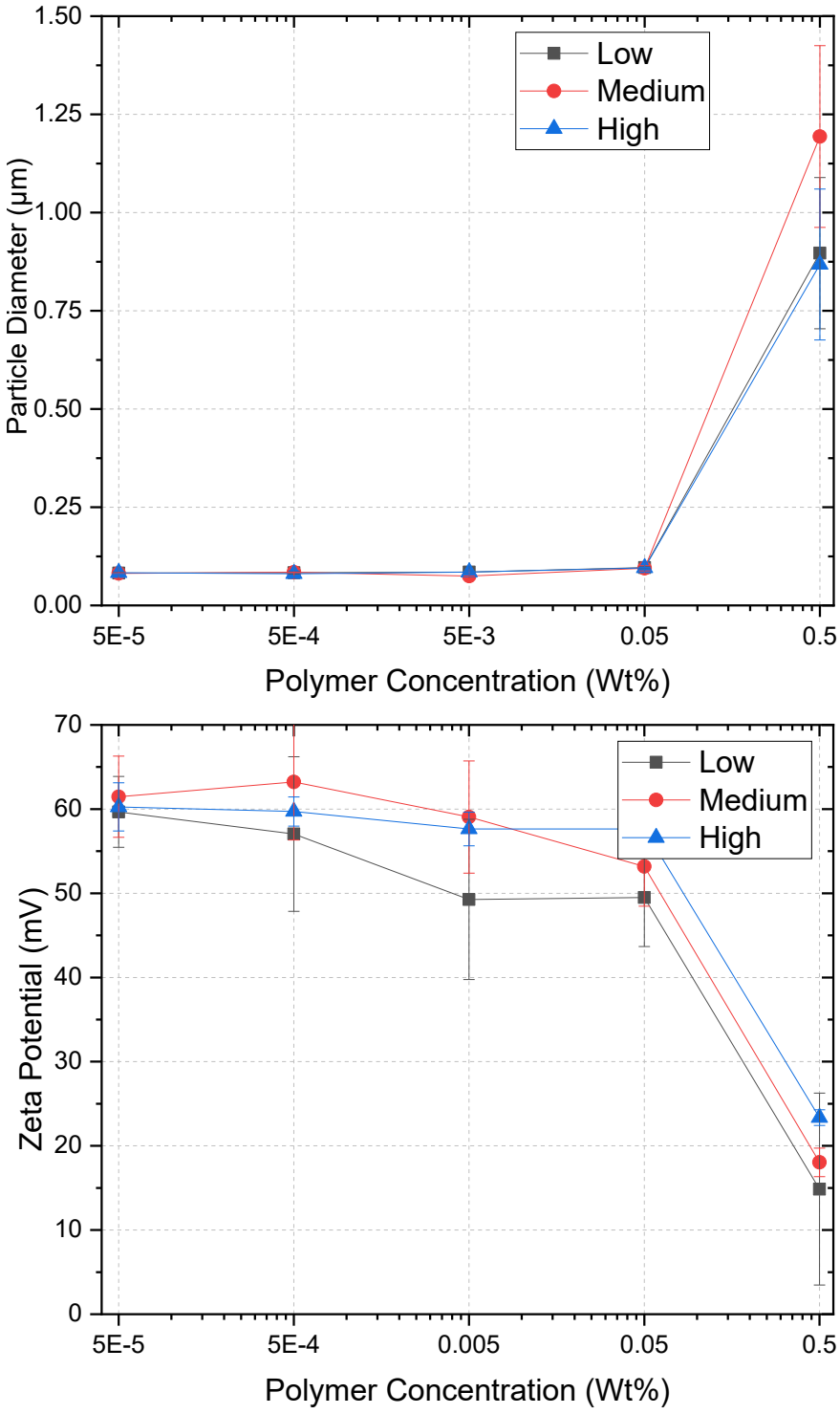


Figure 7.17: Plots of the mean particle diameter and zeta potential of a DIPED-MAMS vesicle dispersion as a function of increasing poly-DADMAC concentration and molecular weights.

0.05 wt% a 10% to 18 % increase in the mean particle size was observed for all poly-DADMAC molecular weights. Increasing the concentration to 0.5 wt% resulted in a large increase in the mean particle diameter for all molecular weights. The mean particle diameter increased by more than a factor of 10. Whilst some difference in the particle diameter is observed between the different molecular weights the large variation in the experimental measurements makes the resolving of any dependency problematic.

The initial zeta potential measurements in 5×10^{-5} wt% poly-DADMAC were measured as 61 ± 6 mV at all molecular weights. As the polyelectrolyte concentration was increased from 5×10^{-5} to 0.05 wt% a slight decline in the zeta potential was observed for all molecular weights. There was some variation in the measured zeta potentials at all concentrations making it difficult to resolve if there are any dependency on the molecular weight. As the concentration was increased further to 0.5 wt% the zeta potential fell steeply to 18 ± 5 mV. This was true for all molecular weights. Despite the variation in the measured zeta potential at this concentration it is not believed that there is any observed dependency on the molecular weight.

The initial zeta potential values at 5×10^{-5} wt% poly-DADMAC compare well with the surface potentials calculated from the colloidal probe direct force measurements. With the experimental surface potentials being slightly higher than the zeta potential measurements as would be expected. However whilst the zeta potential values show a slight decline up to 0.05 wt% poly-DADMAC and a sharp decline at 0.5 wt% poly-DADMAC, the surface potentials, table 7.1 show a steady decline with each increase in the polymer concentration.

The effect of increasing concentrations and molecular weights of PEO on the mean particle size and zeta potential of DIPEDMAMS vesicle dispersions are shown in figure 7.18. For clarity, the PEO concentration has been plotted on a $\log_{10}$ scale. The initial particle size and therefore vesicle diameter was measured as 81 ± 6 nm. No significant change in the mean particle diameter was observed as the polymer concentration was increased form 5×10^{-5} to 5×10^{-3} wt%. At 0.05 wt% a 20% to 30% increase in the mean particle size was observed for all PEO molecular weights. Increasing the concentration to 0.5 wt% resulted in a large increase in the mean

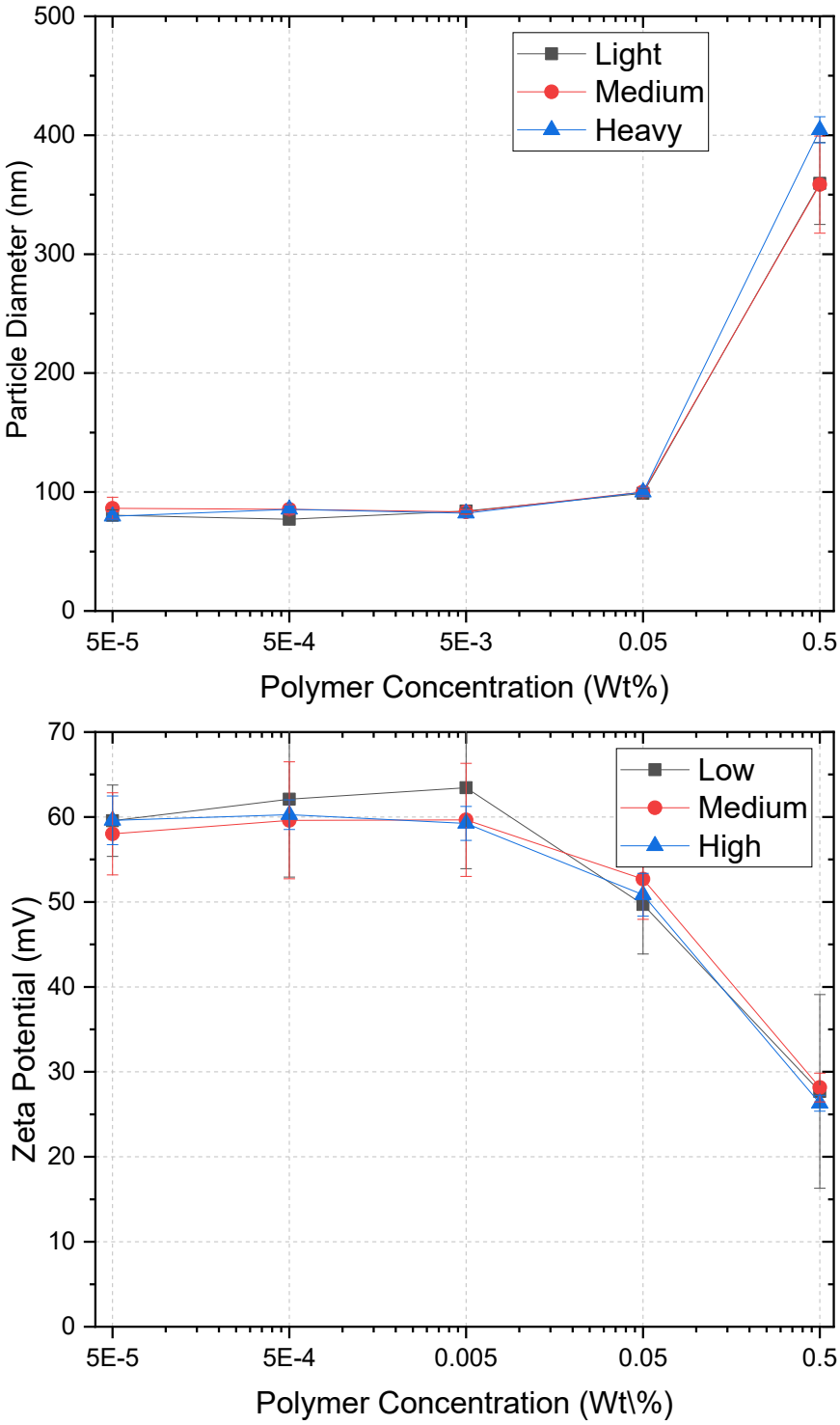


Figure 7.18: Plots of the mean particle diameter and zeta potential of a DIPED-MAMS vesicle dispersion as a function of increasing PEO concentration and molecular weights.

particle diameter for all molecular weights. The mean particle diameter increased by approximately five times the initial vesicle diameter. Taking into account the variation and range of the measured particle diameters at each polymer concentration the molecular weight of the polymer does not appear to have an impact on the mean particle size at any concentration.

The initial zeta potential measurements in 5×10^{-5} wt% PEO were measured as 58 ± 6 mV at all molecular weights. Within error the zeta potential remains constant as the polymer concentration was increased from 5×10^{-5} to 5×10^{-3} wt%. However due to the variation in the measured values this does not appear significant and can not be stated with much certainty. Whilst there is some difference in the values for the different molecular weights at these concentrations they are not significant enough to suggest any dependency on the molecular weights. A significant decrease in the zeta potential is observed as the polymer concentration is increased to 0.05 and 0.5 wt%. At 0.5 wt% the zeta potential has fallen to 27 ± 8 mV. The decrease in the zeta potential observed at 0.05 and 0.5 wt% do not appear to show any dependency on the molecular weight of the polymer.

The large increases in the mean particle diameter measured at high polymer and polyelectrolyte concentrations are suggested to be caused by aggregation of the DIEDMAMS surfactant vesicles. These aggregates form when the interactions between the surfactant vesicles are not sufficiently repulsive to prevent them from coming into contact with one another. Once in contact interactions including the attractive van der Waals interaction, hydration effects, and depletion interactions cause the vesicle to adhere to one another. This may also involve vesicles merging or engulfing one another. The growth of these aggregates may eventually lead to the system separating into a surfactant rich phase and an aqueous phase.

With the addition of poly-DADMAC the colloidal probe microscopy show that the interaction between the surfactant bilayers was strongly repulsive up to 5×10^{-3} wt%. This is reflected in the particle sizing data which showed no change in the mean particle diameter at these concentrations. At 0.05 wt% a weak depletion interaction was observed, for all molecular weights, in the forces measured between the bilayers. A small but not insignificant increase in the mean particle diameter was observed

at this concentration potentially suggesting that the system has begun to flocculate. Whilst the colloidal probe data suggested a relationship between the strength of the depletion interaction and the molecular weight of the polyelectrolyte this was not reflected in the DLS data. At the highest poly-DADMAC concentration of 0.5 wt% only minimally repulsive interactions were measured between the bilayers which, from the large increase in the mean particle size observed in the DLS data, are weak enough to cause the system to flocculate.

The changes in the zeta potential with increasing poly-DADMAC concentration are similar to those observed with the addition of NaCl. Supporting the suggestion that it is chloride counter ions which are having the largest impact in the changes in electrical repulsion between the bilayers. The ionic pair model of electrical double layers, as discussed in Chapter 6 suggests that the increased counterion binding at the head group of the surfactant bilayers can decrease the surface potential and therefore the measured zeta potential. This also reduces the thickness of the double layer and reduces the repulsion between the vesicles.

In PEO the size of the vesicles is constant up to 0.05 wt% at which a small increase is observed then large increase at 0.5 wt% but not as much as poly-DADMAC. The colloidal probe data however shows the interactions between the supported bilayers as strongly repulsive up to 0.05 wt%. There appears to be a contrast between the measured forces and the particle size data suggesting that the system is beginning to flocculate. However there is another potential explantation for the observed increase in the particle size. From the AFM imaging data of DIPEDMAMS bilayers with the addition of PEO adsorption of the polymer coils onto the bilayers were observed. If this was also occurring in the bulk vesicle systems it would show an increase in the mean particle diameter of the vesicles. The system does then show a significant increase in the mean particle diameter at 0.5 wt% PEO which can only be understood in terms of vesicle aggregation and the beginnings of system instability. The increase in vesicle diameter at 0.5 wt% PEO however is about half that observed for the poly-DADMAC. The bilayer - bilayer interactions at these concentrations do show a stronger repulsive interaction than their poly-DADMAC counter parts which could explain why the aggregation is not to the same extent. Steric effects caused by the adsorption of the PEO polymer coils to the bilayers may also have an effect.

The decrease in the zeta potential with the addition of PEO is only observed at 0.05 wt% and above, echoing the observed decrease in the surface potentials observed from the colloidal probe work. It is suggested that the adsorption of the polymer coils to the bilayer surface as observed in the AFM data may be acting to shield the surface charge or causing a shift in the shear plane thus reducing the measured zeta potential.

7.4 Conclusions

Colloidal probe force spectroscopy was used to directly measure the interactions between two supported cationic surfactant bilayers in aqueous polymer and polyelectrolyte environments. The measured interactions before the addition of polymers or polyelectrolytes were exponentially repulsive. With the addition of poly-DADMAC the strength and range of the repulsive interaction declined with increasing polyelectrolyte concentration, in a similar manner observed to the impact of electrolyte on the measured interactions. At 0.05 wt% poly-DADMAC a small but not insignificant attractive interaction was observed. This is thought to be a depletion attraction.

Comparing the measured interaction with the theoretical EDL model the electrical double layer forces were observed to decay at rates in agreement with theoretical Debye lengths, where the polyelectrolyte were treated as monomers, with some deviation at extremes of electrolyte concentrations. The good agreement of the theoretical and measured Debye lengths suggested that treating the polyelectrolyte as a normal electrolyte is sufficient to describe their impact on the range of the measured interactions. There did not appear to be any strong correlation between the molecular weight of the poly-DADMAC and its impact on the bilayer - bilayer interactions.

Topographical AFM images of the supported surfactant bilayers with increasing concentrations of poly-DADMAC showed the formation of holes in bilayers penetrating down to the mica support. The size and number of these holes appeared

to increase as the polyelectrolyte concentration increased. The hole formation did not appear to show any dependence on the molecular weight of the polyelectrolyte. This generally supported the trend observed in the colloidal probe force microscopy. The hole formation provided an additional explanation for the observation that the surface potential fell with increasing poly-DADMAC concentration. The similarity of the impact of the polyelectrolytes on the bilayers with the effect of the halide salts on the bilayers suggested that the polymer coils had only minimal impact on the bilayers and the responsibility for the changes in the bilayers lay with the chloride counter ions.

Looking at bulk DIPEDMAMS vesicle dispersions the systems appeared stable as measured by DLS and zeta potential up to 5×10^{-3} wt% poly-DADMAC. However the vesicles were observed to aggregate and flocculate at higher concentrations. At 0.05 wt% poly-DADMAC, at which a depletion attraction was observed, showed only a modest increase in the mean particle diameter. There were no significant variations between the changes observed in the mean particle diameter and zeta potential with the different molecular weights investigated.

The addition of PEO at similar concentration to the polyelectrolyte had a much smaller impact on the measured forces up to 0.05 wt%. No significant change in the repulsive interactions were observed as the concentration of PEO was increased to 5×10^{-3} wt% in contrast to the steady decline in strength and range of the interactions observed with poly-DADMAC. A sharp decline in the repulsive interactions was observed at 0.05 wt% PEO followed by a short range attraction not observed at higher concentrations. The interactions measured at 0.5 wt% were variable and often showed behaviour not consistent with EDL interactions.

Topographical AFM images of the supported bilayers in increasing concentrations of PEO showed no significant changes up to 5×10^{-3} wt%. At 0.05 wt% and above polymer coils and aggregates were observed to have adhered to the surface of the bilayers. The number of which increased as the concentration was raised further. The number adhered polymers decreased and the size of the features increased with increasing polymer molecular weight.

Finally the impact of PEO on the mean particle size and zeta potential of bulk surfactant vesicle dispersions was investigated. No significant changes were observed up to a concentration of 5×10^{-3} wt%. At 0.05 wt% a small increase in the mean particle size was observed, this is suggested to be related to the adhesion of polymers to the vesicles as opposed to vesicles aggregation. A large increase in the particle size is observed at 0.5 wt% where the measured forces are sufficiently low that the system begins to flocculate and destabilise.

Chapter 8

The Impact of Fatty Acids on Bilayer-Bilayer Interactions to Simulate Surfactant Ageing

8.1 Introduction

The cationic double tailed surfactant di(alkyl iso-propyl ester) dimethyl ammonium methylsulfate (DIPEDMAMS), which has been the main focus of the work so far has been designed to contain two ester bonds. This is a deliberate design decision based around the need to make such industrial surfactant and surfactant systems more environmentally friendly than those containing alkyl or ether linkages. The ester enables the surfactant to under go hydrolysis reducing it to its consultant parts. The resulting fatty acids can be broken down in the environment as they are a natural product. [344] Whilst this design reduces the long term environmental impact of the surfactant system on the environment it means that the composition of the system will change over time.

The DIPEDMAMS system is synthesised using a industrial fatty acid mixture primarily comprised of stearic, palmitic and oleic acid. Corresponding to the chain

lengths C18, C16, and C18:1 respectively. The mixture is generally sourced from tallow or a vegetable based system with similar fatty acid ratios. A typical tallow composition is as follows 14% stearic acid, 26% Palmitic acid, and 47% oleic acid any other constituents are typically present at concentrations of $< 3\%$. [345]

Ageing or chemically inducing the breakdown of the surfactant molecules would be both laborious and inconsistent with precisely controlling the amount of decomposition being problematic. Instead, it was decided to mimic the decomposition of the system by adding the fatty acids to the system. This was done in a manner that endured the fatty acid were incorporated into the bilayers as they would be if produced within the bilayers. This enabled the effect of increasing the bilayer content of each individual fatty acid to be investigated as well as the impact of the mixed tallow on the system.

Colloidal probe microscopy was used to investigate the impact of increasing fatty acid content on the forces measured between the supported cationic bilayers in an attempt to understand if this would be a potential cause of system instability. Atomic force microscopy was used to image the supported bilayers to investigate how the addition of the different fatty acids to the bilayers impacted upon the topography and nano-mechanical properties of the surfactant bilayers. This was in an attempt to decouple the impact of the polymers on the forces between the bilayers and changes to bilayers themselves. Small and wide angle x-ray scattering was used to try and understand if the impact of the fatty acids on the supported bilayers was present in the bulk system.

8.2 Experimental

The cationic surfactant, di(alkyl iso-propyl ester) dimethyl ammonium methylsulfate (DIPEDMAMS) was provided by Procter and Gamble. Synthesised using an industrial fatty acid mixture of C18, C16 and C18:1 chains, therefore the aliphatic tails are a statistical mixture of the three fatty acids see section 4. Stearic, palmitic, and oleic acid were obtained from Sigma-Aldrich. All solutions were prepared with

deionised water, $<$ 18 mS, filtered through an activated carbon filter to remove organic impurities.

8.2.1 Preparation of supported lipid bilayers

Supported surfactant bilayers were formed by the vesicle deposition technique from DIPEDMAMS/fatty acid vesicle dispersions, as described in Chapter 3. Bilayers were formed on both mica and the glass colloidal probe in situ at 60 °C.

8.2.2 Atomic Force Microscopy

All measurements were made using a JPK Nano wizard 4 AFM and analysed using the JPK data processing software as detailed in Chapter 3

Colloid Probe Atomic Force Spectroscopy

Colloidal probe force spectroscopy was used to measure force distance curves between a colloidal sphere, attached to an AFM probe, and a flat substrate. By forming a supported cationic surfactant bilayer on both surfaces the interactions between the bilayers could be investigated. Force curves were collected in multiple positions across the surface for each fatty acid composition. For more details please see Chapter 3

AFM Imaging

All imaging was performed in quantitative imaging (QI) mode. Multiple images of different areas of each supported bilayer were collected. All imaging was performed at 23 ± 2 °C. Further details on QI mode and on the imaging protocols can be found in Chapter 3

8.2.3 Small Angle X-ray Scattering (SAXS)

Sample Preparation

DIPEDMAMS/fatty acid/water systems were fabricated according to the protocols discussed in Chapter 3. Samples were hydrated at 20 wt% by mass.

Beamline set up

SAXS was performed at the Diamond Light Source (Oxfordshire) on beamline I22, as detailed in Chapter 3

8.2.4 Dynamic Light Scattering and Zeta Potential

Sample Preparation

DIPEDMAMS/fatty acid vesicle dispersions were fabricated according to the protocols described in Chapter 3.

Particle sizing and zeta potential measurements

Particle sizing and zeta measurements were performed using a A Brookhaven zeta-PALS as detailed in Chapter 3. All measurements were performed at 25 °C.

8.3 Results and Discussion

8.3.1 The impact of bilayer compositions on the interactions measured between supported cationic bilayers

Earlier work required the addition of periyl alcohol to the surfactant vesicle dispersion to reduce the transition temperature of the system enabling the formation of supported DIPEDMAMS bilayers at room temperature. At this stage in the project a sample heating stage had been acquired for the AFM enabling imaging and force spectroscopy to be performed at temperatures above ambient. This enabled the formation of supported DIPEDMAMS bilayers in situ on both the probe and the mica substrate by heating the system. The system was then allowed to cool and treated in the same manner as those formed in the earlier work. Being able to form supported bilayers this way opened up the opportunity to study the impact of changing surfactant compositions on the interaction between two supported surfactant bilayers.

When investigating how additives to the system affected the interactions between the bilayers it was possible to create the supported bilayers then measure how the interactions changed as the system was flushed to replace the aqueous environment with another of interest. That is clearly not possible when investigating the composition of the surfactant bilayers. As has been mentioned previously there is some variation between the initial interactions. This however is thought to be primarily caused by different cantilevers as the exact spring constant is not known and they can be impacted by variations in the size and position of the colloidal sphere. To compensate for this variation each fatty acid series was performed using a single probe. This was repeated several times for each fatty acid until the trend with the probe increasing and decreasing the fatty acid content exhibited a similar pattern.

The interactions between two supported DIPEDMAMS bilayers containing increasing ratios of stearic, and palmitic acid are shown in figure 8.1. The interactions shown in for each fatty acid were performed using the same probe to minimise variation in the force measurements. At each each fatty acid concentration the forces

shown are typical of those observed at each concentration as there was little variation across the surface for each sample. Force curves shown are those on approach as those on withdrawal showed no significant difference to those on approach.

The interactions between the pure DIPEDMAMS bilayers and those containing the C18 fatty acid, stearic acid, and the C16 fatty acid, palmitic acid, exhibited similar behaviour. All exhibited almost solely repulsive interactions on approach. The onset of the repulsive interaction was between a separation of 300 and 350 nm. As the separation was decreased the force measured between the bilayers appeared to increase exponentially. At shorter separations the repulsive interactions appeared to increase further an a purely exponential relationship would suggest. Further decreasing the separation resulted in one of two behaviours. Most often the repulsive interaction would increase further until it became indistinguishable from the compliance region and hard contact between the bilayers was assumed to have been achieved. In a minority of areas a small attractive force was observed between 2 and 5 nm with an attractive force of < 0.5 nN which lead to contact between the bilayers.

For both of the stearic and palmitic acid as the fatty acid content of the bilayers was increased the strength and range of the repulsive interactions appeared to decrease. However this decrease is subtle compared to those observed in previous work. The relationship between the fatty acid content and the measured forces was observed using several probes both increasing and decreasing the fatty acid content. This suggests that the observations are not just the result of variation between experimental runs. No significant difference is observed between the impact of stearic and palmitate acid on the interactions.

The interactions between two supported DIPEDMAMS bilayers containing increasing ratios of oleic acid and a simulated tallow mixture are shown in figure 8.2. The simulated tallow was formed by melting together stearic, palmitic and oleic acid in the following ratio 16:30:54 in order to mimic the industrial product used the create the surfactant and simulate the hydrolysis of the statistical surfactant system.

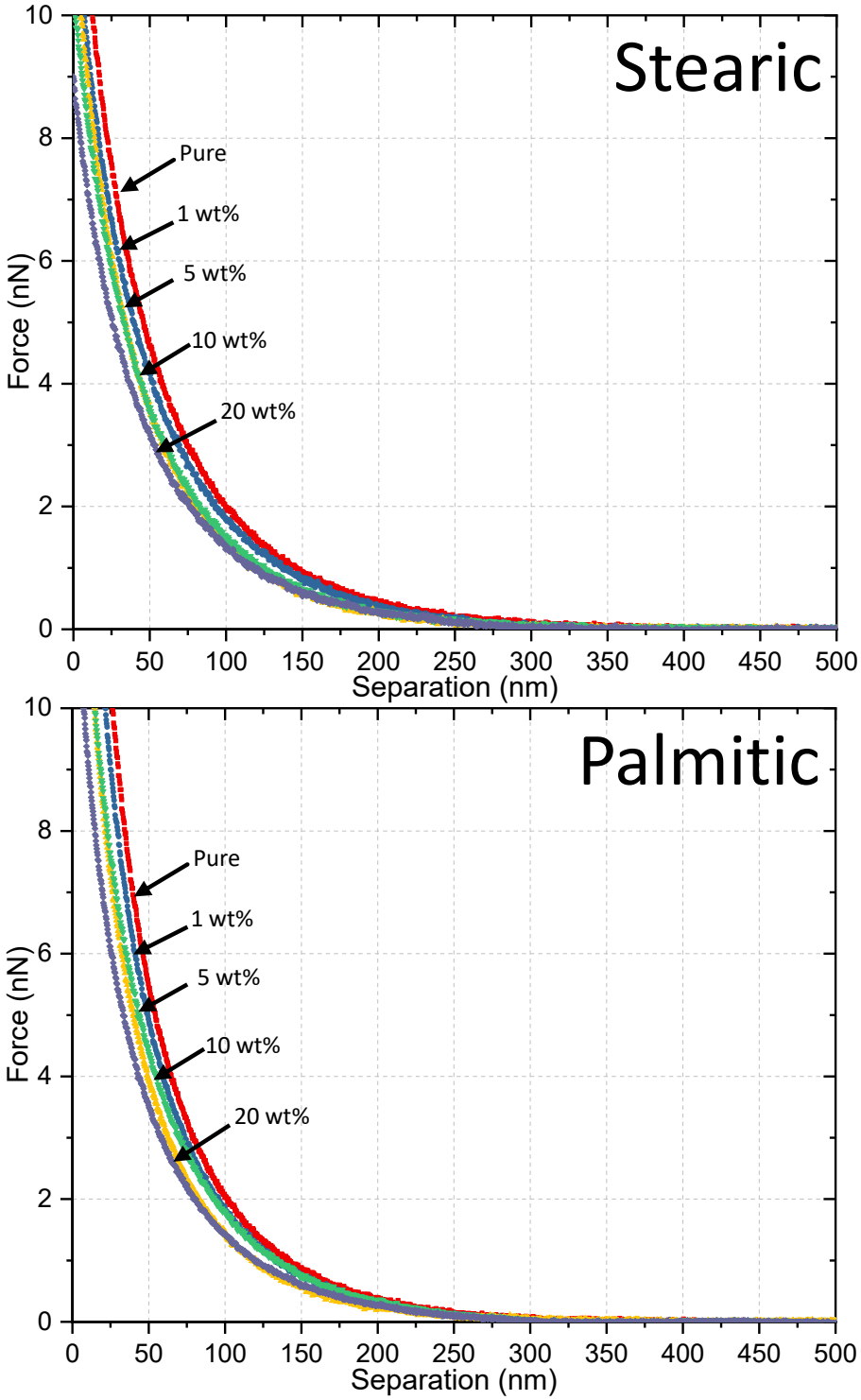


Figure 8.1: Forces measured on approach between DIPEDMAMS bilayers containing increasing concentrations of stearic acid and palmitic acid. Fatty acid concentrations and identity are shown in the figure.

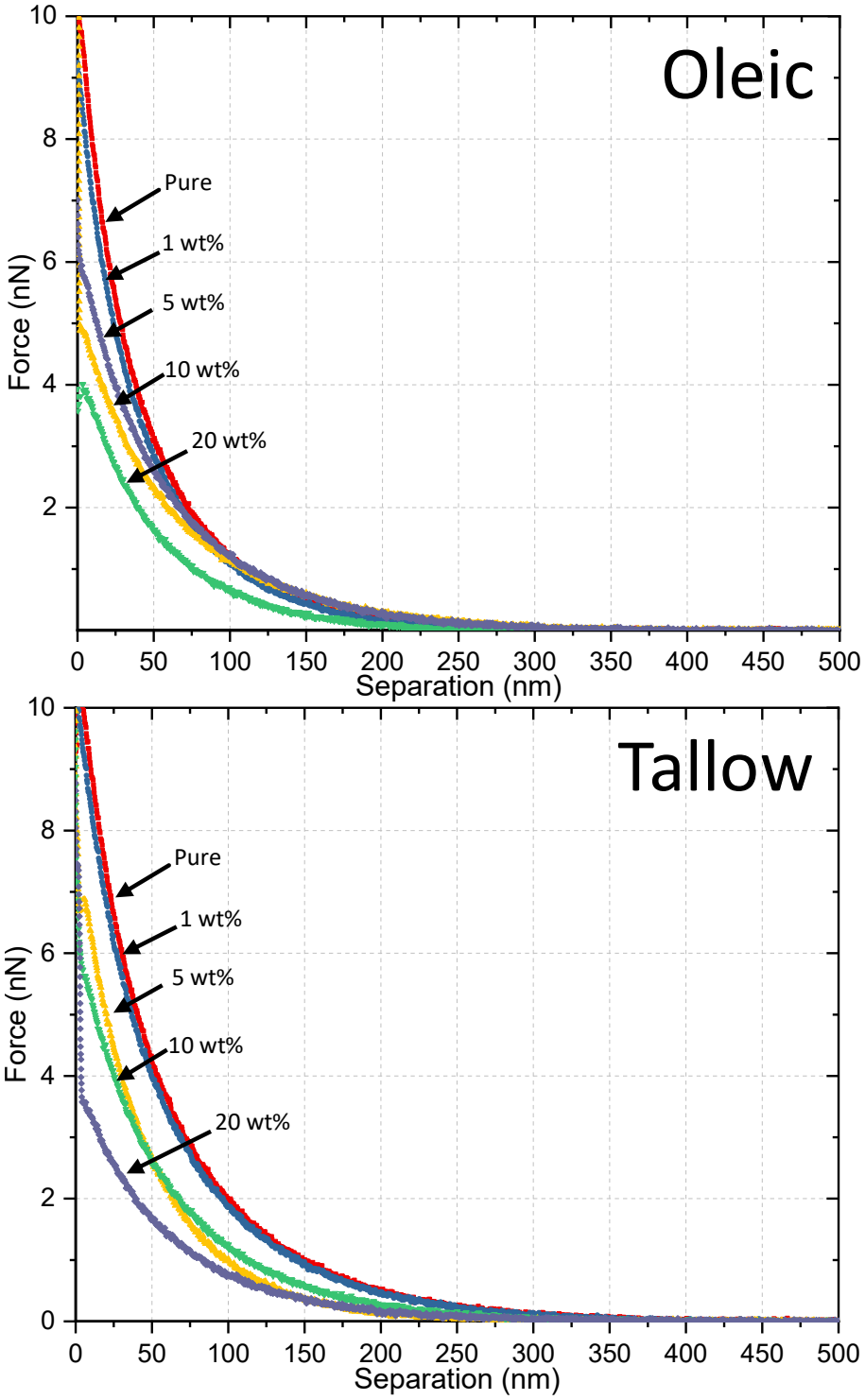


Figure 8.2: Forces measured on approach between DIPEDMAMS bilayers containing increasing concentrations of oleic acid and tallow mixture. Fatty acid concentrations and identity are shown in the figure.

The interactions between the surfactant bilayers with increasing oleic acid content and those with increasing tallow composition exhibited almost solely repulsive interactions on approach. The range and strength of these repulsive interactions are observed to decrease with increasing oleic acid concentration and the increasing inclusion of the tallow mixture showed a similar pattern. These interactions were observed with different probes and on decreasing the fatty acid content. The onset of the repulsive interactions were observed between a separation of 300 and 350 nm for pure DIPEDMAMS bilayers falling to between 200 and 250 nm at the highest fatty acid contents. The measured forces appear to increase exponentially at all concentrations but does deviate at shorter separations as discussed earlier. Near to contact two different behaviours, as discussed above, are observed. One showing a very short range attraction of < 0.5 nN around a separation of 2 to 5 nm. More dominantly an increase in the repulsion becoming indistinguishable from the compliance region. The decreasing strength and range of the repulsive interactions observed with increasing oleic acid or tallow is more marked than the changes observed with the inclusion of stearic or palimitic acid.

The experimental interactions between the supported DIPEDMAMS bilayers containing increasing ratios of stearic, palmitic, and oleic acid, as well as those containing increasing amounts of the simulated tallow mixture are shown along side the theoretical model EDL interactions for each composition in figure 7.4 and 7.5 on a semi-log scale. Only the EDL model has been used here as the attractive van der Waal's component of the DLVO theory is not observed, as discussed in Chapter 6.

From the semi-log plots it is clear that the observed repulsive interactions are exponential in nature for all bilayer compositions and fatty acid content. As discussed earlier at small separations the repulsive interactions are observed to increase further than an exponential relationship would suggest. This was observed for all compositions but the degree of this increase is observed to decline at higher concentrations of oleic acid or with the tallow mixture. This has been observed for almost all other bilayer-bilayer interactions measured using this technique and has been attributed to additional short range repulsive interactions not accounted for by the DLVO theory such as hydration effects or stearic interactions, or the result of charge regulating interactions between the two bilayers in close proximity. For all

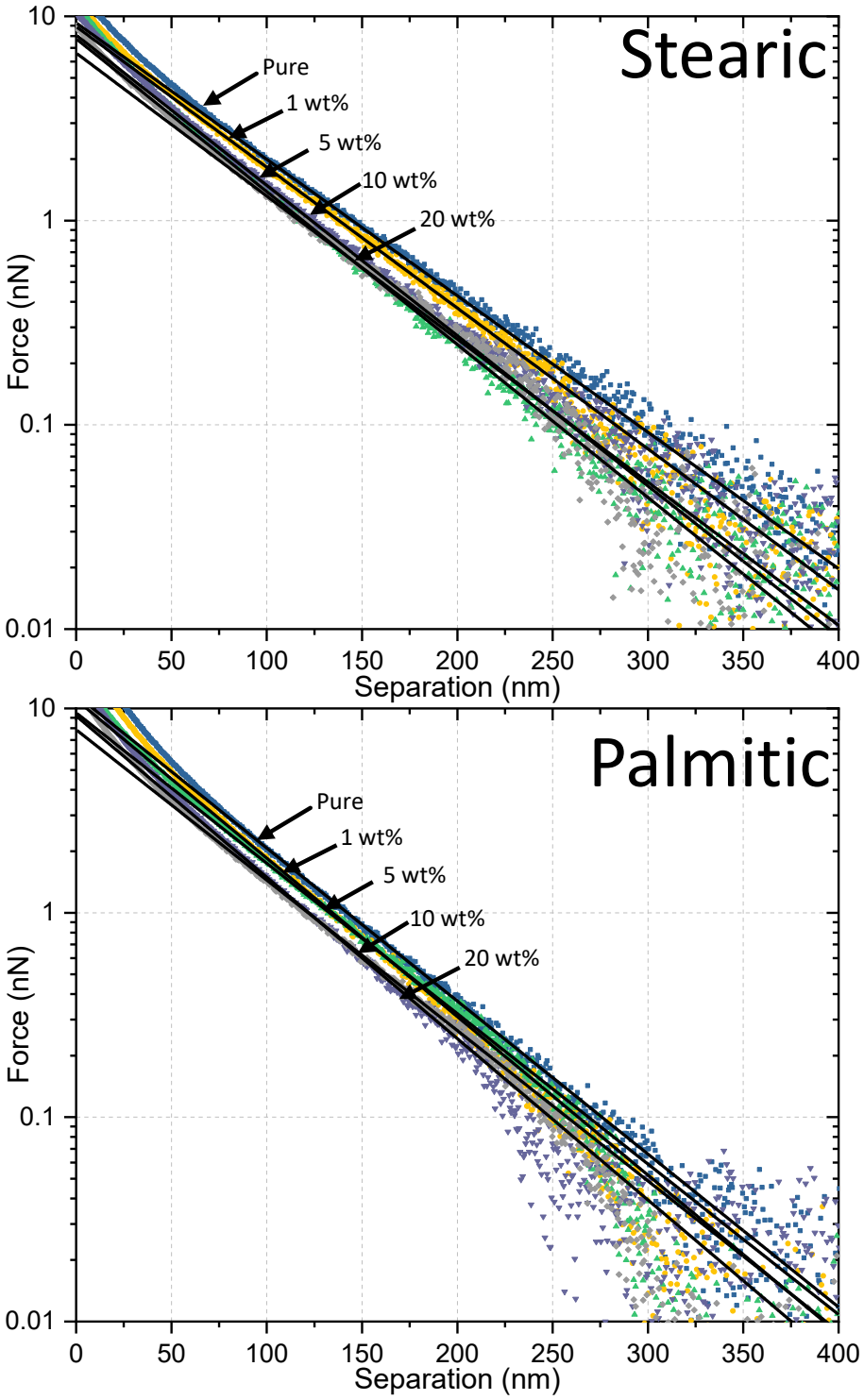


Figure 8.3: Forces measured on approach between DIPEDMAMS bilayers containing increasing concentrations of stearic acid and palmitic acid on a semi-log scale. Solid black lines show the theoretical model EDL interactions interactions for each composition. Fatty acid concentrations and identity are shown in the figure.

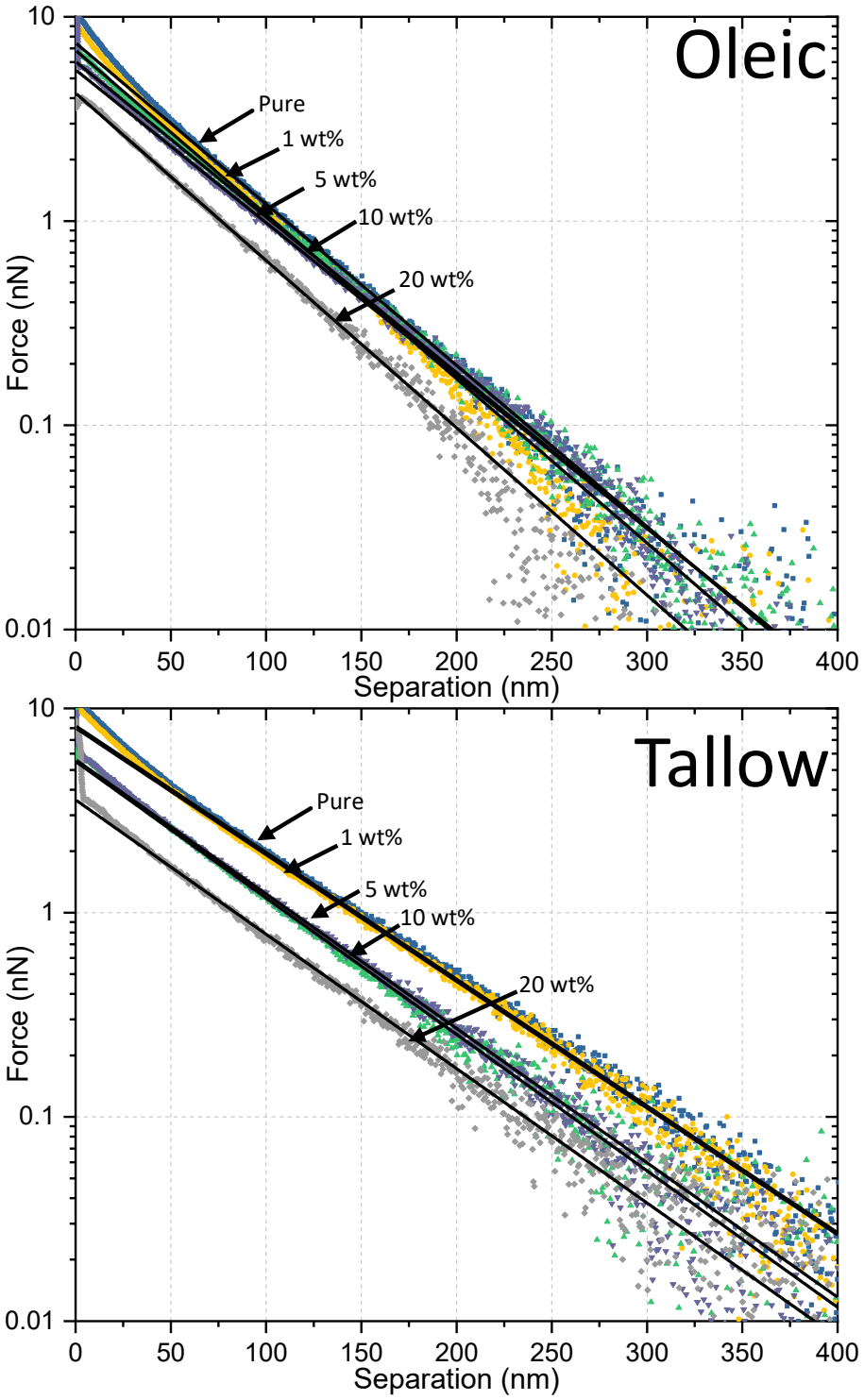


Figure 8.4: Forces measured on approach between DIPEDMAMS bilayers containing increasing concentrations of oleic acid and the tallow mixture on a semi-log scale. Solid black lines show the theoretical model EDL interactions interactions for each composition. Fatty acid concentrations and identity are shown in the figure.

fatty acid contents and identities the model EDL interactions generally fit the data well but data and the model do diverge at shorter separations, as discussed, where the model suggests a lesser repulsive interactions than those measured.

As the concentration of stearic or palmitic acid incorporated into the supported bilayers increases no significant change is observed, although there is some variation, in the absolute gradients of the model interactions for either fatty acid. There does however appear to be a decrease in the intercepts of the model forces as the concentration is increased. This decrease however is small compared to the changes observed with the addition of polymers or electrolytes to the system. There does not appear to be any significant difference between the addition of stearic or palmitic acid.

The increasing oleic acid or tallow mixture content of the supported bilayers as with the stearic and palmitic acids did not appear to have a significant impact on the absolute gradient of the model interactions. Although there were some variation in the absolute gradient no clear trend was apparent. The intercept of the model forces however did show a more significant decrease with increasing oleic acid or tallow content than the observed with the two saturated fatty acids. This decrease in the model intercepts is more more pronounced for the oleic acid samples than with the tallow containing bilayers.

The results of the EDL fitting operation are shown in table 8.1 for all fatty acid bilayer compositions. The table shows the experimental values for the Debye length and experimentally determined values for the surface potential for each composition and molecular weight. As discussed previously there is some variation in the initial experimental surface potentials therefore a column normalising the surface potential at the pure DIPEDMAMS values has been included for ease of comparison.

The experimentally derived Debye lengths appear to show no clear dependency on neither the identity nor the concentration of the fatty acid content of the supported bilayers. However the experimentally determined surface potentials do show a dependency on the fatty acid content in terms of both identity and concentration. Overall the increasing fatty acid content of the bilayers resulted in a decrease in the

Table 8.1: Fitting parameters used in DLVO and EDL fits to the CP-AFM data in figure 7.9 and 7.10

	Debye length/κ^{-1}	Fitted Surface Potential	
[Stearic]/wt%	Fitted/nm	ψ/mV	Normalised ψ
5×10^{-5}	65±2	66±6	1
5×10^{-4}	63±2	63±5	0.95
5×10^{-3}	58±3	55±5	0.83
0.05	59±1	57±2	0.86
0.5	62±2	52±0.5	0.78
[Palmitic]/wt%			
5×10^{-5}	58±2	71±9	1
5×10^{-4}	56±2	67±4	0.94
5×10^{-3}	59±2	63±3	0.88
0.05	55±1	59±2	0.83
0.5	59±1	56±1	0.79
[Oleic]/wt%			
5×10^{-5}	55±3	62±7	1
5×10^{-4}	54±3	59±4	0.95
5×10^{-3}	57±1	47±2	0.76
0.05	58±1	45±2	0.72
0.5	53±1.5	37±0.5	0.60
[Tallow]/wt%			
5×10^{-5}	70±3	64±7	1
5×10^{-4}	70±3	61±4	0.95
5×10^{-3}	65±1	48±2	0.75
0.05	66±1	49±2	0.75
0.5	66±1.5	38±0.5	0.59

measured surface potentials. This decrease appears to be greater for the bilayers containing oleic acid or the tallow mixture than for those containing stearic acid or palmitic acid.

The Debye lengths of the pure DIPEDMAMS bilayers are observed to be between 55 and 70 nm. With no clear trend observed as the concentration is increased for any of the fatty acids. At the highest fatty acid concentrations the Debye lengths were observed between 53 and 66 nm which whilst appear to be a decrease is well within error of the initial experimental Debye lengths and the values are observed to fluctuate as the concentration increases. This degree of variation may make any small tends unresolvable.

The experimental surface potentials from the fitting of the EDL model to the experimental data range from 62 to 70 nN for the pure DIPEDMAMS bilayers. This variation appears to be related to the individual probe used. With the addition of stearic or palmitic acid to the surfactant bilayers a small but steady decline in the measured surface potentials is observed. The addition of oleic acid or tallow to the bilayers resulted in more pronounced decline the in the measured surface potentials. Whilst this decline is fairly well pronounced across the range of concentrations for each fatty acid composition the degree of error between concentration can sometimes be larger than the observed changing. As such it is difficult to comment on the direct dependency of the forces on the bilayer composition.

The lack of any clear trend in the experimental Debye lengths is to be expected. As has been previously discussed the Debye length can be understood as the distance over which a charge can be "felt". Changes to the composition of the surfactant bilayers is not expected to have an impact on the Debye length. The variation in the Debye lengths is put down to impurities within the deionised water used to prepare the vesicle dispersion and the imaging buffer.

Stearic and palmitic acid are observed to to have a similar impact on the experimental surface potentials with increasing fatty acid content. A simple explanation for this observation would be the reduction in the DIPEDMAMS content and hence the number of charged head groups in the bilayers as the fatty acid content increases. However the inclusion of oleic acid to the system had a much greater impact on the surface potentials than the stearic or palmitic acid suggesting that the structure of the added fatty acid plays a role. The obvious difference between oleic acid and stearic or plamitic acid is the unsaturation in the hydrocarbon chain of the oleic acid. The addition of unsaturated fatty acids to lipid or surfactant bilayers have been shown to causes changes in the arrangement or organisation of the bilayers. [278] It is suggested that a rearrangement or reorganisation of the surfactant bilayers due to the addition of oleic acid may be responsible for the observed changes in the measured surface potentials.

Whilst this may explanation the differing impact of oleic acid compared with stearic or palmitic acid the changes observed. The impact of the addition of the

tallow mixture on the measure interactions can not be understood in this manner as it is approximately 50% oleic acid.

However if the addition of fatty acids was causing some form of rearrangement of the bilayers one would expect the impact to be more closely tied to the content. For example 20 mol% having twice the impact on the surface potential then the 10 mol% sample. This may however be the result of the innate variation in the system and as these are relatively small changes and may not be resolvable due to this variation.

8.3.2 AFM Imaging

AFM imaging was used to investigate the impact of increasing fatty acid content on the topographical structure of supported DIPEDMAMS bilayers. This was to gain a more complete understanding of the impact of the bilayers fatty acid content on the system and to try to understand how changes to the structure of the bilayers to impact on the forces measured between the bilayers.

The DIPEDMAMS bilayers were formed using the same vesicle deposition technique as used for the colloidal probe force microscopy. The vesicle dispersions were formed from a homogenous DIPEDMAMS/fatty acid system. Several images of the bilayers were taken for each bilayer composition.

Figure 8.5 shows typical height, adhesion, and measured slope maps of the supported DIPEDMAMS bilayers containing increasing concentrations of stearic acid. At 1 mol% stearic acid the system adopts the two phase configuration where the two phases have different surface properties and nano-mechanics. As no discernable difference was observed between pure DIPEDMAMS bilayers and those containing 1 mol% stearic acid the pure bilayers have not been shown in the figure. As the stearic acid content is increased the thicker phase appears to become dominant, the area covered by the thicker phase appears to increase. Whilst the coverage by the thicker phase appears to increase the number of domains within the thicker phase which adopt the thinner appear to increase but their size decreases. At 20 mol%

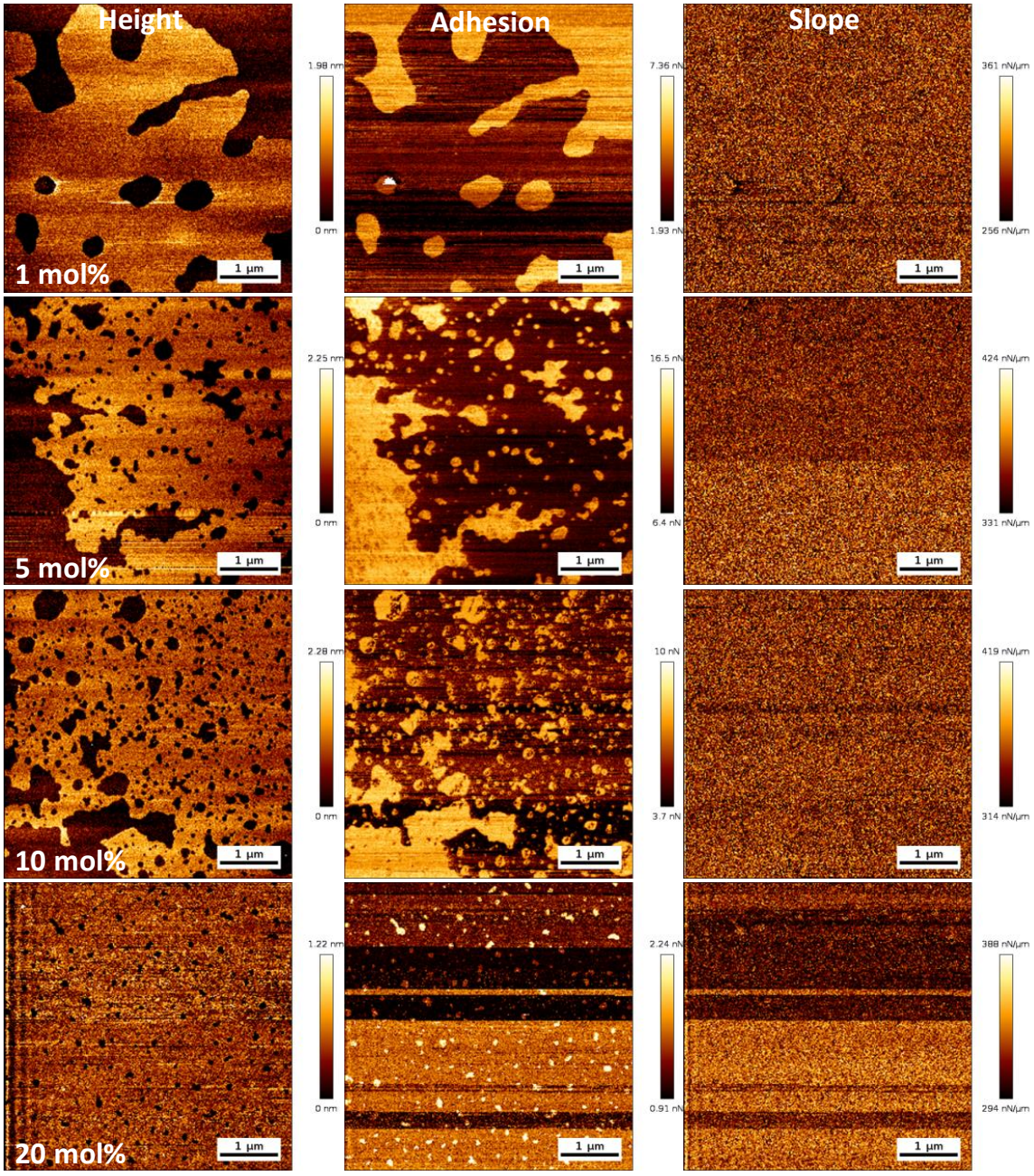


Figure 8.5: Typical QI AFM topographical images, with associated typical maps of surface adhesion and measured slope, for supported DIPEDMAMS bilayers containing increasing concentrations of stearic acid. Concentrations shown in figure.

the bilayer adopts almost solely the thicker phase only exhibiting some small, < 150 nm diameter, regions of the thinner phase. The increasing stearic acid content does not appear to have a significant impact on the tip to sample adhesion of the two different surfactant phases. The measured slope also shows no significant change in the properties of the two areas as the stearic acid content is increased.

The impact of the addition of palmitic acid on the structure of supported DIPEDMAMS bilayers exhibited practically identical behaviour to the addition of stearic acid. At 1 mol% palmitic acid the bilayers exhibited the two phase behaviour that has come to be expected for DIPEDMAMS bilayers. No significant difference was observed between those formed from pure DIPEDMAMS and those containing 1 mol% palmitic acid. As the palmitic acid content increased the area covered by the thicker phase increased until at 20 mol% only the thicker phase was observed. No significant changes in the adhesion or nano-mechanical properties between the two phases were observed with increasing palmitic acid content.

Figure 8.6 shows topographical AFM images, with corresponding cross-sections at 1 and 20 mol% for stearic and palmitic acid. As mentioned at 1 mol% both the palmitic and stearic containing samples show the two phase behaviour. From the cross-section it is observed that the height difference between these two phases is 1 - 1.5 nm as expected. At 20 mol% whilst the two phase behaviour is about observable due to small areas of the thinner bilayer the thicker bilayer phase is dominant. The cross-sections show the height difference between the two phases at this fatty acid content to still be between 1 and 1.5 nm.

Typical AFM images showing the height, adhesion, and measured slope maps of supported DIPEDMAMS bilayers containing increasing concentrations of oleic acid are shown in figure 8.7. No significant differences were observed between the bilayers containing 1 mol% oleic acid and those of pure DIPEDMAMS. These bilayers exhibited the two phase behaviour, as observed earlier, for supported DIPEDMAMS bilayers. The adhesion maps show how that the thicker bilayer phase has a lower tip to sample adhesion than the thinner phase and the the measured slope plots suggest that the thicker phase is relatively more stiff than the the thinner one. As the oleic acid content of the bilayers is increased the area of the bilayers adopting

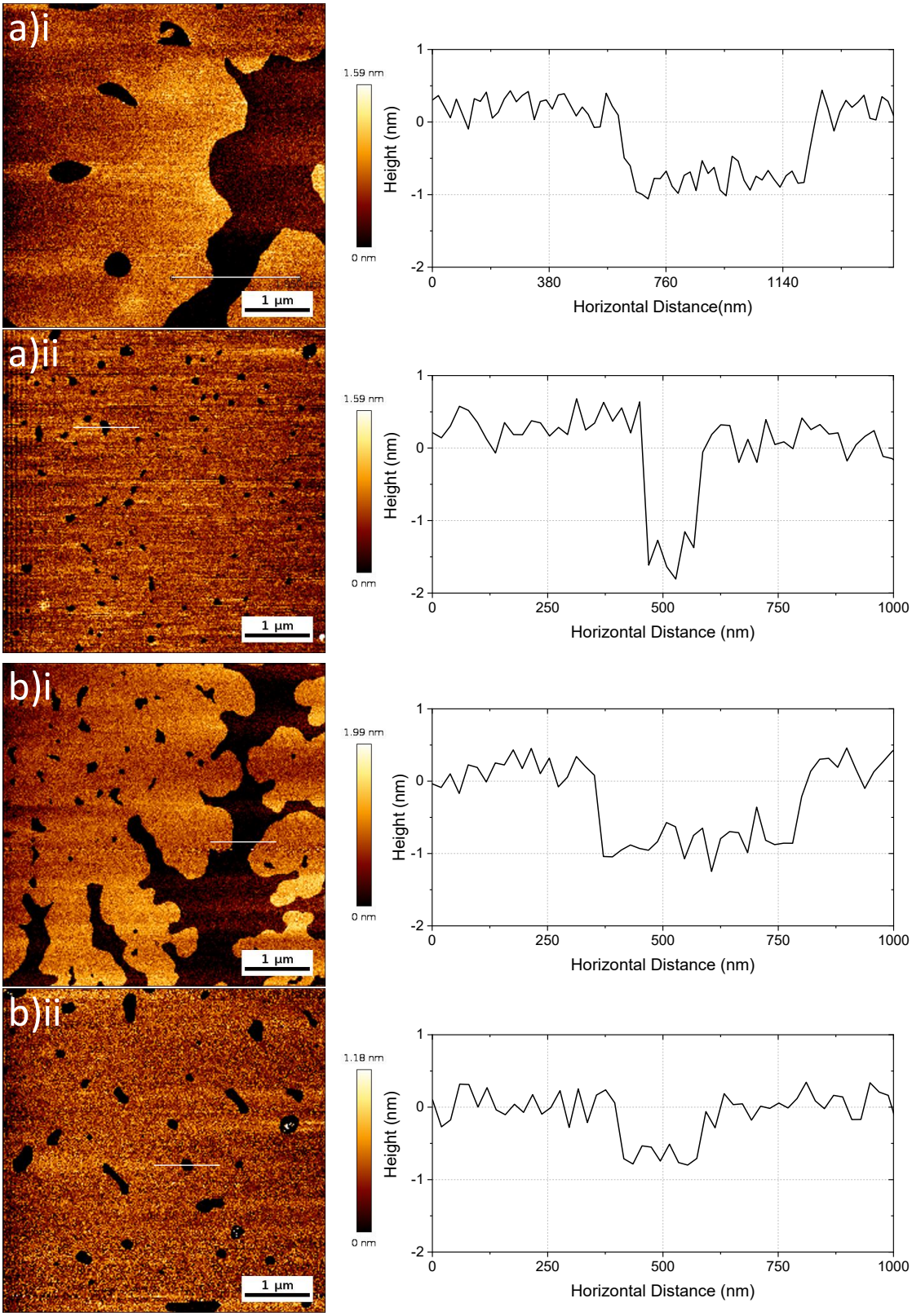


Figure 8.6: AFM images, 5 x 5 μm and associated cross-sections of DIPEDMAMS bilayers containing a)i 1 mol% stearic acid a)ii 20 mol% stearic acid b)i 1 mol% palmitic acid b)ii 20 mol% palmitic acid.

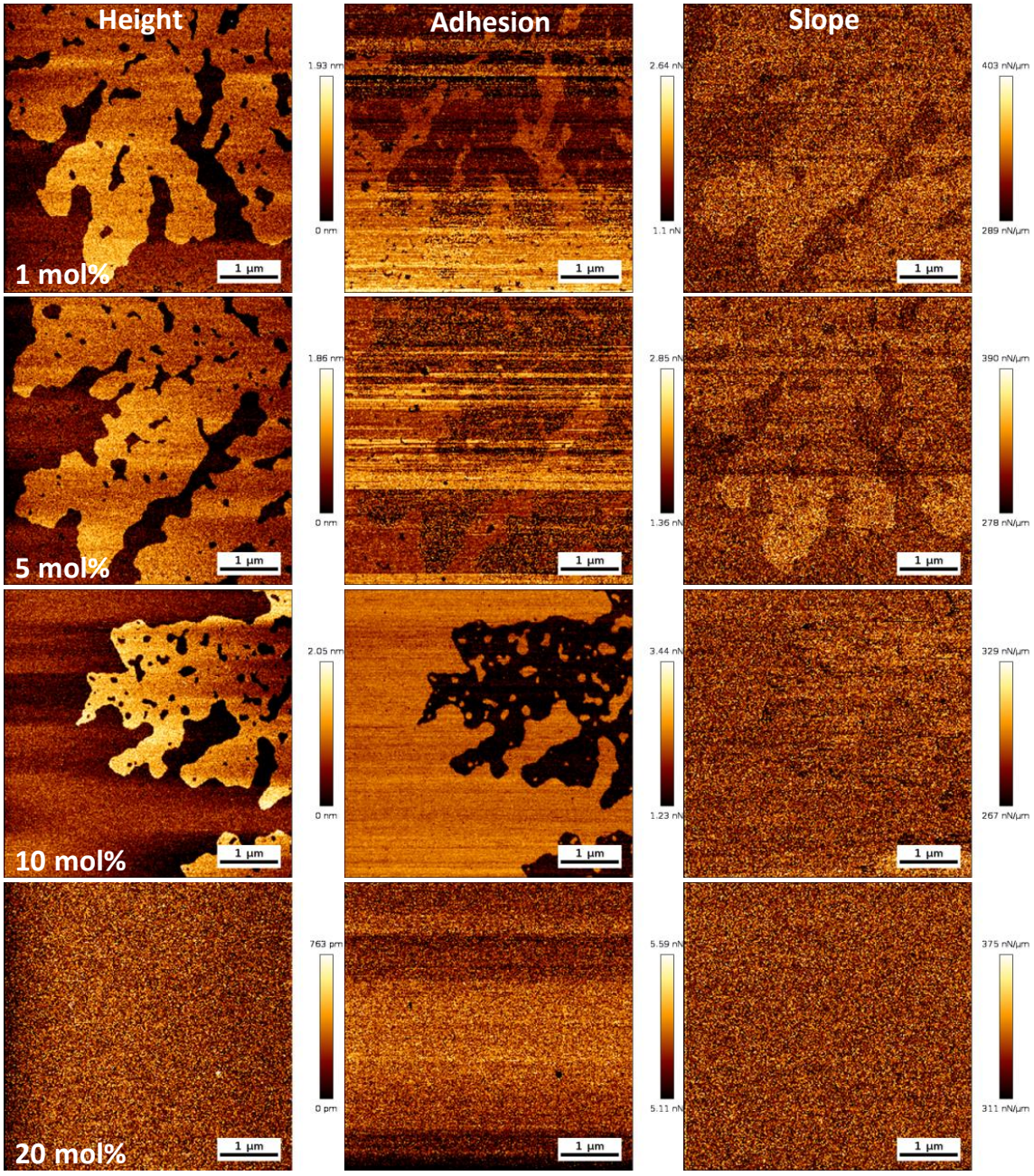


Figure 8.7: Typical QI AFM topographical images, with associated typical maps of surface adhesion and measured slope, for supported DIPEDMAMS bilayers containing increasing concentrations of oleic acid. Concentrations shown in figure.

the thicker bilayer arrangement decreases. At 20 mol% only one continuous bilayer phase is observed, this is suggested to the the thinner phase due to the previously mentioned trend. There does not appear to be any significant impact on the tip to sample adhesion as the oleic acid content is increased however there does appear to be a slight fall in the difference between he relative stiffness of the two phases at 10 mol%.

AFM images showing typical height, adhesion, and measured slope maps of supported DIPEDMAMS bilayers containing increasing concentrations of the fatty acid tallow mixture are shown in figure 8.8. No significant change is observed between the pure DIPEDMAMS bilayers and those containing 1 mol% tallow mixture. These bilayers exhibited the two phase behaviour, as observed earlier, for supported DIPEDMAMS bilayers. The adhesion maps show how that the thicker bilayer phase has a lower tip to sample adhesion than the thinner phase and the the measured slope plots suggest that the thicker phase is relatively more stiff than the the thinner one. As the tallow content of the surfactant bilayers is increased there does not appear to be any significant changes in the ratios between the two bilayer phases. However at 20 mol% gaps in the bilayers are observed penetrating down to the mica substrate. The tip to sample adhesion and the relative stiffness of the two phases does not appear to show any significant change with the increasing tallow content. The images at 20 mol% show the tip to sample adhesion and the measured slope for the areas suspected of being bare mica are significantly higher than the surrounding bilayers.

Stearic and palmitic acid had a similar impact on the supported bilayers to each other. They both result in a change in the arrangement of the supported bilayers away from the two co-existing phases towards the dominance of the thicker bilayer phase. This similarity in impact on the bilayers is not unexpected as stearic and palmitic acid only differer by 2 °C. The addition of long chain fatty acids or alcohols to surfactant or lipid system have been shown increase the packing order of the bilayers and stiffen them. [279, 346] It is suggested that the addition of stearic or palmitic acid to the DIPEDMAMS bilayers results in the conversion of the thinner bilayer phase into the thicker phase. It is not certain if the addition of the fatty acids has a significant impact on the thicker phase or not.

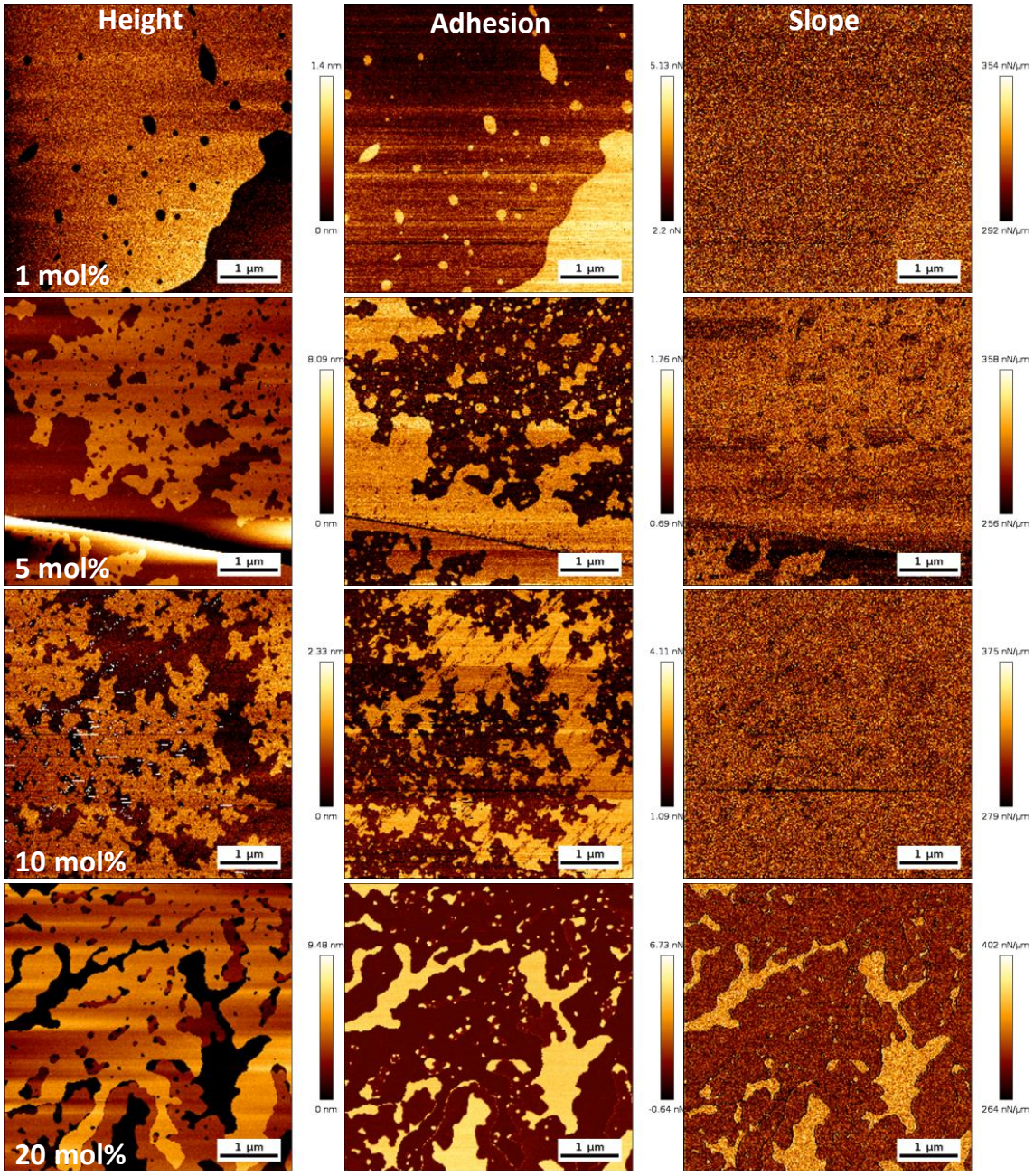


Figure 8.8: Typical QI AFM topographical images, with associated typical maps of surface adhesion and measured slope, for supported DIPEDMAMS bilayers containing increasing concentrations of the tallow fatty acid mixture. Concentrations shown in figure.

Oleic acid has a similar impact on the bilayers in that it results in a change in the arrangement of the supported bilayers away from the two co-existing phases towards the dominance of one one of the bilayer phases. In the case of oleic acid the thinner phase becomes dominant. Stearic and oleic acid have identical alkyl chain lengths but oleic acid contains an unsaturation, an alkene in the 9 position, about halfway along the alkyl chain. Unsaturated alkyl alcohols or fatty acids have been shown to decrease the packing order of surfactant and lipid systems and to fluidise the bilayers. [347–349] It is suggested that the addition of oleic acid to the system results in the conversion of the thicker phase into the thinner one possibly by fluidising and disrupting the local packing of the surfactants in those regions. It is not clear if the oleic acid has a significant impact on the thinner phase.

These observations that the saturated fatty acids cause the conversion of the thinner phase into the the thicker and the unsaturated fatty acids cause the conversion the thicker phase into the thinner phase may suggest a cause of the two phase behaviour. This may suggest that the thinner phase is enriched in surfactants which contain an unsaturated alkyl chain where as the thicker phase is enriched in surfactants which do not have an unsaturated tail. The addition of the saturated fatty acids to the sample causes the stiffening of the thinner phase reducing the impact of the unsaturated tails resulting in the phase converting to the thicker phase, with the inverse holding true for the oleic acid and the thicker phase. It is unlikely that the added fatty acids are concentrated in those regions which have been converted from one phase to another therefore it is suggested that the impact of the addition fatty acid to those regions which are already enriched in surfactants containing those alkyl chains is minimal at these molar ratios. Less closely packed bilayers may be an explanation for the fall in the surface potential as observed in the colloidal probe data.

The addition of the tallow mixture was designed to simulate the break down of the statistical surfactant mixture as opposed to looking at the impact of the individual fatty acids used to produce the surfactant system. It did not appear to cause any significant changes to the ratio of the two bilayer phases observed before the addition of the fatty acids, unlike the addition of the single fatty acids. However it does cause the supported bilayers to become patchy showing incomplete coverage

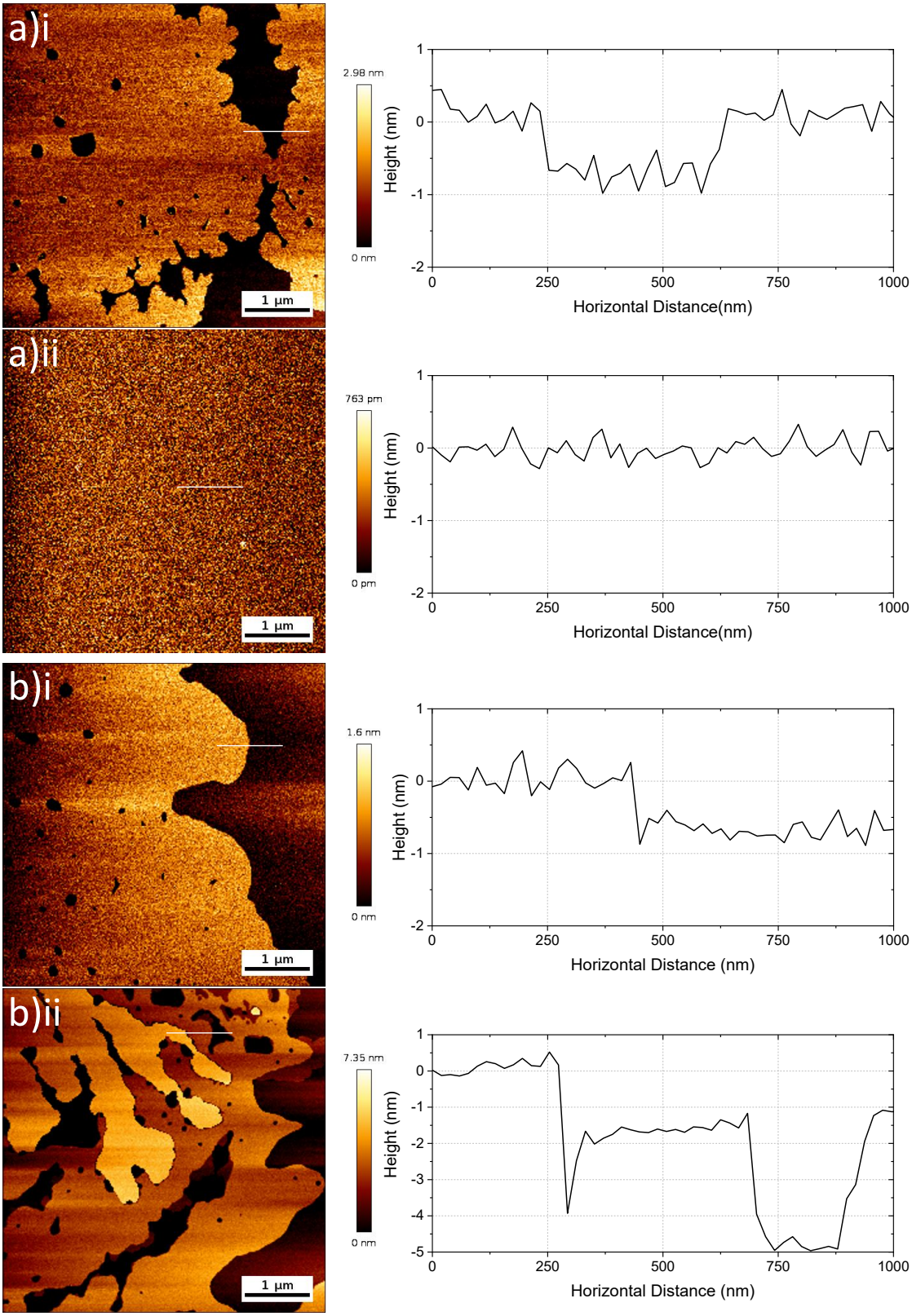


Figure 8.9: AFM images, 5 x 5 μm and associated cross-sections of DIPEDMAMS bilayers containing a)i 1 mol% oleic acid a)ii 20 mol% oleic acid b)i 1 mol% tallow b)ii 20 mol% tallow.

of the mica. It is not certain as to why the addition of the fatty acid mixture would cause holes to form in the bilayers when this was not observed for any of the individual fatty acids. However it does offer an explanation to the decreasing surface potentials observed in the colloidal probe data.

8.3.3 Small and Wide Angle X-ray Scattering

Small angle x-ray scattering was used to investigate the changes to the structure of the bulk lamellar system brought about by the addition of fatty acids to the system. The systems were fabricated by dissolving the required mass of DIPEDMAMS and the fatty acids of interest in chloroform before reprecipitating the mixture to ensure that the fatty acids were evenly dispersed throughout the system. It was hoped that small and wide angle x-ray scattering would aid in the understanding of the changes observed in the supported bilayers as studied by AFM imaging.

Linear intensity plots from the radial integration of the SAXS patterns for DIPEDMAMS/fatty acid/water systems with increasing fatty acid content are shown in figure 8.10. The SAXS patterns for increasing content of stearic, palmitic, and oleic acid, as well as the tallow mixture are shown. The SAXS patterns of pure DIPEDMAMS/water systems, as discussed in Chapter 4, exhibit two series of equally spaced Bragg peaks indicating two co-existing lamellar phases. At low scattering angles it can be problematic differentiating the two peaks due to the overlapping of the peaks. The broadness of the scattering peaks also does not help in differentiating the two series. At higher scattering angles it is easier to resolve the two series.

Stearic and palmitic acid had a similar effect on the SAXS patterns to each other. Up to 20 mol% content of either palmitic or stearic acid two sets of equally spaced Bragg peaks are observed. As the content of these fatty acids increased, the scattering angle of the peaks decreased. Above 20 mol% only one set of equally spaced Bragg peaks are observed. The increasing content of the saturated fatty acids resulted in a change in the intensities of the two sets of Bragg peaks observed in the pure DIPEDMAMS systems. The intensity of the lower scattering angle Bragg

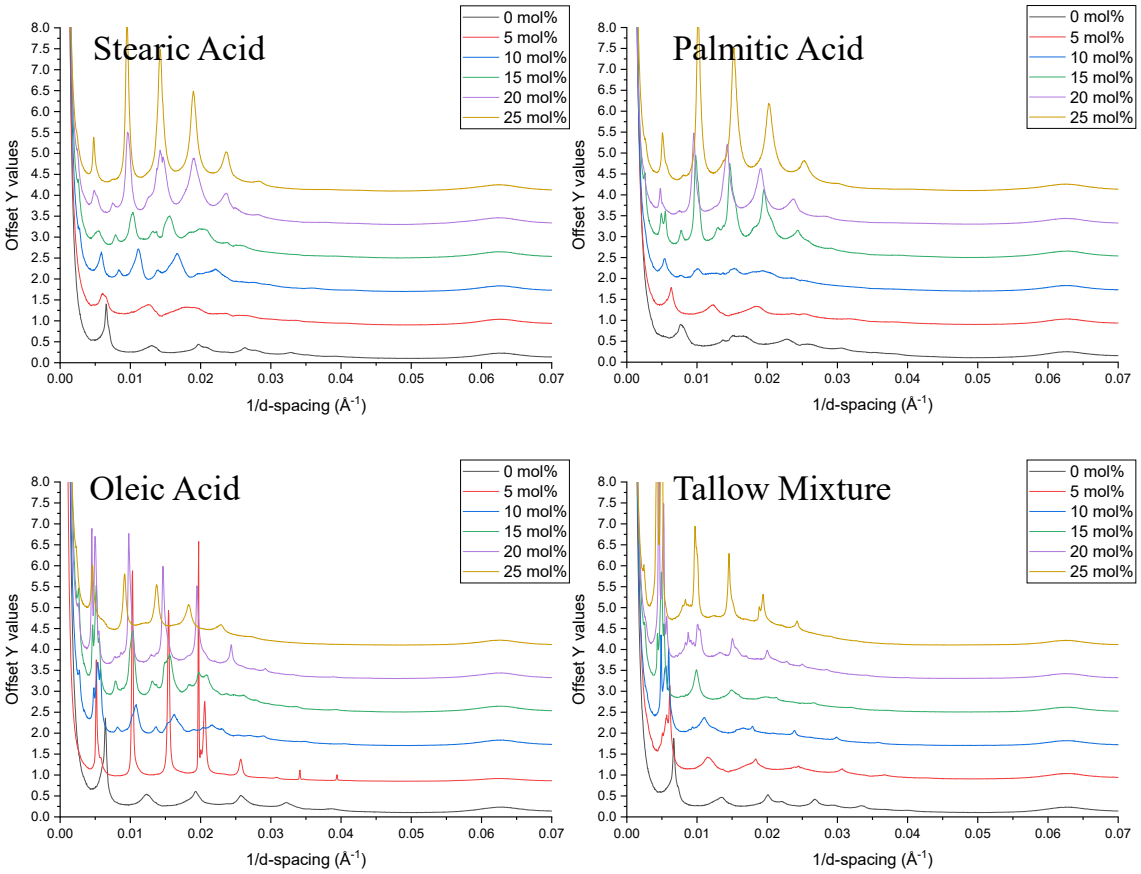


Figure 8.10: Linear intensity plots of the SAXS patterns of DIPEDMAMS/water systems with varying fatty acid content. Fatty acid concentrations and identity are shown in the figure.

peaks appears to increase until at 20 mol% only one set of evenly spaced Bragg peaks are observed.

Increasing the oleic acid content of the surfactant/water system has a similar impact to the stearic or palmitic acid. At low oleic acid content the SAXS patterns show two sets of evenly spaced Bragg peaks. The scattering angle of these peaks appears to decrease as the oleic acid content increases. With the addition of oleic acid at between 5 and 15 mol% there are additional peaks apart from the two sets previously mentioned. As these often appear as shoulders on more prominent peaks it is difficult to assign them. However they do also appear to be of even spacing. At 20 mol% only one set of Bragg peaks can be observed. The intensity of the most dominant set of peaks does appear to increase with increasing oleic acid content.

The addition of the tallow mixture was designed to mimic the breakdown of the statistical surfactant tail composition as opposed to looking at the impact of the individual fatty acids. The SAXS patterns of the initial pure DIPEDMAMS system showed the expected two series of equally spaced Bragg peaks. As the tallow content was increased the peaks for both series were observed to shift and move to a lower angle. The two sets of Bragg peaks are clear up to 10 mol%, above which additional peaks are observed. As with the addition of oleic acid these often appear as shoulders on broader or more intensely scattering peaks making assigning the peaks difficult. At 20 mol% multiple sets of Bragg peaks are observed, as discussed, however the pattern is dominated by two sets of equally spaced Bragg peaks which are still observed. The intensity of both these sets of Bragg peaks appears to increase with increasing tallow content.

Equally spaced Bragg peaks, as previously discussed in Chapter 4, correspond to a lamellar phase. With a series of stacked surfactant bilayers separated by a layer of water. The d-spacing of these lamellar phases, thickness of the bilayer and water layer, is inversely proportional to the separation of the Bragg peaks. The two sets of equally spaced peaks, observed for most of the DIPEDMAMS/fatty acid systems, indicates two co-existing lamellar phases with different d-spacings. This co-existing behaviour has been observed earlier when investigating the impact of temperature on the surfactant system and the effect of halide salts on the bulk lamellar system. The difference between the d-spacing of the two different lamellar phases was between 1 and 2 nm.

The d-spacings for each of the DIPEDMAMS/fatty acid samples are shown in figure 8.11, lines have been included only to help guide the eye. For clarity only the d-spacings for the most intensely scattering Bragg peaks have been shown, however for those systems that did exhibit two co-existing lamellar phases the d-spacing of the other phase was typically 10 to 20 Å smaller with no clear trend in the difference between the two phases observed with increasing fatty acid content.

In general the d-spacings were observed to increase with increasing fatty acid composition for all of the fatty acids investigated. The d-spacing of the pure DIPEDMAMS/water systems was observed to be around 150 ± 5 Å. With the addition of

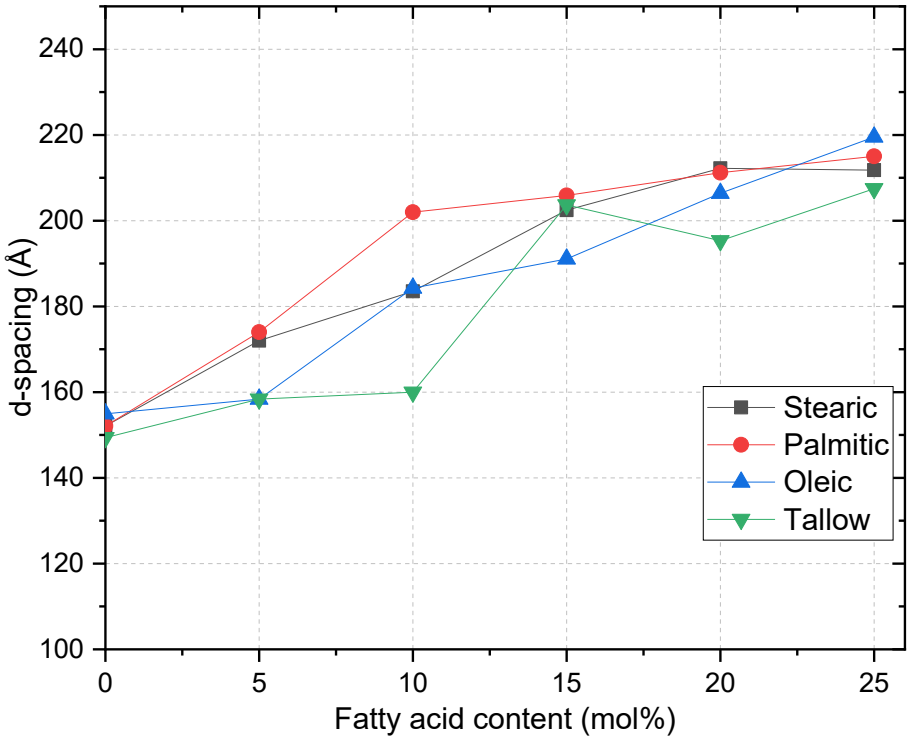


Figure 8.11: Plot of the d-spacing of DIPEDMAMS lamellar phases as a function of increasing fatty acid content.

stearic, palmitic, or oleic acid the the d-spacing increased up to 210 ± 10 Å. No significant jumps in the d-spacing or plateaus were observed as the concentration was increased. Taking into account the variation in the measured d-spacings there did not appear to any significant difference between the three fatty acids. The d-spacings with he tallow mixture however exhibited a slightly different behaviour. A small increase from around 150 to 160 Å was observed as the tallow content was increased to 10 mol%. The d-spacing then increased from 160 to 200 Å at 15 mol% before increasing to 210 ± 10 Å.

The d-spacing is a measure of the length of the repeating unit within the lamellar phase. It is the sum of the bilayer thickness and the thickness of the aqueous layer separating the surfactant bilayers. Therefore changes in the d-spacing can only be the result of changes to the thickness of the bilayer, the aqueous phase, or both. Changes to the water layer would not be observable by AFM imaging of supported bilayers however changes to the bilayer itself may show some correlation.

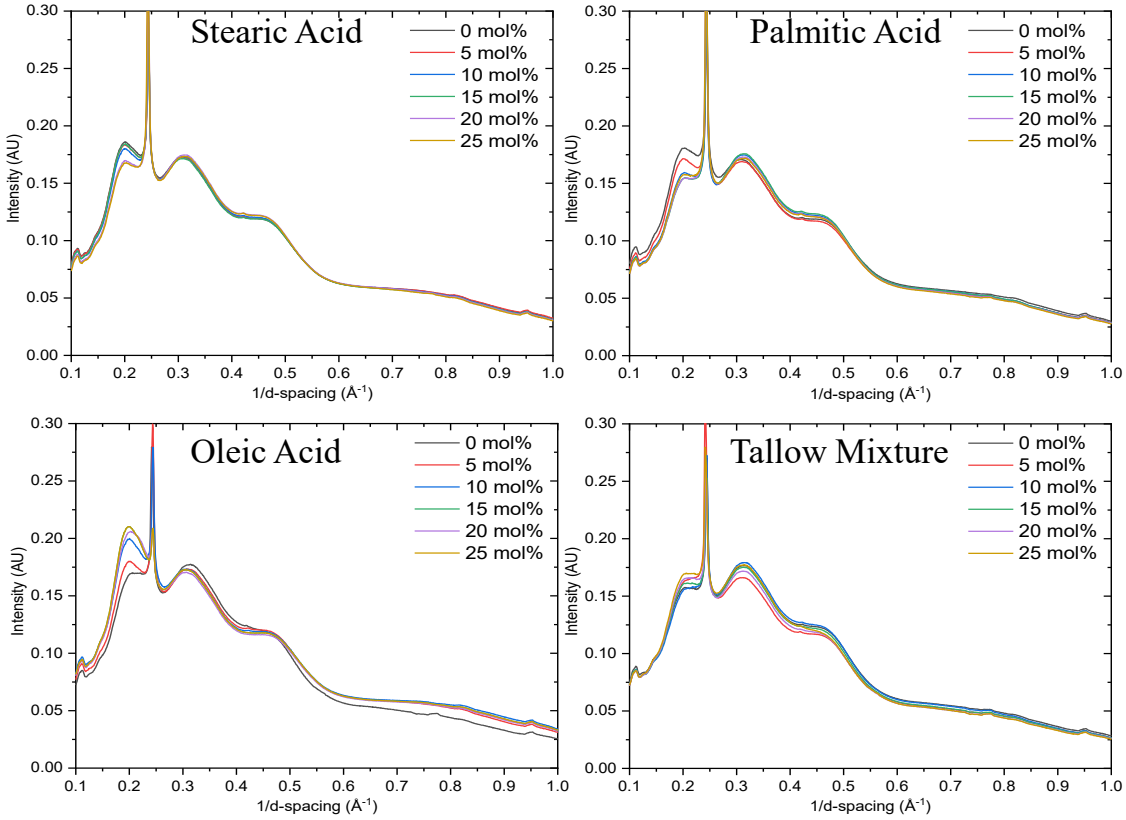


Figure 8.12: Linear intensity plots of the WAXS patterns of DIPEDMAMS/water systems with varying fatty acid content. Fatty acid concentrations and identity are shown in the figure.

The observed increase in the d-spacing with increasing fatty acid content was observed to be independent of the fatty acid identity. As the fatty acid content is increased the DIPEDMAMS water ratio decreases. It is suggested that this change in the surfactant water ratio is the cause of the d-spacing increase as opposed to the impact of the fatty acids on the system.

As discussed in section 3.3 and Chapter 4 WAXS can be used to probe shorter range ordering than SAXS. For surfactant/water systems the WAXS can provide information on the state of the alkyl chains within the lamellar bilayers. Linear intensity plots from the radial integration of the WAXS patterns for DIPEDMAMS/fatty acid/water systems with increasing fatty acid content are shown in figure 8.12. The WAXS patterns for increasing content of stearic, palmitic, and oleic acid, as well as the tallow mixture are shown.

The WAXS patterns for all samples show three main features. A diffuse peak around 0.2 $Å^{-1}$, a sharp peak at 0.24 $Å^{-1}$ and a series of broad diffuse peaks between 0.3 and 0.6 $Å^{-1}$. The peaks at 0.2 and 0.24 $Å^{-1}$ provide information on the alkyl chains within the lamellar bilayers whist the peaks between 0.3 and 0.6 $Å^{-1}$ are due to short range ordering of the water molecules. A broad peak at 0.2 $Å^{-1}$ is indicative of the fluid phase and a sharp peak at 0.24 $Å^{-1}$ is caused by the alkyl chains being in the gel phase. The pure DIPEDMAMS/water systems exhibited a weak diffuse fluid peak at 0.2 $Å^{-1}$ and a sharp intensely scattering gel peak at 0.24 $Å^{-1}$.

Increasing content of stearic or palmitic acid had a similar effect on the WAXS patterns. The intensity of the gel peak was observed to increase and the intensity of the fluid peak was observed to decrease as the fatty acid content was increased. The intensity of the 0.3 and 0.6 $Å^{-1}$ peaks remained relatively unchanged. The addition of oleic acid had the opposite effect from that of the two saturated fatty acids. The gel peak was observed to decrease in intensity with increasing concentration of oleic acid whilst the intensity of the diffuse fluid peak was observed to increase. With the tallow mixture no significant changes in the relative intensities of the gel or fluid peaks was observed although there was some variation in the overall scattering intensity.

The WAXS observation and low fatty acid content could suggest that the two co-existing lamellar phases observed in the SAXS are the result of co-existing lamellar gel and lamellar fluid phases. The addition of stearic and palmitic acid appear to increase the ratio of gel to fluid phases. This is believed to be due to their impact as long saturated alkyl chains inserted into and stiffening the bilayer. The addition of the unsaturated oleic acid having the opposite effect, disrupting the bilayer and resulting in an increase in the amount of fluid phase. The tallow mixture, being a statistical mixture of the fatty acids present in the surfactant tails, does not appear to cause a significant change in the ratio of the two phases.

The two co-existing lamellar phases observed from the SAXS patterns for the pure DIPEDMAMS system and those containing low fatty acid concentrations are suggest to correspond to the two bilayer phases observed in the AFM images of the supported bilayers. The SAXS patterns for the DIPEDMAMS systems containing

increasing concentrations of stearic and palmitic acid showed the disappearance of one of the lamellar phases as the concentration was increased until only one was present at 25 mol%. This compares rather favourably with the observations from the AFM imaging of the supported bilayers which showed an increase in the area covered by one of the surfactant phases until at 20 mol% where the thicker phase is dominant with only small areas of the lower phase observed. From the WAXS it is believed that this is due to an increase in the lamellar gel phase at the expense of the fluid phase.

With the addition of oleic acid to the system the SAXS patterns showed the two co-existing lamellar phases giving way to a single lamellar phase above 20 mol% oleic acid. This again compares well with the observations from the AFM images of the supported DIPEDMAMS bilayers. The images showed an increase in the size of the areas covered by the thinner surfactant phase until only one phase, assumed to be the thinner one, is observed at 20 mol%. It is not possible from the SAXS patterns to comment on which of the two phases are present above 20 mol% but the WAXS suggests that the fluid lamellar phase is now dominant.

The SAXS patterns of the DIPEDMAMS systems with addition of the tallow mixture showed a retention of the two co-existing lamellar phase configuration as the the fatty acid concentration was increased. This is reflected in the AFM images of supported DIPEDMAMS bilayers containing increasing concentration of the tallow mixture. However the formation of holes in the supported bilayers is not reflected in the SAXS data.

8.3.4 Particle sizing and zeta potential of vesicles

The colloidal probe force microscopy data showed how the forces between supported cationic bilayers were effected by the increasing content of fatty acids within the bilayers. The AFM imaging of the supported bilayers and the x-ray scattering of bulk surfactant/water system provided information on how they effected the structure of the bilayers. However it is not clear how these will impact on the stability of bulk vesicle dispersions. To further explore the relationship between the changing

structure of the bilayers, and the interactions between them, the particle size and zeta potential of DIPEDMAMS vesicles with increasing fatty acid content were investigated.

The size and zeta potential of DIPEDMAMS/fatty acid vesicle dispersions with increasing fatty acid content are shown in figure 8.13. The impact of the increasing content of stearic, palmitic, and oleic acid, as well as the tallow mixture are shown. The initial, pure DIPEDMAMS, vesicle size was 84 ± 4 nm. As the fatty acid content was increased from 0 to 15 mol% no significant increase in the vesicle size was observed for any of the fatty acids. For the stearic and palmitic acid containing samples a small increase in the average vesicle size is observed. With the average size increasing from 86 ± 5 nm to 100 nm. A further increase at 25 mol% to < 120 nm is also observed. However due to the associated error with the DLS measurements this observation is not considered to be significant. Increasing the oleic acid and tallow content of the vesicle dispersion to 20 and 15 mol% did not show any significant changes to the mean particle diameter.

The zeta potential for the pure DIPEDMAMS vesicles was observed to be 64 ± 8 mV. As the content of stearic and palmitic acid was increased the zeta potentil was observed to increase to around 75 ± 8 mV for the palmitic and 85 ± 12 mV for stearic as the fatty acid content increased to 10 mol%. The zeta potential was then observed to fall to 48 ± 6 mV as the content was increased to 25 mol%. The zeta potentials for the oleic acid containing vesicle showed a small increase at 5 mol% followed by decrease to 44 ± 6 mV at 15 mol% with no significant further changes in the zeta potential as the concentration was increased further to 25 mol%. The tallow mixture had a similar effect on the zeta potential as stearic and palmitic acid. A small rise in the zeta potential is observed as the fatty acid composition is increased to 10 mol% follow by a decrease in the zeta potential to 47 ± 6 mV at 25 mol%.

Due to the large uncertainty associated with the zeta potential measurements it would be problematic to comment and draw conclusions on the observations of increasing and then declining zeta potential. However the overall trend of decreasing zeta potential as the fatty acid content increases may be real.

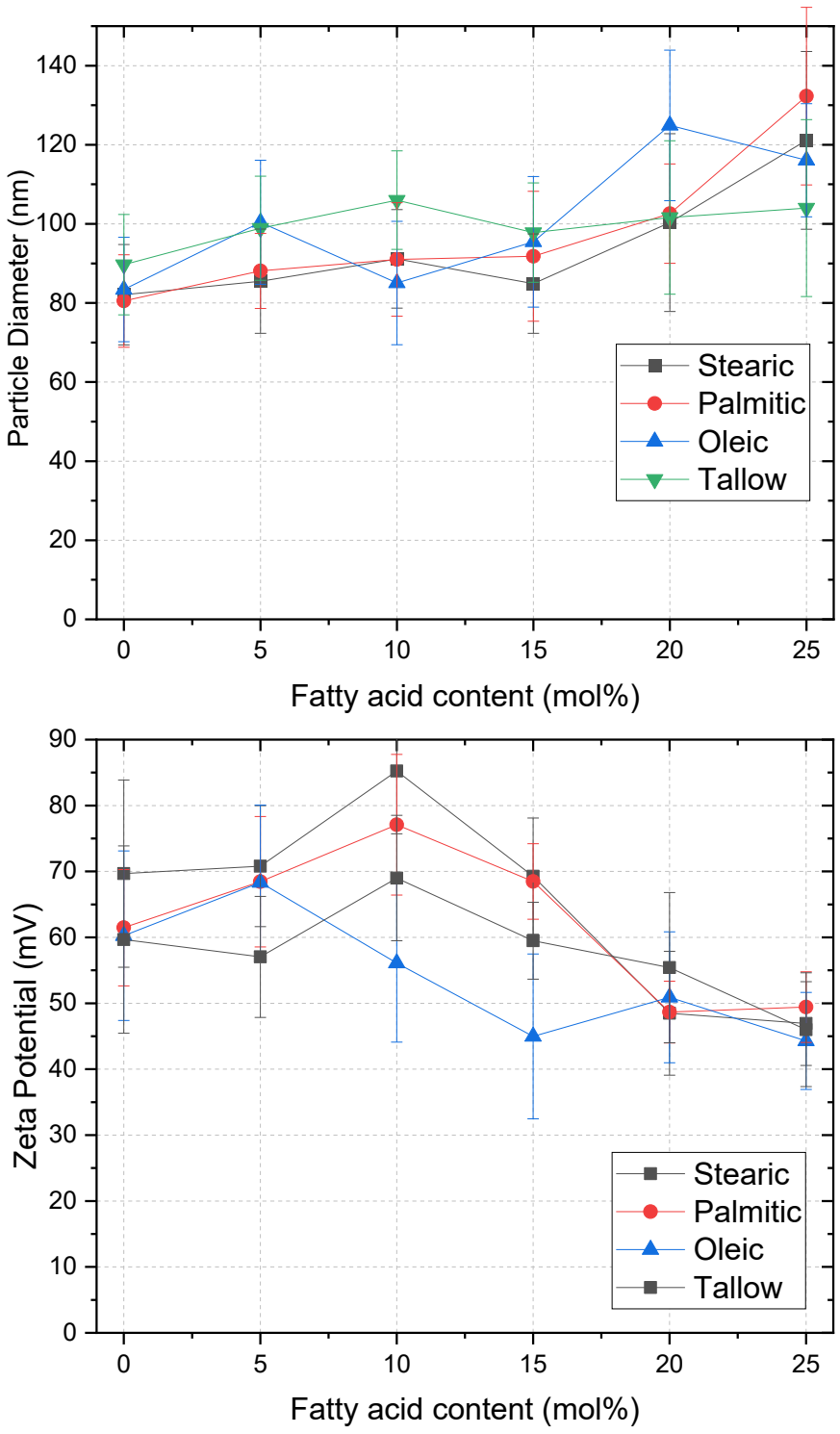


Figure 8.13: Plots of the mean particle diameter and zeta potential of a DIPED-MAMS vesicle dispersion as a function of increasing fatty acid content.

The increase in mean particle size with increasing palmitic and stearic content is believed to be caused by an increase in the mean vesicle size, unlike with the addition of electrolytes or polymers, discussed in Chapters 6 and 7, where a large increase in the mean particle size was attributed to vesicle aggregation. There is a significant difference between these particle sizing experiments and those carried out for the salts and polymers. With the previous experiments it was possible to form the vesicle dispersion and then increase the additive content. Here, as the additives are incorporated into the surfactant bilayers, the vesicles have to be formed from a surfactant dispersion containing the fatty acids. This increase in the mean vesicle size may be result of the added stearic and palmitic acids stiffening the bilayers, reducing the amount of curvature the membrane can achieve, therefore forming larger vesicles. With the increasing content of oleic acid and tallow mixture did not exhibit any significant change in the vesicle diameter as the fatty acid content was increased.

The zeta potential measurements overall showed a slight decrease as the fatty acid concentration was increased to 25 mol%. As discussed it is problematic to comment on the trends observed due to the uncertainty in the measurements. A decrease in the zeta potential could be explained by increased fatty acid content resulting in a decrease in the number of surfactant molecules in the vesicle bilayers. As the fatty acids are uncharged a decrease in the ratio of surfactant to fatty acid in the vesicle bilayers could result in a decreased surface charge density and therefore the zeta potential.

Due to the variation in the system and the small size of the changes observed from the particle sizing and the zeta potential it is problematic to offer any strong suggestion on the impact of the increasing fatty acid content on the vesicle size and zeta potential. Any effect specific to the different fatty acid is also difficult to comment on. However it can be concluded that the fatty acid content, at these concentrations, does not cause the system to destabilise in the manner observed with the addition of salts, polyelectrolytes or polymers.

8.4 Conclusions

Colloidal probe force spectroscopy was used to directly measure the interactions between catioinc surfactant bilayers containing increasing fractions of long chained fatty acids. The impact of increasing content of stearic, palmitic, and oleic acid were investigated as well as the impact of a statistical mixture of the fatty acids which matched the statistical make up of the surfactant tails. The interactions between the bilayers were observed to be exponentially repulsive at all fatty acid concentrations investigated. Increasing the content of palmitic or stearic acid in the bilayers did not have a significant impact on the range nor strength of the repulsive interactions. The addition of oleic acid or the tallow mixture did however result in a decrease in strength the repulsive interaction but the range did not appear to have been significantly effected.

Comparing the measured interactions with the theoretical EDL model the surface potential was shown to decrease slightly with the addition of stearic or palmitic acid whilst the Debye lengths remained, within error, constant. The addition of oleic acid or the tallow mixture resulted in a more significant reduction in the experimental surface potentials but no significant change was observed in the Debye lengths.

Topographical AFM imaging of supported DIPEDMAMS bilayers containing increasing fatty acid concentrations exhibit different behaviour depending on the fatty acid. Stearic and palmitic acid had a similar effect on the bilayer structure. At low fatty acid concentrations the bilayers formed two distinct phases. Increasing the content of stearic or palmitic acid the coverage of the thicker phase increased until it became the dominant phase and the thinner phase was not observed. The addition of oleic acid had the opposite effect. It increased the ratio of the sample that adopted the thinner phase until at 20 mol% only the thinner phase was observed. The two phase behaviour persisted with the addition of the tallow mixture but holes in the bilayers penetrating down to the mica were formed at higher concentrations.

The SAXS experiments of the surfactant/fatty acid/water systems showed the impact increasing fatty acid contents on the surfactant lamellar phases. Pure DIPEDMAMS/water systems were observed to form two co-existing lamellar phases. In-

creasing the content of stearic, palmitic, or oleic acid resulted in the in a single lamellar phase at higher fatty acid concentrations. However with the mixed fatty acids the two phase behaviour was still present at higher concentrations. These observations reflected those observed for the supported bilayers. The wide angle experiments suggested that both the lamellar gel and fluid lamellar phases are present in the pure DIEPDMAMS systems. The addition of stearic or palmitic acid resulted in an increase in the gel signal and a decrease of the fluid signal, whilst the opposite was observed with oleic acid. No significant changes were observed with he tallow mixture. Assuming the thinner supported bilayer phase is in the fluid state and the thicker the gel phase this further supports the observations from the AFM imaging.

The bulk vesicle dispersions did not show any significant instability with the increasing fatty acid content. A small increase in the vesicle size was observed with the addition of stearic or palmitic acid but no significant changes were measured with increasing oleic acid or tallow mixture. A small decrease was observed in the measure zeta potential with increasing fatty acid content. This appeared to be mostly independent of the identity of the fatty acids.

Chapter 9

Conclusions and Outlook

The aim of this work was to understand the stability of vesicle dispersions, fabricated from the cationic surfactant DIPEDMAMS, by directly measuring the interactions between supported surfactant bilayers. The interactions between the supported bilayers was directly measured using the colloidal probe AFM technique. Whilst interactions between surfactant and lipid bilayers had been investigated previously using the surface forces apparatus minimal literature is available using the colloidal probe technique.

The first steps were to understand the aqueous phase behaviour of the surfactant system. This was investigated using SAXS/WAXS, and DSC which, showed that the surfactant system adopted two co-existing lamellar gel phases below the transition temperature and a single fluid lamellar phase above the transition temperature of 40 ± 2 °C. This enabled the development of protocols for the formation of supported surfactant bilayers for use in AFM experiments. Imaging of these supported bilayers by AFM showed that they adopted two distinct bilayer phases which transitioned to a single bilayer phase on heating, the two phases re-emerging on cooling. This supported the idea that supported surfactant bilayers would exhibit similar behaviour to bilayers in a bulk system or a vesicle dispersion, and justified the use of supported bilayers for investigating and understanding the impact of additives on vesicle dispersions.

The direct measurement of the interactions between two supported DIPEDMAMS bilayers required the simultaneous in-situ formation of surfactant bilayers on both the mica substrate and glass colloidal probe. Initial studies demonstrated that complete bilayer formation was only achieved when the surfactant system was in the fluid phase. It was therefore necessary to find a method of decreasing the transition temperature of the surfactant system so that it would be in the fluid phase at room temperature. To this end the impact of different alkyl alcohols on the structure and behaviour of the DIPEDMAMS system was investigated. It was shown that it was possible to change the transition temperature of the surfactant system with the addition of different alkyl alcohols. The impact of their addition on the bulk DIPEDMAMS/water structure and the topographical and nanomechanical properties of the supported bilayers was also investigated. This enabled the control of the transition temperature of the DIPEDMAMS system with minimal impact on the surface interactions and nanomechanical properties of the surfactant bilayers leading to the formation and measurement of the interactions between supported DIPEDMAMS bilayers.

Salts and electrolytes are common additives in industrial vesicle vesicle dispersions such as liquid fabric enhancers, in which they are used to adjust the rheology of the system and modify the commercial properties of the product. Therefore an investigation into the impact of electrolytes on the DIPEDMAMS vesicle system was conducted. The interactions between supported DIPEDMAMS bilayers were shown to be dependent on the identity of the electrolyte and its concentration within the aqueous environment. Whilst the concentration dependency was predicted by the DLVO theory the impact of the salt identity was not. It was observed that larger halide ions had a greater impact on the forces measured between the supported bilayers whilst changing the cation had little effect. This trend was observed not only with the direct measurement of the interactions but by the impact of the the electrolytes on the structure of the supported bilayers, the bulk lamellar phase, and the behaviour of the bulk vesicle dispersions. The impact on the interactions between the supported bilayers was believed to be the combined impact of the electrolytes interacting with the bilayers themselves and by mediating the interactions through the aqueous medium.

Polymers and polyelectrolytes are regularly used in commercial vesicle dispersion and other surfactant systems to adjust the rheological properties of the systems and to control other behaviour such as rate of deposition. Therefore the impact of like charged and uncharged polymers on the interactions between the supported bilayers and the impact of different molecular weights was investigated. Like charged polymers, or polyelectrolytes, were observed to affect the measured interactions in a similar manner to other electrolytes, however an attractive interaction was observed at certain concentrations. This is believed to the depletion interaction and is possibly the first direct measurement of the depletion interaction between two supported surfactant bilayers using the colloidal probe technique. Uncharged polymers had a different impact on the measured interactions believed to be caused by the adhesion of the polymer coils to the surface of the bilayers. This was confirmed by AFM imaging of the bilayers. The impact of the polymers and polyelectrolytes on the behaviour of the bulk DIPEDMAMS vesicle dispersions compared well the measured forces. This offers insight into the mechanisms behind the complex behaviour of polymers and polyelectrolytes within vesicle dispersions and could be developed to create accurate predictions of the stability of such systems.

With the later capability to heat the AFM environment it was possible to form bilayers in-situ on both substrate and probe from vesicle dispersions not in the fluid phase at room temperature. This enabled the study of the role the bilayer composition has on the bilayer-bilayer interactions. Due to the design of the DIPEDMAMS surfactant it is predicted to breakdown over time and in the environment releasing free fatty acids. The impact of increasing fatty acid content of the bilayers to mimic the break down of the surfactant system was investigated. It showed that increasing saturated fatty acids had a minimal impact on the measured interactions but AFM imaging and SAXS of the lamellar system showed a conversion from the two phase behaviour to a single bilayer phase on increasing concentration. Unsaturated fatty acids had a small but not insignificant impact on the directly measured forces compared with the saturated fatty acids but also exhibited a transition from a two phase system to a single lamellar phase at higher concentrations. Increasing the concentration of a statistical mixture of the fatty acids within the bilayers showed a measurable decrease in the strength of the repulsive interactions between the surfactant bilayers. This showed a breakdown in the coverage of the supported bilayers.

These interactions for all fatty acids compared well with the behaviour of the bulk vesicle dispersions. Whilst this simulated ageing did show a measurable impact on the bilayer-bilayer interactions they were relativity minor compared to the impact of additives to the aqueous phase such as salts and polymers. This suggests that whilst the degradation of the surfactant may play a role in the stability of these systems it is not as significant as the role of additives.

Whilst the colloidal probe technique was able to directly measure the interactions between DIPEDMAMS bilayers in changing environment and bilayer compositions and show the trends in the these interactions. It was problematic, especially where the forces remained weakly repulsive, to identify the exact concentration of additive that would lead to the instability of the vesicle dispersion. Further work around these points could develop this technique into a useful and practical analysis tool for predicting the stability of vesicle dispersions.

References

[1] Alan D McNaught and Alan D McNaught. *Compendium of chemical terminology*, volume 1669. Blackwell Science Oxford, 1997.

[2] Robert G. Laughlin. *The Aqueous phase behavior of surfactants*. Achademic Press Limited, London, 1st editio edition, 1994.

[3] Xikui Jiang. Hydrophobic-lipophilic interactions. aggregation and self-coiling of organic molecules. *Accounts of Chemical Research*, 21(10):362–367, 1988.

[4] Michael J Owen. Silicone hydrophobicity and oleophilicity. *Silicon*, 9(5):651–655, 2017.

[5] Ian Hamley. *Introduction to Soft Matter*. John Wiley & sons, Ltd, Chicester, 1 edition, 2000.

[6] Gold Book. Compendium of chemical terminology. *International Union of Pure and Applied Chemistry*, 528, 2014.

[7] Helmut Hauser. Some aspects of the phase behaviour of charged lipids. *Biochimica et Biophysica Acta (BBA)-Biomembranes*, 772(1):37–50, 1984.

[8] Hector L Casal and Henry H Mantsch. Polymorphic phase behaviour of phospholipid membranes studied by infrared spectroscopy. *Biochimica et Biophysica Acta (BBA)-Reviews on Biomembranes*, 779(4):381–401, 1984.

[9] Gerrit Van Meer, Dennis R Voelker, and Gerald W Feigenson. Membrane lipids: where they are and how they behave. *Nature reviews Molecular cell biology*, 9(2):112, 2008.

[10] PR Cullis and B De Kruijff. Polymorphic phase behaviour of lipid mixtures as detected by 31p nmr. evidence that cholesterol may destabilize bilayer structure in membrane systems containing phosphatidylethanolamine. *Biochimica et Biophysica Acta (BBA)-Biomembranes*, 507(2):207–218, 1978.

[11] B Lühmann and H Finkelmann. A lyotropic nematic phase of lamellar micelles (n l) obtained by a non-ionic surfactant in aqueous solution. *Colloid and Polymer Science*, 264(2):189–192, 1986.

[12] Chao Wang, Zhiqiang Wang, and Xi Zhang. Amphiphilic building blocks for self-assembly: from amphiphiles to supra-amphiphiles. *Accounts of chemical research*, 45(4):608–618, 2012.

[13] Jacob N Israelachvili, D John Mitchell, and Barry W Ninham. Theory of self-assembly of hydrocarbon amphiphiles into micelles and bilayers. *Journal of the Chemical Society, Faraday Transactions 2: Molecular and Chemical Physics*, 72:1525–1568, 1976.

[14] Gordon JT Tiddy. Surfactant-water liquid crystal phases. *Physics reports*, 57(1):1–46, 1980.

[15] M Kahlweit, R Strey, P Firman, D Haase, J Jen, and R Schomäcker. General patterns of the phase behavior of mixtures of water, nonpolar solvents, amphiphiles, and electrolytes. 1. *Langmuir*, 4(3):499–511, 1988.

[16] Abraham Marmur. Dissolution and self-assembly: the solvophobic/hydrophobic effect. *Journal of the American Chemical Society*, 122(9):2120–2121, 2000.

[17] Lutz Maibaum, Aaron R Dinner, and David Chandler. Micelle formation and the hydrophobic effect. *The Journal of Physical Chemistry B*, 108(21):6778–6781, 2004.

[18] Pasupati Mukerjee and Karol J Mysels. Critical micelle concentrations of aqueous surfactant systems. Technical report, National Standard reference data system, 1971.

[19] Li-Jen Chen, Shi-Yow Lin, Chiung-Chang Huang, and En-Ming Chen. Temperature dependence of critical micelle concentration of polyoxyethylenated non-ionic surfactants. *Colloids and Surfaces A: Physicochemical and Engineering Aspects*, 135(1-3):175–181, 1998.

[20] A Patist, SS Bhagwat, KW Penfield, P Aikens, and DO Shah. On the measurement of critical micelle concentrations of pure and technical-grade nonionic surfactants. *Journal of Surfactants and Detergents*, 3(1):53–58, 2000.

[21] Ana Domínguez, Aurora Fernandez, Noemi Gonzalez, Emilia Iglesias, and Luis Montenegro. Determination of critical micelle concentration of some surfactants by three techniques. *Journal of chemical education*, 74(10):1227, 1997.

[22] Raoul Zana, M Benrraou, and R Rueff. Alkanediyl-. alpha.,. omega.-bis (dimethylalkylammonium bromide) surfactants. 1. effect of the spacer chain length on the critical micelle concentration and micelle ionization degree. *Langmuir*, 7(6):1072–1075, 1991.

[23] P Somasundaran, Thomas W Healy, and DW Fuerstenau. Surfactant adsorption at the solid—liquid interface—dependence of mechanism on chain length. *The Journal of Physical Chemistry*, 68(12):3562–3566, 1964.

[24] K o z o Shinoda. The effect of chain length, salts and alcohols on the critical micelle concentration. *Bulletin of the Chemical Society of Japan*, 26(2):101–105, 1953.

[25] Pieter R Cullis, Michael J Hope, and Colin PS Tilcock. Lipid polymorphism and the roles of lipids in membranes. *Chemistry and physics of lipids*, 40(2-4):127–144, 1986.

[26] Pierre-Gilles De Gennes and Jacques Prost. *The physics of liquid crystals*, volume 83. Oxford university press, 1993.

[27] Qizhen Liang, Pengtao Liu, Cheng Liu, Xigao Jian, Dingyi Hong, and Yang Li. Synthesis and properties of lyotropic liquid crystalline copolyamides containing phthalazinone moiety and ether linkages. *Polymer*, 46(16):6258–6265, 2005.

[28] K Larsson. Cubic lipid-water phases: structures and biomembrane aspects. *The Journal of Physical Chemistry*, 93(21):7304–7314, 1989.

[29] Per-Olof Eriksson and G Lindblom. Lipid and water diffusion in bicontinuous cubic phases measured by nmr. *Biophysical journal*, 64(1):129–136, 1993.

[30] Gemma C Shearman, Arwen II Tyler, Nicholas J Brooks, Richard H Templer, Oscar Ces, Robert V Law, and John M Seddon. A 3-d hexagonal inverse micellar lyotropic phase. *Journal of the American Chemical Society*, 131(5):1678–1679, 2009.

[31] K Fontell. Cubic phases in surfactant and surfactant-like lipid systems. *Colloïd and polymer science*, 268(3):264–285, 1990.

[32] P Sakya, JM Seddon, RH Templer, RJ Mirkin, and GJT Tiddy. Micellar cubic phases and their structural relationships: The nonionic surfactant system c12eo12/water. *Langmuir*, 13(14):3706–3714, 1997.

[33] Z Lin, JJ Cai, LE Scriven, and HT Davis. Spherical-to-wormlike micelle transition in ctab solutions. *The Journal of Physical Chemistry*, 98(23):5984–5993, 1994.

[34] V Luzzati and F Husson. The structure of the liquid-crystalline phases of lipid-water systems. *The Journal of cell biology*, 12(2):207–219, 1962.

[35] Jacob N. Israelachvili. *Intermolecular and Surface Forces*. Academic Press Limited, Burlington, 3rd edition, 2011.

[36] Gregory L Kirk, Sol M Gruner, and DL Stein. A thermodynamic model of the lamellar to inverse hexagonal phase transition of lipid membrane-water systems. *Biochemistry*, 23(6):1093–1102, 1984.

[37] Michael Rappolt, Andrea Hickel, Frank Bringezu, and Karl Lohner. Mechanism of the lamellar/inverse hexagonal phase transition examined by high resolution x-ray diffraction. *Biophysical journal*, 84(5):3111–3122, 2003.

[38] John M Seddon. An inverse face-centered cubic phase formed by diacylglycerol-phosphatidylcholine mixtures. *Biochemistry*, 29(34):7997–8002, 1990.

[39] Duncan JP Yeardley, Goran Ungar, Virgil Percec, Marian N Holerca, and Gary Johansson. Spherical supramolecular minidendrimers self-organized in an "inverse micellar"-like thermotropic body-centered cubic liquid crystalline phase. *Journal of the American Chemical Society*, 122(8):1684–1689, 2000.

[40] R Lipowsky and E Sackmann. *Structure and Dynamics of Membranes—from Cells to Vesicles (Handbook of Biological Physics vol 1)*. Amsterdam: Elsevier, 1995.

[41] Jesús Sot, Francisco J Aranda, M-Isabel Collado, Félix M Goni, and Alicia Alonso. Different effects of long-and short-chain ceramides on the gel-fluid and lamellar-hexagonal transitions of phospholipids: a calorimetric, nmr, and x-ray diffraction study. *Biophysical journal*, 88(5):3368–3380, 2005.

[42] Raymond E Goldstein and Stanislas Leibler. Model for lamellar phases of interacting lipid membranes. *Physical review letters*, 61(19):2213, 1988.

[43] SC Costigan, PJ Booth, and RH Templer. Estimations of lipid bilayer geometry in fluid lamellar phases. *Biochimica et Biophysica Acta (BBA)-Biomembranes*, 1468(1-2):41–54, 2000.

[44] Derek Marsh. Analysis of the chainlength dependence of lipid phase transition temperatures: main and pretransitions of phosphatidylcholines; main and non-lamellar transitions of phosphatidylethanolamines. *Biochimica et Biophysica Acta (BBA)-Biomembranes*, 1062(1):1–6, 1991.

[45] Ruthven NAH Lewis, David A Mannock, Ronald N McElhaney, David C Turner, and Sol M Gruner. Effect of fatty acyl chain length and structure on the lamellar gel to liquid-crystalline and lamellar to reversed hexagonal phase transitions of aqueous phosphatidylethanolamine dispersions. *Biochemistry*, 28(2):541–548, 1989.

[46] Leif Rilfors, Ali Khan, Ingvar Brentel, Åke Wieslander, and Göran Lindblom. Cubic liquid crystalline phase with phosphatidyl-ethanolamine from bacillus megaterium containing branched acyl chains. *FEBS Letters*, 149(2):293–298, 1982.

[47] Yoji Inoko and Toshio Mitsui. Structural parameters of dipalmitoyl phosphatidylcholine lamellar phases and bilayer phase transitions. *Journal of the Physical Society of Japan*, 44(6):1918–1924, 1978.

[48] Joke A Bouwstra, Gert S Gooris, K Cheng, A Weerheim, Wim Bras, and Maria Ponec. Phase behavior of isolated skin lipids. *Journal of lipid research*, 37(5):999–1011, 1996.

[49] RP Rand and V Luzzati. X-ray diffraction study in water of lipids extracted from human erythrocytes: the position of cholesterol in the lipid lamellae. *Biophysical journal*, 8(1):125–137, 1968.

[50] H Lecuyer and DG Dervichian. Structure of aqueous mixtures of lecithin and cholesterol. *Journal of molecular biology*, 45(1):39–57, 1969.

[51] Ali KHAN, Leif RILFORS, Åke WIESLANDER, and Göran LINDBLOM. The effect of cholesterol on the phase structure of glucolipids from acholeplasma laidlawii membranes. *European journal of biochemistry*, 116(2):215–220, 1981.

[52] Gerald W Feigenson and Jeffrey T Buboltz. Ternary phase diagram of dipalmitoyl-pc/dilauroyl-pc/cholesterol: nanoscopic domain formation driven by cholesterol. *Biophysical journal*, 80(6):2775–2788, 2001.

[53] Daniel Lingwood and Kai Simons. Lipid rafts as a membrane-organizing principle. *science*, 327(5961):46–50, 2010.

[54] Frederick A Heberle and Gerald W Feigenson. Phase separation in lipid membranes. *Cold Spring Harbor perspectives in biology*, 3(4):a004630, 2011.

[55] Edward J Shimshick and Harden M McConnell. Lateral phase separation in phospholipid membranes. *Biochemistry*, 12(12):2351–2360, 1973.

[56] Raghuveer Parthasarathy, Cheng-han Yu, and Jay T Groves. Curvature-modulated phase separation in lipid bilayer membranes. *Langmuir*, 22(11):5095–5099, 2006.

[57] Eric W Kaler, Kathleen L Herrington, A Kamalakara Murthy, and Joseph AN Zasadzinski. Phase behavior and structures of mixtures of anionic and cationic surfactants. *The Journal of Physical Chemistry*, 96(16):6698–6707, 1992.

[58] Michael C Holmes. Intermediate phases of surfactant-water mixtures. *Current opinion in colloid & interface science*, 3(5):485–492, 1998.

[59] SA Safran, PA Pincus, David Andelman, and FC MacKintosh. Stability and phase behavior of mixed surfactant vesicles. *Physical Review A*, 43(2):1071, 1991.

[60] J Oberdisse, C Couve, J Appell, JF Berret, Ch Ligoure, and G Porte. Vesicles and onions from charged surfactant bilayers: a neutron scattering study. *Langmuir*, 12(5):1212–1218, 1996.

[61] BD Simons and ME Cates. Vesicles and onion phases in dilute surfactant solutions. *Journal de Physique II*, 2(7):1439–1451, 1992.

[62] H Hoffmann, C Thunig, P Schmiedel, and U Munkert. Surfactant systems with charged multilamellar vesicles and their rheological properties. *Langmuir*, 10(11):3972–3981, 1994.

[63] Danilo D Lasic. The mechanism of vesicle formation. *Biochemical Journal*, 256(1):1, 1988.

[64] Eric W Kaler, A Kamalakara Murthy, Beatriz E Rodriguez, and JA Zasadzinski. Spontaneous vesicle formation in aqueous mixtures of single-tailed surfactants. *Science*, 245(4924):1371–1374, 1989.

[65] SA Safran, P Pincus, and David Andelman. Theory of spontaneous vesicle formation in surfactant mixtures. *Science*, 248(4953):354–356, 1990.

[66] Harry G Enoch and Philipp Strittmatter. Formation and properties of 1000-a-diameter, single-bilayer phospholipid vesicles. *Proceedings of the National Academy of Sciences*, 76(1):145–149, 1979.

[67] Johannes Zipfel, Peter Lindner, Marina Tsianou, Paschalis Alexandridis, and Walter Richtering. Shear-induced formation of multilamellar vesicles ("onions") in block copolymers. *Langmuir*, 15(8):2599–2602, 1999.

[68] D Mayrand and D Grenier. Biological activities of outer membrane vesicles. *Canadian journal of microbiology*, 35(6):607–613, 1989.

[69] Sriram Vemuri and CT Rhodes. Preparation and characterization of liposomes as therapeutic delivery systems: a review. *Pharmaceutica Acta Helvetiae*, 70(2):95–111, 1995.

[70] Maria Laura Immordino, Franco Dosio, and Luigi Cattel. Stealth liposomes: review of the basic science, rationale, and clinical applications, existing and potential. *International journal of nanomedicine*, 1(3):297, 2006.

[71] D Fennell Evans, Hakan Wennerstrom, and Raj Rajagopalan. The colloidal domain: where physics, chemistry, biology, and technology meet. *Journal of Colloid and Interface Science*, 172(2):541–541, 1995.

[72] DH Everett. Manual of symbols and terminology for physicochemical quantities and units, appendix ii: Definitions, terminology and symbols in colloid and surface chemistry. *Pure and Applied Chemistry*, 31(4):577–638, 1972.

[73] Puthusserickal A Hassan, Suman Rana, and Gunjan Verma. Making sense of brownian motion: colloid characterization by dynamic light scattering. *Langmuir*, 31(1):3–12, 2014.

[74] Evert Johannes Willem Verwey. Theory of the stability of lyophobic colloids. *The Journal of Physical Chemistry*, 51(3):631–636, 1947.

[75] Neer Asherie, Aleksey Lomakin, and George B Benedek. Phase diagram of colloidal solutions. *Physical Review Letters*, 77(23):4832, 1996.

[76] Stanislaw Slomkowski, José V Alemán, Robert G Gilbert, Michael Hess, Kazuyuki Horie, Richard G Jones, Przemyslaw Kubisa, Ingrid Meisel, Werner Mormann, Stanisław Penczek, et al. Terminology of polymers and polymerization processes in dispersed systems (iupac recommendations 2011). *Pure and Applied Chemistry*, 83(12):2229–2259, 2011.

[77] Paul Jenkins and Martin Snowden. Depletion flocculation in colloidal dispersions. *Advances in colloid and interface science*, 68:57–96, 1996.

[78] Igor Ekhiel'evich Dzyaloshinskii, Efrat M Lifshitz, Lev P Pitaevskii, MG Priestley, et al. The general theory of van der waals forces. In *Perspectives in Theoretical Physics*, pages 443–492. Elsevier, 1992.

[79] Edmund S Rittner. Binding energy and dipole moment of alkali halide molecules. *The Journal of Chemical Physics*, 19(8):1030–1035, 1951.

[80] Christopher Kelk Ingold and Edith Hilda Ingold. CLXIX.—The nature of the alternating effect in carbon chains. Part V. A discussion of aromatic substitution with special reference to the respective roles of polar and non-polar dissociation; and a further study of the relative directive efficiencies of o. *J. Chem. Soc.*, 129(1310):1310–1328, 1926.

[81] Linus Pauling. The nature of the chemical bond. iv. the energy of single bonds and the relative electronegativity of atoms. *Journal of the American Chemical Society*, 54(9):3570–3582, 1932.

[82] William B Jensen. Electronegativity from avogadro to pauling: part 1: origins of the electronegativity concept. *Journal of chemical education*, 73(1):11, 1996.

[83] Frank J Lovas. Microwave spectral tables ii. triatomic molecules. *Journal of Physical and Chemical Reference Data*, 7(4):1445–1750, 1978.

[84] H Margenau. Van der waals forces. *Reviews of Modern Physics*, 11(1):1, 1939.

[85] RP Bell. The calculation of dipole interaction. *Transactions of the Faraday Society*, 31:1557–1560, 1935.

[86] GS Rushbrooke. On the statistical mechanics of assemblies whose energy-levels depend on the temperature. *Transactions of the Faraday Society*, 36:1055–1062, 1940.

[87] WH Keesom. The second viral coefficient for rigid spherical molecules, whose mutual attraction is equivalent to that of a quadruplet placed at their centre. *Proc. R. Acad. Sci*, 18:636–646, 1915.

[88] KG Denbigh. The polarisabilities of bonds—i. *Transactions of the Faraday Society*, 36:936–948, 1940.

[89] JO Hirschfelder. Curtiss ch. *F., Bird RB: Molecular theory of gases and liquids. J*, 1954.

[90] Young Kee Kang and Mu Shik Jhon. Additivity of atomic static polarizabilities and dispersion coefficients. *Theoretica chimica acta*, 61(1):41–48, Jan 1982.

[91] John C Slater and John G Kirkwood. The van der waals forces in gases. *Physical Review*, 37(6):682, 1931.

[92] Fritz London. The general theory of molecular forces. *Transactions of the Faraday Society*, 33:8b–26, 1937.

[93] Hendrik BG Casimir and Dirk Polder. The influence of retardation on the london-van der waals forces. *Physical Review*, 73(4):360, 1948.

[94] Joseph E Mayer. Dispersion and polarizability and the van der waals potential in the alkali halides. *The Journal of Chemical Physics*, 1(4):270–279, 1933.

[95] Roberto Cambi, David Cappelletti, Giorgio Liuti, and Fernando Pirani. Generalized correlations in terms of polarizability for van der waals interaction potential parameter calculations. *The Journal of chemical physics*, 95(3):1852–1861, 1991.

[96] AD McLachlan. Retarded dispersion forces between molecules. *Proceedings of the Royal Society of London. Series A. Mathematical and Physical Sciences*, 271(1346):387–401, 1963.

[97] Hugo C Hamaker. The london—van der waals attraction between spherical particles. *physica*, 4(10):1058–1072, 1937.

[98] NG Van Kampen, BRA Nijboer, and K Schram. On the macroscopic theory of van der waals forces. *Physics letters A*, 26(7):307–308, 1968.

[99] J Visser. On hamaker constants: A comparison between hamaker constants and lifshitz-van der waals constants. *Advances in colloid and interface science*, 3(4):331–363, 1972.

[100] AD McLachlan. Van der waals forces between an atom and a surface. *Molecular Physics*, 7(4):381–388, 1964.

[101] LD Landau and EM Lifshitz. Sov. phys. *Jetp*, 3:920, 1956.

[102] AD McLachlan. Effect of the medium on dispersion forces in liquids. *Discussions of the Faraday Society*, 40:239–245, 1965.

[103] David C Grahame. The electrical double layer and the theory of electrocapillarity. *Chemical reviews*, 41(3):441–501, 1947.

[104] H von Helmholtz. Ueber einige gesetze der vertheilung elektrischer ströme in körperlichen leitern, mit anwendung auf die thierisch-elektrischen versuche (schluss.). *Annalen der Physik*, 165(7):353–377, 1853.

[105] M Gouy. Sur la constitution de la charge électrique à la surface d'un électrolyte. *J. Phys. Theor. Appl.*, 9(1):457–468, 1910.

[106] GH Bolt. Analysis of the validity of the gouy-chapman theory of the electric double layer. *Journal of Colloid Science*, 10(2):206–218, 1955.

[107] Adolph Stern. On the counter-transference in psychoanalysis. *Psychoanalytic Review*, 11(2):166–174, 1924.

[108] P Debye. Introductory paper—part i: Mobilities of ions. report on conductivity of strong electrolytes in dilute solutions. *Transactions of the Faraday Society*, 23:334–340, 1927.

[109] Mika M Kohonen, Marilyn E Karaman, and Richard M Pashley. Debye length in multivalent electrolyte solutions. *Langmuir*, 16(13):5749–5753, 2000.

[110] Kenneth S Pitzer. Electrolyte theory-improvements since debye and hückel. *Accounts of Chemical Research*, 10(10):371–377, 1977.

[111] Peter Debye and Erich Hückel. Zur theorie der elektrolyte. ii. *Phys. Zft*, 24:305–325, 1923.

[112] Petrus Josephus Wilhelmus Debye. *Osmotische Zustandsgleichung und Aktivität verdünnter starker Elektrolyte*. Hirzel, 1924.

[113] Boris V Derjaguin. Acta physicochim. *USSR*, 14, 1941.

[114] Evert Johannes Willem Verwey, Jan Theodoor Gerard Overbeek, and K Van Nes. *Theory of the stability of lyophobic colloids: the interaction of sol particles having an electric double layer*. Elsevier Publishing Company, 1948.

[115] Robert L Scott and Peter H van Konynenburg. Static properties of solutions. van der waals and related models for hydrocarbon mixtures. *Discussions of the Faraday society*, 49:87–97, 1970.

[116] JH Schenkel and JA Kitchener. A test of the derjaguin-verwey-overbeek theory with a colloidal suspension. *Transactions of the Faraday Society*, 56:161–173, 1960.

[117] Barry W Ninham. On progress in forces since the dlvo theory. *Advances in colloid and interface science*, 83(1-3):1–17, 1999.

[118] Hugo K Christenson. Non-dlvo forces between surfaces-solvation, hydration and capillary effects. *JOURNAL OF DISPERSION SCIENCE ANDTECHNOLOGY*, 9(2):171–206, 1988.

[119] Maurice L Huggins and Joseph E Mayer. Interatomic distances in crystals of the alkali halides. *The Journal of Chemical Physics*, 1(9):643–646, 1933.

[120] FG Fumi and MP Tosi. Ionic sizes and born repulsive parameters in the nacl-type alkali halides—i: the huggins-mayer and pauling forms. *Journal of Physics and Chemistry of Solids*, 25(1):31–43, 1964.

[121] Johan van Dranen. Born repulsion and restricted free rotation. *The Journal of Chemical Physics*, 20(12):1982–1983, 1952.

[122] Felix Franks. The hydrophobic interaction. In *Water a comprehensive treatise*, pages 1–94. Springer, 1975.

[123] Robert L Baldwin. Temperature dependence of the hydrophobic interaction in protein folding. *Proceedings of the National Academy of Sciences*, 83(21):8069–8072, 1986.

[124] S Levine and GP Dube. Interaction between two hydrophobic colloidal particles, using the approximate debye-hückel theory. i. general properties. *Transactions of the Faraday Society*, 35:1125–1140, 1939.

[125] BV Derjaguin. Interaction forces between hydrophobic and hydrophilic self-assembled monolayers. *Kolloid Zeits*, 69:155–164, 1934.

[126] Y Mao, ME Cates, and HNW Lekkerkerker. Depletion force in colloidal systems. *Physica A Statistical Mechanics and its Applications*, 222(1-4):10–24, 1995.

[127] Sho Asakura and Fumio Oosawa. On interaction between two bodies immersed in a solution of macromolecules. *The Journal of Chemical Physics*, 22(7):1255–1256, 1954.

[128] Sho Asakura and Fumio Oosawa. Interaction between particles suspended in solutions of macromolecules. *Journal of polymer science*, 33(126):183–192, 1958.

[129] R Tuinier, HNW Lekkerkerker, and DGAL Aarts. Interaction potential between two spheres mediated by excluded volume polymers. *Physical Review E*, 65(6):060801, 2002.

[130] J.Th.G Overbeek and M.J Sparnaay. Experiments on long-range attractive forces between macroscopic objects. *Journal of Colloid Science*, 7(3):343–345, jun 1952.

[131] B. V. Derjaguin, I. I. Abrikosova, and E. M. Lifshitz. Direct measurement of molecular attraction between solids separated by a narrow gap. *Quarterly Reviews, Chemical Society*, 10(3):295, 1956.

[132] P. M. Claesson, T. Ederth, V. Bergeron, and M. W. Rutland. Techniques for measuring surface forces. *Advances in Colloid and Interface Science*, 67(1996):119–183, 1996.

[133] R. G. Horn, D. R. Clarke, and M. T. Clarkson. Direct measurement of surface forces between sapphire crystals in aqueous solutions. *Journal of Materials Research*, 3(3):413–416, jun 1988.

[134] Roger G Horn and Douglas T Smith. Contact Electrification and Adhesion Between Dissimilar Materials. *Science*, 256(5055):362–364, apr 1992.

[135] R. G. Horn, D. T. Smith, and W Haller. Surface forces and viscosity of water measured between silica sheets. *Chemical Physics Letters*, 162(4-5):404–408, oct 1989.

[136] Gene Vigil, Zhenghe Xu, Suzi Steinberg, and Jacob Israelachvile. Interactions of silica surfaces. *Journal of Colloid And Interface Science*, 165(2):367–385, jul 1994.

[137] J. Israelachvili, Y. Min, M. Akbulut, A. Alig, G. Carver, W. Greene, K. Kristiansen, E. Meyer, N. Pesika, K. Rosenberg, and H. Zeng. Recent advances in the surface forces apparatus (SFA) technique. *Reports on Progress in Physics*, 73(3), 2010.

[138] S. Tolansky. The intensity efficiency of the fabry-repot interferometer. Both in transmission and reflection. *Physica*, 12(9-10):649–655, dec 1946.

[139] S Tolansky. Applications of Multiple-Beam Interferometry. *Nature*, (167):815–816, 1951.

[140] A.M. Stewart. Measuring the Radii of Curvature of the Surfaces in a Surface Force Apparatus. *Journal of Colloid and Interface Science*, 170(1):287–289, mar 1995.

[141] M. Heuberger, G. Luengo, and J. Israelachvili. Topographic information from multiple beam interferometry in the surface forces apparatus. *Langmuir*, 13(14):3839–3848, 1997.

[142] D. Tabor and R. H S Winterton. The Direct Measurement of Normal and Retarded van der Waals Forces. *Proceedings of the Royal Society A: Mathematical, Physical and Engineering Sciences*, 312(1511):435–450, sep 1969.

[143] J. N. Israelachvili and D. Tabor. The Measurement of Van Der Waals Dispersion Forces in the Range 1.5 to 130 nm. *Proceedings of the Royal Society A: Mathematical, Physical and Engineering Sciences*, 331(1584):19–38, 1972.

[144] Jacob N. Israelachvili. Direct measurement of long range forces between two mica surfaces in aqueous KNO3 solutions. *Nature*, 262(1967):349–351, 1976.

[145] Jacob Israelachvili. Direct measurements of forces between surfaces in liquids at the molecular level. *Proceedings of the Natural Academy of Science*, 84:4722–4724, aug 1987.

[146] Jacob N. Israelachvili and Patricia M. McGuiggan. Adhesion and short-range forces between surfaces. part i: New apparatus for surface force measurements. *Journal of Materials Research*, 5(10):2223–2231, 1990.

[147] Vincent S.J. Craig. An historical review of surface force measurement techniques. *Colloids and Surfaces A: Physicochemical and Engineering Aspects*, 129-130:75–93, 1997.

[148] Jacob N. Israelachvili and Gayle E. Adams. Measurement of forces between two mica surfaces in aqueous electrolyte solutions in the range 0-100 nm. *Journal of the Chemical Society, Faraday Transactions 1: Physical Chemistry in Condensed Phases*, 74:975–1001, 1977.

[149] R. M. Pashley. DLVO and hydration forces between mica surfaces in Li+, Na+, K+, and Cs+ electrolyte solutions: A correlation of double-layer and hydration forces with surface cation exchange properties. *Journal of Colloid And Interface Science*, 83(2):531–546, 1981.

[150] R. M. Pashley and J. N. Israelachvili. Dlvo and hydration forces between mica surfaces in Mg2+, Ca2+, Sr2+, and Ba2+ chloride solutions. *Journal of Colloid And Interface Science*, 97(2):446–455, 1983.

[151] R.M. Pashley and J.P. Quirk. The effect of cation valency on DLVO and hydration forces between macroscopic sheets of muscovite mica in relation to clay swelling. *Colloids and Surfaces*, 9(1):1–17, mar 1984.

[152] R.M. Pashley. Hydration forces between mica surfaces in electrolyte solutions. *Advances in Colloid and Interface Science*, 16(1):57–62, jul 1982.

[153] R.M Pashley. Hydration forces between mica surfaces in aqueous electrolyte solutions. *Journal of Colloid and Interface Science*, 80(1):153–162, mar 1981.

[154] Richard M. Pashley and Jacob N. Israelachvili. Molecular layering of water in thin films between mica surfaces and its relation to hydration forces. *Journal of Colloid and Interface Science*, 101(2):511–523, oct 1984.

[155] Roger G. Horn and Jacob N. Israelachvili. Direct measurement of structural forces between two surfaces in a nonpolar liquid. *The Journal of Chemical Physics*, 75(3):1400–1411, 1981.

[156] Hugo K. Christenson. Experimental measurements of solvation forces in nonpolar liquids. *The Journal of Chemical Physics*, 78(11):6906–6913, 1983.

[157] Jacob N. Israelachvili, Stephen J. Kott, Michelle L. Gee, and Thomas A. Witten. Forces between Mica Surfaces across Hydrocarbon Liquids: Effects of Branching and Polydispersity. *Macromolecules*, 22(11):4247–4253, 1989.

[158] Sanjay Patel. Measurement of Forces between surfaces in polymer fluids. *Annual Review of Physical Chemistry*, 40:597–635, 1989.

[159] J. N. Israelachvili, R. K. Tandon, and L. R. White. Measurement of forces between two mica surfaces in aqueous polyethylene oxide solution. *Journal of Colloid And Interface Science*, 78(2):430–443, 1980.

[160] Ya'acov Almog and Jacob Klein. Interactions between mica surfaces in a polystyrene-cyclopentane solution near the θ-temperature. *Journal of Colloid And Interface Science*, 106(1):33–44, 1985.

[161] J. N. Israelachvili, R. K. Tandon, and L. R. White. Measurement of forces between two mica surfaces in aqueous poly(ethylene oxide) solutions. *Nature*, 277(11):120–121, 1979.

[162] JN Israelachvili. Measurements of hydration forces between macroscopic surfaces. *Chemica Scripta*, 25(1):7–14, 1985.

[163] Jacob Klein and P F Luckham. Long-range attractive forces between two mica surfaces in an aqueous polymer solution. *Nature*, 308(26):836–837, 1984.

[164] L. R. Dix, C. Toprakcioglu, and R. J. Davies. Surface force measurements for poly-l-lysine: Effect of ionic strength. *Colloids and Surfaces*, 31(C):147–149, 1988.

[165] Johan Marra and Michael L. Hair. Forces between two poly(2-vinylpyridine)-covered surfaces as a function of ionic strength and polymer charge. *Journal of Physical Chemistry*, 92(21):6044–6051, 1988.

[166] Johan Marra and Michael L. Hair. Double-layer forces in nonadsorbing ionic micellar solutions and polyelectrolyte solutions. *Journal of Colloid And Interface Science*, 128(2):511–522, 1989.

[167] Jacob Israelachvili and Richard Pashley. The hydrophobic interaction is long range, decaying exponentially with distance. *Nature*, 300(5890):341–342, 1982.

[168] J. N. Israelachvili and R. M. Pashley. Measurement of the hydrophobic interaction between two hydrophobic surfaces in aqueous electrolyte solutions. *Journal of Colloid And Interface Science*, 98(2):500–514, 1984.

[169] Richard M. Pashley, Patricia M. Mcguiggan, Barry W. Ninham, and D. Fennell Evans. Attractive forces between uncharged hydrophobic surfaces: Direct measurements in aqueous solution. *Science*, 229(4718):1088–1089, 1985.

[170] R M Pashley and Jacob N. Israelachvili. A comparison of surface forces and interfacial properties of mica in purified surfactant solutions. *Colloids and Surfaces*, 2:169–187, 1981.

[171] Y. L.E. Chen, M. L. Gee, C. A. Helm, J. N. Israelachvili, and P. M. McGuiggan. Effects of humidity on the structure and adhesion of amphiphilic monolayers on mica. *Journal of Physical Chemistry*, 93(20):7057–7059, 1989.

[172] Johan Marra and Jacob Israelachvili. Direct Measurements of Forces between Phosphatidylcholine and Phosphatidylethanolamine Bilayers in Aqueous Electrolyte Solutions. *Biochemistry*, 24(17):4608–4618, 1985.

[173] Per Claesson, Ana Maria Carmona-Ribeiro, and Kazue Kurihara. Dihexadecyl phosphate monolayers: Intralayer and interlayer interactions. *Journal of Physical Chemistry*, 93(2):917–922, 1989.

[174] J. Marra. Direct measurement of the interaction between phosphatidylglycerol bilayers in aqueous electrolyte solutions. *Biophysical Journal*, 50(5):815–825, 1986.

[175] Johan Marra. Direct measurements of attractive Van der Waals and adhesion forces between uncharged lipid bilayers in aqueous solutions. *Journal of Colloid And Interface Science*, 109(1):11–20, 1986.

[176] Per M. Claesson, Roland Kjellander, Per Stenius, and Hugo K. Christenson. Direct measurement of temperature-dependent interactions between non-ionic surfactant layers. *Journal of the Chemical Society, Faraday Transactions 1: Physical Chemistry in Condensed Phases*, 82(9):2735–2746, 1986.

[177] R. M. Pashley, P. M. McGuiggan, B. W. Ninham, J. Brady, and D. F. Evans. Direct measurements of surface forces between bilayers of double-chained quaternary ammonium acetate and bromide surfactants. *Journal of Physical Chemistry*, 90(8):1637–1642, 1986.

[178] Johan Marra. Effects of counterion specificity on the interactions between quaternary ammonium surfactants in monolayers and bilayers. *The Journal of Physical Chemistry*, 90(10):2145–2150, 1986.

[179] R. G. Horn. Direct Measurement of the Force Between two Lipid Bilayers and Observation of their Fusion. *Biochimica et biophysica acta*, 778:224–228, 1984.

[180] Christiane A. Helm, Jacob N. Israelachvili, and Patricia M. McGuiggan. Molecular mechanisms and forces involved in the adhesion and fusion of amphiphilic bilayers. *Science*, 246(4932):919–922, 1989.

[181] Saurabh Das, Stephen H. Donaldson Jr., Yair Kaufman, and Jacob N. Israelachvili. Interaction of adsorbed polymers with supported cationic bilayers. *RSC Advances*, 3(43):20405, 2013.

[182] Travers H. Anderson, Stephen H. Donaldson, Hongbo Zeng, and Jacob N. Israelachvili. Direct measurement of double-layer, van der waals, and polymer depletion attraction forces between supported cationic bilayers. *Langmuir*, 26(18):14458–14465, sep 2010.

[183] Hans Jürgen Butt, Brunero Cappella, and Michael Kappl. Force measurements with the atomic force microscope: Technique, interpretation and applications. *Surface Science Reports*, 59(1-6):1–152, 2005.

[184] G. Binnig, H. Rohrer, Ch. Gerber, and E. Weibel. Surface Studies by Scanning Tunneling Microscopy. *Physical Review Letters*, 49(1):57–61, jul 1982.

[185] G. Binnig and H. Rohrer. Scanning tunneling microscopy. *Surface Science*, 126(1-3):236–244, mar 1983.

[186] J. Tersoff and D. R. Hamann. Theory and Application for the Scanning Tunneling Microscope. *Physical Review Letters*, 50(25):1998–2001, jun 1983.

[187] G. Binnig, C. F. Quate, and Ch. Gerber. Atomic Force Microscope. *Physical Review Letters*, 56(9):930–933, mar 1986.

[188] Gerhard Meyer and Nabil M. Amer. Novel optical approach to atomic force microscopy. *Applied Physics Letters*, 53(12):1045–1047, sep 1988.

[189] S. Alexander, L. Hellemans, O. Marti, J. Schneir, V. Elings, P. K. Hansma, Matt Longmire, and John Gurley. An atomic-resolution atomic-force microscope implemented using an optical lever. *Journal of Applied Physics*, 65(1):164–167, jan 1989.

[190] Nancy A. Burnham, Dawn D. Dominguez, Robert L. Mowery, and Richard J. Colton. Probing the surface forces of monolayer films with an atomic-force microscope. *Physical Review Letters*, 64(16):1931–1934, 1990.

[191] Y. Martin, C. C. Williams, and H. K. Wickramasinghe. Atomic force microscope-force mapping and profiling on a sub 100-Å scale. *Journal of Applied Physics*, 61(10):4723–4729, 1987.

[192] U. Dürig, J. K. Gimzewski, and D. W. Pohl. Experimental observation of forces acting during scanning tunneling microscopy. *Physical Review Letters*, 57(19):2403–2406, 1986.

[193] A. L. Weisenhorn, P. K. Hansma, T. R. Albrecht, and C. F. Quate. Forces in atomic force microscopy in air and water. *Applied Physics Letters*, 54(26):2651–2653, jun 1989.

[194] J. H. Hoh, J. P. Revel, and P. K. Hansma. Tip-sample interactions in atomic force microscopy: I. Modulating adhesion between silicon nitride and glass. *Nanotechnology*, 2(3):119–122, 1991.

[195] Hans Jürgen Butt. Measuring electrostatic, van der Waals, and hydration forces in electrolyte solutions with an atomic force microscope. *Biophysical Journal*, 60(6):1438–1444, 1991.

[196] Hans Jüurgen Butt. Electrostatic interaction in atomic force microscopy. *Biophysical Journal*, 60(4):777–785, 1991.

[197] William A. Ducker and Robert F. Cook. Rapid measurement of static and dynamic surface forces. *Applied Physics Letters*, 56(24):2408–2410, 1990.

[198] N. Hilal, W.R. R Bowen, L. Alkhatib, and O. Ogunbiyi. A Review of Atomic Force Microscopy Applied to Cell Interactions with Membranes. *Chemical Engineering Research and Design*, 84(4):282–292, 2006.

[199] William A. Ducker, Tim J. Senden, and Richard M. Pashley. Direct measurement of colloidal forces using an atomic force microscope. *Nature*, 353(6341):239–241, 1991.

[200] William A. Ducker, Tim J. Senden, and Richard M. Pashley. Measurement of Forces in Liquids Using a Force Microscope. *Langmuir*, 8(7):1831–1836, 1992.

[201] G. Peschel, P. Belouschek, M. M. Müller, M. R. Müller, and R. König. The interaction of solid surfaces in aqueous systems. *Colloid & Polymer Science*, 260(4):444–451, 1982.

[202] Laurence Meagher. Direct measurement of forces between silica surfaces in aqueous CaCl2 solutions using an atomic force microscope, aug 1992.

[203] Hans Jürgen Butt, Manfred Jaschke, and William Ducker. Measuring surface forces in aqueous electrolyte solution with the atomic force microscope. *Bioelectrochemistry and Bioenergetics*, 38(1):191–201, 1995.

[204] Y. Q. Li, N. J. Tao, J. Pan, A. A. Garcia, and S. M. Lindsay. Direct Measurement of Interaction Forces between Colloidal Particles Using the Scanning Force Microscope. *Langmuir*, 9(3):637–641, 1993.

[205] Tim J. Senden and Calum J. Drummond. Surface chemistry and tip-sample interactions in atomic force microscopy. *Colloids and Surfaces A: Physicochemical and Engineering Aspects*, (96):29–51, 1996.

[206] Gary Toikka, Robert A. Hayes, and John Ralston. Surface forces between spherical ZnS particles in aqueous electrolyte. *Langmuir*, 12(16):3783–3788, 1996.

[207] Grit Hüttl, Dirk Beyer, and Eberhard Müller. AFM investigation of electrical double layers on SiO2 surfaces. *Key Engineering Materials*, 132-136(February):726–729, 1997.

[208] Mahdy M. Elmahdy, Astrid Drechsler, Christof Gutsche, Alla Synytska, Petra Uhlmann, Friedrich Krerner, and Manfred Stamm. Forces between blank surfaces as measured by the colloidal probe technique and by optical tweezers - A comparison. *Langmuir*, 25(22):12894–12898, 2009.

[209] Aysen Tulpar, Vivek Subramanian, and William Ducker. Decay lengths of double-layer forces in solutions of partly associated ions. *Langmuir*, 17(26):8451–8454, 2001.

[210] Luke M. Mosley, Keith A. Hunter, and William A. Ducker. Forces between colloid particles in natural waters. *Environmental Science and Technology*, 37(15):3303–3308, 2003.

[211] Gary Toikka and Robert A. Hayes. Direct measurement of colloidal forces between mica and silica in aqueous electrolyte. *Journal of Colloid and Interface Science*, 191(1):102–109, 1997.

[212] Gregor Trefalt, Thomas Palberg, and Michal Borkovec. Forces between colloidal particles in aqueous solutions containing monovalent and multivalent ions. *Current Opinion in Colloid and Interface Science*, 27:9–17, 2017.

[213] F. Javier Montes Ruiz-Cabello, Mohsen Moazzami-Gudarzi, Magdalena Elzbieciak-Wodka, Plinio Maroni, Christophe Labbez, Michal Borkovec, and Gregor Trefalt. Long-ranged and soft interactions between charged colloidal particles induced by multivalent coions. *Soft Matter*, 11(8):1562–1571, 2015.

[214] Ohad Zohar, Ilya Leizerson, and Uri Sivan. Short range attraction between two similarly charged silica surfaces. *Physical Review Letters*, 96(17):1–4, 2006.

[215] Prashant Sinha, Istvan Szilagyi, F. Javier Montes Ruiz-Cabello, Plinio Maroni, and Michal Borkovec. Attractive forces between charged colloidal particles induced by multivalent ions revealed by confronting aggregation and direct force measurements. *Journal of Physical Chemistry Letters*, 4(4):648–652, 2013.

[216] Valentina Valmacco, Magdalena Elzbieciak-Wodka, David Herman, Gregor Trefalt, Plinio Maroni, and Michal Borkovec. Forces between silica particles in the presence of multivalent cations. *Journal of Colloid and Interface Science*, 472:108–115, 2016.

[217] A. J. Milling. Depletion and structuring of sodium poly(styrenesulfonate) at the silica-water interface. *Journal of Physical Chemistry*, 100(21):8986–8993, 1996.

[218] Andrew J. Milling and Brian Vincent. Depletion forces between silica surfaces in solutions of poly(acrylic acid). *Journal of the Chemical Society - Faraday Transactions*, 93(17):3179–3183, 1997.

[219] A. J. Milling and K. Kendall. Depletion, adsorption, and structuring of sodium poly(acrylate) at the water-silica interface. 1. An atomic force microscopy force study. *Langmuir*, 16(11):5106–5115, 2000.

[220] Simon Biggs, Janine L. Burns, Yao De Yan, Graeme J. Jameson, and Paul Jenkins. Molecular weight dependence of the depletion interaction between silica surfaces in solutions of sodium poly(styrene sulfonate). *Langmuir*, 16(24):9242–9248, 2000.

[221] Martin Piech and John Y. Walz. Direct measurement of depletion and structural forces in polydisperse, charged systems. *Journal of Colloid and Interface Science*, 253(1):117–129, 2002.

[222] Simon Biggs. Steric and Bridging Forces between Surfaces Bearing Adsorbed Polymer: An Atomic Force Microscopy Study. *Langmuir*, 11(1):156–162, 1995.

[223] G. J.C. Braithwaite, A. Howe, and P. F. Luckham. Interactions between poly(ethylene oxide) layers adsorbed to glass surfaces probed by using a modified atomic force microscope. *Langmuir*, 12(17):4224–4237, 1996.

[224] Stéphanie Pasche, Marcus Textor, Laurence Meagher, Nicholas D. Spencer, and Hans J. Griesser. Relationship between interfacial forces measured by colloid-probe atomic force microscopy and protein resistance of poly(ethylene glycol)-grafted poly(L-lysine) adlayers on niobia surfaces. *Langmuir*, 21(14):6508–6520, 2005.

[225] P. G. Hartley and P. J. Scales. Electrostatic properties of polyelectrolyte modified surfaces studied by direct force measurement. *Langmuir*, 14(24):6948–6955, 1998.

[226] Ramon Pericet-Camara, Georg Papastavrou, Sven H. Behrens, Christiane A. Helm, and Michal Borkovec. Interaction forces and molecular adhesion between pre-adsorbed poly(ethylene imine) layers. *Journal of Colloid and Interface Science*, 296(2):496–506, 2006.

[227] Stephan Block and Christiane A. Helm. Single polyelectrolyte layers adsorbed at high salt conditions: polyelectrolyte brush domains coexisting with flatly adsorbed chains. *Macromolecules*, 42(17):6733–6740, 2009.

[228] Michal Borkovec, Istvan Szilagyi, Ionel Popa, Marco Finessi, Prashant Sinha, Plinio Maroni, and Georg Papastavrou. Investigating forces between charged particles in the presence of oppositely charged polyelectrolytes with the multiparticle colloidal probe technique. *Advances in Colloid and Interface Science*, 179-182:85–98, 2012.

[229] Luke J. Kirwan, Plinio Maroni, Sven H. Behrens, Georg Papastavrou, and Michal Borkovec. Interaction and structure of surfaces coated by poly(vinyl amines) of different line charge densities. *Journal of Physical Chemistry B*, 112(46):14609–14619, 2008.

[230] Laurence Meagher, George Maurdev, and Michelle L. Gee. Interaction forces between a bare silica surface and an α-alumina surface bearing adsorbed polyelectrolyte and surfactant. *Langmuir*, 18(7):2649–2657, 2002.

[231] Marilyn E. Karaman, Laurence Meagher, and Richard M. Pashley. Surface Chemistry of Emulsion Polymerization. *Langmuir*, 9(5):1220–1227, 1993.

[232] Stephen B. Johnson, Calum J. Drummond, Peter J. Scales, and Satoshi Nishimura. Comparison of Techniques for Measuring the Electrical Double Layer Properties of Surfaces in Aqueous Solution: Hexadecyltrimethylammonium Bromide Self-Assembly Structures as a Model System. *Langmuir*, 11(7):2367–2375, 1995.

[233] Ioana Pera, Rüdiger Stark, Michael Kappl, Hans Jürgen Butt, and Fabio Benfenati. Using the atomic force microscope to study the interaction between two solid supported lipid bilayers and the influence of synapsin I. *Biophysical Journal*, 87(4):2446–2455, 2004.

[234] Bärbel Lorenz, Rabea Keller, Eva Sunnick, Burkhard Geil, and Andreas Janshoff. Colloidal probe microscopy of membrane-membrane interactions: From ligand-receptor recognition to fusion events. *Biophysical Chemistry*, 150(1-3):54–63, 2010.

[235] 4PK Hansma, JP Cleveland, M Radmacher, DA Walters, PE Hillner, M Bezanilla, M Fritz, D Vie, HG Hansma, CB Prater, et al. Tapping mode atomic force microscopy in liquids. *Applied Physics Letters*, 64(13):1738–1740, 1994.

[236] Laura Picas, Pierre Emmanuel Milhiet, and Jordi Hernández-Borrell. Atomic force microscopy: A versatile tool to probe the physical and chemical prop-

erties of supported membranes at the nanoscale. *Chemistry and Physics of Lipids*, 165(8):845–860, 2012.

[237] Dmitri I Svergun and Michel H J Koch. Small-angle scattering studies of biological macromolecules in solution. *Reports on Progress in Physics*, 66(10):1735–1782, sep 2003.

[238] LA Feigin, Dimitrij I Svergun, et al. *Structure analysis by small-angle X-ray and neutron scattering*, volume 1. Springer, 1987.

[239] W Bras, IP Dolbnya, D Detollenaere, R van Tol, M Malfois, GN Greaves, AJ Ryan, and E Heeley. Recent experiments on a small-angle/wide-angle x-ray scattering beam line at the esrf. *Journal of Applied Crystallography*, 36(3):791–794, 2003.

[240] William Henry Bragg and William Lawrence Bragg. The reflection of x-rays by crystals. *Proceedings of the Royal Society of London. Series A, Containing Papers of a Mathematical and Physical Character*, 88(605):428–438, 1913.

[241] William Lawrence Bragg. The analysis of crystals by the x-ray spectrometer. *Proceedings of the Royal Society of London. Series A, Containing Papers of a Mathematical and Physical Character*, 89(613):468–489, 1914.

[242] Arsenij Aleksandrovič Sokolov and Igor Michajlovic Ternov. Synchrotron radiation. *Akademia Nauk SSSR, Moskovskoie Obshchestvo Ispytatelei prirody. Sektsia Fiziki. Sinkhrotron Radiation, Nauka Eds., Moscow, 1966 (Russian title: Sinkhrotronnoie izluchenie), 228 pp.*, 1966.

[243] MJ O'neill. The analysis of a temperature-controlled scanning calorimeter. *Analytical chemistry*, 36(7):1238–1245, 1964.

[244] Marjorie J Vold. Differential thermal analysis. *Analytical chemistry*, 21(6):683–688, 1949.

[245] Bruce J Berne and Robert Pecora. *Dynamic light scattering: with applications to chemistry, biology, and physics*. Courier Corporation, 2000.

[246] Robert J Hunter. *Zeta potential in colloid science: principles and applications*, volume 2. Academic press, 2013.

[247] Marie-Paule Mingeot-Leclercq, Magali Deleu, Robert Brasseur, and Yves F Dufrêne. Atomic force microscopy of supported lipid bilayers. *Nature protocols*, 3(10):1654–9, jan 2008.

[248] RN Lewis, Walter Pohle, and Ronald N McElhaney. The interfacial structure of phospholipid bilayers: differential scanning calorimetry and fourier transform infrared spectroscopic studies of 1, 2-dipalmitoyl-sn-glycero-3-phosphorylcholine and its dialkyl and acyl-alkyl analogs. *Biophysical journal*, 70(6):2736–2746, 1996.

[249] M Dubois and Th Zemb. Phase behavior and scattering of double-chain surfactants in diluted aqueous solutions. *Langmuir*, 7(7):1352–1360, 1991.

[250] RG Laughlin, RL Munyon, YC Fu, and AJ Fehl. Physical science of the dioctadecyldimethylammonium chloride-water system. 1. equilibrium phase behavior. *Journal of Physical Chemistry*, 94(6):2546–2552, 1990.

[251] Michael Rappolt, Georg Pabst, Gert Rapp, Manfred Kriechbaum, Heinz Amenitsch, Christian Krenn, Sigrid Bernstorff, and Peter Laggner. New evidence for gel-liquid crystalline phase coexistence in the ripple phase of phosphatidylcholines. *European Biophysics Journal*, 29(2):125–133, May 2000.

[252] Hongguang Li, Stefan A Wieczorek, Xia Xin, Tomasz Kalwarczyk, Natalia Ziebacz, Tomasz Szymborski, Robert Hołyst, Jingcheng Hao, Ewa Gorecka, and Damian Pociecha. Phase transition in salt-free catanionic surfactant mixtures induced by temperature. *Langmuir*, 26(1):34–40, 2009.

[253] Håkan Edlund, Alireza Sadaghiani, and Ali Khan. Phase behavior and phase structure for catanionic surfactant mixtures: dodecyltrimethylammonium chloride- sodium nonanoate- water system. *Langmuir*, 13(19):4953–4963, 1997.

[254] J Bouwstra, G Gooris, and Maria Ponec. The lipid organisation of the skin barrier: liquid and crystalline domains coexist in lamellar phases. *Journal of biological physics*, 28(2):211–223, 2002.

[255] Joke A Bouwstra, Gert S Gooris, FER Dubbelaar, and Maria Ponec. Phase behavior of lipid mixtures based on human ceramides: coexistence of crystalline and liquid phases. *Journal of lipid research*, 42(11):1759–1770, 2001.

[256] John L. Parker, Hugo K. Christenson, and Barry W. Ninham. Forces between bilayers of a cationic surfactant with hydroxylated headgroups: Effects of interbilayer adhesion on the interactions. *Journal of Physical Chemistry*, 92(14):4155–4159, 1988.

[257] J. N. Israelachvili and P. M. McGuiggan. Forces Between Surfaces in Liquids. *Science*, 241(4867):795–800, aug 1988.

[258] Stephen B. Johnson, Calum J. Drummond, Peter J. Scales, and Satoshi Nishimura. Comparison of Techniques for Measuring the Electrical Double Layer Properties of Surfaces in Aqueous Solution: Hexadecyltrimethylammonium Bromide Self-Assembly Structures as a Model System. *Langmuir*, 11(7):2367–2375, 1995.

[259] P F Luckham and K Smith. Direct measurement of recognition forces between proteins and membrane receptors. *Faraday Discussions*, (111):307–343, 1998.

[260] S. Chiruvolu, J. N. Israelachvili, E. Naranjo, Z. Xu, J. A. Zasadzinski, E. W. Kaler, and K. L. Herrington. Measurement of Forces between Spontaneous Vesicle-Forming Bilayers. *Langmuir*, 11(11):4256–4266, 1995.

[261] You Lung Chen, Shaun Chen, Curtis Frank, and Jacob Israelachvili. Molecular mechanisms and kinetics during the self-assembly of surfactant layers. *Journal of Colloid And Interface Science*, 153(1):244–265, 1992.

[262] J A N Zasadzinski, J T Woodward, and M L Longo. scanning probe microscopy of surfactant bilayers and monolayers. pages 242–255, 1992.

[263] William A. Ducker and David R. Clarke. Controlled modification of silicon nitride interactions in water via zwitterionic surfactant adsorption. *Colloids and Surfaces A: Physicochemical and Engineering Aspects*, 93(C):275–292, 1994.

[264] Amber Sharma and John Y. Walz. Direct measurement of the depletion interaction in a charged colloidal dispersion. *Journal of the Chemical Society - Faraday Transactions*, 92(24):4997–5004, 1996.

[265] Hilde A. Rinia and Ben De Kruijff. Imaging domains in model membranes with atomic force microscopy. *FEBS Letters*, 504(3):194–199, 2001.

[266] Yves F Dufrêne and Gil U Lee. Advances in the characterization of supported lipid films with the atomic force microscope. *Biochimica et Biophysica Acta (BBA) - Biomembranes*, 1509(1–2):14–41, 2000.

[267] Y F Dufrêne. Application of atomic force microscopy to microbial surfaces: from reconstituted cell surface layers to living cells. *Micron*, 32(2):153–165, 2001.

[268] Katharine B Blodgett. Films built by depositing successive monomolecular layers on a solid surface. *Journal of the American Chemical Society*, 57(6):1007–1022, 1935.

[269] Ralf Richter, Anneke Mukhopadhyay, and Alain Brisson. Pathways of lipid vesicle deposition on solid surfaces: a combined qcm-d and afm study. *Biophysical journal*, 85(5):3035–3047, 2003.

[270] B Seantier, C Breffa, O Felix, and G Decher. Dissipation-enhanced quartz crystal microbalance studies on the experimental parameters controlling the formation of supported lipid bilayers. *The Journal of Physical Chemistry B*, 109(46):21755–21765, 2005.

[271] Simon J. Attwood, Youngjik Choi, and Zoya Leonenko. Preparation of DOPC and DPPC supported planar lipid bilayers for atomic force microscopy and atomic force spectroscopy. *International Journal of Molecular Sciences*, 14(2):3514–3539, 2013.

[272] Erik Reimhult, Fredrik Höök, and Bengt Kasemo. Intact vesicle adsorption and supported biomembrane formation from vesicles in solution: Influence of surface chemistry, vesicle size, temperature, and osmotic pressure. *Langmuir*, 19(5):1681–1691, 2003.

[273] E. Reimhult, F. Höök, and B. Kasemo. Temperature dependence of formation of a supported phospholipid bilayer from vesicles on [formula presented]. *Physical Review E - Statistical Physics, Plasmas, Fluids, and Related Interdisciplinary Topics*, 66(5):4, 2002.

[274] K. Dimitrievski, E. Reimhult, B. Kasemo, and V. P. Zhdanov. Simulations of temperature dependence of the formation of a supported lipid bilayer via vesicle adsorption. *Colloids and Surfaces B: Biointerfaces*, 39(1-2):77–86, 2004.

[275] Tania Kjellerup Lind, Marité Cárdenas, and Hanna Pauliina Wacklin. Formation of supported lipid bilayers by vesicle fusion: Effect of deposition temperature. *Langmuir*, 30(25):7259–7263, 2014.

[276] M. V. Maslova, L. G. Gerasimova, and W. Forsling. Surface properties of cleaved mica. *Colloid Journal*, 66(3):322–328, 2004.

[277] Dalei Jing and Bharat Bhushan. Quantification of surface charge density and its effect on boundary slip. *Langmuir : the ACS journal of surfaces and colloids*, 29(23):6953–63, 2013.

[278] Ruthven NAH Lewis, David A Mannock, Ronald N McElhaney, David C Turner, and Sol M Gruner. Effect of fatty acyl chain length and structure on the lamellar gel to liquid-crystalline and lamellar to reversed hexagonal phase transitions of aqueous phosphatidylethanolamine dispersions. *Biochemistry*, 28(2):541–548, 1989.

[279] Susan Mabrey and Julian M Sturtevant. Incorporation of saturated fatty acids into phosphatidylcholine bilayers. *Biochimica et Biophysica Acta (BBA)-Lipids and Lipid Metabolism*, 486(3):444–450, 1977.

[280] Ruthven NAH Lewis and Ronald N McElhaney. Thermotropic phase behavior of model membranes composed of phosphatidylcholines containing methyl iso-branched fatty acids. 1. differential scanning calorimetric studies. *Biochemistry*, 24(10):2431–2439, 1985.

[281] Shuji Kitagawa, Junko Endo, and Fujio Kametani. Effects of long-chain cis-unsaturated fatty acids and their alcohol analogs on aggregation of bovine platelets and their relation with membrane fluidity change. *Biochimica et Biophysica Acta (BBA)-Biomembranes*, 818(3):391–397, 1985.

[282] Thomas J McIntosh, Hainan Lin, Shusen Li, and Ching-hsien Huang. The effect of ethanol on the phase transition temperature and the phase structure of monounsaturated phosphatidylcholines. *Biochimica et Biophysica Acta (BBA)-Biomembranes*, 1510(1-2):219–230, 2001.

[283] Elizabeth S Rowe. Lipid chain length and temperature dependence of ethanol-phosphatidylcholine interactions. *Biochemistry*, 22(14):3299–3305, 1983.

[284] R Ganguly, VK Aswal, PA Hassan, IK Gopalakrishnan, and JV Yakhmi. Sodium chloride and ethanol induced sphere to rod transition of triblock copolymer micelles. *The Journal of Physical Chemistry B*, 109(12):5653–5658, 2005.

[285] ES Rowe. The effects of ethanol on the thermotropic properties of dipalmitoylphosphatidylcholine. *Molecular pharmacology*, 22(1):133–139, 1982.

[286] Steven L Krill, Kristine Knutson, and William I Higuchi. Ethanol effects on the stratum corneum lipid phase behavior. *Biochimica et Biophysica Acta (BBA)-Biomembranes*, 1112(2):273–280, 1992.

[287] Julian Eastoe, Marios Hopkins Hatzopoulos, and Peter J Dowding. Action of hydrotropes and alkyl-hydrotropes. *Soft Matter*, 7(13):5917–5925, 2011.

[288] PA Hassan, Srinivasa R Raghavan, and Eric W Kaler. Microstructural changes in sds micelles induced by hydrotropic salt. *Langmuir*, 18(7):2543–2548, 2002.

[289] Michael Patra, Emppu Salonen, Emma Terama, Ilpo Vattulainen, Roland Faller, Bryan W. Lee, Juha Holopainen, and Mikko Karttunen. Under the influence of alcohol: The effect of ethanol and methanol on lipid bilayers. *Biophysical Journal*, 90(4):1121–1135, 2006.

[290] Colley C.M. and Metcalfe J.C. Localisation of Small Molecules in Lipid Membranes. *FEBS Letters*, 24(3):241–246, 1972.

[291] R Zana. AQUEOUS SURFACTANT-ALCOHOL SYSTEMS : A REVIEW. *Advances in Colloid and Interface Science*, 57:1–64, 1995.

[292] Werner Kunz, Krister Holmberg, and Thomas Zemb. Hydrotropes. *Current Opinion in Colloid and Interface Science*, 22:99–107, 2016.

[293] Martin Caffrey. Kinetics and mechanisms of the lamellar gel/lamellar liquid-crystal and lamellar/inverted hexagonal phase transition in phosphatidylethanolamine: a real-time x-ray diffraction study using synchrotron radiation. *Biochemistry*, 24(18):4826–4844, 1985.

[294] Ryugo Tero. Substrate effects on the formation process, structure and physicochemical properties of supported lipid bilayers. *Materials*, 5(12):2658–2680, dec 2012.

[295] Sergi Garcia-Manyes and Fausto Sanz. Nanomechanics of lipid bilayers by force spectroscopy with AFM: A perspective. *Biochimica et Biophysica Acta - Biomembranes*, 1798(4):741–749, 2010.

[296] Yinli Li, Changjiang Zhu, Jichun Zhu, Hao Liang, Dong Chen, Huiling Zhao, and Bo Liu. Nanomechanics of phospholipid LB film studied layer by layer with AFM. pages 1–8, 2014.

[297] C. Canale, M. Jacono, a. Diaspro, and S. Dante. Force spectroscopy as a tool to investigate the properties of supported lipid membranes. *Microscopy Research and Technique*, 73(10):965–972, 2010.

[298] L.T. Boni, J.S. Hah, S.W. Hui, P. Mukherjee, J.T. Ho, and C.Y. Jung. Aggregation and fusion of unilamellar vesicles by poly(ethylene glycol). *Biochimica et Biophysica Acta (BBA) - Biomembranes*, 775(3):409 – 418, 1984.

[299] J. C. Fröberg, O. J. Rojas, and P. M. Claesson. Surface forces and measuring techniques. *International Journal of Mineral Processing*, 56:1–30, 1999.

[300] Tonya Kuhl, Yuqing Guo, James L Alderfer, Alan D Berman, Deborah Leckband, Jacob Israelachvili, and Sek Wen Hui. Direct measurement of polyethylene glycol induced depletion attraction between lipid bilayers. *Langmuir*, 12(12):3003–3014, 1996.

[301] Tonya L Kuhl, Alan D Berman, Sek Wen Hui, and Jacob N Israelachvili. Part 1. direct measurement of depletion attraction and thin film viscosity between lipid bilayers in aqueous polyethylene glycol solutions. *Macromolecules*, 31(23):8250–8257, 1998.

[302] G. Hema Sagar and Jayesh R. Bellare. Estimation of mechanical strength of unilamellar and multilamellar AOT/Water vesicles and their rupture using micropipet aspiration. *Journal of Physical Chemistry B*, 113(42):13805–13810, 2009.

[303] Youhei Kawabata, Tomoaki Shinoda, and Tadashi Kato. Vesicle growth and deformation in a surfactant solution below the Krafft temperature. *Physical Chemistry Chemical Physics*, 13(8):3484, 2011.

[304] Matthew Leivers, John M Seddon, Marc Declercq, Eric Robles, and Paul Luckham. Measurement of forces between supported cationic bilayers by colloid probe atomic force microscopy: Electrolyte concentration and composition. *Langmuir*, 35(3):729–738, 2018.

[305] J. C. Berg. *An Introduction to Interfaces & Colloids*. World Scientific, Singapore, 2012.

[306] Matan Dishon, Ohad Zohar, and Uri Sivan. Effect of cation size and charge on the interaction between silica surfaces in 1:1, 2:1, and 3:1 aqueous electrolytes. *Langmuir*, 27(21):12977–12984, 2011.

[307] Lorena Redondo-Morata, Marina I Giannotti, and Fausto Sanz. Structural impact of cations on lipid bilayer models: Nanomechanical properties by AFM-force spectroscopy. *Molecular membrane biology*, 31(1):17–28, 2014.

[308] Franz Hofmeister. Zur Lehre von der Wirkung der Salze. *Archiv für Experimentelle Pathologie und Pharmakologie*, 24(4-5):247–260, feb 1888.

[309] Yanjie Zhang and Paul S. Cremer. Interactions between macromolecules and ions: the Hofmeister series. *Current Opinion in Chemical Biology*, 10(6):658–663, 2006.

[310] V. V. Kalinin and C. J. Radke. An ion-binding model for ionic surfactant adsorption at aqueous-fluid interfaces. *Colloids and Surfaces A: Physicochemical and Engineering Aspects*, 114:337–350, 1996.

[311] Ali Khan. Phase science of surfactants. *Current Opinion in Colloid & Interface Science*, 1(5):614–623, 1996.

[312] John F. Nagle and Stephanie Tristram-Nagle. Structure of lipid bilayers. *Biochimica et Biophysica Acta - Reviews on Biomembranes*, 1469(3):159–195, 2000.

[313] Shuang Yang, Dadong Yan, Hongge Tan, and An Chang Shi. Depletion interaction between two colloidal particles in a nonadsorbing polymer solution. *Physical Review E - Statistical, Nonlinear, and Soft Matter Physics*, 74(4):1–10, 2006.

[314] Y. K. Leong. Depletion interaction in colloidal suspensions: A comparison between theory and experiment. *Colloids and Surfaces A: Physicochemical and Engineering Aspects*, 118(1-2):107–114, 1996.

[315] Sugam Kumar, A. J. Chinchalikar, V. K. Aswal, and R. Schweins. Tuning of adsorption vs. depletion interaction in nanoparticle-polymer system. *AIP Conference Proceedings*, 1512(February 2013):152–153, 2013.

[316] Gerard J. Fleer. Polymers at interfaces and in colloidal dispersions. *Advances in Colloid and Interface Science*, 159(2):99–116, 2010.

[317] Andrei V. Petukhov, Remco Tuinier, and Gert Jan Vroege. Entropic patchiness: Effects of colloid shape and depletion. *Current Opinion in Colloid and Interface Science*, 30:54–61, 2017.

[318] Alberto Striolo, Coray M. Colina, Keith E. Gubbins, Nicola Elvassore, and Leo Lue. The depletion attraction between Pairs of colloid particles in polymer solution. *Molecular Simulation*, 30(7):437–499, 2004.

[319] S. Ramakrishnan, M. Fuchs, K. S. Schweizer, and C. F. Zukoski. Entropy driven phase transitions in colloid-polymer suspensions: Tests of depletion theories. *Journal of Chemical Physics*, 116(5):2201–2212, 2002.

[320] To Ngai, Xiaochen Xing, and Fan Jin. Depletion attraction between a polystyrene particle and a hydrophilic surface in a Pluronic aqueous solution. *Langmuir*, 24(24):13912–13917, 2008.

[321] L. Helden, R. Roth, G. H. Koenderink, P. Leiderer, and C. Bechinger. Direct Measurement of Entropic Forces Induced by Rigid Rods. *Physical Review Letters*, 90(4):4, 2003.

[322] D. Ray and V. K. Aswal. Tuning of depletion interaction in nanoparticle-surfactant systems. *AIP Conference Proceedings*, 1591(February):175–177, 2014.

[323] Robert I Feigin and Donald H Napper. Depletion stabilization and depletion flocculation. *Journal of Colloid and Interface Science*, 75(2):525–541, jun 1980.

[324] O. Théodoly, J. S. Tan, R. Ober, C. E. Williams, and V. Bergeron. Oscillatory forces from polyelectrolyte solutions confined in thin liquid films. *Langmuir*, 17(16):4910–4918, 2001.

[325] Roland R. Netz and David Andelman. Neutral and charged polymers at interfaces. *Physics Reports*, 380(1-2):1–95, 2003.

[326] Hugo K. Christenson and Roger G. Horn. Forces between mica surfaces in ethylene glycol. *Journal of Colloid And Interface Science*, 103(1):50–55, 1985.

[327] T. L. Kuhl, D. E. Leckband, D. D. Lasic, and J. N. Israelachvili. Modulation of interaction forces between bilayers exposing short-chained ethylene oxide headgroups. *Biophysical Journal*, 66(5):1479–1488, 1994.

[328] Janine L. Burns, Yao De Yan, Graeme J. Jameson, and Simon Biggs. The effect of molecular weight of nonadsorbing polymer on the structure of depletion-induced flocs. *Journal of Colloid and Interface Science*, 247(1):24–32, 2002.

[329] Shunxi Ji and John Y. Walz. Depletion forces and flocculation with surfactants, polymers and particles - Synergistic effects. *Current Opinion in Colloid and Interface Science*, 20(1):39–45, 2015.

[330] Xiaochen Xing, Li Hua, and To Ngai. Depletion versus stabilization induced by polymers and nanoparticles: The state of the art. *Current Opinion in Colloid and Interface Science*, 20(1):54–59, 2015.

[331] G. K. James and J. Y. Walz. Experimental investigation of the effects of ionic micelles on colloidal stability. *Journal of Colloid and Interface Science*, 418:283–291, 2014.

[332] R. Tuinier, J. Rieger, and C. G. De Kruif. Depletion-induced phase separation in colloid-polymer mixtures. *Advances in Colloid and Interface Science*, 103(1):1–31, 2003.

[333] Janine L. Burns, Yao De Yan, Graeme J. Jameson, and Simon Biggs. Relationship between interaction forces and the structural compactness of depletion flocculated colloids. *Colloids and Surfaces A: Physicochemical and Engineering Aspects*, 162(1-3):265–277, 2000.

[334] Aysen Tulpar, Robert D. Tilton, and John Y. Walz. Synergistic effects of polymers and surfactants on depletion forces. *Langmuir*, 23(8):4351–4357, 2007.

[335] Yao De Yan, Janine L. Burns, Graeme J. Jameson, and Simon Biggs. Structure and strength of depletion force induced particle aggregates. *Chemical engineering journal*, 80(1-3):23–30, 2000.

[336] Cathy E. McNamee, Yoshinobu Tsujii, Hiroyuki Ohshima, and Mutsuo Matsumoto. Interaction forces between two hard surfaces in particle-containing aqueous systems. *Langmuir*, 20(5):1953–1962, 2004.

[337] Annalisa Caria, Oren Regev, and Ali Khan. Surfactant-polymer interactions: Phase diagram and fusion of vesicle in the didodecyldimethylammonium bromide-poly(ethylene oxide)-water system. *Journal of Colloid and Interface Science*, 200(1):19–30, 1998.

[338] Simon Aben, Christian Holtze, Tharwat Tadros, and Peter Schurtenberger. Rheological investigations on the creaming of depletion-flocculated emulsions. *Langmuir*, 28(21):7967–7975, 2012.

[339] D. Meyuhas, S. Nir, and D. Lichtenberg. Aggregation of phospholipid vesicles by water-soluble polymers. *Biophysical Journal*, 71(5):2602–2612, 1996.

[340] J. C. van de Pas and C. J. Buytenhek. The effects of free polymers on osmotic compression, depletion flocculation and fusion of lamellar liquid-crystalline droplets. *Colloids and Surfaces*, 68(1-2):127–139, 1992.

[341] O. Théodoly, J. S. Tan, R. Ober, C. E. Williams, and V. Bergeron. Oscillatory forces from polyelectrolyte solutions confined in thin liquid films. *Langmuir*, 17(16):4910–4918, 2001.

[342] P. R. Suresha, Manohar V. Badiger, and Bernhard a. Wolf. Polyelectrolytes in dilute solution: viscometric access to coil dimensions and salt effects. *RSC Adv.*, 5(35):27674–27681, 2015.

[343] Regine V. Klitzing, Branko Kolarić, Werner Jaeger, and Astrid Brandt. Structuring of poly(DADMAC) chains in aqueous media: A comparison between bulk and free-standing film measurements. *Physical Chemistry Chemical Physics*, 4(10):1907–1914, 2002.

[344] S.T. Giolando, R.A. Rapaport, R.J. Larson, T.W. Federle, M. Stalmans, and P. Masscheleyn. Environmental fate and effects of DEEDMAC: A new rapidly biodegradable cationic surfactant for use in fabric softeners. *Chemosphere*, 30(6):1067–1083, mar 1995.

[345] National Research Council et al. *Fat Content and Composition of Animal Products: Proceedings of a Symposium*. National Academies Press, 1976.

[346] David P Cistola, David Atkinson, James A Hamilton, and Donald M Small. Phase behavior and bilayer properties of fatty acids: hydrated 1: 1 acid-soaps. *Biochemistry*, 25(10):2804–2812, 1986.

[347] JR Usher, RM Epand, and D Papahadjopoulos. The effect of free fatty acids on the thermotropic phase transition of dimyristoyl glycerophosphocholine. *Chemistry and physics of lipids*, 22(3):245–253, 1978.

[348] Noriyuki Muranushi, Noriko Takagi, Shozo Muranishi, and Hitoshi Sezaki. Effect of fatty acids and monoglycerides on permeability of lipid bilayer. *Chemistry and physics of lipids*, 28(3):269–279, 1981.

[349] William Ehringer, Daniel Belcher, Stephen R Wassall, and William Stillwell. A comparison of the effects of linolenic (18: 3ω3) and docosahexaenoic (22: 6ω3) acids on phospholipid bilayers. *Chemistry and physics of lipids*, 54(2):79–88, 1990.